

https://dspace.org/

Fluid-rock interaction in carbonatite and alkaline composite intrusions and implications for rare earth element mineralization

Ozturk, Anil

2019

https://hdl.handle.net/10539/29586

Ozturk, Anil (2019) Fluid-rock interaction in carbonatite and alkaline composite intrusions and implications for rare earth element mineralization, University of the Witwatersrand, Johannesburg, <http://hdl.handle.net/10539/29586>

Downloaded from a DSpace repository. https://dspace.org/

Fluid-Rock Interaction in Carbonatite and Alkaline Composite Intrusions and Implications for Rare Earth Element Mineralization

by

Anıl Öztürk



Supervisors

Associate Professor Paul A. M. Nex

Professor Judith A. Kinnaird

A FULL THESIS SUBMITTED IN FULLFILMENT OF THE REQUIREMENTS FOR A MASTER DEGREE IN GEOLOGY, SCHOOL OF GEOSCIENCES, UNIVERSITY OF THE WITWATERSRAND

October 25, 2018

School of Geosciences

University of the Witwatersrand

DECLARATION

I declare that this dissertation is my own, unaided work. It is being submitted for the Degree of Master in Science at the University of the Witwatersrand, Johannesburg. It has not been submitted before for any degree or examination in any other university.



Signature of Candidate

17st day of April 2019

ABSTRACT

The Spitskop Igneous Complex is a carbonatite-alkaline silicate complex located 190 km northeast of Pretoria and 48 km east of Groblersdal in South Africa. It covers an area of 50 km^2 and intruded into the Bushveld Complex on the Kaapvaal Craton at 1.3 Ga. It is considered a part of the Pilanesberg Alkaline Province, as it contains similar rock types such as nepheline syenites, ijolites and carbonatites and has a similar age. The carbonatite component of the Spitskop Complex consists primarily of dolomite carbonatite, calcite-dolomite carbonatite and calcite carbonatite with an apatite-rich zone. The outer part of the complex comprises alkaline rocks including ijolite and nepheline syenite, surrounded by the Rustenburg Layered Suite and the Lebowa Granite Suite of the Bushveld Complex. It is a unique complex, where both felsic and mafic fenites occur together. REE mineralization is hosted in carbonatites, however it is not considered an economic mineral deposit.

This study characterizes the alteration stages that led to the formation of fenites and alkaline rocks, and the petrology and geochemistry of the Spitskop Complex. It shows that the fluids controlled the rare earth element content of Spitskop and affected the mobility of REE.

The Spitskop Complex was mapped and samples were collected from different lithologies. Thin section petrology was used to determine the characteristic features and distribution of minerals. A total of 125 polished thin sections were studied using transmitted-reflected light microscopy and scanning electron microscopy (SEM). XRF and ICP-MS data of rocks have been obtained and the distribution of major-, trace- and rare earth elements of different lithologies were studied. The chemical composition of the fenitized Bushveld rocks have been compared with the unfenitized Bushveld rocks.

The carbonatites all have similar major element concentrations except for CaO, MgO and MnO. The CaO and MgO concentrations reflect the type of carbonatite and the carbonatite mineralogy. Trace element and REE patterns of the different carbonatites are similar. The REE content of Spitskop carbonatites is up to 740 ppm. Nepheline syenites show metasomatic REE alteration patterns.

Fenites are divided into two groups in the Spitskop Complex, mafic fenites and granite fenites. Mafic fenites represent metasomatized Upper Zone gabbro, whereas granite fenites represent metasomatized Nebo Granite. Moreover, granite fenites are subdivided into feldspar fenite,

which contains mostly feldspar; and quartz-feldspar fenite, which contains quartz and feldspar together. Mafic fenites are enriched in Na_2O-K_2O and P_2O_5 relative to the likely parental Upper Zone gabbros. Most of the trace element and all of the REE content of the mafic fenites are higher than the Upper Zone gabbros except Sc, V, Ni, Cu and U. Feldspar fenites are enriched in Na_2O, K_2O and MgO, and depleted in SiO_2 compared to the parental Bushveld Granites.

There are only some limited locations in the world where mafic and granitic rocks are extensively metasomatized together, therefore the Spitskop Complex is an ideal place to investigate the metasomatic geochemical processes.

The mobility of the trace elements changes with increased fenitization. Nebo Granite has the highest trace elements concentrations, rather than in the quartz-feldspar fenite, with the feldspar fenite most depleted. However Cu, Sc and Eu are depleted in Nebo Granite.

The REE data shows that the fenites compositionally lie between the unaltered Nebo Granite and the unaltered Upper Zone rocks. Fenitized Nebo Granite is depleted in REE and fenitized Upper Zone rocks are enriched in REE. The unaltered Upper Zone country rocks defines the lower REE boundary and the Nebo Granite defines the upper REE abundances.

It is suggested that the metasomatic fluids caused a depletion of REE in the felsic rocks, whereas the same fluids caused an enrichment of REE in the mafic rocks. In mafic rocks the enrichment is dispersed through the whole rock across a broad zone and is therefore not economic.

The data from thin section petrography and SEM suggests that the fenitization evolved in multiple steps at the Spitskop Complex. Alteration minerals show that there is a systematic change of minerals, from plagioclase to albite or nepheline, from olivine and orthopyroxene to clinopyroxene, from nepheline to analcite and from clinopyroxene to amphibole, which represent mafic fenites.

Geochemical data, particularly REE patterns, suggests that the nepheline syenite at Spitskop is not a magmatic nepheline syenite, rather it is a product of fenitization. The REE patterns of the nepheline syenites are similar to the fenites of the Spitskop Complex and differ from other Pilanesberg nepheline syenites such as those in Pilanesberg, which are not fenitized. REE geochemistry also suggested that the syenites produced from fenitization (feldspar fenites) can be distinguished from magmatic syenite with the same REE patterns.

Table of Contents

Chapter 1. Introduction 22

1.1 Kaapvaal Craton 22

1.2 Pilanesberg Alkaline Province 24

1.3 Carbonatites and REE Mineralization 26

1.4 Fluids as a Metasomatism Tool 30

1.5 Introduction to the Spitskop Complex 32

1.6 Methodology 37

1.7 Objectives 38

Chapter 2. Field Relationships 39

2.1 Introduction 39

2.2 Carbonatites 40

2.3 Nepheline Syenites 43

2.4 Mafic Fenites 45

2.5 Granite Fenites 48

Chapter 3. Petrology/Petrography and SEM 52

3.1 Introduction 52

3.2 Carbonatites 53

3.3 Nepheline Syenites and Ijolite 58

3.4 Original Bushveld Upper Zone Rocks and the Mafic Fenites 62

3.5 Granite Fenites 72

3.6 Conclusion of Metasomatic Alteration 75

3.7 Discussion on Alteration Assemblages 75

Chapter 4. Geochemistry 78

4.1 Carbonatites 79

4.1.1 Major element geochemistry 79

4.1.2 Trace element geochemistry 81

4.1.3 REE geochemistry 84
4.2 Nepheline Syenites and Ijolite 85
4.2.1 Major element geochemistry 86
4.2.2 Trace element geochemistry 88
4.2.3 REE geochemistry 92
4.3 Mafic Fenites 94
4.3.1 Major element geochemistry 95
4.3.2 Trace element geochemistry 97
4.3.3 REE geochemistry 101
4.3.4 Isocon geochemistry 102
4.4 Granitic Fenites 104
4.4.1 Major element geochemistry 105
4.4.2 Trace element geochemistry 106
4.4.3 REE geochemistry 109
4.4.4 Isocon geochemistry 111
4.5 Summary of Geochemistry Results 113
4.6 Discussion 116
Chapter 5. Conclusions, Discussion and Suggestions 119
5.1 Spitskop Alkaline Complex 119
5.2 Fenites 119
5.2.1 Mafic Fenites – implications from Spitskop 121
5.2.2 Granitic Fenites – implications from Spitskop 121
5.2.3 Fenites – implications 122
5.3 Implications for REE Mineralization and Exploration 123
5.4 Conclusions 125
5.5 Discussion 126
5.5.1 Discussion of the Mafic Fenites at Spitskop 126

5.5.2 Discussion of the Granitic Fenites at Spitskop 129

5.5 Suggestions for Further Work 130

References 133

Supplementary Data 142

List of Figures

Figure 1. 1: Simplified geological map of the northeastern part of the Kaapvaal Craton, modified from Olsson et al. (2010), showing the location of the Busveld Complex, the Pilanesberg Complex and the Spitskop Complex and the distribution of the different sedimentary successions deposited on the Kaapvaal craton. 24

Figure 1. 2: Map showing the distribution of the carbonatite-alkaline complexes of the Pilanesberg alkaline province on the Kaapvaal Craton. The inset map on the right shows the Archean Kaapvaal and Zimbabwe cratons together with the Limpopo Belt (Gose et al., 2013). 26

Figure 1. 3: Chemical classification of carbonatites, edited from Le Maitre (2002). Weight percent of oxides are used for this classification. 27

Figure 1. 4: Distribution of carbonatites worldwide from Jones et al. (2013). 28

Figure 1. 5: Distribution of carbonatites by geographic regions, from Woolley and Kjarsgaard (2008). 29

Figure 1. 6: Mineral assemblages of the different stages of metasomatism (Elliott et al., 2018) 31

Figure 1. 7: Total alkalis vs silica of fenites and their protoliths around the world (Elliott et al., 2018). 31

Figure 1. 8: Google earth image showing the location of the Spitskop Complex, Groblersdal, Johannesburg and Pretoria. 32

Figure 1. 9: Geological map of the Spitskop Complex displaying carbonatite, nepheline syenite, ijolite and fenitized rocks surrounded by Bushveld granite (Gose et al., 2013). The box shows the outline of Figure 1.8. 33

Figure 1. 10: Geological map of the Spitskop carbonatite, modified after Verwoerd (1967). 34

Figure 1. 11: Typical field photographs of the Spitskop alkaline rocks (a) ijolite, (b) nepheline syenite, (c) calcite carbonatite, (d) dolomite carbonatite. 36

Figure 2. 1: 3-D Google Earth image showing the location of the stream section travers (blue) along the Tshweneng River, Spitskop Hill, Mare Hill and the location of nepheline syenites, carbonatites, mafic fenites and granite fenites (feldspar fenite and quartz-feldspar fenite)…. 40

Figure 2. 2: Google Earth image showing location of carbonatites, nepheline syenites, mafic fenites and granite fenites…… 40

Figure 2. 3: Field photographs of carbonatites showing (a) euhedral coarse-grained white calcite carbonatite near the Tshweneng River with calcite grains up to 5 cm in size (X-East: 786776, Y-North: 7234740, Z-Elevation: 1345) (b) the boundary between medium-grained whitish calcite-dolomite carbonatite (left) and fine-grained brown dolomite carbonatite (right) near Spitskop Hill, note the sharp colour change. The dolomite carbonatite is younger than the calcite-dolomite carbonatite (X-East: 786342, Y-North: 7233540, Z-Elevation: 1395) (c) brown-coloured fine-grained magnetite-bearing dolomite carbonatite, from an outcrop located northeastern of Tshweneng River between Mare- and Spitskop Hill (X-East: 786322, Y-North: 7234469, Z-Elevation: 1354) (d) yellowish-brown fine-grained apatite in dolomite carbonatite near Spitskop Hill, note that apatite is mostly found with dolomite carbonatite (X-East: 786506, Y-North: 7233596, Z-Elevation: 1391)…… 43

Figure 2. 4: Field photographs of nepheline syenite showing the various textural features (a) intrusion of medium-grained nepheline syenite into alkali feldspar-rich porphyritic nepheline syenite on Spitskop Hill. Alkali feldspars are 2-5 cm in length (X-East: 785595, Y-North: 7233095, Z-Elevation: 1579) (b) porphyritic nepheline syenite with alkali feldspars 1-4 cm in length on Spitskop Hill (X-East: 785595, Y-North: 7233095, Z-Elevation: 1579) (c) acicular green-black coloured aegirine 1-2 cm in length within massive nepheline syenite on Spitskop Hill (X-East: 785592, Y-North: 7233118, Z-Elevation: 1581) (d) medium- to coarse-grained nepheline syenite with flow banding textures at the top of Mare Hill (X-East: 786676, Y-North: 7235210, Z-Elevation:1513) (e) equant square alkali feldspars in typical massive nepheline syenite on Spitskop Hill (X-East: 785683, Y-North: 7233151, Z-Elevation: 1506) (f) tabular-shaped feldspars in pegmatitic nepheline syenite on Spitskop Hill, note that the alkali feldspars can be more than 7-8 cm in length (X-East: 785595, Y-North: 7233095, Z-Elevation: 1579)…… 45

Figure 2. 5: Field photographs of mafic fenites in the Tshweneng River. (a) typical blue to dark blue mafic fenite consisting of nepheline and clinopyroxene with a single perthite vein, note that ijolite also looks like this mafic fenite in the field (X-East: 787597, Y-North: 7234691, Z-Elevation: 1330) (b) light blue mafic fenite with dark green clinopyroxene patches and some alkali feldspars, note that zoned clinopyroxenes near alkali feldspars are coarser than the clinopyroxenes within mafic fenite (X-East: 787716, Y-North: 7234180, Z-Elevation: 1322) (c) typical perthitic vein within mafic fenite; the size of the alkali feldspars are mostly 1-3 cm in

size, note that there is a clinopyroxene zone within the vein (X-East: 787603, Y-North: 7234664, Z-Elevation: 1330 (d) alkali feldspar patch within mafic fenite (X-East: 787691, Y-North: 7234216, Z-Elevation: 1323) (e) perthite vein within mafic fenite, note that clinopyroxenes within the vein are coarser than the clinopyroxenes within the mafic fenite (X-East: 787616, Y-North: 7234380, Z-Elevation: 1325) (f) The main magnetite zone in the middle of the Tshweneng River, the light blue-blue rock is mafic fenite and dark parts are the massive magnetites. There is a thick white perthite vein within this magnetite zone (X-East: 787598, Y-North: 7234454, Z-Elevation: 1324) (g) Plagioclase inclusions within magnetite, note that inclusions are oriented parallel to the margin of the magnetite (X-East: 787598, Y-North: 7234454, Z-Elevation: 1324). …….. 48

Figure 2. 6: Field photographs of granite fenite in the south-eastern part of the Tshweneng River showing (a) typical coarse-grained feldspar fenite with dark-coloured mafic veins, note that there is a gradual colour change near vein boundaries (X-East: 787974, Y-North: 7233907, Z-Elevation: 1312) (b) feldspar fenite with light- and dark-coloured veins. Note that the feldspar fenite contains more veins than the quartz-feldspar fenite (X-East: 787974, Y-North: 7233907, Z-Elevation: 1312) (c) typical whitish coarse-grained quartz-feldspar fenite with very fine-grained black veins, the mineralogical composition of the vein is not known (X-East: 788168, Y-North: 7233828, Z-Elevation: 1311) (d) the boundary between feldspar fenite (right) and quartz-feldspar fenite (left). Note that there are two different colours of quartz-feldspar fenite, both pink and white (X-East: 788155, Y-North: 7233843, Z-Elevation: 1310)……... 50

Figure 3. 1: 3-D Google Earth image showing the location of the Spitskop Complex together with the number of samples collected from the different lithologies. The blue line is the Tshweneng River, where ijolite, mafic fenite and granite fenite samples come from……..52

Figure 3. 2: Minerals and textures in calcite carbonatite (a) PPL image showing igneous coarse-grained subhedral to euhedral calcite crystals with fine-grained apatite zones and medium-grained anhedral magnetite grains; accessory fine-grained dolomite is present but rare in this image. Sample 7-85. (b) XPL image showing coarse-grained calcite crystals with good cleavages and fine-grained apatite zones, anhedral to subhedral magnetite grains are present. Sample 6-69B. (c) PPL image showing fine-grained apatite with moderate relief and medium- to coarse-grained subhedral magnetite crystals within the groundmass of medium- to coarse-grained calcite. Sample 8-88-2B. (d) PPL image showing medium- to coarse-grained subhedral

magnetite grains and a thin apatite vein 0.1 to 0.5 mm in width within the groundmass of coarse-grained calcite. Sample 8-90. (e) PPL image showing fine-grained pale yellow-pale green REE-bearing mineral within a coarse-grained calcite crystal. Sample 6-69B. (f) fine-grained REE-bearing minerals between the boundary of hornblende and calcite crystals and within the hornblende crystal in BSE. Sample 6-69-1. Abbreviation of minerals are from Krest (1983). Calcite (Cal), apatite (Ap), magnetite (Mag), dolomite (Dol) and hornblende (Hbl)……...55

Figure 3. 3: Minerals and textures in calcite-dolomite carbonatite (a) PPL image showing medium-grained subhedral calcite crystals rimmed by fine-grained dolomite crystals, fine-grained anhedral magnetite grains are present within the groundmass. Sample 8-91. (b) primary- and secondary replacement of calcite by late dolomite, apatite crystals are found in the primary replacement zone, but disappear in the secondary replacement zone. Complete- and incomplete replacement are found together in the primary zone. Sample 8-91. (c) BSE image of calcite crystals and dolomite rims, apatite is mostly found within dolomite. Sample 8-91. (d) PPL image of a fine-grained apatite vein containing medium- to coarse-grained anhedral magnetite grains and fine-grained dolomite. Accessory calcite is present, but rare in this image. Sample 8-100B. Calcite (Cal), dolomite (Dol), apatite (Ap), magnetite (Mag), primary replacement zone (prz), secondary replacement zone (srz)……...56

Figure 3. 4: Minerals and textures in dolomite carbonatite (a) PPL image of a fine-grained anhedral dolomite (Dol) and a fine-grained anhedral apatite (Ap) with medium-grained magnetite grains. Sample 8-93. b) PPL image of coarse-grained subhedral magnetite (Mag) and medium-grained magnetite grains surrounded by fine-grained apatite within the groundmass of dolomite. Sample 8-103-2B. c) XPL image of coarse-grained magnetite with cracks filled by fine-grained apatite; the groundmass consists of dolomite. Sample 8-103-1B. d) BSE image of coarse-grained subhedral magnetite, filled and rimmed by fine-grained apatite within the groundmass of dolomite. Sample 8-103-1A. Dolomite (Dol), apatite (Ap), magnetite (Mag). …….. 58

Figure 3. 5: Minerals and textures in nepheline syenite (a) XPL image of medium- to coarse-grained subhedral equant nepheline, medium-grained subhedral aegirine-augite within the groundmass of the tabular-shaped medium-grained alkali feldspar. Sample 3-23-1. (b) BSE image of subhedral perthitic alkali feldspar composed of albite within microcline crystals, subhedral aegirine-augite crystals and subhedral to euhedral nepheline. Sample 3-24. (c) XPL image of coarse-grained euhedral equant nepheline with interstitial medium- to coarse-grained aegirine-augite within the groundmass of medium-grained aegirine-augite and medium-grained

tabular alkali feldspar. Sample 3-23-1. (d) BSE image showing seriate texture of nepheline syenite composed of fine- to coarse-grained anhedral to euhedral aegirine-augite within the groundmass of nepheline. Sample 3-30-1. (e) PPL image showing acicular and fibrous texture of fine-grained aegirine-augite together with medium-grained subhedral nepheline and altered coarse-grained alkali feldspar crystals. Sample 3-31-1-2. (f) PPL image showing tabular coarse-grained euhedral feldspar crystals containing subhedral medium-grained nepheline and fine-grained clinopyroxene inclusions. Sample 3-31-3-1. (g) PPL image showing acicular and dendritic overgrowths of fine-grained aegirine-augite around the coarse-grained subhedral alkali feldspar and the medium-grained euhedral nepheline. Sample 3-31-3-1. Nepheline (Ne), aegirine-augite (Agt), alkali feldspar (Afs)……...60

Figure 3. 6: Minerals and textures in ijolite (a) XPL image of typical ijolite showing medium-grained euhedral equant nepheline and medium-grained subhedral aegirine-augite, tabular coarse-grained alkali feldspar is also present. Sample 2-11-1-1. (b) XPL image showing medium-grained euhedral equant nepheline and acicular medium-grained aegirine-augite with coarse-grained alkali feldspar. Note that alkali feldspar contains aegirine-augite inclusions. Sample 2-11-1-1. (c) PPL image showing subhedral hexagonal- and square nepheline together with interstitial medium-grained aegirine-augite. Sample 2-11-1-3. (d) BSE image of euhedral hexagonal- to square nepheline with interstitial anhedral to subhedral aegirine-augite. Note that there is an analcite rim around nepheline crystals. Sample 2-11-1-1. (e) BSE image showing analcite vein and the metasomatic alteration of euhedral nepheline to anhedral analcite, subhedral to euhedral titanite and minor magnetite. Sample 2-12-1-1. Nepheline (Ne), aegirine-augite (Agt), alkali feldspar (Afs), analcite (Anl), titanite (Ttn), magnetite (Mag)……. 62

Figure 3. 7: Minerals and textures in the Bushveld Upper Zone rocks, from Bierkraal (a) XPL image of a magnetitite layer showing the massive magnetite and coarse-grained subhedral plagioclase minerals within magnetitite. Note that some clinopyroxene is also present within the magnetitite. Sample IW1459.3. (b) PPL image of a gabbro showing medium-grained anhedral to subhedral ortho- and clinopyroxene, and tabular shaped medium- to coarse-grained plagioclase crystals. Sample IW403.4. c) PPL image of a gabbro showing medium-grained subhedral orthopyroxene with tabular shaped plagioclase crystals and medium-grained anhedral magnetite. Sample IW403.4. d) XPL image of gabbro showing plagioclase crystals, medium-grained anhedral magnetite, anhedral apatite and anhedral olivine. Magnetite (Mag), plagioclase (Pl), clinopyroxene (Cpx), orthopyroxene (Opx), apatite (Ap) and olivine (Ol)...64

Figure 3. 8: Minerals and textures in magnetite-bearing mafic fenites (a) PPL image of a typical mafic fenite showing colourless medium- to coarse-grained anhedral nepheline, medium- to coarse-grained anhedral aegirine-augite and medium-grained anhedral magnetite grains. Note that fine-grained stilpnomelane is also present within some aegirine-augite crystals. Sample 1-2-2-2. (b) XPL image of a typical mafic fenite showing medium-grained anhedral to subhedral nepheline, medium-grained anhedral aegirine-augite and fine-grained magnetite crystals with accessory medium-grained subhedral diamond-shaped titanite. Sample 1-2-2-2. (c) PPL image showing seriate texture of fine- to coarse-grained anhedral aegirine-augite, fine-grained anhedral magnetite and colourless nepheline. Note that the amount of magnetite increases near or around aegirine-augite and nepheline. Sample 6-64-1B. (d) PPL image showing tabular colourless medium-grained subhedral plagioclase, medium-grained anhedral olivine, medium-grained anhedral apatite and medium- to coarse-grained subhedral aegirine-augite. Note that nepheline is also present in this thin section. Sample 6-64-2A. (e) XPL image of the mafic fenite showing medium-grained anhedral nepheline, medium- to coarse-grained tabular subhedral plagioclase, medium-grained anhedral olivine, fine- to medium-grained anhedral magnetite and medium- to coarse-grained subhedral aegirine-augite. Sample 6-64-2A. (f) XPL image showing medium-grained olivine rimmed by fine- to medium-grained aegirine-augite, and medium-grained plagioclase together with anhedral nepheline. Sample 6-64-2B. (g) PPL image showing fine- to medium-grained anhedral augite-aegirine, medium-grained anhedral to subhedral stilpnomelane and colourless anhedral nepheline. Note that aegirine-augite near or around nepheline is always fine-grained. Sample 1-1-1. (h) XPL image of a perthite vein showing coarse-grained tabular euhedral perthitic feldspar consists of microcline and albite, and some medium-grained anhedral aegirine-augite. Note that stilpnomelane and nepheline are also present. Sample 1-2-2-2. (i) PPL image of a perthite vein showing coarse-grained subhedral aegirine-augite interstitial to the perthitic feldspar, and medium-grained anhedral magnetite crystals. Note the change of the size of the clinopyroxene, aegirine-augite outside of the perthite vein is fine- to medium-grained. Sample 2-14-5-2. Nepheline (Ne), aegirine-augite (Agt), magnetite (Mag), stilpnomelane (Stp), titanite (Ttn), plagioclase (Pl), olivine (Ol), apatite (Ap), perthitic feldspar (Afs)…….. 67

Figure 3. 9: Minerals and textures in magnetite-bearing mafic fenites (a) XPL image showing a part of the massive magnetite and the vein within the magnetite. Medium-grained subhedral to euhedral diamond-shaped titanite with simple twinning and medium- to coarse-grained anhedral nepheline together with some medium-grained aegirine-augite are common and some

fine-grained magnetite grains are also present within the vein. Sample 1-8-2-1. (b) PPL image showing the anhedral to subhedral diamond-shaped titanite rim to the magnetite, medium-grained anhedral aegirine-augite and colourless medium-grained nepheline. Sample 2-14-6-2. (c) PPL image showing fine- to medium-grained subhedral stilpnomelane crystals and fine-grained aegirine-augite grains within the magnetite inclusion. Sample 1-6-1. (d) XPL image of the magnetite filled with fine-grained anhedral aegirine-augite and medium-grained subhedral nepheline with some fine-grained magnetite crystals. Note that few anhedral titanite crystals are present. Sample 2-14-3. (e) BSE image of the magnetite filled with nepheline and plagioclase. Sample 1-8-2-1. (f) BSE image showing anhedral aegirine-augite and anhedral nepheline near the massive titaniferous magnetite. Note that the massive magnetite is rimmed by titanite. Sample 2-12-1-1. Magnetite (Mag), titanite (Ttn), nepheline (Ne), aegirine-augite (Agt), stilpnomelane (Stp), plagioclase (Pl)…… 69

Figure 3. 10: Metasomatic alteration textures in mafic fenites (a) XPL image of a mafic fenite showing the beginning of alteration of a medium-grained subhedral olivine to fine- to medium-grained aegirine-augite, and the alteration of medium-grained plagioclase to anhedral nepheline. Note that the irregular fractures in olivine are filled by aegirine-augite. Sample 6-64-2A. (b) PPL image showing the beginning of an alteration of another medium-grained olivine to anhedral medium-grained aegirine-augite. Note that the cracks are filled by aegirine-augite. Sample 6-64-2B. (c) PPL image showing the initial alteration of olivine to fine-grained aegirine-augite, and subsequently to stilpnomelane. Note that small pale-yellow to pale-brown crystals within aegirine-augite are remnant olivine. Sample 1-4. (d) XPL image of the same thin section of (c). Sample 1-4. (e) PPL image of medium-grained subhedral olivine rimmed and filled by fine-grained anhedral aegirine-augite. Note that some aegirine-augite was subsequently altered to anhedral stilpnomelane. Sample 1-1-1. (f) XPL image of the transformation of coarse-grained subhedral orthopyroxene rimmed and filled by fine-grained anhedral aegirine-augite. Sample 1-4. (g) XPL image of a medium-grained subhedral orthopyroxene rimmed and cross-cut by fine-grained anhedral aegirine-augite. Sample 1-1-1. (h) XPL image showing the beginning of alteration of subhedral orthopyroxene to fine- and medium-grained anhedral to subhedral aegirine-augite. Sample 1-4. (i) XPL image showing medium-grained subhedral orthopyroxene rimmed by fine-grained anhedral aegirine-augite. Sample 1-1-1. (j)PPL image showing the alteration of medium-grained anhedral aegirine-augite to stilpnomelane. Sample 2-14-4-2. (k) PPL image showing the beginning of alteration of medium- to coarse-grained subhedral aegirine-augite to medium-grained anhedral

stilpnomelane. Sample 2-14-4-1. (l) XPL image showing alteration of anhedral nepheline possibly to analcite, near a perthite vein. Sample 2-16-1. Olivine (Ol), aegirine-augite (Agt), plagioclase (Pl), nepheline (Ne), stilpnomelane (Stp), orthopyroxene (Opx)…….. 71

Figure 3. 11: Minerals and textures in feldspar fenite and quartz feldspar fenite (a) PPL image showing coarse-grained subhedral perthitic feldspar and coarse-grained anhedral clinopyroxene. Sample 4-48-4. (b) PPL image showing coarse-grained altered patch perthitic feldspar with domains of K and microcline and albite with some fine-grained anhedral magnetite grains. Sample 5-52-1. (c) XPL image showing radiating clusters of needle-like aegirines and tabular-shaped medium-grained alkali feldspars. Sample 4-48-10. (d) BSE image showing coarse-grained microcline with albite inclusions, and radiating clusters of needle-like coarse-grained aegirine. Sample 5-50-1. (e) BSE image showing coarse-grained anhedral-subhedral albite crystals and subhedral aegirines, note that there is no K-spar in this zone. Sample 5-50-1. (f) PPL image showing coarse-grained subhedral alkali feldspar, medium- to coarse-grained anhedral to subhedral quartz crystals with fine-grained anhedral clinopyroxene and medium-grained anhedral hornblende. Sample 5-56-2. (g) XPL image of coarse-grained anhedral to subhedral quartz with coarse-grained alkali feldspar. Sample 5-56-1. (h) PPL image showing a clinopyroxene vein within a coarse-grained perthitic feldspar. Sample 5-56-1. Perthitic feldspar (Afs), clinopyroxene (Cpx), microcline (Mc), albite (Ab), magnetite (Mag), aegirine (Aeg), quartz (Qtz), hornblende (Hbl)…… 74

Figure 3. 12: Metasomatic alteration textures in quartz-feldspar fenite (a) XPL image showing an alteration of coarse-grained subhedral plagioclase feldspar of the Bushveld Nebo granite. Note that the altered anhedral mineral may be nepheline. Sample 5-56-1. (b) XPL image showing the alteration of coarse-grained subhedral quartz of the Bushveld Nebo granite possibly to nepheline. Sample 5-56-1. Plagioclase (Pl), quartz (Qtz)…….. 74

Figure 4. 1: Chemical classification of the Spitskop carbonatites. Note that there is no separate field in Woolley and Kempe's (1989) diagram for calcite-dolomite carbonatite. Harmer's (1992) data is also used. ……...80

Figure 4. 2: Selected Harker diagrams of major element compositions of the Spitskop carbonatites. (a) MgO versus CaO contents, (b) MnO versus MgO contents…….. 80

Figure 4. 3: Chondrite-normalized trace element abundance diagrams for whole rocks of (a) calcite carbonatite, (b) calcite-dolomite carbonatite, (c) dolomite carbonatite and (d) the average abundances. Chondrite values are taken from McDonough and Sun (1995)……83

Figure 4. 4: Selected Harker diagrams of trace element compositions in the Spitskop calcite carbonatite, calcite-dolomite carbonatite and dolomite carbonatite. (a) Co versus Sc contents, (b) Zn versus Pb contents, (c) Pb versus MgO contents and (d) Co versus MgO contents…. 84

Figure 4. 5: Chondrite-normalized REE diagrams of (a) calcite carbonatite, (b) calcite-dolomite carbonatite, (c) dolomite carbonatite and (d) average of the carbonatites of the Spitskop Complex. Chondrite values are taken from Sun and McDonough (1989). Note that samples of Harmer (1992), which contain all REE data are shown as green in diagrams……..85

Figure 4. 6: Selected Harker diagrams of major element composition of the Mare nepheline syenite, Spitskop nepheline syenite and Pilanesberg nepheline syenite. (a) Na_2O+K_2O versus SiO_2 contents, (b) K_2O versus Na_2O contents, (c) Al_2O_3 versus SiO_2 contents, (d) MgO versus SiO_2 contents, (e) CaO versus SiO_2 contents, (f) TiO_2 versus SiO_2 contents, (g) P_2O_5 versus SiO_2 contents, (h) CaO versus Al_2O_3 contents, (i) MgO versus Al_2O_3 contents and (j) P_2O_5 versus TiO_2 contents. Pilanesberg nepheline syenite data are from Elburg and Cawthorn (2017)……88

Figure 4. 7: Chondrite-normalized trace element abundance diagrams for whole rocks of (a) Spitskop nepheline syenite samples, (b) Mare nepheline syenite samples, (c) Pilanesberg nepheline syenite samples, and (d) average values of Spitskop-, Mare- and Pilanesberg nepheline syenite. Normalized values are taken from McDonough and Sun (1995)……90

Figure 4. 8: Harker diagrams showing the trace element compositions of nepheline syenites of the Mare, Spitskop and Pilanesberg areas. (a) Th versus Co contents, (b) Ba versus Co contents, (c) Sr versus Ba contents, (d) Nb versus Y contents of Spitskop-Mare nepheline syenite, and (e) Nb versus Y contents of Spitskop-Mare and Pilanesberg nepheline syenite together. Pilanesberg nepheline syenite data are from Elburg and Cawthorn (2017)……..92

Figure 4. 9: Chondrite-normalized rare earth element diagram of (a) Spitskop nepheline syenites, (b) Mare nepheline syenites, (c) Rietfontein nepheline syenites, (d) Pilanesberg nepheline syenites, (e) average values of Spitskop, Mare, Rietfontein and Pilanesberg nepheline syenites, and (f) Spitskop nepheline syenite average and Spitskop ijolite. Pilanesberg nepheline syenite data are from Elburg and Cawthorn (2017) and Rietfontein REE data are from Harmer (1992). Chondrite values are taken from Sun and McDonough (1989)……94

Figure 4. 10: Selected Harker diagrams of major element composition of the Spitskop mafic fenites, Bushveld Upper Zone gabbros of van Tongeren (2011) and Bushveld Upper Zone gabbros of Scoon and Mitchell (2012). (a) MgO versus SiO_2 contents, (b) CaO versus SiO_2 contents, (c) Na_2O versus SiO_2 contents, (d) K_2O versus SiO_2 contents, (e) Na_2O+K_2O versus SiO_2 contents, (f) MgO+CaO versus SiO_2 contents and (g) TiO_2 versus SiO_2 contents…….. 97

Figure 4. 11: Chondrite-normalized trace element abundance diagrams for whole rocks of (a) Spitskop mafic fenites, (b) Bushveld Upper Zone gabbros and (c) average values of the mafic fenites and the Upper Zone gabbros. Trace element values of the Upper Zone gabbros are from van Tongeren (2011). Normalized values are taken from McDonough and Sun (1995)……..99

Figure 4. 12: Harker diagrams showing the trace element compositions of Spitskop mafic fenites. (a) V versus Sc contents, (b) Co versus Sc contents, (c) Ni versus Sc contents, (d) Ni versus V contents, (e) Ni versus Co contents, (f) Nb versus Ga contents, (g) Y versus Zn contents, (h) Nb versus Zr contents. Trace element values of the Upper Zone gabbros are from van Tongeren (2011) and Scoon and Mitchell (2012). Note that some diagrams do not contain Upper Zone trace element compositions because of unavailability of data……101

Figure 4. 13: Chondrite-normalized rare earth element diagrams of (a) mafic fenites, (b) the Bushveld Upper Zone gabbros, (c) their average values. The values of the Bushveld Upper Zone gabbros were taken from van Tongeren (2011). Normalized values are taken from Sun and McDonough (1989)…….102

Figure 4. 14: Isocon diagram of mafic fenite samples versus Bushveld Upper Zone gabbros. The X-axis represent the concentration of the Upper Zone gabbros, and the Y-axis represent the concentration of the mafic fenites. The concentration of major- (blue square) and trace elements (purple diamonds) are multiplied by a constant for each element for easy representation. (a) mafic fenite sample 1-2-2-1 versus original Bushveld Upper Zone gabbro 6-39; (b) mafic fenite sample 4-43-2 versus original Bushveld Upper Zone gabbro 7-57; (c) mafic fenite sample 4-43-1 versus original Bushveld Upper Zone gabbro 6-21; (d) mafic fenite sample 4-48-2 versus original Bushveld Upper Zone gabbro 6-54. The grey zone represents the elements that can be immobile during metasomatism. Isocon line is within or in the boundary of this grey zone. The values of Bushveld Upper Zone gabbro samples are taken from van Tongeren (2011)…….104

Figure 4. 15: Selected Harker diagrams showing major element compositions of Spitskop feldspar fenite, quartz-feldspar fenite and Nebo granite (Kleeman and Twist (1989) and Hill et al. (1996)). (a) K_2O versus SiO_2 contents, (b) Na_2O versus SiO_2 contents, (c) Na_2O+K_2O versus

SiO_2 contents, (d) MgO versus SiO_2 contents, (e) TiO_2 versus SiO_2 contents and (f) MnO versus SiO_2 contents. The values of Nebo granites are taken from Kleeman and Twist (1989) and Hill et al. (1996). The samples of Kleeman and Twist are shown as yellow and the samples of Hill are shown as turquois. ……106

Figure 4. 16: Chondrite-normalized trace element abundance diagrams for whole rocks of (a) Spitskop feldspar fenite, (b) Spitskop quartz-feldspar fenite, (c) Nebo granite and (d) their average values. Trace element values of the Nebo granite are taken from Kleeman and Twist (1989) and Hill et. al. (1996). Chondrite values are taken from McDonough and Sun (1995)……..108

Figure 4. 17: Selected Harker diagrams showing important trace element compositions of Spitskop feldspar fenite, quartz-feldspar fenite and Nebo granite. (a) TiO_2 versus Zr contents, (b) Zr versus Sr contents, and (c) Y versus Th contents. Data for the Nebo granites are from Kleeman and Twist (1989). ……109

Figure 4. 18: Chondrite-normalized REE diagrams of (a) feldspar fenite, (b) quartz-feldspar fenite and (c) Bushveld Nebo granite and (d) average values of them. Pr, Dy, Ho, Er and Tm data are missing in the Nebo granite. REE values of the Nebo granite are taken from Hill et. al. (1996). Chondrite values are taken from Sun and McDonough (1989)……..111

Figure 4. 19: Isocon diagram of quartz-feldspar fenite and feldspar fenite samples versus Nebo granite samples. The average value of Nebo granite is used for the isocon diagrams. The concentration of major- (red square for quartz-feldspar fenite, orange square for feldspar fenite) and trace elements (light blue diamonds for quartz-feldspar fenite, green diamonds for feldspar fenite) are multiplied by a constant for easy representation. (a) quartz-feldspar fenite sample 5-56-1 versus Bushveld Nebo granite average, (b) quartz-feldspar fenite sample 5-56-2 versus Bushveld Nebo granite average, (c) feldspar fenite sample 5-50-2 versus Bushveld Nebo granite average, (d) feldspar fenite sample 5-52-2 versus Bushveld Nebo granite average, (e) feldspar fenite sample 4-48-1 versus Bushveld Nebo granite average and (f) feldspar fenite sample 4-48-6 versus Bushveld Nebo granite average. The grey zone represents the elements that can be immobile during metasomatism. The values of Bushveld Nebo Granite samples are taken from Kleeman and Twist (1989) and Hill (1996)……113

Figure 4. 20: Chondrite-normalized REE diagram of the fenites of the Spitskop Complex (quartz-feldspar fenite, feldspar fenite and mafic fenite) and their parental rocks (Nebo granite and Upper Zone rocks). Normalized values are taken from Sun and McDonough (1989)… 115

Figure 4. 21: Trace elements and REE diagrams of the mafic fenites, Mare nepheline syenite and Spitskop nepheline syenite (a) chondrite-normalized trace element abundance diagram for whole rock averages of the mafic fenites and nepheline syenites and (b) chondrite-normalized REE diagram of average values of mafic fenites and nepheline syenites. Chondrite values are taken from McDonough and Sun (1995)…… 117

Figure 5. 1: Geological map of the Spitskop Complex displaying carbonatite, nepheline syenite, ijolite and fenitized rocks surrounded by Bushveld granite (Gose et al., 2013)……120

Figure 5. 2: Fenitized outcrops in the Spitskop Complex. After alkali metasomatism, granitic rocks transformed to syenitic rocks…… 122

Figure 5. 3: Chondrite-normalized rare earth element diagram of (a) Spitskop feldspar fenites, (b) quartz-feldspar fenites, (c) mafic fenites, and (d) fenitized nepheline syenite. Chondrite values are taken from Sun and McDonough (1989)……... 124

Figure 5. 4: Small scale of albitization zones of metasomatic rocks. (a) is taken from quartz-feldspar fenite and (b) is taken from feldspar fenite. Pink zones are albititic zones…….. 130

Figure 5. 5: Chondrite-normalized rare earth element diagram of (a) fenitized Spitskop nepheline syenites, (b) fenitized Mare nepheline syenites, (c) Pilanesberg nepheline syenites, and (d) average values of the Spitskop Nebo granite (yellow), quartz-feldspar fenite (red) and feldspar fenite (orange). Pilanesberg nepheline syenite data are from Elburg and Cawthorn (2017) and Nebo granite are taken from Hill et. al. (1996). Chondrite values are taken from Sun and McDonough (1989)……..132

List of Tables

Table 1: Geochronological data of the important complexes of the Mesoproterozoic Pilanesberg alkaline province with sizes and predominant rock types, based on Hanson et al. (2006), ([1]Verwoerd, 1967; [2]Mcdougall, 1963; [3]Nelson et al., 1988; [4]Harmer, 1992; [5]van Niekerk, 1962; [6]Harmer, 1999; [7]Hanson et. al, 2006; [8]Elburg and Cawthorn, 2017; [9]Woolley, 2001). 25

Table 2: Carbonatite classification by chemical characteristics, extended from Jones et al. (2013), calcite-dolomite carbonatite is added. FeO^T is total iron, RE_2O_3 is total REE oxides. 27

Table 3: Some of the important carbonatite deposits and their reserves and grades, from Jones et al. (2013). 30

Table 4: Rock types, number of samples and number of thin sections of the rocks of the Spitskop Complex. 53

Table 5: Total number of samples of rocks of the Spitskop Complex and number of the samples that are used for XRF and ICP-MS analysis. 78

Table 6: Trace element averages of all carbonatites, calcite carbonatite, calcite-dolomite carbonatite and dolomite carbonatite from the most enriched elements to the least enriched elements. 81

Table 7: Carbonatite types and their total REE-, LREE- and HREE averages. 84

Table 8: Average trace element data for nepheline syenites of Mare, Spitskop, Rietfontein and Pilanesberg in descending order of abundance. Data for the Rietfontein nepheline syenite and Pilanesberg nepheline syenite are taken from Harmer (1992) and Elburg and Cawthorn (2017) respectively. 89

Table 9: Nepheline syenites and their total REE-, LREE- and HREE averages. Data for the Rietfontein nepheline syenite is taken from Harmer (1992). 92

Table 10: Trace element averages of the Spitskop mafic fenites and the Upper Zone data of van Tongeren (2011) and Scoon and Mitchell (2012) from the most enriched elements to the least enriched elements. 98

Table 11: Total REE-, LREE- and HREE averages of mafic fenites and the Upper Zone gabbros. 101

Table 12: Trace element averages of the feldspar fenite and the quartz feldspar fenite of the Spitskop Complex and the Bushveld Nebo Granite from Kleeman and Twist (1989) from the most enriched elements to the least enriched elements. 107

Table 13: REE-, LREE- and HREE averages of feldspar fenite, quartz-feldspar fenite and the Nebo granite. *Note that 1 LREE (Pr) and 4 HREEs (Dy, Ho, Er, Tm) are missing in Nebo granite. 110

Table 14: Mafic fenites in the world. 126

Chapter 1.

Introduction

This study focuses on the fluid-rock interaction between a series of magmatic rocks and igneous carbonatitic-alkaline intrusions emplaced into these rocks. Heat and volatile elements are transported to the surrounding magmatic rocks during this emplacement, as part of the metasomatic processes (Harlov and Austrheim, 2012). The term metasomatism was originally introduced by Naumann (1826) and the general definition suggested by the IUGS Subcommission on the Systematics of Metamorphic Rocks (SSMR) is ‘‘-a metamorphic process by which the chemical composition of a rock or rock portion is altered in a pervasive manner and which involves the introduction and/or removal of chemical components as a result of the interaction of the rock with aqueous fluids (solutions). During metasomatism the rock remains in a solid state.’’ These carbonatitic-alkalic igneous rocks are elements of the Spitskop Complex, which intruded the Bushveld Igneous Complex on the Kaapvaal Craton at approximately 1.3 Ga (Harmer, 1999).

This study has an importance in understanding rare earth element (REE) mineralization processes in carbonatites and composite alkaline rocks, and gives unique information about metasomatism processes, which may cause major- and trace element mobility and may change the concentration of REE of the rocks at the Spitskop Complex. There is a huge interest in REE and critical metals in the world, as these are used for high-technology, hybrid car technology, strategic/military use and renewable energy applications among others. Great progress has been achieved in this decade in the understanding of the mineralization processes of REE/critical metals and the metal mobility due to the metasomatic processes. This study aims to give a better perspective to the metasomatic processes and REE mineralization systems in the aureole of the Spitskop Complex.

1.1 Kaapvaal Craton

The Kaapvaal Craton is one of the most comprehensively studied and best preserved Archean cratons known (De Wit et al., 1992). It was part of the Vaalbara supercontinent (2.7-2.1 Ga) and covers an area of 1,200,000 km^2 in South Africa, Botswana and Mozambique (Cheney, 1996). Primitive crustal growth (3.7-3.1 Ga) was followed by cratonic integration and stabilization from 3.1 to 2.6 Ga (De Wit et al., 1992).

The Kaapvaal Craton consists of 3.6 to 2.7 Ga granite-gneiss and greenstone terrains, distinguished by structural trends, overlain by metamorphosed volcano-sedimentary cover sequences of Archean and Proterozoic age (Zegers et. al, 1998). On the Kaapvaal Craton the Witwatersrand-Pongola Supergroups are the oldest sedimentary cover sequences (Beukes and Cairncross, 1991), followed by the Ventersdorp Supergroup, Wolkberg-Schmidtsdrif Supergroup, Transvaal Supergroup, Waterberg Group and Soutpansberg-Olifantshoek Group. The craton was intruded by the Bushveld Igneous Complex at 2.06 Ga (Zeh et al., 2015), which is the largest layered intrusion on Earth (Fig. 1.1).

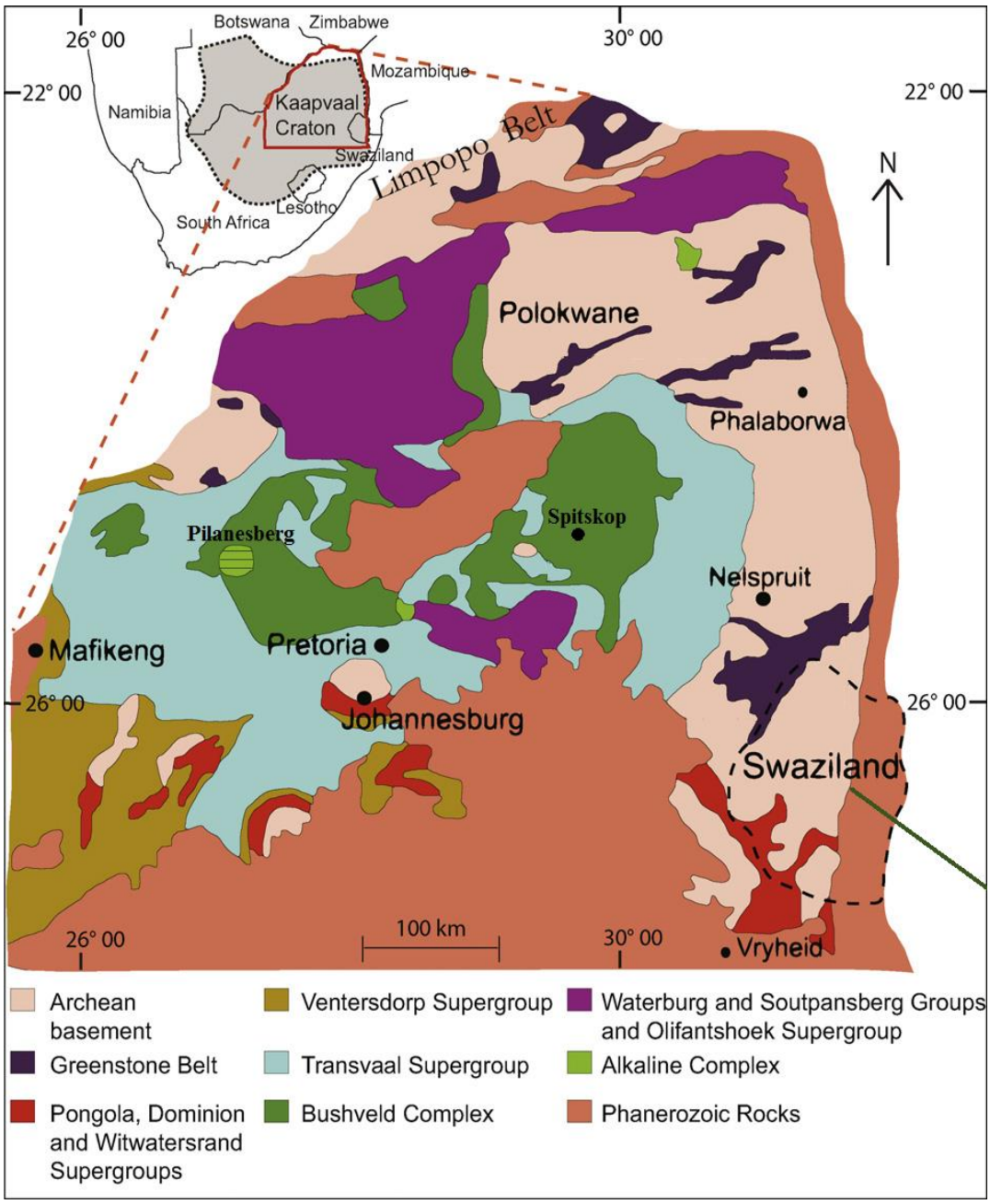

Figure 1. 1: Simplified geological map of the northeastern part of the Kaapvaal Craton, modified from Olsson et al. (2010), showing the location of the Busveld Complex, the Pilanesberg Complex and the Spitskop Complex and the distribution of the different sedimentary successions deposited on the Kaapvaal craton.

The Paleoproterozoic Bushveld Igneous Complex consists of the Rooiberg Volcanic Group, the Rustenburg Layered Suite, the Rashoop Granophyre Suite and the Lebowa Granite Suite. These suites has been studied extensively because they contain considerable ore deposits of chromium, vanadium, palladium, rhodium and platinum (Kinnaird, 2005).

The movement of the Kaapvaal Craton to the north between 2.9 and 2.7 Ga, caused a collision with the Zimbabwe Craton at 2.68 Ga and formed the Limpopo Belt, an east-west trending zone of granulite facies metamorphic rocks located in the border area between South Africa, Zimbabwe and Botswana (de Wit et al., 1992). The Limpopo Belt is divided into a Southern, a Central and a northern Marginal zone, which are separated from each other by shear zones.

The Limpopo belt has long been accepted as an important example of an Archean orogeny in the modern style as well as one of the oldest orogenic belts in the world (Van Breemen and Dodson, 1972). Hence it is regarded as evidence for plate tectonics acting early in the Earth's geological history. As a result of collision between two cratons, the high metamorphic grade of rocks has been attributed to crustal thickening at 2.7 Ga.

The Kalahari Craton, formed as a result of the collision between the Kaapvaal and Zimbabwe cratons, comprises the core of southern Africa and is surrounded by Proterozoic fold belts and is limited by the Phanerozoic Lebombo and Sabi monoclines in the south (Brandl and de Wit, 1997).

1.2 Pilanesberg Alkaline Province

The Kaapvaal craton includes some extraordinary igneous suites including the Bushveld Complex, the Phalaborwa Complex, various diamondiferous kimberlites and the Pilanesberg Alkaline Province (Fig. 1.1).

The Pilanesberg Alkaline Province comprises a series of at least 22 Mesoproterozoic alkaline intrusions, some with a carbonatite component, some solely carbonatite that intruded the Kaapvaal Craton between 1.4-1.0 Ga (Table 1). In addition, the best documented Mesoproterozoic kimberlite, the Premier cluster, intruded during the same time interval. The Pilanesberg Alkaline Province intruded over an area of ~110.000 km^2 (Fig. 1.2). The Pilanesberg Complex is the largest member of the Pilanesberg Alkaline Province with a size of

530 km^2 and it is also one of the world's largest alkaline complexes. It consists mainly of syenite and nepheline syenite, and is thought to have intruded during an intraplate extension event (Lee et al., 2013).

It has been suggested that Mesoproterozoic orogenesis in the Namaqua–Natal–Maud Belt initiated this intraplate magmatism including the Pilanesberg Alkaline Province of the Kalahari Craton (Gose et. al, 2013; Friese et al., 1995). The Pilanesberg Dyke Swarm, which has the same orientation as normal faults located in the same area near the Pilanesberg complex (Fig. 1.2), is regarded as an example of coexisting extensional tectonic movements and alkaline magmatism (Friese et al., 1995).

The geographically isolated Spitskop Complex, located approximately 290 km east of the Pilanesberg Complex, is also considered a member of the Pilanesberg Alkaline Province (Verwoerd, 2006), due to the fact that it contains nepheline syenites, ijolites and carbonatites that have been dated at 1341 ± 37 Ma (Harmer, 1999).

Table 1: Geochronological data of the important complexes of the Mesoproterozoic Pilanesberg alkaline province with sizes and predominant rock types, based on Hanson et al. (2006), ([1]Verwoerd, 1967; [2]Mcdougall, 1963; [3]Nelson et al., 1988; [4]Harmer, 1992; [5]van Niekerk, 1962; [6]Harmer, 1999; [7]Hanson et. al, 2006; [8]Elburg and Cawthorn, 2017; [9]Woolley, 2001).

Complex	Predominant Rock Type	Age (Ma)	Size
Glenover	Carbonatite, pyroxenite, brec.	1000 ± 200[1]	5 km in diameter
Stukpan	Carbonatite, syenite	1130 ± 45[2]	3 km in diameter
Goudini	Carbonatite, volcanic brec.	1190 ± 80[3]	6 km in diameter
Kruidfontein (CR)	Pyroclastic rocks, carbonatite dyke	1246 ± 26[4]	5 km in diameter
Tweerivier (CR)	Carbonatite, fenite, dolomite	1269 ± 171[4]	2.5 km x 5 km
Bulhoekkop (CR)	Carbonatite, fenite, gabbroic brec.	1269 ± 171[4]	1.5 km in diameter
Bulhoek South (CR)	Carbonatite, fenite, gabbroic brec.	1269 ± 171[4]	1 km in diameter
Derdepoort (PR)	Carbonatite, syenite, brec.	1269 ± 171[4]	1 km^2
Pilanesberg dykes	Dolerite	1302 ± 80[5]	400 km length
Spitskop	Carbonatite, neph. syenite, ijolite	1341 ±37[6]	50 km^2
Leeuwfontein (PR)	Syenite, monzonite, neph. syenite	1374 ± 10[7]	4 km x 2 km
Rondavel (PR)	Quartz syenite	1381 ± 10[7]	1 km in diameter
Klipdrift (PR)	Quartz syenite	1385 ± 5[7]	1 km in diameter
Haakdoomfont (PR)	Quartz syenite	1385 ± 5[7]	< 1 km in diameter
Leeuwkraal (PR)	Phonolite	1395 ± 80[7]	1.5 km in diameter
Pilanesberg	Syenite, neph. syenite	1395 ± 10[8]	530 km^2
Franspoort (PR)	Neph. syenite	1420 ± 70[9]	1.6 km in diameter

Buffelskraal (CR)	Pyroxenite, ijolitic dyke	not known	no surface outcrop
Nooitgedacht (CR)	Carbonatite, neph. syenite, fenite	not known	2 km in diameter
Elandskraal (PR)	Basalt, trachyte, pyroxenite	not known	16 km x 14 km
Klopperbos (PR)	neph. syenite	not known	3 km in diameter
Roodeplaat (PR)	Trachyte, neph. syenite, tuff	not known	16 km x 12 km

CR: Crocodile River Alkaline Complexes

PR: Pienaars River Alkaline Complexes

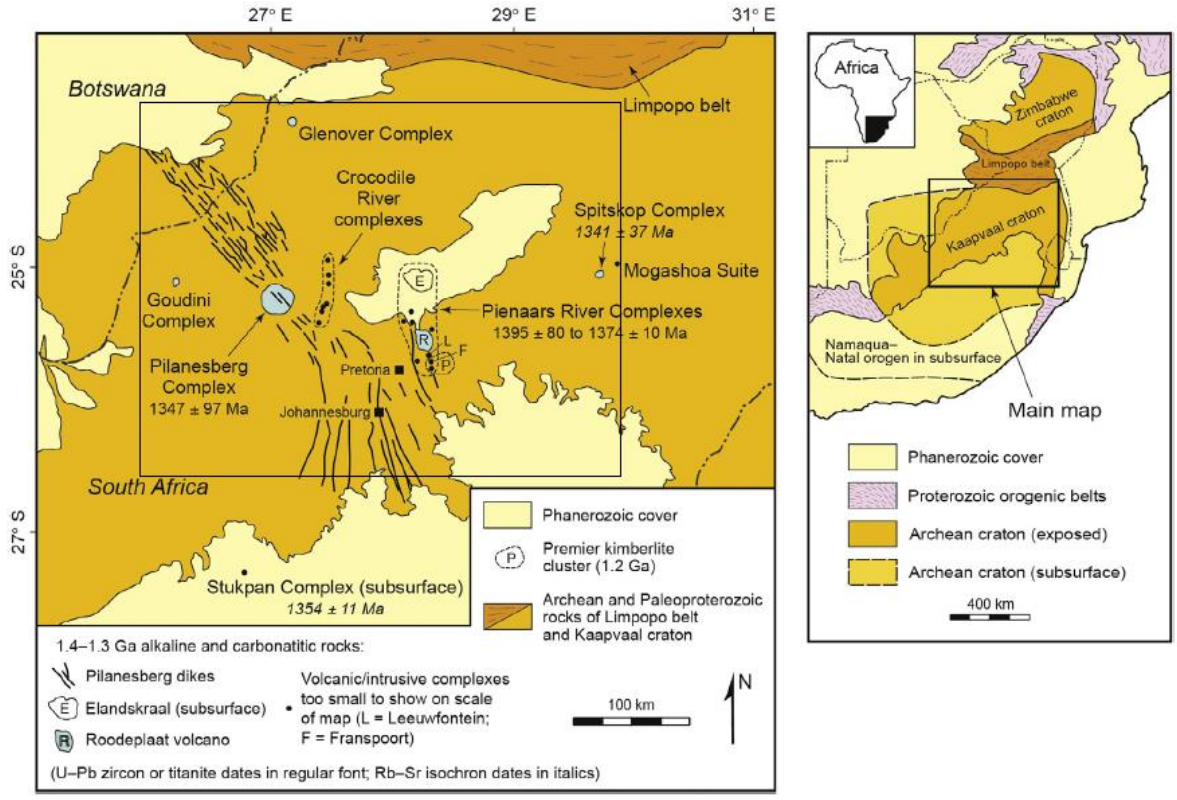

Figure 1. 2: Map showing the distribution of the carbonatite-alkaline complexes of the Pilanesberg alkaline province on the Kaapvaal Craton. The inset map on the right shows the Archean Kaapvaal and Zimbabwe cratons together with the Limpopo Belt (Gose et al., 2013).

1.3 Carbonatites and REE Mineralization

Carbonatites are igneous rocks containing more than 50% modal carbonate minerals (Le Maitre, 2002). The general classification of carbonatites is made either on the basis of major element geochemistry or on the basis of dominant carbonate mineral (Fig. 1.3) (Table 2).

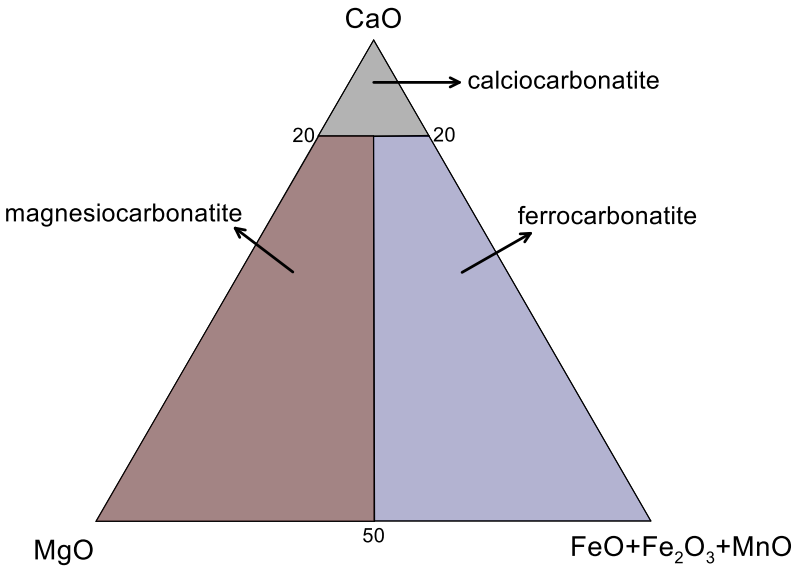

Figure 1. 3: Chemical classification of carbonatites, edited from Le Maitre (2002). Weight percent of oxides are used for this classification.

These enigmatic rocks are usually found together with alkalic silicate igneous rocks, either in individual complexes or in a regional association within magmatic provinces. Associated silicates are generally alkaline ultramafic rocks, typically pyroxenites and ijolites, but may also include more evolved types such as phonolites and nepheline syenites. An ijolite is a coarse-grained alkaline igneous rock containing essential clinopyroxene and nepheline (Le Maitre, 2002).

Table 2: Carbonatite classification by chemical characteristics, extended from Jones et al. (2013), calcite-dolomite carbonatite is added. FeO^T is total iron, RE_2O_3 is total REE oxides.

Class	**Chemical Characteristic**
Calcite carbonatite	$CaO/(CaO + FeO + MgO) > 0.80$
Calcite-dolomite carbonatite*	$CaO/(CaO + FeO + MgO) < 0.80$ & (Ca, Mg)-rich
Dolomite carbonatite	(Ca, Mg)-rich
Ferrocarbonatite	$(FeO^T + MnO) > MgO$
Magnesiocarbonatite	$MgO > (FeO + MnO)$
Rare earth carbonatite	$RE_2O_3 > 1$ wt. %
Natrocarbonatite	$(Na_2O + K_2O) > (CaO + MgO + FeO)$

Carbonatites occur mostly within stable, intraplate environments, and can be found both in continental and, sometimes, in oceanic crust (Le Bas, 1987; Jones et al., 2013) (Fig. 1.4). They usually intrude in a continental rift environment, such as in the East African Rift Valley System (Mitchell and Garson, 1981; Bell and Tilton, 2001). Many carbonatitic complexes have a large

diversity of different carbonatites (Le Bas, 1987). There are at least 527 carbonatite occurences worldwide and more than 60 % of them are located in Africa and Asia (Woolley and Kjarsgaard, 2008) (Fig. 1.5).

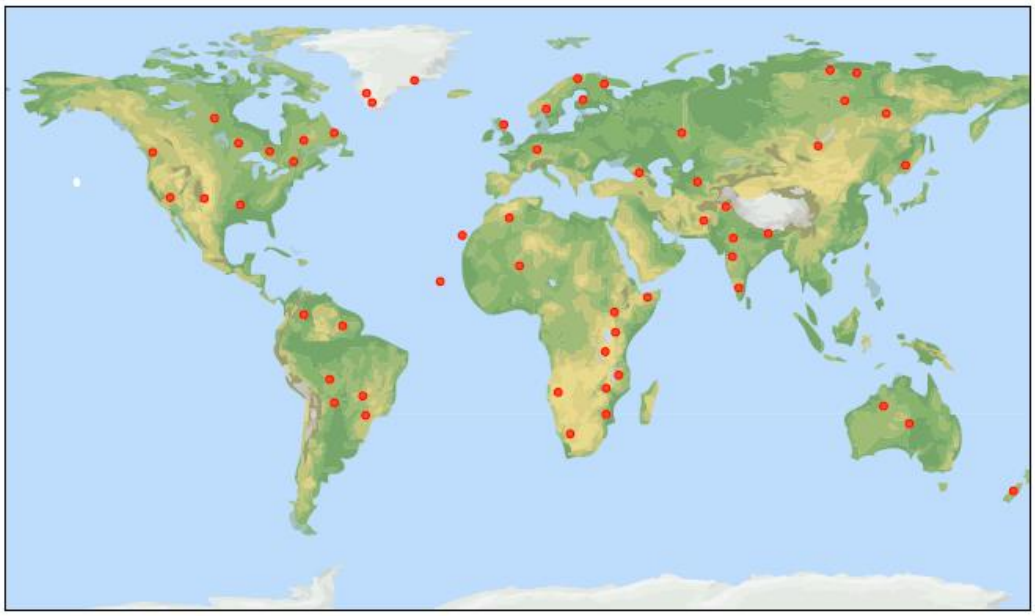

Figure 1. 4: Distribution of carbonatites worldwide from Jones et al. (2013).

There is still scientific debate as to the formation of carbonatites, but theories exist to understand the origin of carbonatites as well as carbonatite magmas, and these can be summarized into three main theories:

- formation of melts from partial melting of carbonated peridotite mantle (Harmer and Gittins, 1998; Ying et al. 2004; Brey et al., 2009)
- extensive silicate magma fractionation from carbonate-bearing liquid (Lee and Wyllie, 1994)
- liquid immiscibility models (Mitchell, 2009; Guzmics et al., 2011).

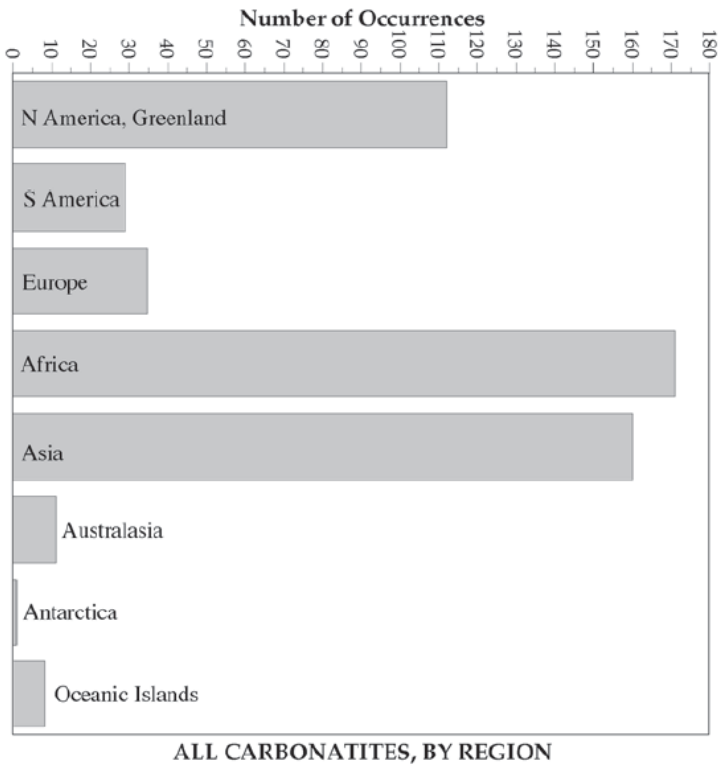

Figure 1. 5: Distribution of carbonatites by geographic regions, from Woolley and Kjarsgaard (2008).

Carbonatites are the most REE-enriched type of igneous rocks and as a consequence many carbonatites generate economic REE deposits (Hornig-Kjarsgaard, 1998; Rankin, 2003). They also host some key elements of economic interests, such as niobium, phosphorus, fluorite, barium and uranium (Jones et al., 2013) (Table 3). Carbonatite fluids play a significant role in mineralization in REE deposits. The formation and evolution of carbonatite- and ore-forming fluids has become a key topic of current geological research. A classification of REE deposits related to carbonatites has been proposed by Mariano (1989):

- Primary: REE enrichment by magmatic processes (eg. Mountain Pass, USA).
- Hydrothermal: REE in most carbonatites concentrated into late hydrothermal fluids. The temperatures may vary from a few hundred degrees celsius to almost ambient conditions (eg. Lofdal, Namibia).
- Supergene/Epigenetic: REE enrichment achieved through alteration processes. When carbonatites are subjected to chemical weathering, the carbonate minerals are easily dissolved, Ca and Mg can be selectively removed from the system, leaving behind the less mobile elements (eg. Mount Weld, Australia; Zandkopfsdrift, South Africa).

Table 3: Some of the important carbonatite deposits and their reserves and grades, from Jones et al. (2013).

Deposit	Reserve and Grade	Comments
Oka carbonatite, Quebec	112,7 Mt at 0.44 % Nb_2O_5 23.8 Mt at 0,2-0,5 % REO	Hydrothermal REE mineralization
Phalaborwa, South Africa	600 Mt at 7 % P_2O_5 286 Mt at 0,69 % Cu 2,16 Mt REO	Banded carbonatite contains Cu sulphides, magnetite and baddeleyite
Bayan Obo, Inner Mongolia	37 Mt at 6 % REO 1 Mt at 0,1 % Nb	Largest mined REE deposit
Amba Dongar, India	11,6 Mt at 30 % CaF_2	Ore associated with fenite units between carbonatite-country rocks
Panda Hill, Tanzania	113 Mt at 0,3 % Nb_2O_5	Disseminated pyrochlore, apatite, magnetite in carbonatite plug

REE deposits associated with carbonatites usually result from a combination of two or more enrichment processes. It is sometimes difficult to distinguish igneous carbonatites from sedimentary carbonates, therefore the amount of REE's and isotopic studies can be used to distinguish between the two. The REE content in sedimentary carbonates is approximately 200 ppm., whereas in carbonatites the range is from 500 to > 10,000 ppm. (Loubet et al., 1972; Eby, 1975; Moller et al., 1980). In addition isotopic determination such as $^{87}Sr/^{86}Sr$, $^{143}Nd/^{144}Nd$, $^{206}Pb/^{204}Pb$, $^{207}Pb/^{204}Pb$ and $^{208}Pb/^{204}Pb$ can also provide evidence for the carbonatite source (Kalt et al., 1997; Bell and Tilton, 2001), and Holmes (1958) produced the first geochemical evidence for the magmatic origin of the Spitskop carbonatite.

Fenitization or alkali metasomatism is one of the most common metasomatic processes, in which Na and K are transferred from fluid to the country rocks (Le Bas, 2008).

1.4 Fluids as a Metasomatism Tool

Fenitization is a result of fluids emanating from carbonatites or alkaline magmatism that caused alteration of the surrounding rocks (Le Bas, 2008). It is the most common metasomatic processes, in which Na and K are transferred from fluid to the country rocks, and the rocks

which are affected and altered by these Na-K-rich fluids are composed mainly of K-feldspar, albite and alkali pyroxenes/hornblendes and are called fenites (Zharikov et. al, 2007). The scale of the fenitization depends on the distance of the fluid system and varies from meters up to 2-3 kilometers from the fluid source.

Fluids that cause fenitization can form REE enrichments during fenitization process (Elliott et al., 2016). The mineral assemblages caused from the fluids depends on the country rock, therefore there are some varieties between different complexes in terms of minerals (Le Bas, 1987).

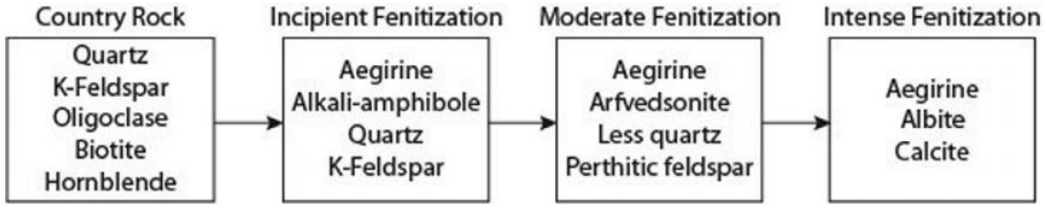

Figure 1. 6: Mineral assemblages of the different stages of metasomatism (Elliott et al., 2018)

There is a general trend that during fenitization alkalis are added and silica is removed from the country rock and other major elements may also be added or removed, which will depend on the mineralogy and the geochemistry of the country rock (Brögger, 1921; Bardina and Popov, 1994).

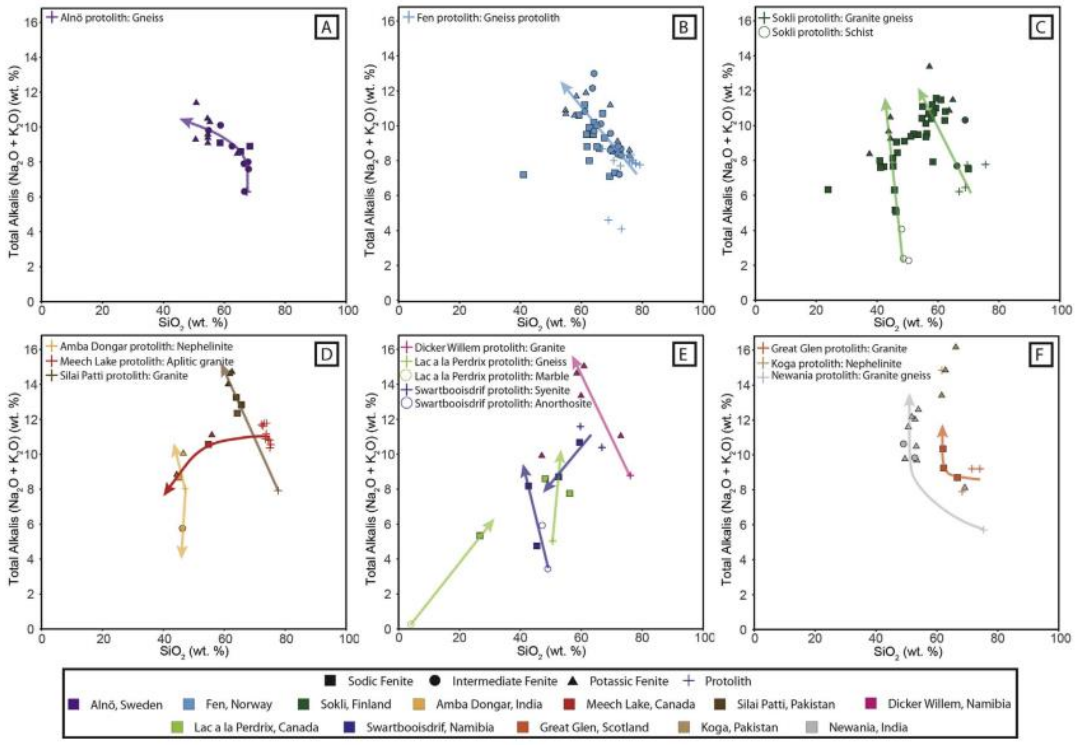

Figure 1. 7: Total alkalis vs silica of fenites and their protoliths around the world (Elliott et al., 2018).

1.5 Introduction to the Spitskop Complex

The Spitskop Complex is located 190 km north-east of Pretoria and 48 km east of Groblersdal (Fig. 1.6). It intruded into the Bushveld Complex at 1341 ± 37 Ma (Harmer, 1992) and is circular in shape, 8 km in diameter and covers an area of 50 km^2. The Spitskopspruit (Tshweneng River) flows through the complex from west to east.



Figure 1. 8: Google earth image showing the location of the Spitskop Complex, Groblersdal, Johannesburg and Pretoria.

The complex was discovered by Hall (1910) and a brief description of the rocks was made. Shand (1921) conceived that the region was a single intrusion of nepheline syenite with urtite and ijolite, in the centre of which, the carbonate rocks were a limestone mass derived from the Transvaal Supergroup dolomites. Further investigations and detailed mapping by Strauss and Truter (1950) led them to suggest that the limestones were not sedimentary, rather they were igneous rocks called carbonatite. Verwoerd (1967) mapped the region in more detail and Harmer (1992) undertook geochemical, petrogenetic and isotopic studies of the Spitskop Complex.

The major components of the Spitskop Complex are alkaline silicate rocks such as ijolite and nepheline syenite, and carbonatites, which are divided into calcite carbonatite, calcite-dolomite carbonatite and iron-bearing dolomite carbonatite with an apatite-rich zone (Fig. 1.7). These alkaline units are cut by the plug of carbonatite, which is the youngest component of the complex.

The Spitskop carbonatite is one of the best studied carbonatites in South Africa (Strauss and Truter, 1950; Verwoerd, 1967; Harmer, 1992, 1999) and consists mainly of calcite, dolomite and apatite with minor magnetite. The carbonatite is composite and comprises an incomplete outer zone of coarse calcite carbonatite, commonly 5-10 mm in grain size (in some outcrops up to 50 mm), which is found only in the eastern and southern part of the Spitskop complex. Dolomite carbonatite, which has a granular grain size of < 0,5 mm, occurs in the centre and is the major component of the Spitskop carbonatite complex. The calcite-dolomite carbonatite forms an intermediate transition zone and is found in northeastern, southeastern and western part of the complex (Fig 1.8).

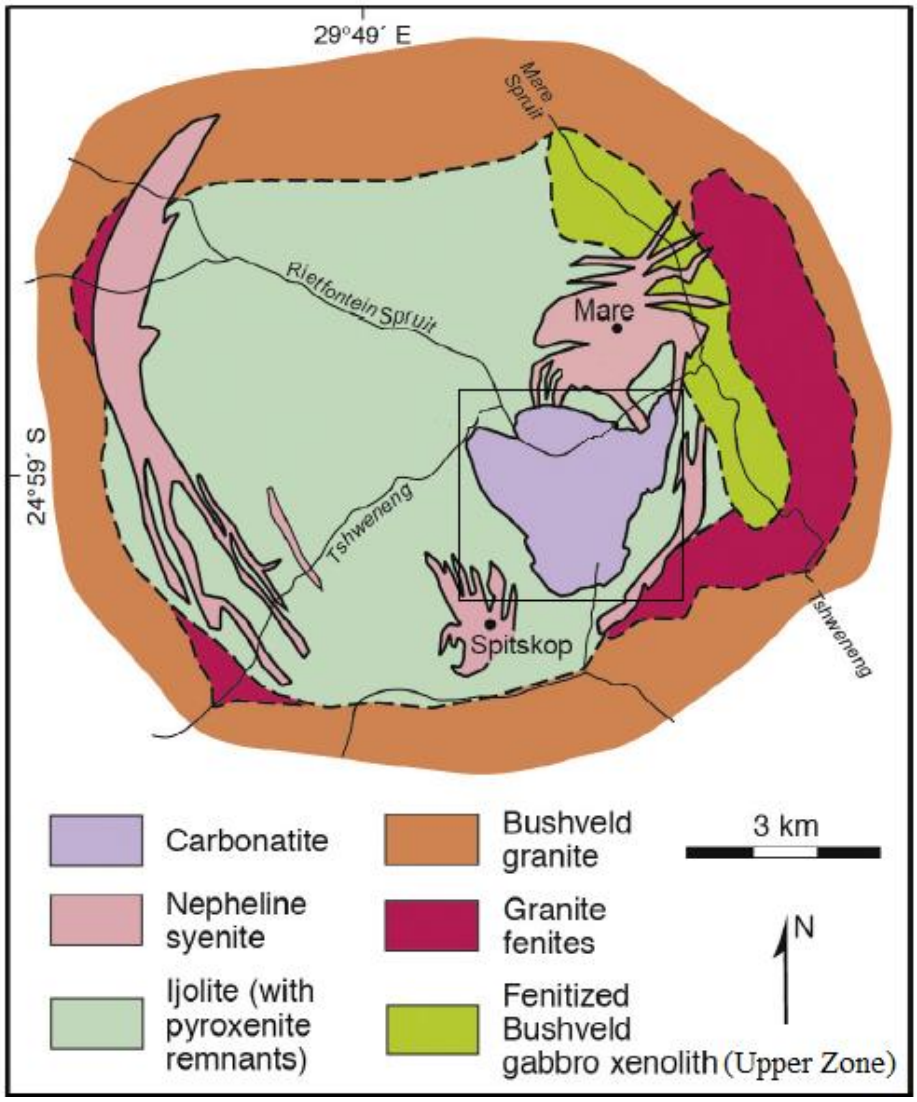

Figure 1. 9: Geological map of the Spitskop Complex displaying carbonatite, nepheline syenite, ijolite and fenitized rocks surrounded by Bushveld granite (Gose et al., 2013). The box shows the outline of Figure 1.8.

Nepheline syenites are the second youngest member of the complex and the main minerals are perthite, nepheline and clinopyroxene. Both carbonatite and nepheline syenite exposures are excellent. It is the closest unit to the carbonatite plug and the best fresh outcrops are seen generally at Mare- and Spitskop Hill.

Nepheline syenite was called “foyaite” by Strauss and Truter (1950). It has a wide range of textures, from a very fine-grained to coarser-grained, and massive to porphyritic types. The different types of nepheline syenite were created from more than one pulse of magma (Harmer, 1999). Nepheline syenites weather less readily than the other rocks in the field and produce higher topographical features.

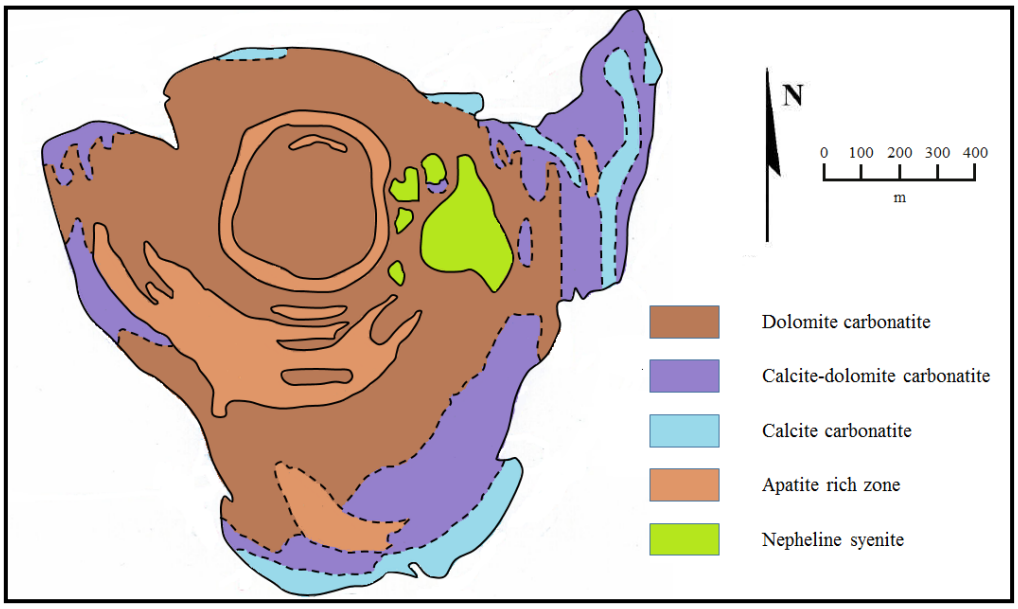

Figure 1. 10: Geological map of the Spitskop carbonatite, modified after Verwoerd (1967).

Ijolites are the oldest alkaline rock in the region. In some outcrops it is found together with pyroxenite. The outcrops are usually very heterogeneous (Harmer, 1992) and the outcrop of ijolite is poor, good outcrops are only found along a small part of stream sections. It consists primarily of nepheline and clinopyroxene and it is very difficult to separate magmatic ijolites from metasomatic ijolites in the field. Pyroxenites are very poorly exposed and their genesis is not well understood, because they are never found in older country rocks and there are no pyroxenite dykes and/or veins (Harmer, 1999). Additionally there is no pyroxenite outcrop along the Tshweneng River, which is the most important study area in the Spitskop Complex. The boundary between carbonatite and ijolite are not seen but it is possible to estimate the location of the contacts within 5-10 m.

Strauss and Truter (1950) distinguished three textural types of ijolite:

Type 1: coarse-grained, red ijolite

Type 2: fine-grained, black ijolite

Type 3: very fine-grained, very dark ijolite (melteigite).

Strauss and Truter (1950) described ijolites type 1 and 2 as being intrusive into pyroxenite. The pyroxenite–ijolite assemblage forms a plug-like framework, which intruded nepheline syenite.

The Spitskop Complex, which was emplaced into the Bushveld Complex, is surrounded by the Rustenburg Layered Suite and the Lebowa Granite Suite. The Rustenburg Layered Suite of southern Africa, consists of mafic and ultramafic rocks in the world's largest layered intrusion and intruded at 2055.91 ± 0.26 Ma (Zeh et al., 2015). It is divided into five main zones: Marginal Zone, Lower Zone, Critical Zone, Main Zone and Upper Zone. The Upper Zone forms one part of the country rocks of the Spitskop Complex. Gabbro, ferrogabbro, gabbronorite and anorthosite are the main rocks and the magnetitite layers are the most important part of this zone because of the enrichment in vanadium.

The Lebowa Granite Suite is divided into seven different types: Nebo Granite, Lease granite, Bobbejaankop Granite, Verena Granite, Balmoral Granite, Klipkloof Granite and Makutso Granite (SACS, 1980). The Nebo Granite, which intruded at 2054 ± 3 Ma (Kinnaird, 2005) constitutes 20% of the volume of the Bushveld Complex (Wilson et al., 2000), and is the dominant type of granite and generates a considerable amount of the felsic portion of the Bushveld Complex (Wilson et al., 2000). The emplacement of the Nebo Granite happened shortly after the emplacement that of the Rustenburg Layered Suite and formed a sheet-like body (Wilson et al., 2000). It is a coarse-grained equigranular felsic rock composed of quartz, plagioclase, perthite and hornblende with accessory biotite (Kleeman and Twist, 1989). It is generally grey and pink in colour and is intruded by the Spitskop alkaline rocks. Fluids from the emplacement of carbonatite and/or alkaline silicates have widely metasomatized the country rocks, reacted with them and changed their mineralogy, which is termed a fenitization process and the resulting rocks are called fenites. Mafic fenites have formed from alteration of the Upper Zone rocks by water-rich fluids emanating from the intrusion of carbonatites and/or alkaline rocks, while granitic fenites formed from fluid interaction with the Nebo Granite. Strauss and Truter (1950) discovered the fenitization of the Bushveld Nebo granite and granophyre of the region and separated these fenitized rocks into two main groups, the red fenites and the white fenites. Red fenites represent the fenitized granite that does not contain quartz and the term 'red fenites' comes from the red coloured feldspar, which is the dominant mineral of this rock. In

white fenites the colour of feldspar changes from red to white, there is an increase in mafic minerals, and again quartz has disappeared. However, this did not include fenitized mafic Bushveld rocks from the Upper Zone of the RLS. It is very hard to distinguish these fenitic rocks from the original rocks in the field, because most of the fenites show significant changes only in their mineral structures and their geochemistry. Therefore fenites of the Spitskop Complex look the same as the original unmetasomatized Bushveld country rocks.

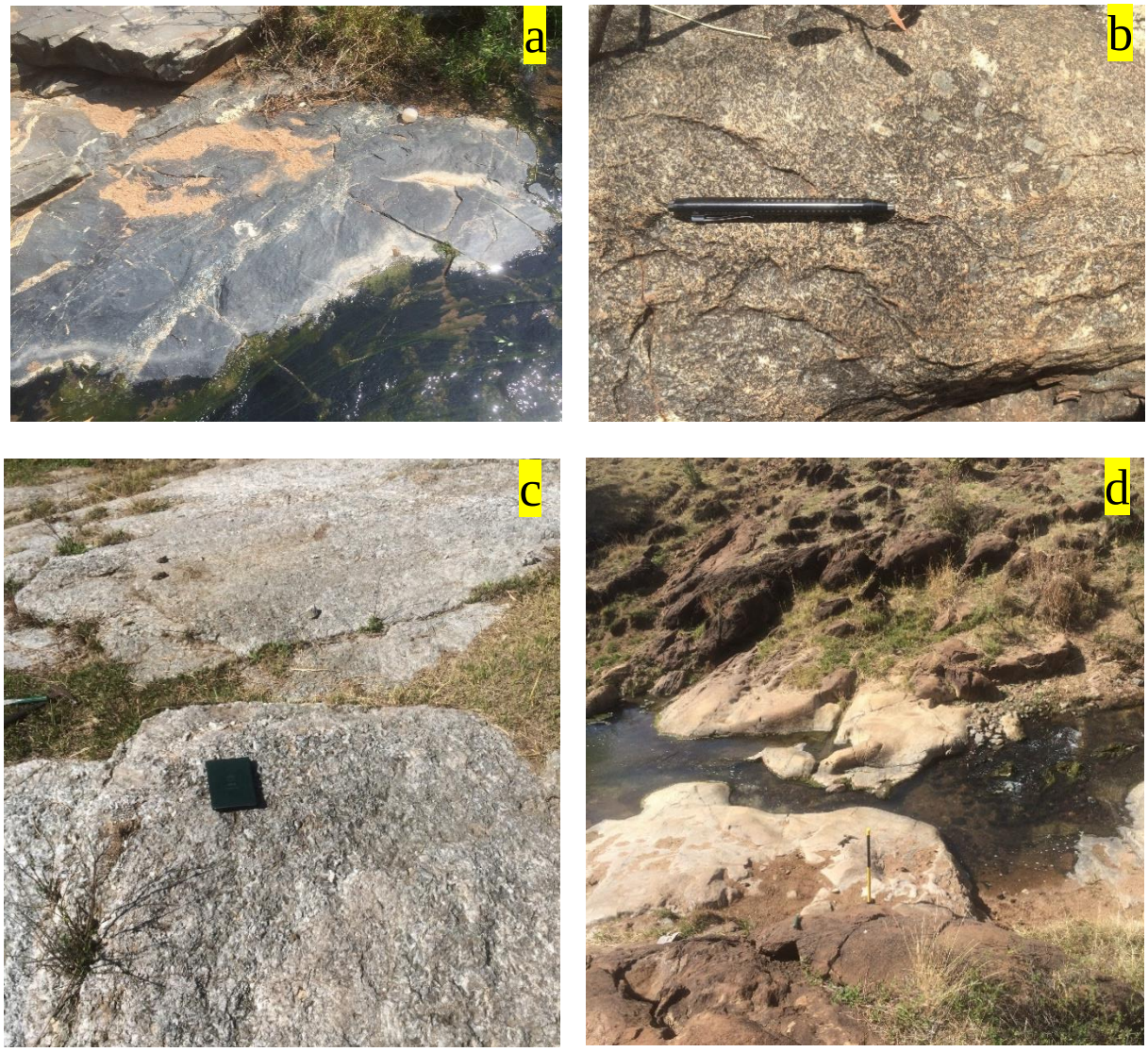

Figure 1. 11: Typical field photographs of the Spitskop alkaline rocks (a) ijolite, (b) nepheline syenite, (c) calcite carbonatite, (d) dolomite carbonatite.

Carbonatites and associated alkaline rocks are typically heterogeneous igneous rocks, and their evolution as well as their fluid chemistry are not well understood. Spitskop presents a perfect opportunity to study the petrogenetic as well as fluid relationship between carbonatite and mafic and felsic silicate magmatism and the associated fenites.

1.6 Methodology

Previous work (Strauss and Truter, 1950; Verwoerd, 1967; Harmer, 1992; Harmer, 1999) on the Spitskop Complex has focused on the distribution of the various lithologies, the mineralogy and the geochemistry. Little attention has been given to the carbonatite-related fluids, their affect on the surrounding rocks and the role in phosphate and rare earth element mineralization.

Fluid-rock interactions are of great importance for understanding the evolution of carbonatites and related REE mineralization. To investigate the effects of fluids, the stream section of the Spitskop Complex, which is the most important place to understand the fluid-rock interactions, was mapped in detail and a large number of samples were collected from different lithologies. These samples include ijolites, carbonatites, fenitized Bushveld granites and fenitized Bushveld Upper Zone rocks. In the stream section, vein-rock relationships at different scales can be seen and each relationship helps in the understanding of the evolution of the complex. With the whole rock geochemistry data, the chemical composition of the fenitized Bushveld rocks can be compared with the original, unmetasomatized Bushveld rocks. These will help to constrain the metasomatism and element movement as a result of the fluid-rock interaction.

Samples were cut and prepared for polished thin sections as well as for the whole rock geochemistry by the candidate of this thesis. After preparing the samples for thin section and whole rock geochemistry, they were given to Wits thin section and geochemistry lab. Thin section petrology has been used to identify and determine the characteristic features and distribution of minerals. A total of 125 polished thin sections have been made and were studied using transmitted and reflected light microscopy. In addition, XRF and ICP-MS data of rocks have been obtained and the distribution of major-, trace- and rare earth elements of different lithologies were studied.

One of the important steps to understand the fluid-rock interaction is to look at the mineral chemistry of rocks by scanning electron microscopy (SEM). With the SEM the first priority is to confirm the identification of minerals based on the thin section petrology. Secondly, unknown minerals, which could not be identified with transmitted and reflected light microscopy, were identified. Semi-quantitative microanalysis carried out on a FEI Quanta 200 scanning electron microscope (SEM) with SE and BSE detectors at University of the Witwatersrand. Microanalyses were done using an Oxford INCA Exact EDS analyzer attached to the SEM. Operating conditions set at 30 kV.

Some of the microanalyses were carried out on a FEI Quanta 450 scanning electron microscope (SEM) with SE and BSE detectors in Turkey. Microanalyses were done using an Oxford INCA EDS analyzer attached to the SEM. Operating conditions set at 30 kV.

1.7 Objectives

The objective of this study is to characterize the fenites and associated rocks in the Spitskop are to provide an insight into the nature and effect of fenitizinf fluids and their control on distribution of rare earth elements. In addition, this study will try to understand the relationships of carbonatites with the associated alkaline rocks.

In this introductory chapter, a review of previous work and unresolved problems has been presented.

Chapter 2.

Field Relationships

2.1 Introduction

The field relationships between magmatic rocks at the Spitskop Complex has been well established by previous workers (Strauss and Truter, 1950; Harmer, 1992, 1999) and important details are described in Chapter 1. But the relationships of the fenitized rocks to the other magmatic rocks have not been looked at in detail. Spitskop Hill, Mare Hill and the Tshweneng River are the best areas to investigate these relationships (Fig. 2.1), because the outcrops are well exposed in these hills and around the river.

Strauss and Truter (1950) clarified that mafic rocks at Spitskop are different than the mafic rocks of the Upper Zone of the Rustenburg Layered Suite of the Bushveld Complex, however the terminalogy they used was complex and there were no information of mafic fenites. After that Verwoerd (1964) and Harmer (1992) identified the existence of mafic fenites and did some preliminary works on these rocks, and they described some of the characteristic features of the mafic fenites.

Rock-vein relationships, boundaries of the fenitized rocks and the range of the metasomatic fluids are crucial for understanding the fluid-rock interaction and element mobility. Therefore extensive fieldwork near- and around the Tshweneng River as well as at the Mare- and Spitskop Hill was undertaken to locate the fenites and other magmatic rocks and examine the relationships between them (Fig. 2.2). More than 150 hand samples were collected to understand the mineralogy of these rocks and the effects of metasomatism.

This chapter provides extensive field observations of mafic- and granite fenites as well as carbonatites and alkaline rocks of the Spitskop Complex.

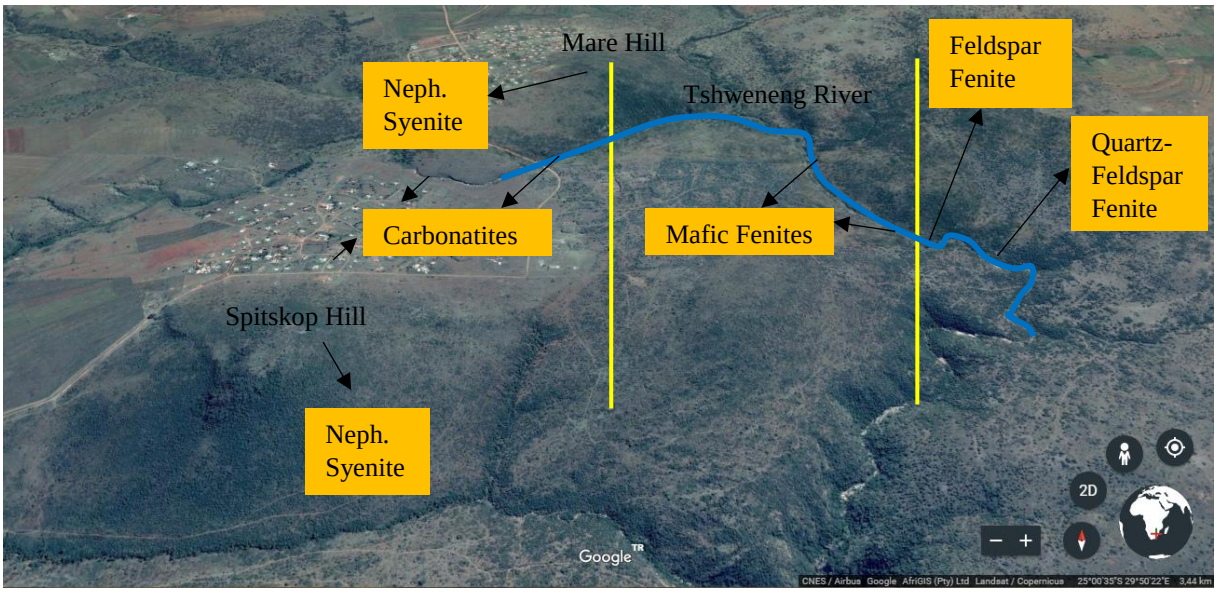

Figure 2. 1: 3-D Google Earth image showing the location of the stream section travers (blue) along the Tshweneng River, Spitskop Hill, Mare Hill and the location of nepheline syenites, carbonatites, mafic fenites and granite fenites (feldspar fenite and quartz-feldspar fenite).

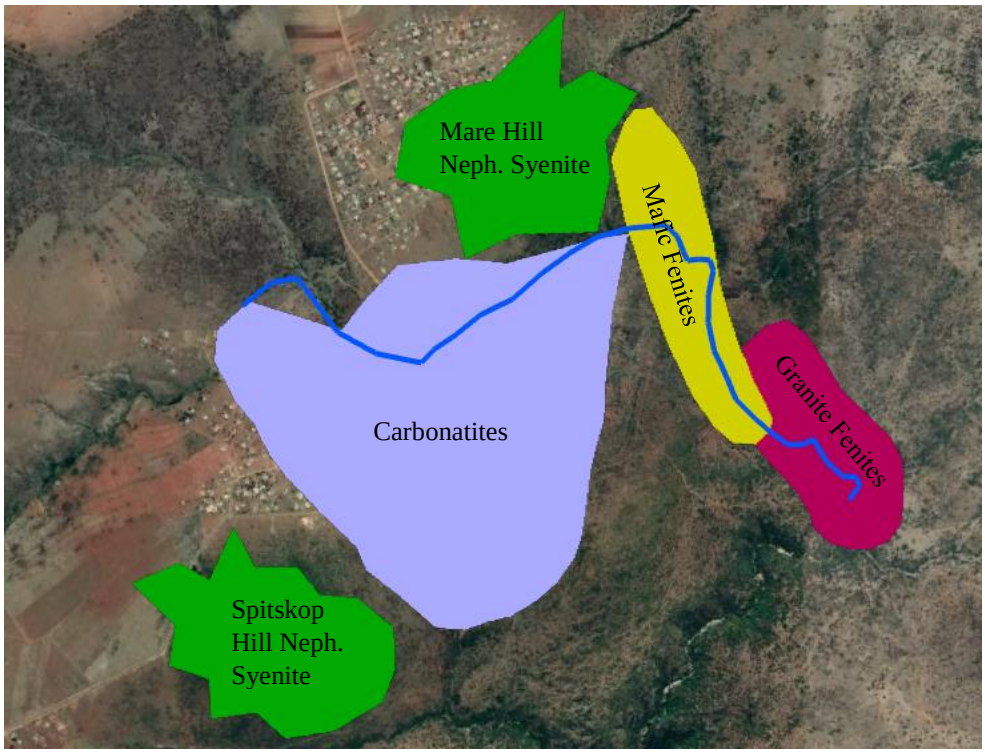

Figure 2. 2: Google Earth image showing location of carbonatites, nepheline syenites, mafic fenites and granite fenites.

2.2 Carbonatites

The carbonatite is heart-shaped in plan, measures 1.6 km across, and it is one of the best known carbonatites in the region, as well as in South Africa (Verwoerd, 1967). It is located between Spitskop- and Mare Hill. Although the surface outcrop covers an area of 2 km^2, the size of the

carbonatite must be much greater at depth, as carbonatite outcrops are also seen to the northeast of the Tshweneng River, which is 1 to 2 km away from the main carbonatite outcrops. Therefore the size of the carbonatite is at least 4 km^2. The topography between the hills is very flat, so the outcrops are poor. Although there is enough outcrop to make useful observations as well as to obtain hand specimens.

The carbonatite at Spitskop is heterogeneous and is divided into three different zones: calcite carbonatite, calcite-dolomite carbonatite and dolomite carbonatite. Calcite carbonatite is the oldest carbonatite unit of the complex and is generally seen at the margin of the intrusion. It is coarse-grained and comprises of holocrystalline euhedral calcite minerals with magnetite and apatite as accessory minerals. Calcite crystals are generally 10 mm in size (Fig. 2.3a), but in some outcrops 30-50 mm crystals are easily observable near the Tshweneng River. The outcrops are whitish grey in colour. Contact boundaries are not clear due to the fact that the outcrop colours of calcite carbonatite and calcite-dolomite carbonatite are very similar.

Calcite-dolomite carbonatite forms the intermediate transition zone between calcite carbonatite and dolomite carbonatite. It is mostly medium-grained and is composed of euhedral-subhedral calcite and dolomite. The outcrops are whitish-blue in colour and are generally seen in the eastern part of the carbonatite plug. The boundary between calcite-dolomite carbonatite and dolomite carbonatite is traceable in some outcrops (Fig. 2.3b). There is no observable calcite-dolomite carbonatite outcrop near the Tshweneng River.

Dolomite carbonatite is the youngest carbonatite unit of the complex. It formed during magnesium alteration of calcite crystals and covers most of the central part of the intrusion. The outcrops are fine- to medium-grained, brown in colour and comprise essentially dolomite with minor apatite and magnetite. Magnetites, which are 3-10 mm in size, are mostly found on the surface of the outcrop (Fig. 2.3c). In the northern part of Tshweneng River, magnetite crystals increase in size to 30-50 mm. Apatite-rich zones, which are mostly found together with dolomite carbonatite, are clearly observed in the field between Mare- and Spitskop Hill (Fig. 2.3d).

It is very hard to locate the contact between carbonatite and other alkaline rocks due to the topography, but estimation of the boundaries can be made in the field. There are no veins observed in the carbonatites.


a


b


c


d

Figure 2. 3: Field photographs of carbonatites showing (a) euhedral coarse-grained white calcite carbonatite near the Tshweneng River with calcite grains up to 5 cm in size (X-East: 786776, Y-North: 7234740, Z-Elevation: 1345) (b) the boundary between medium-grained whitish calcite-dolomite carbonatite (left) and fine-grained brown dolomite carbonatite (right) near Spitskop Hill, note the sharp colour change. The dolomite carbonatite is younger than the calcite-dolomite carbonatite (X-East: 786342, Y-North: 7233540, Z-Elevation: 1395) (c) brown-coloured fine-grained magnetite-bearing dolomite carbonatite, from an outcrop located northeastern of Tshweneng River between Mare- and Spitskop Hill (X-East: 786322, Y-North: 7234469, Z-Elevation: 1354) (d) yellowish-brown fine-grained apatite in dolomite carbonatite near Spitskop Hill, note that apatite is mostly found with dolomite carbonatite (X-East: 786506, Y-North: 7233596, Z-Elevation: 1391).

2.3 Nepheline Syenites

Nepheline syenites in the Spitskop Complex are essentially comprised of alkali feldspar, mainly perthite, nepheline and clinopyroxene. The term ‘‘foyaite’’ is used by Strauss and Truter (1950) to name this rock, while Harmer (1999) called this unit a nepheline syenite due to the fact that syenites at Spitskop are rich in nepheline. The outcrops are brown in colour and are entirely holocrystalline.

Nepheline syenite is the closest unit to the carbonatite intrusion and partly surrounds it from north and south (Fig. 2.2). The best outcrops of nepheline syenites are seen especially at Spitskop- and Mare Hill, therefore all the nepheline syenite samples were obtained from these hills. No nepheline syenite outcrops are observed near the Tshweneng River.

Different textural varieties of nepheline syenites are observed in the outcrops, and three of them are described in detail: a) porphyritic, b) massive, c) pegmatoidal.

a) Porphyritic nepheline syenites: Porphyritic syenites are the most abundant texture for this rock type and it is seen particularly well at Spitskop Hill. In some outcrops tabular alkali feldspars are 3-7 cm in length within a brown groundmass (Fig. 2.4a), but mostly tabular alkali feldspars 1-4 cm in length are present in a fine-medium grained brownish grey groundmass (Fig. 2.4b). Sometimes acicular aegirines 2-3 cm in length are also found in the groundmass but are less common and seen in only a few outcrops (Fig. 2.4c). Some porphyritic outcrops with flow banding textures are also found at the top of the Mare Hill (Fig. 2.4d).

b) Massive nepheline syenites: Massive syenites are less common than those with a porphyritic texture. The minerals are mostly equigranular and medium-grained. The outcrops are extremely fresh and massive textures are generally found at both Spitskop and Mare Hill (Fig. 2.4e)

c) Pegmatoidal nepheline syenites: Pegmatoidal textures are seen at the top of the Spitskop Hill. It is not as common as the porphyritic or massive textures and it is only found at the margins of

syenites. The outcrops are brown in colour, with 10-15 cm of white alkali feldspars and green-black aegirine crystals are specific for this texture (Fig. 2.4f).

Harmer (1992) also found a schistose texture in fine-grained syenite in the western part of the complex, at Rietfontein, but this texture is not common at Spitskop- and Mare Hill.





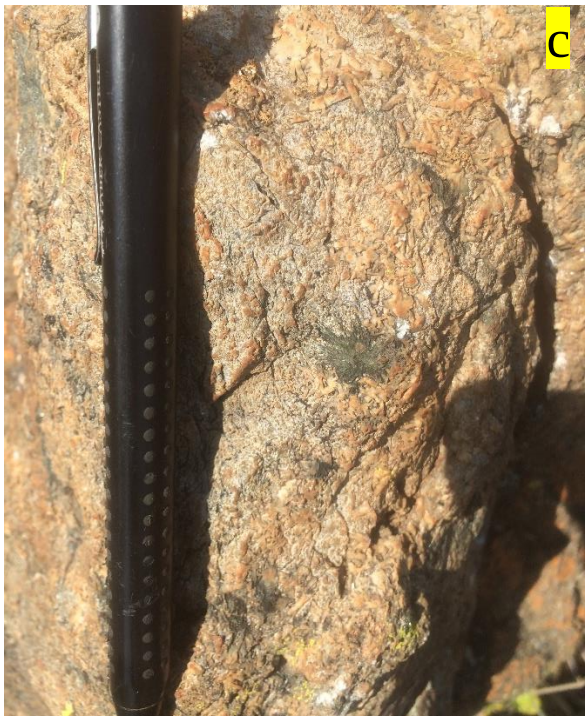





Figure 2. 4: Field photographs of nepheline syenite showing the various textural features (a) intrusion of medium-grained nepheline syenite into alkali feldspar-rich porphyritic nepheline syenite on Spitskop Hill. Alkali feldspars are 2-5 cm in length (X-East: 785595, Y-North: 7233095, Z-Elevation: 1579) (b) porphyritic nepheline syenite with alkali feldspars 1-4 cm in length on Spitskop Hill (X-East: 785595, Y-North: 7233095, Z-Elevation: 1579) (c) acicular green-black coloured aegirine 1-2 cm in length within massive nepheline syenite on Spitskop Hill (X-East: 785592, Y-North: 7233118, Z-Elevation: 1581) (d) medium- to coarse-grained nepheline syenite with flow banding textures at the top of Mare Hill (X-East: 786676, Y-North: 7235210, Z-Elevation:1513) (e) equant square alkali feldspars in typical massive nepheline syenite on Spitskop Hill (X-East: 785683, Y-North: 7233151, Z-Elevation: 1506) (f) tabular-shaped feldspars in pegmatitic nepheline syenite on Spitskop Hill, note that the alkali feldspars can be more than 7-8 cm in length (X-East: 785595, Y-North: 7233095, Z-Elevation: 1579).

2.4 Mafic Fenites

As can be seen on the map (Fig. 2.2), mafic fenites are generally located along the Tshweneng River and they are perhaps the most complicated group of rocks in the Spitskop Complex. They include rocks which were originally gabbros, ferrogabbros, gabbronorites, anorthosites and magnetitites of the Upper Zone of the Rustenburg Layered Suite of the Bushveld Complex. Although there are different rocks in the Upper Zone, mafic fenites look the same at every outcrop, and they also resemble the ijolite of the Spitskop Complex.

The mafic fenites are well exposed along a 4 km length of the river, and are located between the carbonatites in the northwest- and the granite fenites in the southeast of the traverse along the Tshweneng River.

They are mostly blue to dark blue in colour and are medium- to coarse-grained mesocratic to melanocratic rocks composed mainly of nepheline and clinopyroxene, mostly augite-aegirine and/or aegirine (Fig. 2.5a). In some outcrops mafic fenites show a light blue colour (Fig. 2.5b).

The mafic fenites host many different veins with a variety of relationships. Most of the veins are leucocratic, but some melanocratic veins are also seen. Leucocratic veins are perthitic and consist of alkali feldspar 1-5 cm in size (Fig 2.5c), but in some outcrops coarse-grained alkali feldspars are dispersed (Fig. 2.5d). Within or near these veins, the size of the clinopyroxenes increases. These leucocratic veins decrease in number from north to the southeast of the Tshweneng River and disappear at the end of the outcrops of mafic fenites.

Magnetitites of the Upper Zone are the easiest rocks to identify in mafic fenites of the Spitskop Complex, and are located in the middle of the Tshweneng River. The outcrop containing magnetitites is 15 to 20 m in length and 3 m in width (Fig. 2.5e). This area had been termed the main magnetite zone and the massive magnetites are generally 40 to 50 cm thick. There are frequent plagioclase inclusions within the magnetites up to 3 cm in size and they are mostly oriented in a planar texture parallel to the margin of the magnetites (Fig. 2.5f and 2.5g).

In addition to this main magnetite zone, fragments of magnetites are seen within nearly all mafic fenite exposures along the river. These fragments also contain plagioclase inclusions that are generally rounded and 2 to 8 cm in size (Fig. 2.5g).

The north and south contacts of the mafic fenites along the Tshweneng River are observable, carbonatites lie to the north and granite fenites are located in the south.






c


d


e


f



Figure 2. 5: Field photographs of mafic fenites in the Tshweneng River. (a) typical blue to dark blue mafic fenite consisting of nepheline and clinopyroxene with a single perthite vein, note that ijolite also looks like this mafic fenite in the field (X-East: 787597, Y-North: 7234691, Z-Elevation: 1330) (b) light blue mafic fenite with dark green clinopyroxene patches and some alkali feldspars, note that zoned clinopyroxenes near alkali feldspars are coarser than the clinopyroxenes within mafic fenite (X-East: 787716, Y-North: 7234180, Z-Elevation: 1322) (c) typical perthitic vein within mafic fenite; the size of the alkali feldspars are mostly 1-3 cm in size, note that there is a clinopyroxene zone within the vein (X-East: 787603, Y-North: 7234664, Z-Elevation: 1330 (d) alkali feldspar patch within mafic fenite (X-East: 787691, Y-North: 7234216, Z-Elevation: 1323) (e) perthite vein within mafic fenite, note that clinopyroxenes within the vein are coarser than the clinopyroxenes within the mafic fenite (X-East: 787616, Y-North: 7234380, Z-Elevation: 1325) (f) The main magnetite zone in the middle of the Tshweneng River, the light blue-blue rock is mafic fenite and dark parts are the massive magnetites. There is a thick white perthite vein within this magnetite zone (X-East: 787598, Y-North: 7234454, Z-Elevation: 1324) (g) Plagioclase inclusions within magnetite, note that inclusions are oriented parallel to the margin of the magnetite (X-East: 787598, Y-North: 7234454, Z-Elevation: 1324).

2.5 Granite Fenites

Fenitized coarse-grained Nebo granite forms the country rocks that surround the Spitskop Complex (Fig. 1.7). The granite fenites are divided into two different fenites: the first one is a feldspar fenite, which consists mostly of feldspar and is the most fenitized rock, and the second one is a quartz-feldspar fenite, which contains quartz and feldspar together, and is the least fenitized rock. These two types of granite fenites are best preserved in the south eastern part of the Tshweneng River.

Feldspar fenite is located beyond the mafic fenites and covers an area of approximately 90 to 100 m^2. The most fenitized rock is red coloured and (Fig. 2.6a) has a simple mineralogical composition and textural features, composed mainly of alkali feldspar, and contains felsic and mafic veins (Fig. 2.6b). The degree of veining is more than in the quartz-feldspar fenite, but

less than in the mafic fenites. Feldspar fenite has a sharp boundary with the mafic fenites and the contact between them is easily recognizable due to the fact that feldspar fenite has a leucocratic coloration in contrast to the dark mafic fenites.

The quartz-feldspar fenite is located southeast of the feldspar fenite and covers an area of more than 500-600 m^2. It has a similar mineralogy to that of the original Nebo granite, as it is composed mainly of quartz, alkali feldspar and some amphiboles, and there is less vein-rock veining than in the feldspar fenite (Fig. 2.6c). After 250 m in the river section from the quartz-feldspar fenite (X-East: 788168, Y-North: 7233828, Z-Elevation: 1311) to the south of the river, the effect of metasomatism disappears, and the original unmetasomatized Nebo type granites characterize the rest of the river and around the Spitskop Complex. There are no metasomatic veins within the Nebo granite.

One of the most important features of the granite fenites are the gradual colour changes with increasing fenitization: the exposures of feldspar fenite have a distinct red colour whereas the quartz-feldspar fenite has a pink-white colour, and the original Nebo type granite has an orange-red colour (Fig. 2.6d).

The mineralogical changes and the vein-rock relationships of the granite fenites however are simpler than in the mafic fenites. The veins are mostly melanocratic and dominated by clinopyroxene, and there are no leucocratic perthitic veins or magnetite fragments in this part of the river.

To the south of the river, when the outcrops of the white-pink quartz-feldspar fenite begin to disappear, coarse-grained red to orange coloured unmetasomatized Nebo granites are seen everywhere. The change from quartz-feldspar fenite to the Nebo granite is gradual, therefore there is no distinct boundary and there is a transition from fenitized to unaltered over a zone of 200 m in width.



Figure 2. 6: Field photographs of granite fenite in the south-eastern part of the Tshweneng River showing (a) typical coarse-grained feldspar fenite with dark-coloured mafic veins, note that there is a gradual colour change near vein boundaries (X-East: 787974, Y-North: 7233907, Z-Elevation: 1312) (b) feldspar fenite with light- and dark-coloured veins. Note that the feldspar fenite contains more veins than the quartz-feldspar fenite (X-East: 787974, Y-North: 7233907, Z-Elevation: 1312) (c) typical whitish coarse-grained quartz-feldspar fenite with very fine-grained black veins, the mineralogical composition of the vein is not known (X-East: 788168, Y-North: 7233828, Z-Elevation: 1311) (d) the boundary between feldspar fenite (right) and quartz-feldspar fenite (left). Note that there are two different colours of quartz-feldspar fenite, both pink and white (X-East: 788155, Y-North: 7233843, Z-Elevation: 1310).

Carbonatites are the last event of the Spitskop Complex and do not host any veins, either because they were not affected by metasomatic fluids because they are the youngest rocks of the complex and the metasomatism occurred before they intruded, or they may be the source of the metasomatizing fluid, so they do not host any veins or any Na-/K-enriched minerals/zones.

After metasomatism, apart from the magnetitites, it is very difficult to distinguish different Upper Zone lithologies from each other as well as from the magmatic ijolite in the field, because, their fenitized mineralogy resembles that of the ijolite, which also contains nepheline and clinopyroxene in equal amounts. Because Upper Zone rocks of the Bushveld Complex are dominantly plagioclase and pyroxenes, the only way to separate them is to investigate them under the microscope, which will be shown in next chapter.

Perthitic veins are mostly seen in fenitic rocks. Growth of clinopyroxenes near or within the leucocratic perthitic veins in mafic fenites may be the result of metasomatism due to the fact that hot metasomatic fluids can cause an increase the size of the minerals.

Mafic fenites contain more veins than the feldspar fenite and quartz-feldspar fenite, and feldspar fenite contain more veins than the quartz-feldspar fenite. As can be seen in the map (Fig. 2.1), metasomatism decreases from north to south, and the position of the feldspar fenite and quartz-feldspar fenite show this. Therefore there must be a direct relationship between metasomatism and the degree of veining.

Feldspar fenite has a red colour and the reason for that is it consists completely of perthites and quartz has disappeared because of the metasomatic effects. Where the effect of the metasomatic fluids decreases, quartz components are seen in quartz-feldspar fenite, but not as much as in the original Nebo type granites, therefore there is a colour change from red to pink-white.

Field studies show that the metasomatic fluids have occurred over an area of at least 3-4 km^2 and the main metasomatized area is around Tshweneng River. This metasomatized area may be much greater at depth.

A mineralogical and petrological investigation is necessary to distinguish between the different rock types, to look for evidence of fluid-rock interaction in thin section and also to constrain reactions that may have taken place during metasomatism. The next chapter will give detailed descriptions of the mineralogy, petrography, petrology and SEM-EDS of the rocks of the Spitskop Complex.

Chapter 3.

Petrology/Petrography and SEM

3.1 Introduction

In this chapter mineralogy, petrography and petrology of unaltered igneous- and fenitized rocks of the Spitskop Complex are extensively investigated. Optical microscopy was used to identify the different minerals, their textures and their relationships to each other, whereas SEM-EDS was used to confirm the identification of unknown minerals, which could not be identified with transmitted- and reflected light microscopy. Textural relationships between selected minerals were observed and analyzed.

A total of 118 samples were collected of the different lithologies in the field (Fig. 3.1). Thin sections of all of these were made (Table 4) and studied using transmitted- and reflected light microscopy Thin section petrology was used to determine the distribution of calcite and dolomite in a small number of samples as well as some that were studied by SEM-EDS.

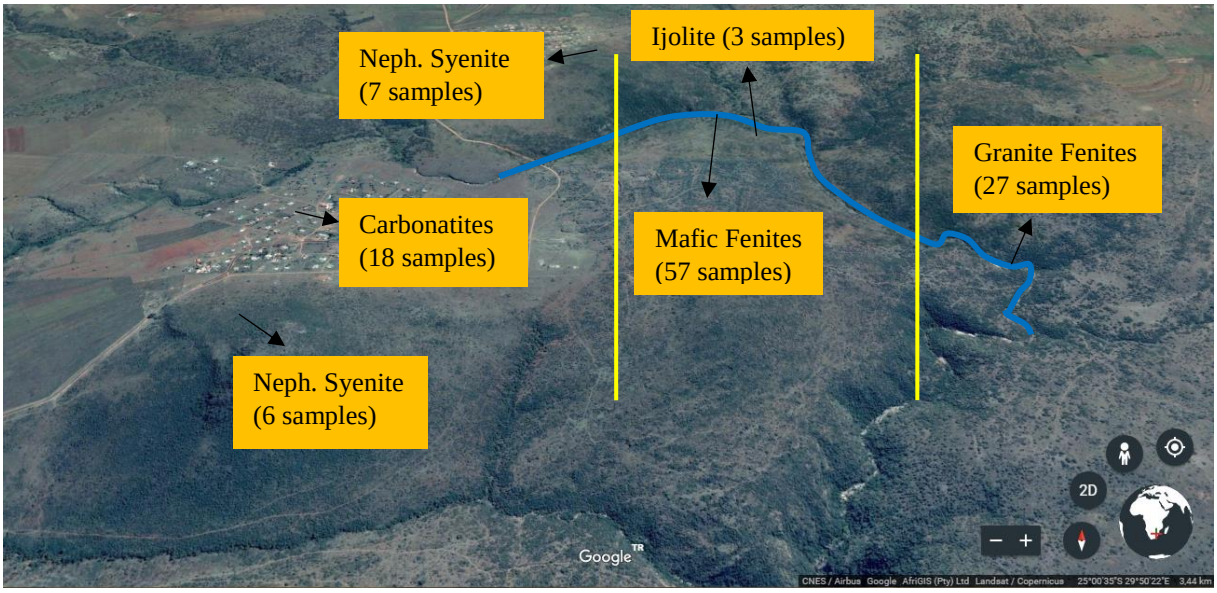

Figure 3. 1: 3-D Google Earth image showing the location of the Spitskop Complex together with the number of samples collected from the different lithologies. The blue line is the Tshweneng River, where ijolite, mafic fenite and granite fenite samples come from.

Table 4: Rock types, number of samples and number of thin sections of the rocks of the Spitskop Complex.

Rock type	Number of samples	Number of thin sections
Calcite carbonatite	7	10
Calcite-dolomite carbonatite	3	5
Dolomite carbonatite	8	11
Nepheline syenite	13	13
Ijolite	3	5
Mafic fenites	57	49
Granite fenites	27	25

3.2 Carbonatites

Before looking at the thin sections of the carbonatites of the Spitskop Complex under a polarized microscope and SEM-EDS, 8 thin sections were stained in the geochemical lab using a carbonate staining method and examined under the microscope. Alizarin red S, potassium ferricyanide and hydrochloric acid were used for the staining procedure. When the staining was completed, calcite minerals turned a red-purple colour, whereas dolomite minerals remained unstained. With this method, calcite was distinguished from dolomite in thin sections. In some samples dolomite forms rims around calcite crystals.

Calcite carbonatite forms the outermost part of the Spitskop carbonatite and consists mainly of calcite, apatite, minor magnetite and accessory dolomite (Fig. 3.2a). Calcite crystals are up to 5-6 cm in size and form up to 75-80 % of the rock. They are coarse-grained and subhedral to euhedral (Fig. 3.2b).

After calcite, apatite is the second most abundant mineral in the calcite carbonatite and forms from 10 to 35-40 % of the rock. Apatite grains are mainly fine-grained, less than 0.2 mm in size, and they are anhedral to subhedral (Fig. 3.2c). Apatites are generally dispersed throughout the carbonatite, however they are mostly found together with magnetite.

Magnetite forms 5 to 10 % of the rock and typically is more abundant when the proportion of apatite increases. Generally, the magnetite is medium to coarse-grained, up to 2 mm in size, with a subhedral to euhedral shape (Fig. 3.2d).

Fine-grained dolomite occurs as an accessory mineral. It has an anhedral shape and is less than 0.4 mm in size. A replacement relationship of dolomite replacing calcite occurs mostly in the calcite-dolomite carbonatite.

Semi-quantitative SEM-EDS results show that the apatite contains approximately 4-5 % fluorine, and should be regarded as fluorapatite. 1-3 % of cobalt was noted by EDS within the magnetites from the carbonatites.

Amphibole, hollandite, ferrihollandite and some REE-bearing minerals were also noted by EDS as accessory minerals in the calcite carbonatite. Amphiboles are commonly found when there is little or no apatite, and mostly occur near or around the REE-bearing minerals. Most of the REE-bearing minerals are clustered together (Fig. 3.2e) and are located at the boundary between calcite and amphibole crystals, and sometimes within amphiboles (Fig. 3.2f). They are medium- to coarse-grained, subhedral in shape and occur only in calcite carbonatite.

Hollandite ($Ba(Mn_6^{4+} Mn_2^{3+})O_{16}$) is generally found within apatites although web-like textures of hollandite are also seen around magnetites. Anhedral ferrihollandites ($Ba(Mn_6^{4+} Fe_2^{3+})O_{16}$) also occur within apatites.

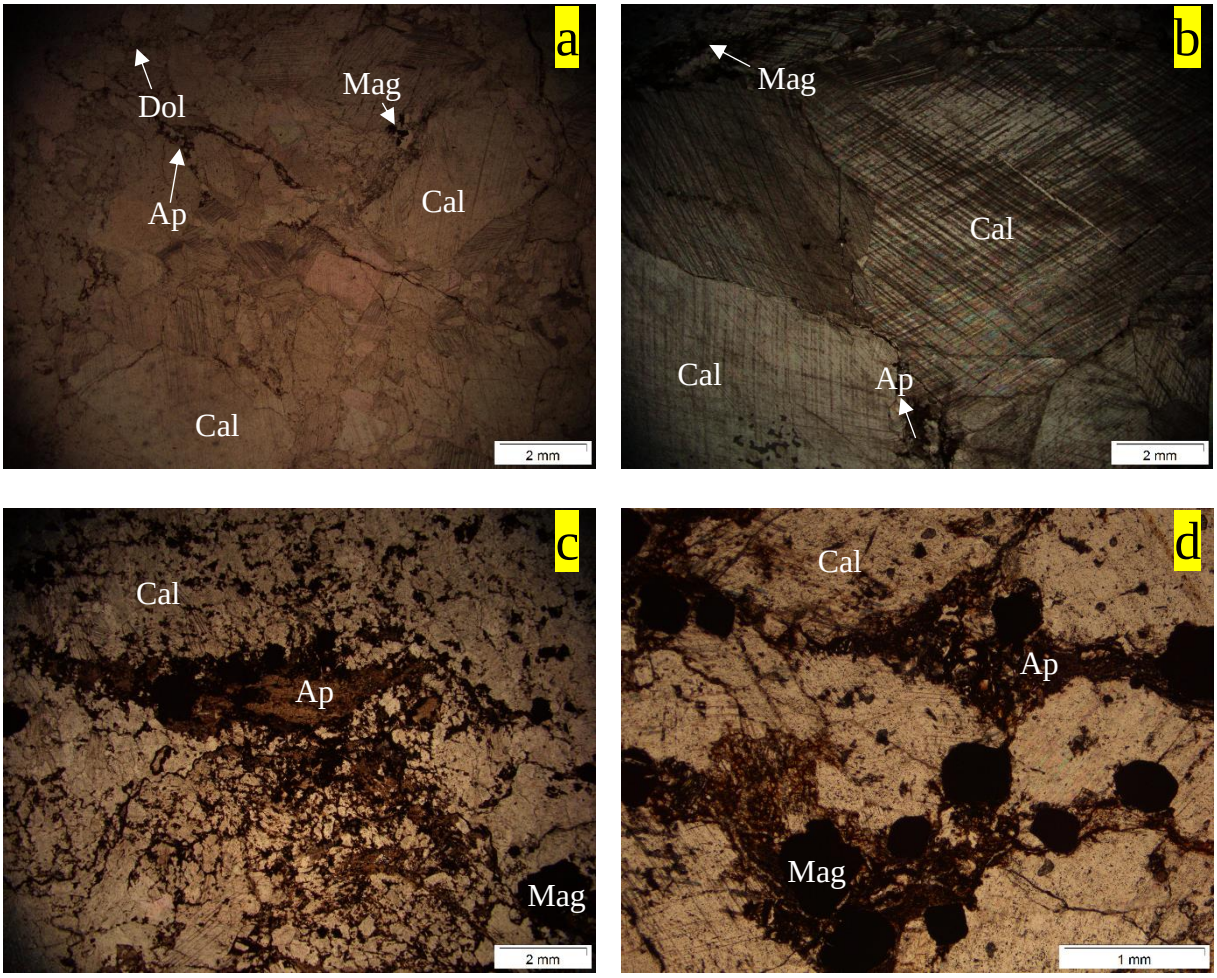

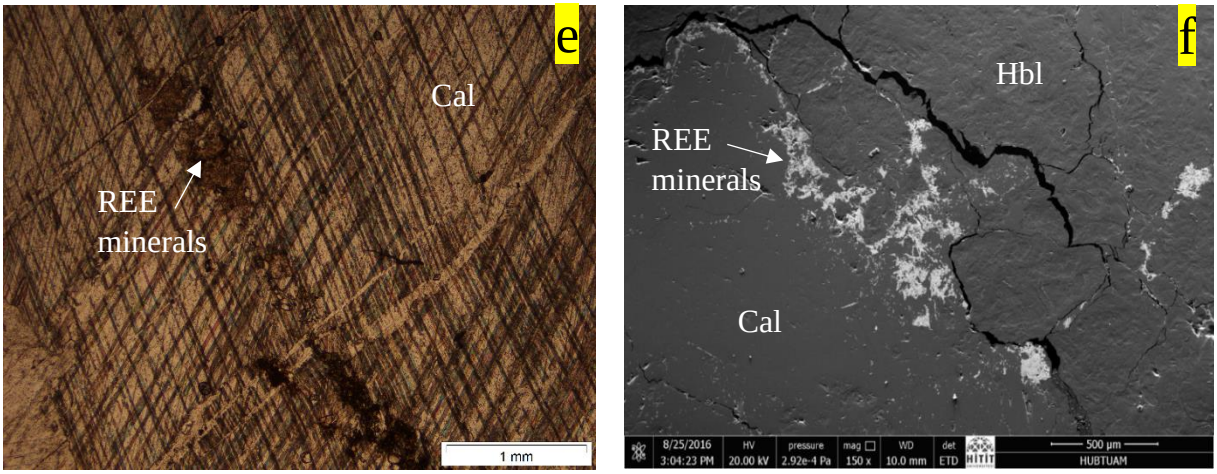

Figure 3. 2: Minerals and textures in calcite carbonatite (a) PPL image showing igneous coarse-grained subhedral to euhedral calcite crystals with fine-grained apatite zones and medium-grained anhedral magnetite grains; accessory fine-grained dolomite is present but rare in this image. Sample 7-85. (b) XPL image showing coarse-grained calcite crystals with good cleavages and fine-grained apatite zones, anhedral to subhedral magnetite grains are present. Sample 6-69B. (c) PPL image showing fine-grained apatite with moderate relief and medium- to coarse-grained subhedral magnetite crystals within the groundmass of medium- to coarse-grained calcite. Sample 8-88-2B. (d) PPL image showing medium- to coarse-grained subhedral magnetite grains and a thin apatite vein 0.1 to 0.5 mm in width within the groundmass of coarse-grained calcite. Sample 8-90. (e) PPL image showing fine-grained pale yellow-pale green REE-bearing mineral within a coarse-grained calcite crystal. Sample 6-69B. (f) fine-grained REE-bearing minerals between the boundary of hornblende and calcite crystals and within the hornblende crystal in BSE. Sample 6-69-1. Abbreviation of minerals are from Krest (1983). Calcite (Cal), apatite (Ap), magnetite (Mag), dolomite (Dol) and hornblende (Hbl).

Calcite-dolomite carbonatite consists mainly of calcite, dolomite, apatite and magnetite. Calcite is the dominant mineral and it forms 45 % to 60 % of the rock. It is medium-grained, 0.5-2 mm in size, and has a subhedral to euhedral shape (Fig. 3.3a). Occasional grains up to 10-15 mm in size have been noted.

Dolomite is the second main mineral and forms 25 to 35 % of the rock, and is generally fine-grained and has a grain size of less than 0.4 mm. Typically, many calcites are rimmed by dolomite, where dolomite replaces calcite. Generally the replacement is incomplete, but complete replacement is also seen. Additionally in some thin sections, after the primary dolomite replacement, secondary dolomite rim traces are seen clearly on the SEM images (Fig. 3.3b). Further to that, apatite crystals are found in the primary calcite-dolomite reaction zone, but disappear in the secondary zone.

Apatite is generally found as a minor mineral or as a vein component. As a minor mineral, it is fine-grained and has a grain size of less than 0.1 mm, anhedral and dispersed throughout the rock. It is commonly found as inclusions within dolomite (Fig. 3.3c). Within veins, it co-exists with magnetite crystals and fine-grained dolomite crystals (Fig. 3.3d). Samples

which contain apatite-bearing veins, do not contain apatite in other areas. Apatite rims 0.1 mm in width are seen at the boundaries between calcite and dolomite. Some magnetites may also have very thin 0.1 mm wide apatite rims.

Subhedral-euhedral magnetite crystals are found in calcite-dolomite carbonatite as a minor mineral, but in some thin sections they form up to 20 % of the rock. REE-bearing minerals, which are noted by EDS, are generally found together with calcite and apatite. SEM-EDS studies show that magnetite contains up to 2 % cobalt and apatite contains up to 4 % fluorine. In one thin section, amphibole is observed as an accessory mineral, however unlike in the calcite carbonatite no REE-bearing minerals are observed in association to the amphibole.

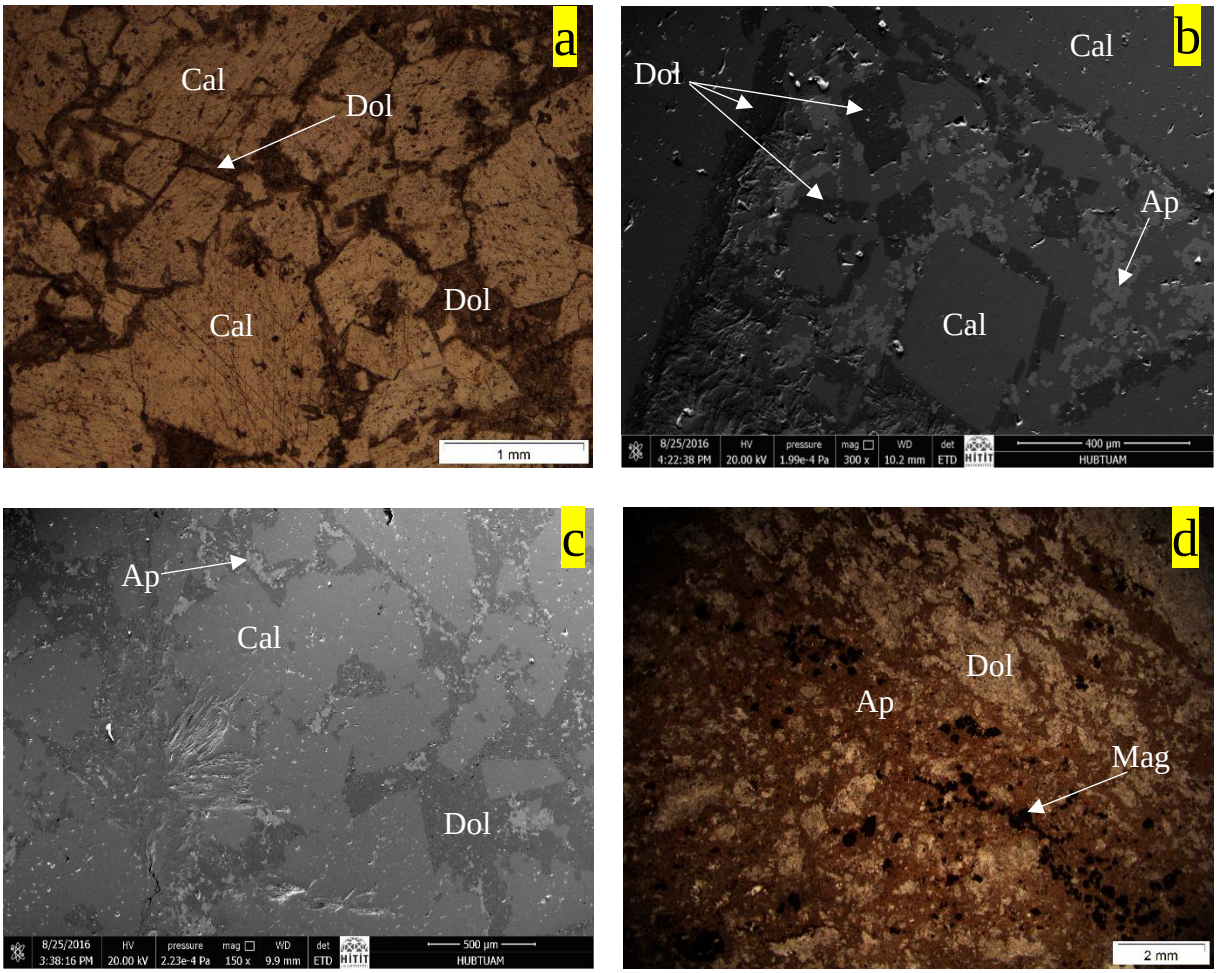

Figure 3. 3: Minerals and textures in calcite-dolomite carbonatite (a) PPL image showing medium-grained subhedral calcite crystals rimmed by fine-grained dolomite crystals, fine-grained anhedral magnetite grains are present within the groundmass. Sample 8-91. (b) primary- and secondary replacement of calcite by late dolomite, apatite crystals are found in the primary replacement zone, but disappear in the secondary replacement zone. Complete- and incomplete replacement are found together in the primary zone. Sample 8-91. (c) BSE image of calcite crystals and dolomite rims, apatite is mostly found within dolomite. Sample 8-91. (d) PPL image of a fine-grained apatite vein containing medium- to coarse-grained anhedral magnetite grains and fine-grained dolomite. Accessory calcite is present, but

rare in this image. Sample 8-100B. Calcite (Cal), dolomite (Dol), apatite (Ap), magnetite (Mag), primary replacement zone (prz), secondary replacement zone (srz).

Dolomite carbonatite is the youngest carbonatite and it forms more than half of the carbonatite at Spitskop. Fine-grained dolomite forms more than 60 % of the rock with varying proportions of magnetite, minor apatite and accessory calcite. Dolomite crystals are generally anhedral or subhedral and between 0.05 to 0.4 mm in size (Fig. 3.4a).

Magnetite crystals are abundant in dolomite carbonatite and can form 20 to 30 % of the rock. In some parts, magnetite displays a close association with apatite, where the apatite completely surrounds the magnetite crystals (Fig. 3.4b). Apatite also occurs filling cracks within the magnetite (Fig. 3.4c and 3.4d). Where there is no apatite rim around the magnetite, medium-grained 0.5 mm in size amphiboles are found adjacent to and as inclusions within magnetite.

Calcite is uncommon, forming less than 3 % of the rock. The crystals are medium-grained, up to 1 mm in size. Some quartz veins are also observable in dolomite carbonatite, especially near apatite and magnetite.

No REE-bearing minerals have been noted in the dolomite carbonatite.

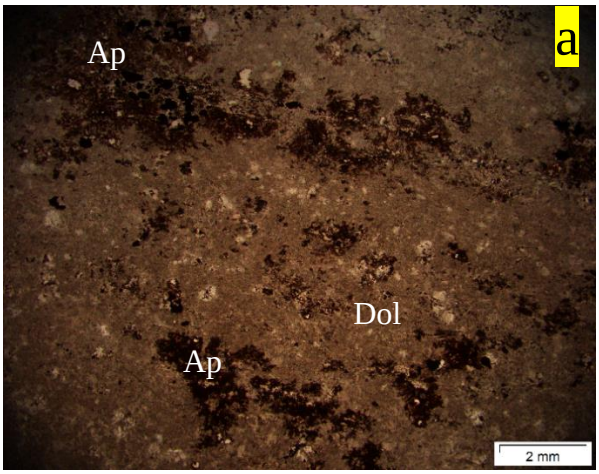

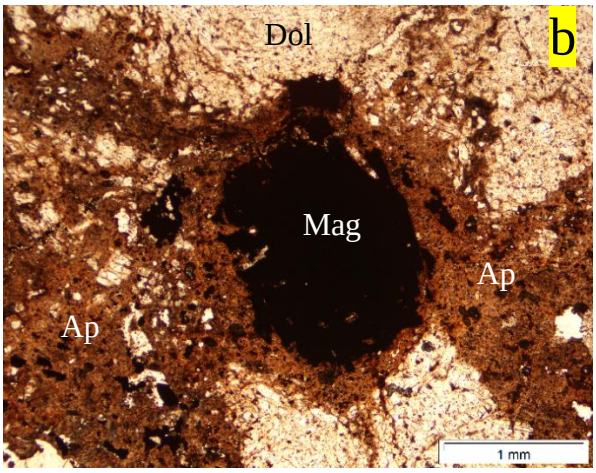

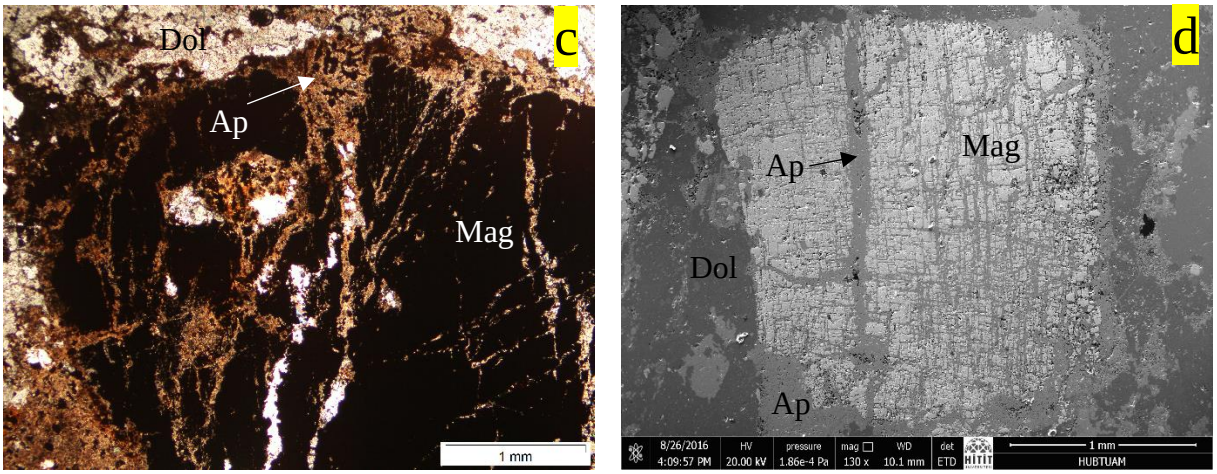

Figure 3. 4: Minerals and textures in dolomite carbonatite (a) PPL image of a fine-grained anhedral dolomite (Dol) and a fine-grained anhedral apatite (Ap) with medium-grained magnetite grains. Sample 8-93. b) PPL image of coarse-grained subhedral magnetite (Mag) and medium-grained magnetite grains surrounded by fine-grained apatite within the groundmass of dolomite. Sample 8-103-2B. c) XPL image of coarse-grained magnetite with cracks filled by fine-grained apatite; the groundmass consists of dolomite. Sample 8-103-1B. d) BSE image of coarse-grained subhedral magnetite, filled and rimmed by fine-grained apatite within the groundmass of dolomite. Sample 8-103-1A. Dolomite (Dol), apatite (Ap), magnetite (Mag).

3.3 Nepheline Syenites and Ijolite

Nepheline syenites of the Mare- and Spitskop Hills have a similar mineralogy and consist mainly of alkali feldspar, nepheline and clinopyroxene with accessory titanite, biotite and sodalite (Fig. 3.5a). The groundmass displays a trachytic texture and consists of alkali feldspar together with euhedral green to dark green clinopyroxenes, which SEM-EDS analyses suggest is mostly aegirine-augite and aegirine. A glomeroporphyritic texture is also present in some outcrops, and porphyritic aegirine-augite are found together.

The alkali feldspars mostly have a perthitic texture and are composed of microcline with elongate inclusions of albite (Fig. 3.5b). These feldspar crystals are the most abundant mineral in the nepheline syenites and generally form 40 to 65 % of the rock. In samples from Mare Hill feldspar crystals are mostly found in the groundmass, and some samples have a porphyritic texture. Crystals are mostly narrow and elongated. In a few outcrops the groundmass is composed entirely of elongated alkali feldspar crystals. Some feldspar crystals from Spitskop Hill are very coarse-grained and these crystals also show a perthitic texture intergrown with albite.

The crystals of colourless nepheline are generally subhedral and medium to coarse-grained, often 1-4 mm in diameter, but in some cases anhedral and euhedral crystals are also found. It forms 15 to 30 % of the nepheline syenites. A few nepheline crystals contain interstitial

aegirine-augite or medium to coarse-grained aegirine-augite inclusions up to 4 mm in size (Fig. 3.5c).

Microphenocrysts of aegirine-augite are the second most abundant mineral in nepheline syenites and they form 35 to 60 % of the rock. The crystals of aegirine-augite display a wide range of grain size from fine-grained to coarse-grained within a very small area (Fig. 3.5d). They are generally medium-grained, less than 2 mm in length. They have an acicular and fibrous texture (Fig. 3.5e). Commonly they are found as single euhedral crystals. Lamellar and simple twining are noted. In some samples clinopyroxenes of the nepheline syenite show a seriate texture (Fig. 3.5d) and some aegirine-augite display simple sector zoning as well as oscillatory zoning.

Bleb-like intergrowths of aegirine-augite in alkali feldspar are common. Feldspar crystals commonly contain green aegirine-augite inclusions and in some cases also contain nepheline inclusions (Fig. 3.5f). In a few outcrops dendritic overgrowths of aegirine-augite surround the phenocrysts of alkali feldspar (Fig. 3.5g). The accessory minerals titanite and biotite are not as abundant as sodalite. Biotites and titanites are generally found in matrix.

Alteration of nepheline in the nepheline syenite is seen in the form of secondary analcite both in the Mare- and Spitskop Hills. Although Harmer (1992) mentioned that nephelines are the most abundant mineral in the nepheline syenites, SEM-EDS results demonstrate two different peaks for nepheline (one peak represents nepheline and the other one represents analcite) and these results show that some of the nephelines are in fact secondary analcite crystals. Complex twining can also be noted in a few thin sections.

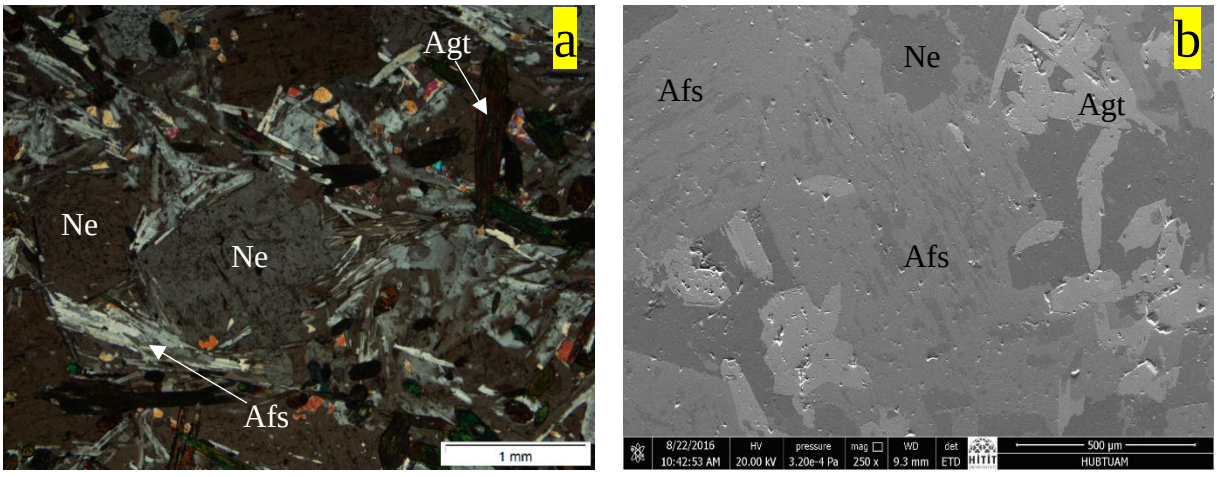

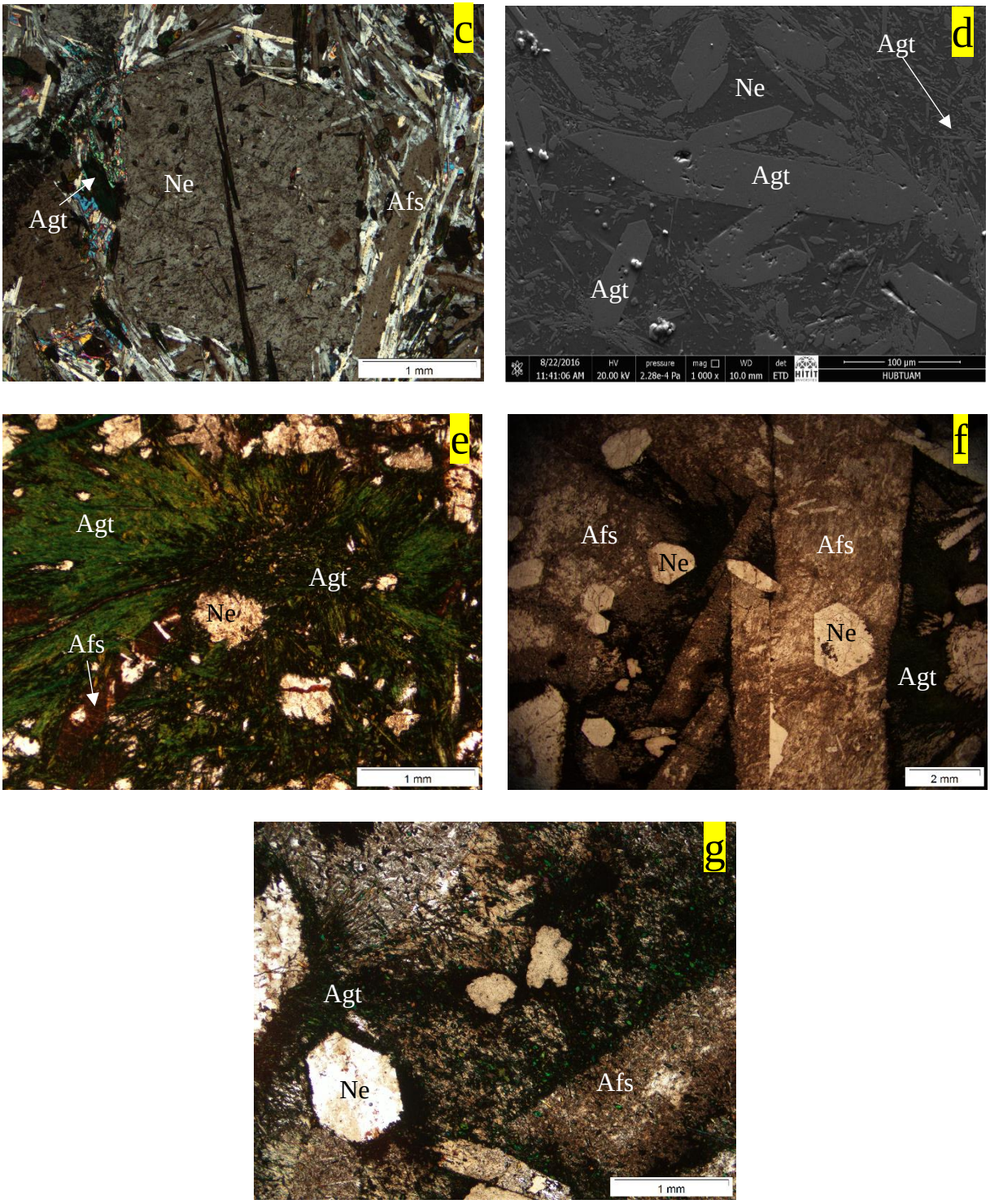

Figure 3. 5: Minerals and textures in nepheline syenite (a) XPL image of medium- to coarse-grained subhedral equant nepheline, medium-grained subhedral aegirine-augite within the groundmass of the tabular-shaped medium-grained alkali feldspar. Sample 3-23-1. (b) BSE image of subhedral perthitic alkali feldspar composed of albite within microcline crystals, subhedral aegirine-augite crystals and subhedral to euhedral nepheline. Sample 3-24. (c) XPL image of coarse-grained euhedral equant nepheline with interstitial medium- to coarse-grained aegirine-augite within the groundmass of medium-grained aegirine-augite and medium-grained tabular alkali feldspar. Sample 3-23-1. (d) BSE image showing seriate texture of nepheline syenite composed of fine- to coarse-grained anhedral to euhedral aegirine-augite within the groundmass of nepheline. Sample 3-30-1. (e) PPL image showing acicular and fibrous texture of fine-grained aegirine-augite together with medium-grained subhedral nepheline

and altered coarse-grained alkali feldspar crystals. Sample 3-31-1-2. (f) PPL image showing tabular coarse-grained euhedral feldspar crystals containing subhedral medium-grained nepheline and fine-grained clinopyroxene inclusions. Sample 3-31-3-1. (g) PPL image showing acicular and dendritic overgrowths of fine-grained aegirine-augite around the coarse-grained subhedral alkali feldspar and the medium-grained euhedral nepheline. Sample 3-31-3-1. Nepheline (Ne), aegirine-augite (Agt), alkali feldspar (Afs).

Ijolite of the Spitskop Complex consists mainly of microcrystalline nepheline and interstitial clinopyroxene in equal amounts and forms the bulk of the rock (Fig. 3.6a and Fig. 3.6b). Uniformly-sized nephelines are equant and have a euhedral shape. The form of the nepheline is hexagonal and square prismatic sections (Fig. 3.6c). They are mainly coarse-grained and form 50 to 60 % of the rock. Very thin incomplete anhedral analcite rims less than 0.01 mm are observed under SEM-EDS around euhedral nepheline crystals (Fig. 3.6d).

Fine- to medium-grained clinopyroxenes in the ijolite are mostly aegirine-augites. They have a subhedral and euhedral shape and an acicular texture. Simple zoning is seen clearly and prominent marginal zoning is also noted in coarse-grained clinopyroxenes. SEM-EDS analyses show that the interstitial needle-like microphenocrysts of aegirine-augite within nephelines also contain up to 20 % barium.

Coarse-grained albitic zones within ijolite host fine-grained analcite inclusions within the albite. SEM-EDS data shows that these analcite inclusions may form approximately 25 to 30 % of the albite grains. Fine-grained anhedral aegirines also occur as inclusions. Analcite veins are not common in the ijolites, but have been noted in one thin section (Fig. 3.6e). A few euhedral sodalite crystals are also noted in the ijolite. Medium-grained crystals of sodalite, 0.5-1 mm in size, are enclosed by an equigranular groundmass composed of fibrous aegirine-augite and equant nepheline.

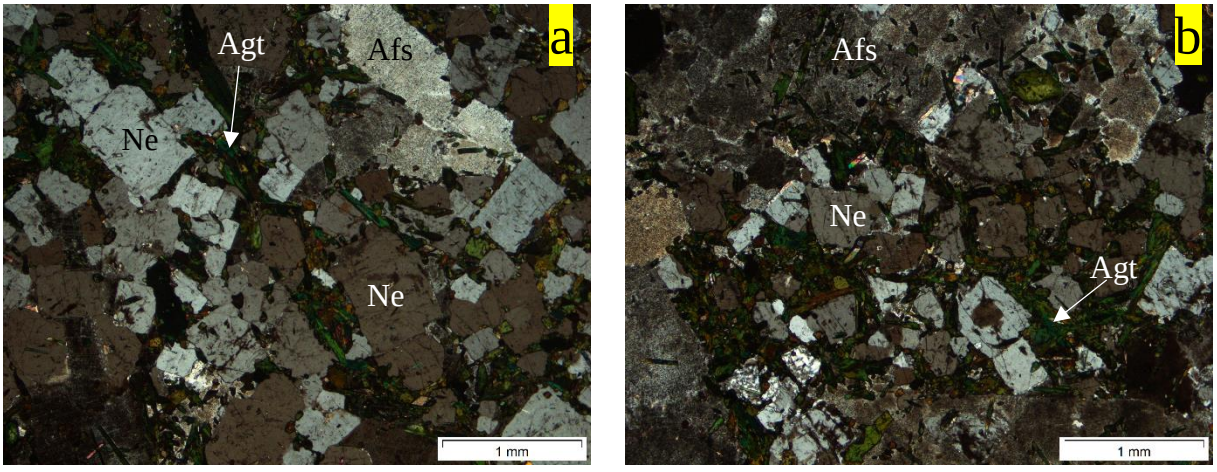

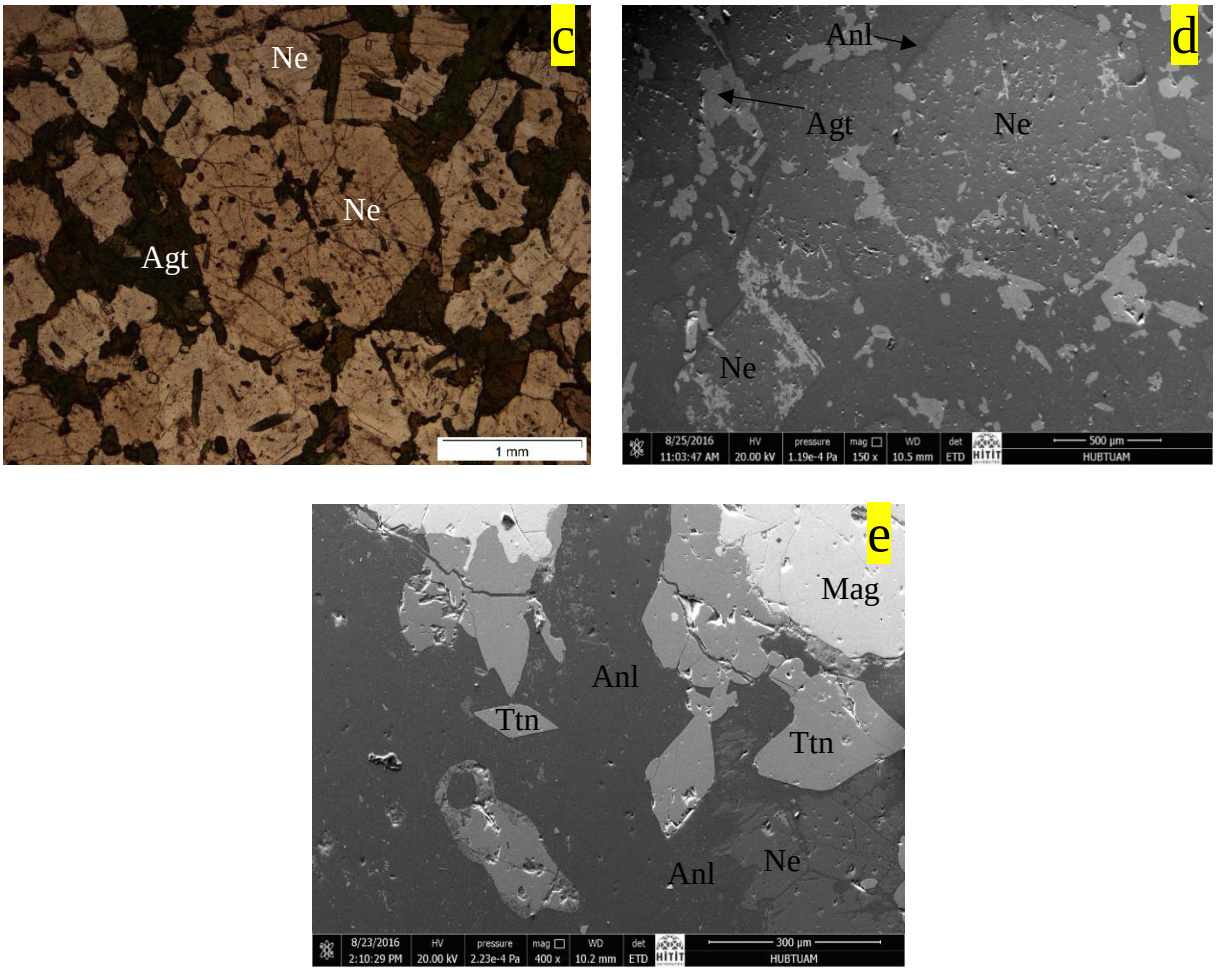

Figure 3. 6: Minerals and textures in ijolite (a) XPL image of typical ijolite showing medium-grained euhedral equant nepheline and medium-grained subhedral aegirine-augite, tabular coarse-grained alkali feldspar is also present. Sample 2-11-1-1. (b) XPL image showing medium-grained euhedral equant nepheline and acicular medium-grained aegirine-augite with coarse-grained alkali feldspar. Note that alkali feldspar contains aegirine-augite inclusions. Sample 2-11-1-1. (c) PPL image showing subhedral hexagonal- and square nepheline together with interstitial medium-grained aegirine-augite. Sample 2-11-1-3. (d) BSE image of euhedral hexagonal- to square nepheline with interstitial anhedral to subhedral aegirine-augite. Note that there is an analcite rim around nepheline crystals. Sample 2-11-1-1. (e) BSE image showing analcite vein and the metasomatic alteration of euhedral nepheline to anhedral analcite, subhedral to euhedral titanite and minor magnetite. Sample 2-12-1-1. Nepheline (Ne), aegirine-augite (Agt), alkali feldspar (Afs), analcite (Anl), titanite (Ttn), magnetite (Mag).

3.4 Original Bushveld Upper Zone Rocks and the Mafic Fenites

Upper Zone (UZ) rocks of the Bushveld Complex are one of the most important group of rocks in this study, and are divided into three subzones, UZa, UZb and UZc, based on the mineralogy of the rocks: such that Uza is the lowest and characterized by the occurrence of magnetite, UZb hosts olivine, while UZc has accessory apatite (Tegner et. al, 2006). The mineralogy of the Upper Zone rocks of ferrogabbro, gabbronorite and diorite are very similar both in the eastern- and western limb (Tegner et. al, 2006) and in this study thin sections from the Bierkraal borehole, from the western limb, were used for the mineralogical and petrological comparison

with the mafic fenites. Based on thin section mineralogy, metasomatized rocks of the UZ associated with the Spitskop Complex include; anorthosite, gabbro, gabbronorite and ferrogabbro.

Anorthosite of the Upper Zone consists mainly of plagioclase crystals comprising up to 90 % of the rock together with the minor magnetite or clinopyroxene, and these have a sharp contact with the magnetitite layer. Magnetitite layers of the Bushveld Upper Zone are the most easily distinguishable lithology. They consist of massive magnetite with plagioclase inclusions (Fig. 3.7a). Subhedral to euhedral plagioclase is mostly medium- to coarse-grained, and up to 1-2 cm in size.

Gabbro/ferrogabbro is one of the main rock types of the Upper Zone. Ortho- and clinopyroxene are mostly anhedral to subhedral and vary in size, from medium- to coarse-grained (Fig. 3.7b-c), while magnetites within gabbro are always anhedral and medium-grained up to 1 mm in size. Apatite and olivine are mostly anhedral, apatite is usually found together with olivine and magnetite (Fig. 3.7d). The occurrence of apatite, olivine and magnetite in gabbro is one of the most characteristic features to identify the Upper Zone ferrogabbros.

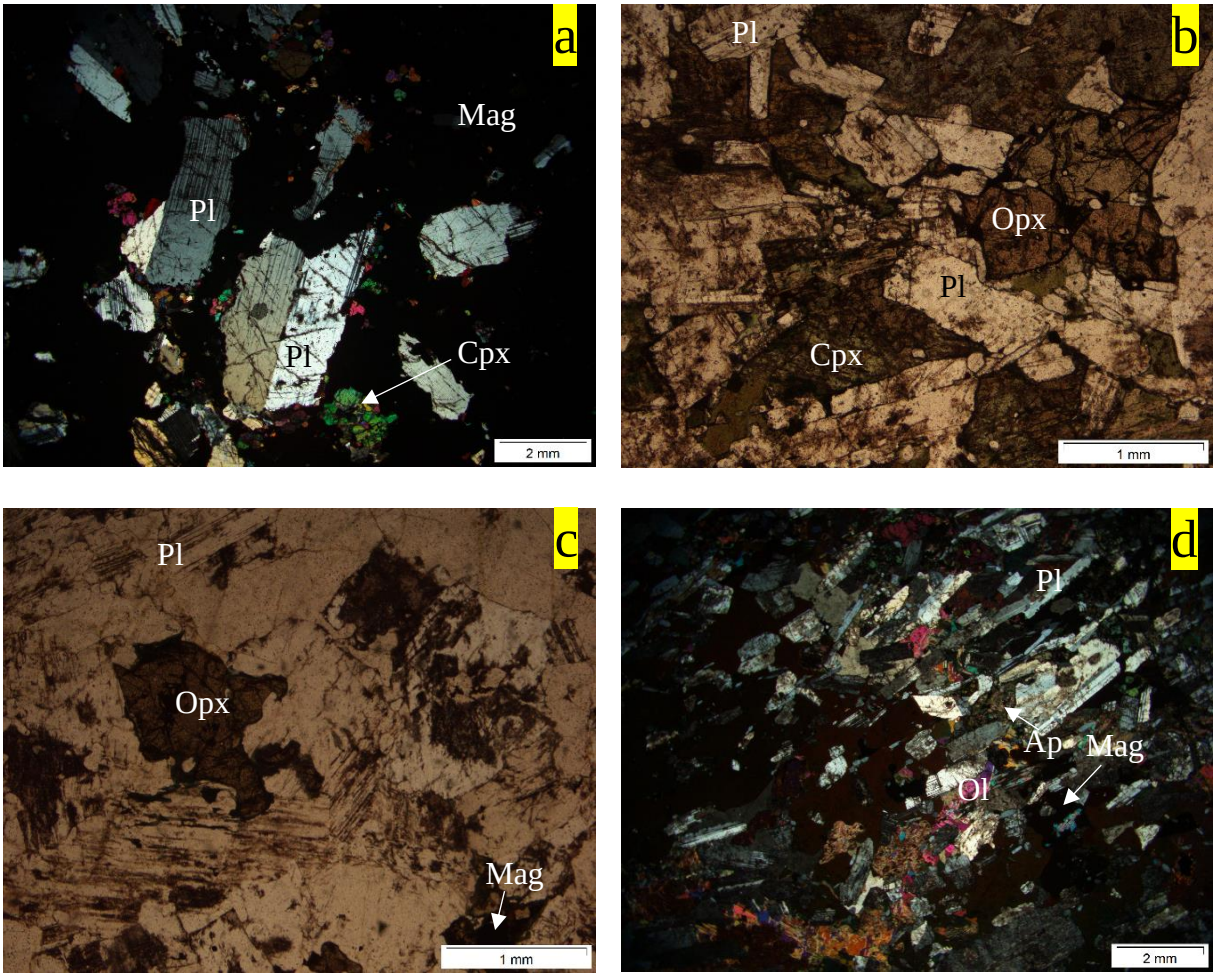

Figure 3. 7: Minerals and textures in the Bushveld Upper Zone rocks, from Bierkraal (a) XPL image of a magnetitite layer showing the massive magnetite and coarse-grained subhedral plagioclase minerals within magnetitite. Note that some clinopyroxene is also present within the magnetitite. Sample IW1459.3. (b) PPL image of a gabbro showing medium-grained anhedral to subhedral ortho- and clinopyroxene, and tabular shaped medium- to coarse-grained plagioclase crystals. Sample IW403.4. c) PPL image of a gabbro showing medium-grained subhedral orthopyroxene with tabular shaped plagioclase crystals and medium-grained anhedral magnetite. Sample IW403.4. d) XPL image of gabbro showing plagioclase crystals, medium-grained anhedral magnetite, anhedral apatite and anhedral olivine. Magnetite (Mag), plagioclase (Pl), clinopyroxene (Cpx), orthopyroxene (Opx), apatite (Ap) and olivine (Ol).

In general, the mafic fenites consist mainly of nepheline, clinopyroxene and magnetite as major minerals together with minor titanite and stilpnomelane, and some accessory minerals such as apatite, ilmenite, hornblende and phlogopite (Fig. 3.8a-b).

Nepheline forms between 40 to 60 % of the rock and is the most abundant mineral of the mafic fenites, it is mostly anhedral and medium-grained, although occasionally subhedral nephelines are also observed in some thin sections. Some nepheline crystals contain a number of fine-grained aegirine-augite crystals as inclusions. In a few thin sections analcite, an alteration product of nepheline, is seen as an incomplete rim around nepheline or in veins where no remnant nepheline remains.

The second most abundant mineral in the mafic fenites is clinopyroxene. SEM-EDS data shows that the subhedral clinopyroxenes are mainly fine- to medium-grained aegirine-augite and sometimes aegirine. A seriate texture occurs in some sections (Fig. 3.8c). The clinopyroxenes contain apatite, calcite, analcite and stilpnomelane inclusions. A few of the aegirine-augite crystals are located within the analcite veins.

Mafic fenites contain fine- to medium-grained anhedral magnetite grains that are always found together with nepheline and aegirine-augite. Coarse-grained magnetite grains within the mafic fenites are rare, except in the main magnetite-bearing zone, which simply consists of massive magnetite.

Thin sections of the mafic fenites, which occur 350-400 meters away from carbonatite outcrops, contain plagioclase crystals together with apatite, magnetite and fayalite (Fig. 3.8d-e), which is also very characteristic for the Upper Zone ferrogabbros (Fig. 3.8d-e). Nepheline can be found with plagioclase and clinopyroxene occurs with olivine (Fig. 3.8f).

SEM-EDS data for the mafic fenites show that nepheline crystals generally contain up to 6 % potassium by weight with up to 6 wt % barium at the edge of the crystal in a zone that is

potassium-free, suggesting that a potassium-barium replacement is possible. Additionally in one sample, barium enrichment is seen in the middle of an analcite crystal.

Mafic fenites also contain accessory stilpnomelane, apatite, ilmenite, calcite, hornblende and pyrrhotite. Medium-grained subhedral stilpnomelanes are found close to titaniferous magnetites, however in some thin sections stilpnomelane can be found together with aegirine-augite (Fig. 3.8g). Fine-grained apatites are always found within aegirine-augite as inclusions and SEM-EDS suggests a fluorine content of 4 % similar to the fluorapatites in carbonatites. Fine-grained ilmenites are seen both inside the mafic fenites and in the magnetite zone. Some ilmenite is rimmed by titanite and most of them contain up to 11 wt % manganese. Rare subhedral calcite was found as inclusions within aegirines. Pyrrhotites are rare and are seen together with aegirine-augite crystals. A poikilitic texture is also found in a few thin sections, chadacrysts of titanium-rich aegirine-augite crystals are observed within oikocrysts of aegirine-augite. The chadacrysts, which have a fairly uniform size, are oriented in one direction. Additionally, Harmer (1992) mentioned that there are also biotites as an accessory mineral, but all the minerals he identified as biotites are probably stilpnomelanes.

One of the most important features of the mafic fenites is the coarse-grained euhedral perthite veins, which are only found in mafic fenites. These veins consist mainly of an intergrowth of microcline and albite (Fig. 3.8h) and the blebs of albite are uniformly distributed. Some of the veins contain coarse-grained euhedral dark green aegirine crystals (Fig. 3.8i). Pure microcline- and pure albite zones are also noted, additionally in one thin section, analcite inclusions are observed within coarse-grained albite.

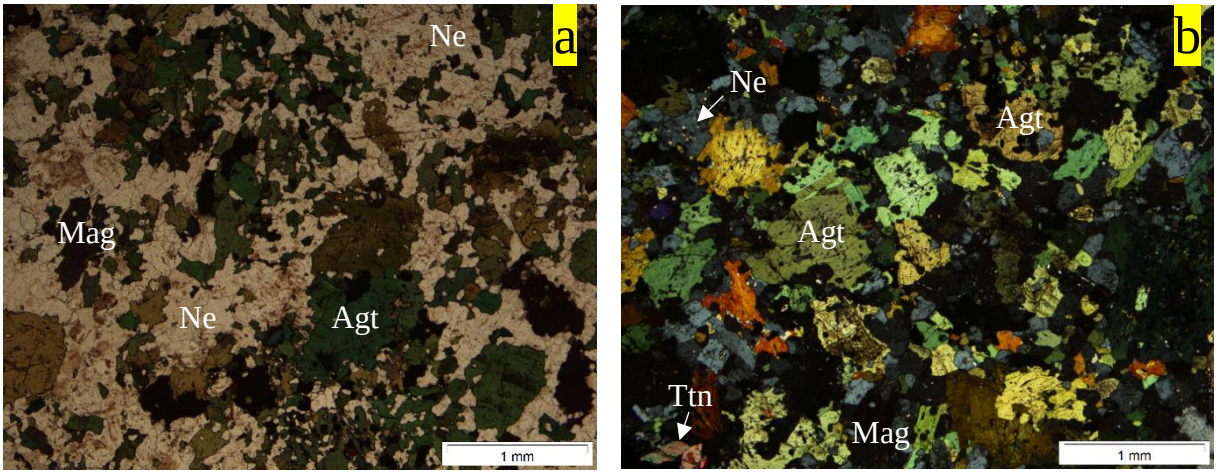

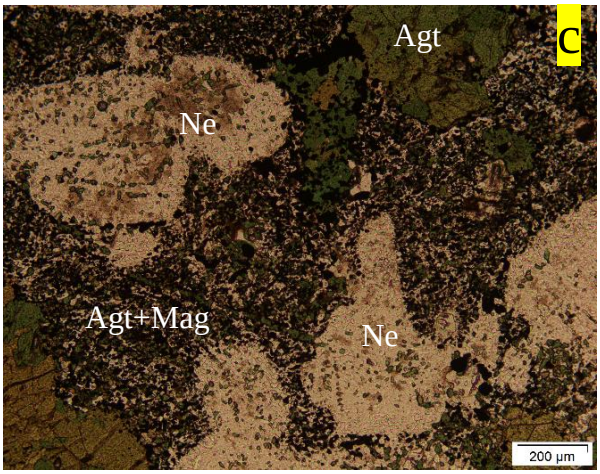
c
Agt
Ne
Agt+Mag
Ne
200 µm

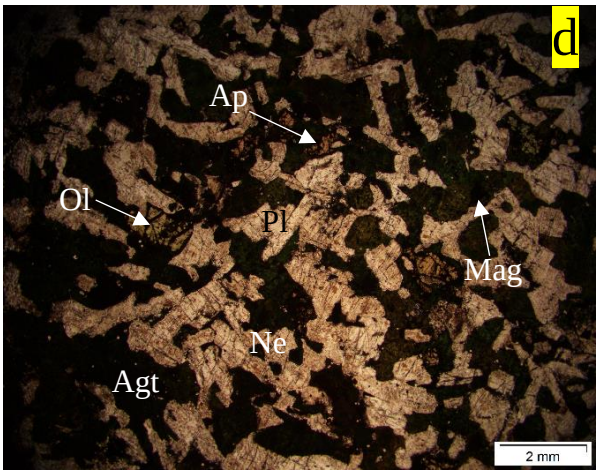
d
Ap
Ol
Pl
Mag
Ne
Agt
2 mm

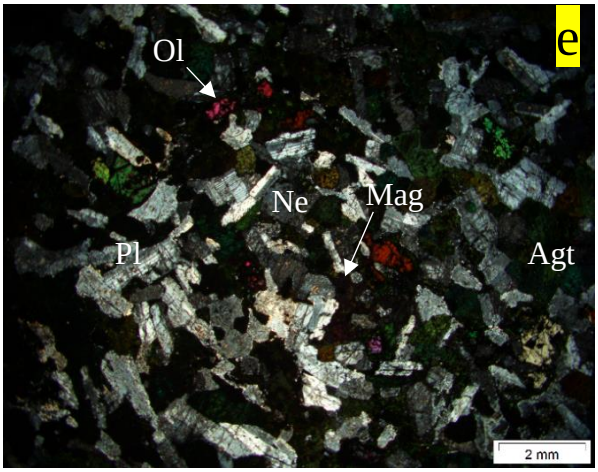
e
Ol
Ne
Mag
Pl
Agt
2 mm

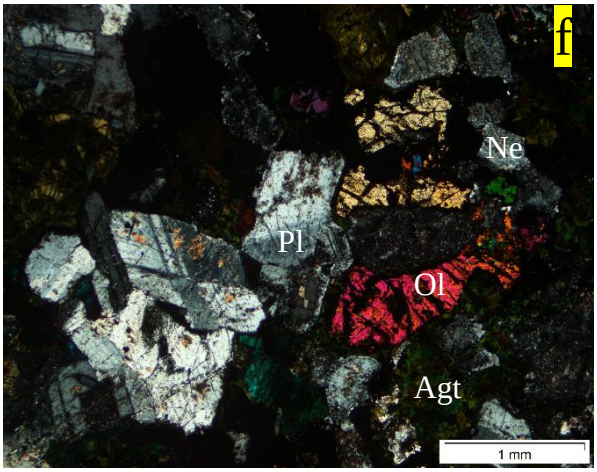
f
Ne
Pl
Ol
Agt
1 mm

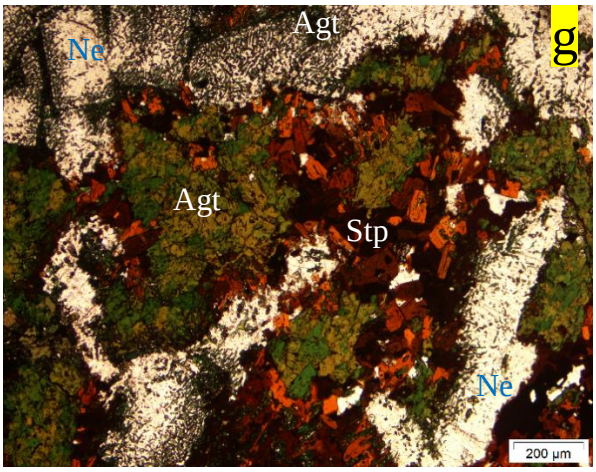
g
Ne
Agt
Agt
Stp
Ne
200 µm

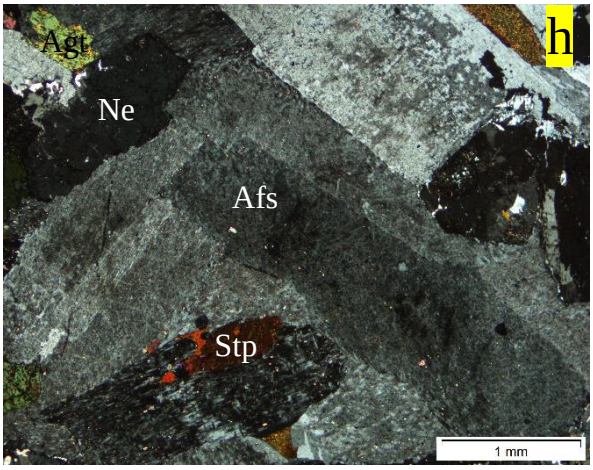
h
Agt
Ne
Afs
Stp
1 mm

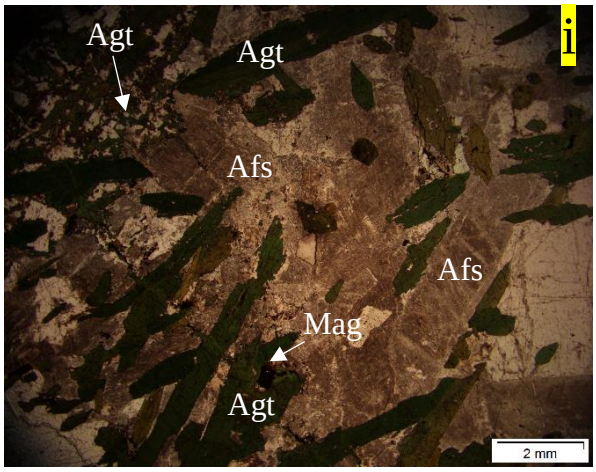

Figure 3. 8: Minerals and textures in magnetite-bearing mafic fenites (a) PPL image of a typical mafic fenite showing colourless medium- to coarse-grained anhedral nepheline, medium- to coarse-grained anhedral aegirine-augite and medium-grained anhedral magnetite grains. Note that fine-grained stilpnomelane is also present within some aegirine-augite crystals. Sample 1-2-2-2. (b) XPL image of a typical mafic fenite showing medium-grained anhedral to subhedral nepheline, medium-grained anhedral aegirine-augite and fine-grained magnetite crystals with accessory medium-grained subhedral diamond-shaped titanite. Sample 1-2-2-2. (c) PPL image showing seriate texture of fine- to coarse-grained anhedral aegirine-augite, fine-grained anhedral magnetite and colourless nepheline. Note that the amount of magnetite increases near or around aegirine-augite and nepheline. Sample 6-64-1B. (d) PPL image showing tabular colourless medium-grained subhedral plagioclase, medium-grained anhedral olivine, medium-grained anhedral apatite and medium- to coarse-grained subhedral aegirine-augite. Note that nepheline is also present in this thin section. Sample 6-64-2A. (e) XPL image of the mafic fenite showing medium-grained anhedral nepheline, medium- to coarse-grained tabular subhedral plagioclase, medium-grained anhedral olivine, fine- to medium-grained anhedral magnetite and medium- to coarse-grained subhedral aegirine-augite. Sample 6-64-2A. (f) XPL image showing medium-grained olivine rimmed by fine- to medium-grained aegirine-augite, and medium-grained plagioclase together with anhedral nepheline. Sample 6-64-2B. (g) PPL image showing fine- to medium-grained anhedral augite-aegirine, medium-grained anhedral to subhedral stilpnomelane and colourless anhedral nepheline. Note that aegirine-augite near or around nepheline is always fine-grained. Sample 1-1-1. (h) XPL image of a perthite vein showing coarse-grained tabular euhedral perthitic feldspar consists of microcline and albite, and some medium-grained anhedral aegirine-augite. Note that stilpnomelane and nepheline are also present. Sample 1-2-2-2. (i) PPL image of a perthite vein showing coarse-grained subhedral aegirine-augite interstitial to the perthitic feldspar, and medium-grained anhedral magnetite crystals. Note the change of the size of the clinopyroxene, aegirine-augite outside of the perthite vein is fine- to medium-grained. Sample 2-14-5-2. Nepheline (Ne), aegirine-augite (Agt), magnetite (Mag), stilpnomelane (Stp), titanite (Ttn), plagioclase (Pl), olivine (Ol), apatite (Ap), perthitic feldspar (Afs).

The main magnetite-bearing zone, which occurs within mafic fenites, is composed of almost entirely massive titaniferous magnetite with a few cracks and/or thin veins, which generally contain nepheline, aegirine-augite and titanite (Fig. 3.9a). Nepheline and aegirine-augite are mostly anhedral and coarse-grained, but in some thin sections fine-grained nepheline and aegirine-augite are also seen within the cracks. Titanite forms anhedral to euhedral diamond-shaped crystals (Fig. 3.9b). The spaces between the massive crystals of magnetite are sometimes filled only by titanite and ilmenite, and some anhedral-subhedral stilpnomelane crystals are also noted near ilmenite.

More importantly, these massive magnetites contain many oriented crystals very similar to the crystals of the Upper Zone magnetitite layer, which are composed of plagioclase. The crystals of the fenitic magnetite zone are composed of stilpnomelane (Fig. 3.9c) and nepheline (Fig. 3.9d). Additionally, in some thin sections plagioclase remnants are seen near anhedral nepheline (Fig. 3.9e).

Generally in all thin sections titanites surround the titaniferous magnetite, and nepheline and aegirine-augite are found near the titanite rim (Fig. 3.9f).

SEM-EDS observations show that the magnetite is rich in titanium with up to 10 wt % Ti. Some of the magnetite crystals contain titanite inclusions and the same crystals are surrounded by stilpnomelane.

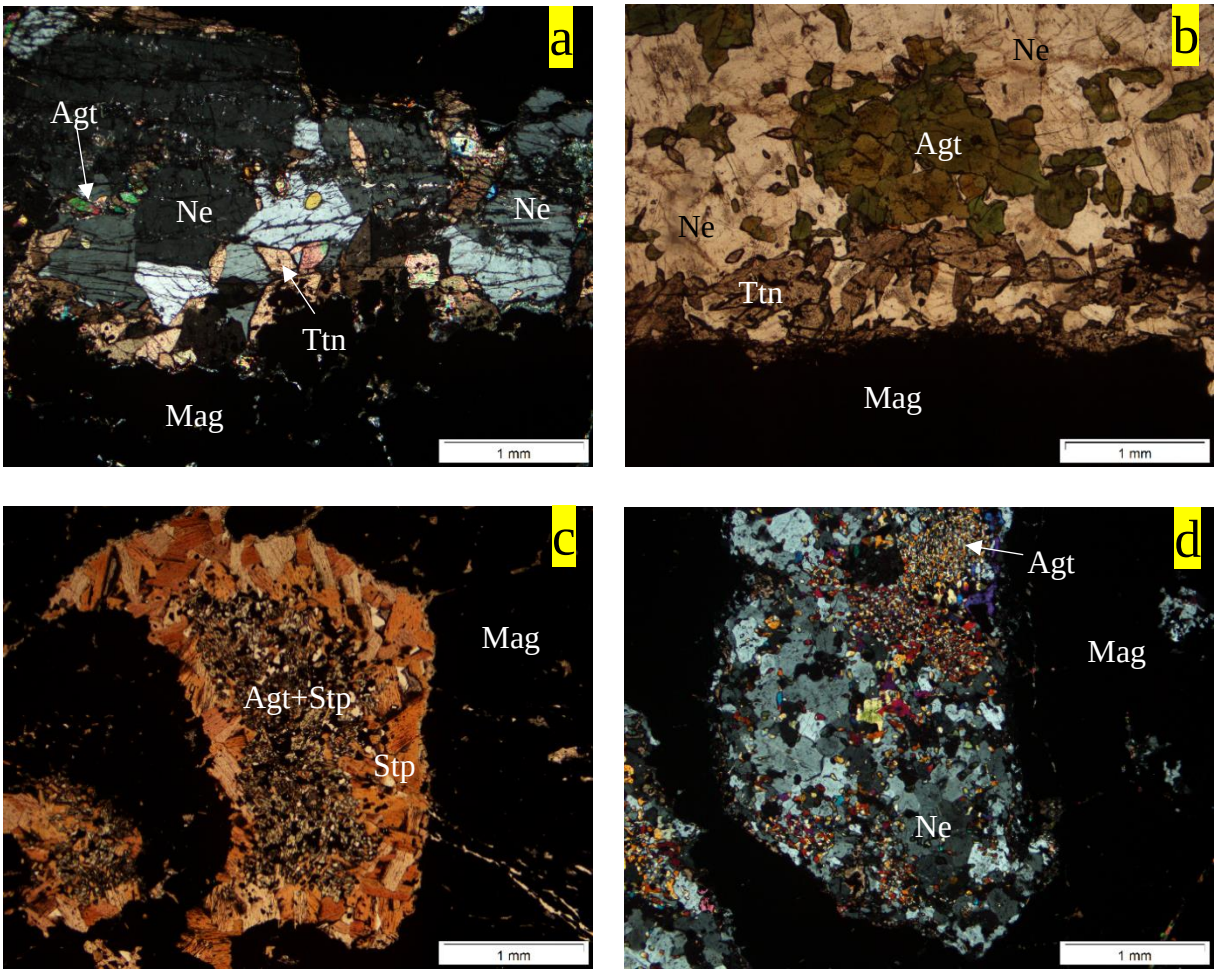

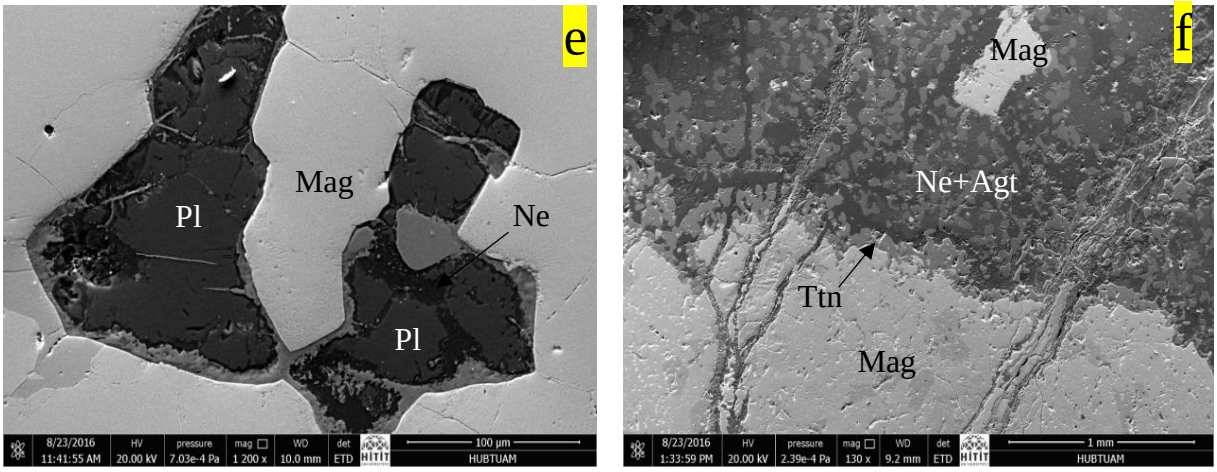

Figure 3. 9: Minerals and textures in magnetite-bearing mafic fenites (a) XPL image showing a part of the massive magnetite and the vein within the magnetite. Medium-grained subhedral to euhedral diamond-shaped titanite with simple twinning and medium- to coarse-grained anhedral nepheline together with some medium-grained aegirine-augite are common and some fine-grained magnetite grains are also present within the vein. Sample 1-8-2-1. (b) PPL image showing the anhedral to subhedral diamond-shaped titanite rim to the magnetite, medium-grained anhedral aegirine-augite and colourless medium-grained nepheline. Sample 2-14-6-2. (c) PPL image showing fine- to medium-grained subhedral stilpnomelane crystals and fine-grained aegirine-augite grains within the magnetite inclusion. Sample 1-6-1. (d) XPL image of the magnetite filled with fine-grained anhedral aegirine-augite and medium-grained subhedral nepheline with some fine-grained magnetite crystals. Note that few anhedral titanite crystals are present. Sample 2-14-3. (e) BSE image of the magnetite filled with nepheline and plagioclase. Sample 1-8-2-1. (f) BSE image showing anhedral aegirine-augite and anhedral nepheline near the massive titaniferous magnetite. Note that the massive magnetite is rimmed by titanite. Sample 2-12-1-1. Magnetite (Mag), titanite (Ttn), nepheline (Ne), aegirine-augite (Agt), stilpnomelane (Stp), plagioclase (Pl).

In the Spitskop Complex, mineral alteration illustrated in Fig. 3.10, is seen clearly and sometimes progressively (Fig. 3.10a-m). The most important alteration is observed in olivine (Fig. 3.10 a-e), in orthopyroxene (Fig. 3.10 f-i), in clinopyroxene (Fig. 3.10j-k), in plagioclase and in nepheline (Fig. 3.10l).

The alteration of olivine and orthopyroxene to aegirine-augite begins at the crystal margins forming an initial fine-grained anhedral rim with acicular aegirine-augite, and progresses inwards or occurs within the fractures (Fig. 3.10e-i).

The alteration of clinopyroxene to stilpnomelane is observed in some samples with one sample showing the transformation of aegirine-augite to stilpnomelane (Fig. 3.10j), whereas generally the stilpnomelane forms rims around magnetite and titanite.

The alteration sequence of plagioclase to nepheline and then nepheline to analcite is not particularly well seen except for in a few samples.

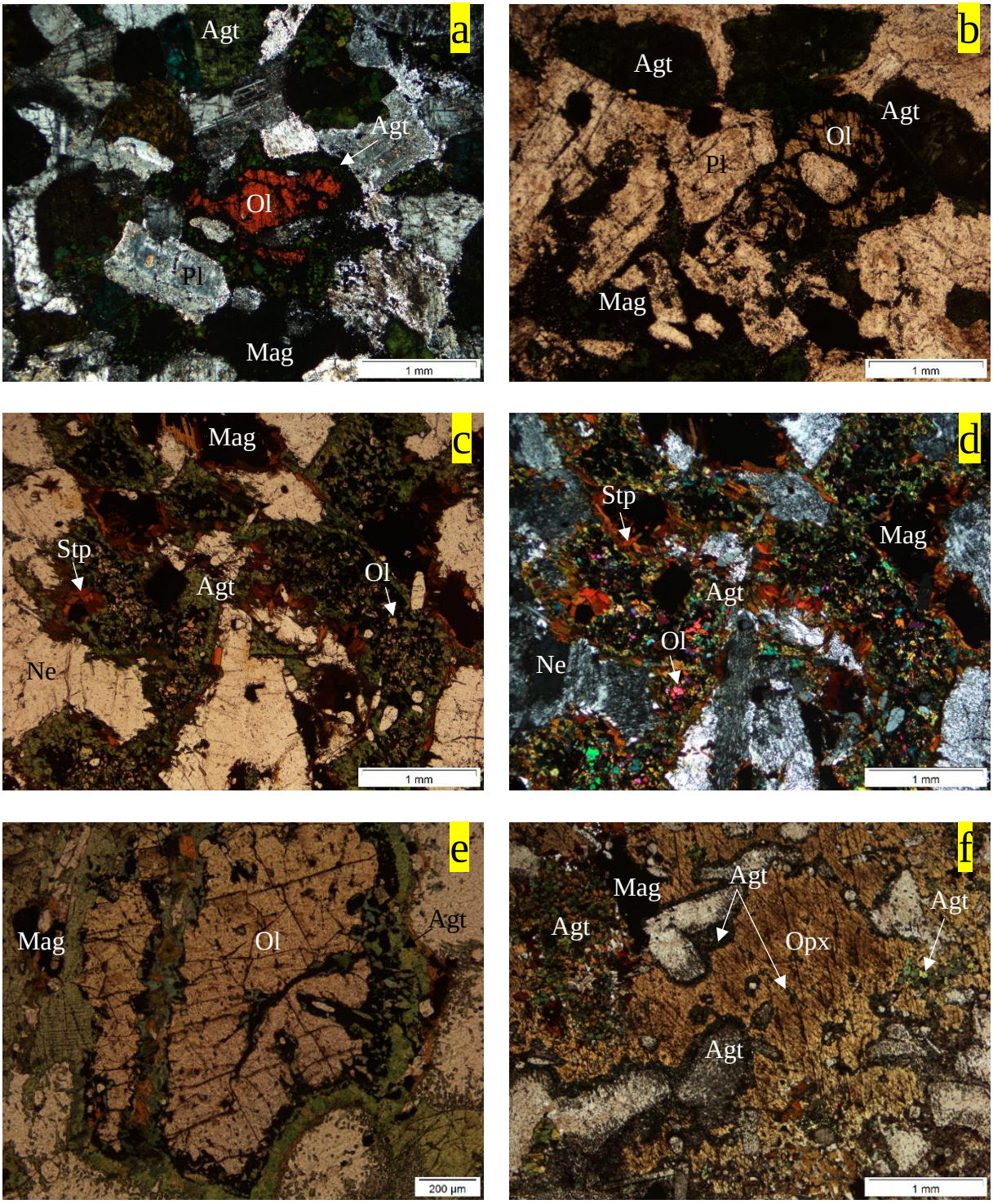
a
Agt
Agt
Ol
Pl
Mag
1 mm
b
Agt
Agt
Ol
Pl
Mag
1 mm
c
Mag
Stp
Agt
Ol
Ne
1 mm
d
Stp
Mag
Agt
Ol
Ne
1 mm
e
Mag
Ol
Agt
200 µm
f
Mag
Agt
Agt
Agt
Opx
Agt
1 mm

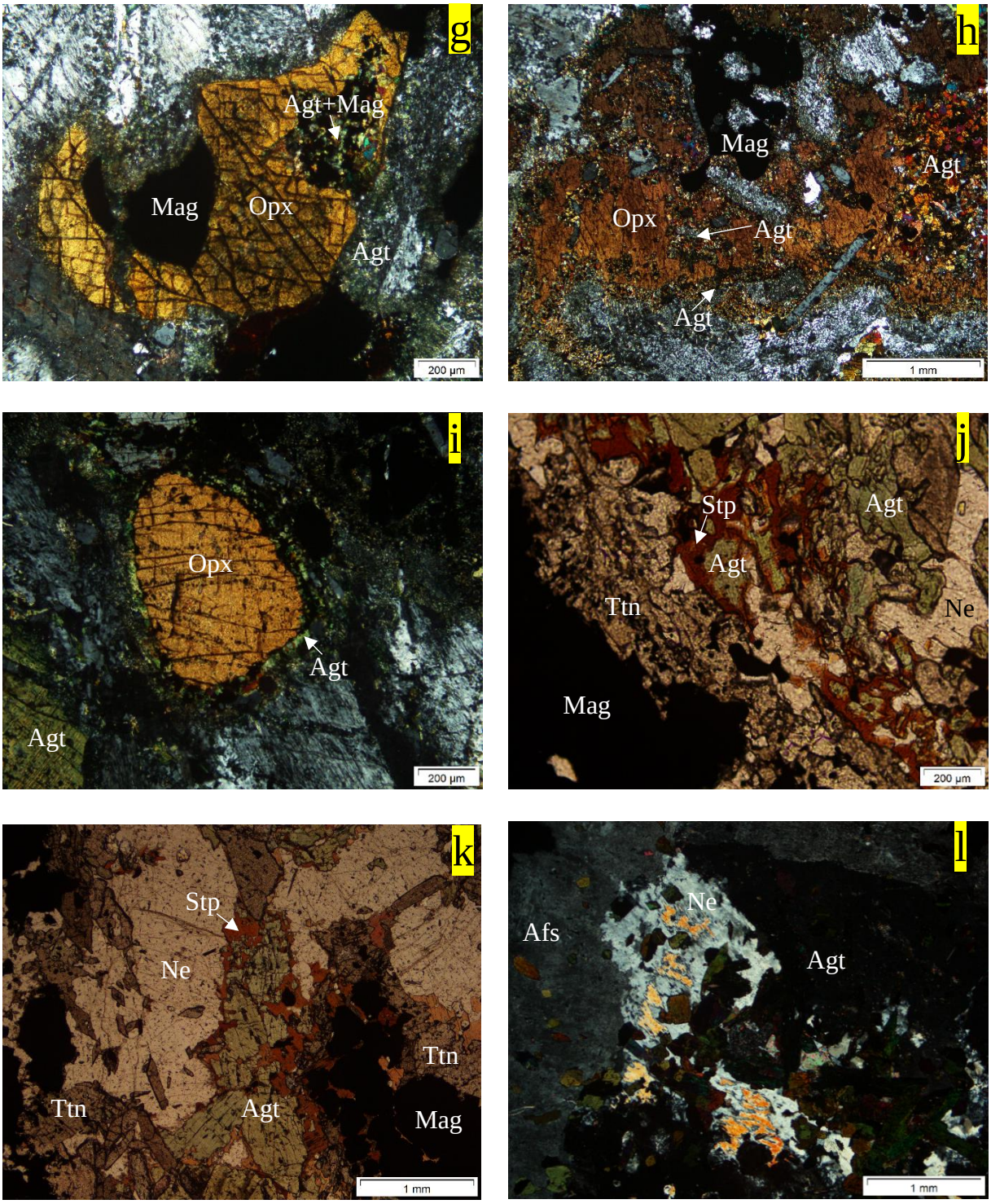

Figure 3. 10: Metasomatic alteration textures in mafic fenites (a) XPL image of a mafic fenite showing the beginning of alteration of a medium-grained subhedral olivine to fine- to medium-grained aegirine-augite, and the alteration of medium-grained plagioclase to anhedral nepheline. Note that the irregular fractures in olivine are filled by aegirine-augite. Sample 6-64-2A. (b) PPL image showing the beginning of an alteration of another medium-grained olivine to anhedral medium-grained aegirine-augite. Note that the cracks are filled by aegirine-augite. Sample 6-64-2B. (c) PPL image showing the initial alteration of olivine to fine-grained aegirine-augite, and subsequently to stilpnomelane. Note that small pale-yellow to pale-brown crystals within aegirine-augite are remnant olivine. Sample 1-4. (d) XPL image of the same thin section of (c). Sample 1-4. (e) PPL image of medium-grained subhedral olivine rimmed and filled by fine-grained anhedral aegirine-augite. Note that some aegirine-augite was

subsequently altered to anhedral stilpnomelane. Sample 1-1-1. (f) XPL image of the transformation of coarse-grained subhedral orthopyroxene rimmed and filled by fine-grained anhedral aegirine-augite. Sample 1-4. (g) XPL image of a medium-grained subhedral orthopyroxene rimmed and cross-cut by fine-grained anhedral aegirine-augite. Sample 1-1-1. (h) XPL image showing the beginning of alteration of subhedral orthopyroxene to fine- and medium-grained anhedral to subhedral aegirine-augite. Sample 1-4. (i) XPL image showing medium-grained subhedral orthopyroxene rimmed by fine-grained anhedral aegirine-augite. Sample 1-1-1. (j)PPL image showing the alteration of medium-grained anhedral aegirine-augite to stilpnomelane. Sample 2-14-4-2. (k) PPL image showing the beginning of alteration of medium- to coarse-grained subhedral aegirine-augite to medium-grained anhedral stilpnomelane. Sample 2-14-4-1. (l) XPL image showing alteration of anhedral nepheline possibly to analcite, near a perthite vein. Sample 2-16-1. Olivine (Ol), aegirine-augite (Agt), plagioclase (Pl), nepheline (Ne), stilpnomelane (Stp), orthopyroxene (Opx).

3.5 Granite Fenites

The phanerocrystalline feldspar fenite is located adjacent to the mafic fenites further downstream of the Tshweneng River. However the mineralogy of the feldspar fenite is very different to that of the mafic fenites and contains up to 90% perthite with minor clinopyroxene (Fig. 3.11a). Perthite consists of microcline and albite, is coarse-grained and subhedral (Fig. 3.11b). Elongate crystals of perthite form a framework in this rock. The transition between the mafic fenites and the feldspar fenite is sharp in the field, however it is not as sharp mineralogically, with some medium-grained nepheline and aegirine-augite zones adjacent to the perthitic zones of the feldspar fenites, although this only persists for 5-10 meters from the contact.

In addition to the perthite, there are microphenocrysts of clinopyroxene, mostly aegirine, forming radiating clusters of acicular crystals (Fig. 3.11c).

Progressive albitization of potassium feldspar is observed in one thin section sample. Coarse-grained microcline crystals with less albite inclusions are noted (Fig. 3.11d), whereas in the upper part of the outcrop coarse-grained albite crystals together with aegirines are common (Fig. 3.11e). Microcline with more albite inclusions is also seen in the same outcrop.

Accessory hornblende forms 2-3 % of the rock. Normally, biotites are found as accessory minerals in Bushveld Nebo granites, but no biotite is found in the feldspar fenites.

The second type of the granite fenite, is quartz-feldspar fenite, located near the feldspar fenite. It is dominated by 50-60% perthite with 30-40% quartz and clinopyroxene, mostly aegirine-augite, with accessory hornblende (Fig. 3.11f and Fig. 3.11g).

In one sample aegirine-augite is found within the perthite as a vein (Fig. 3.11h). There is no aegirine and biotite in this rock.

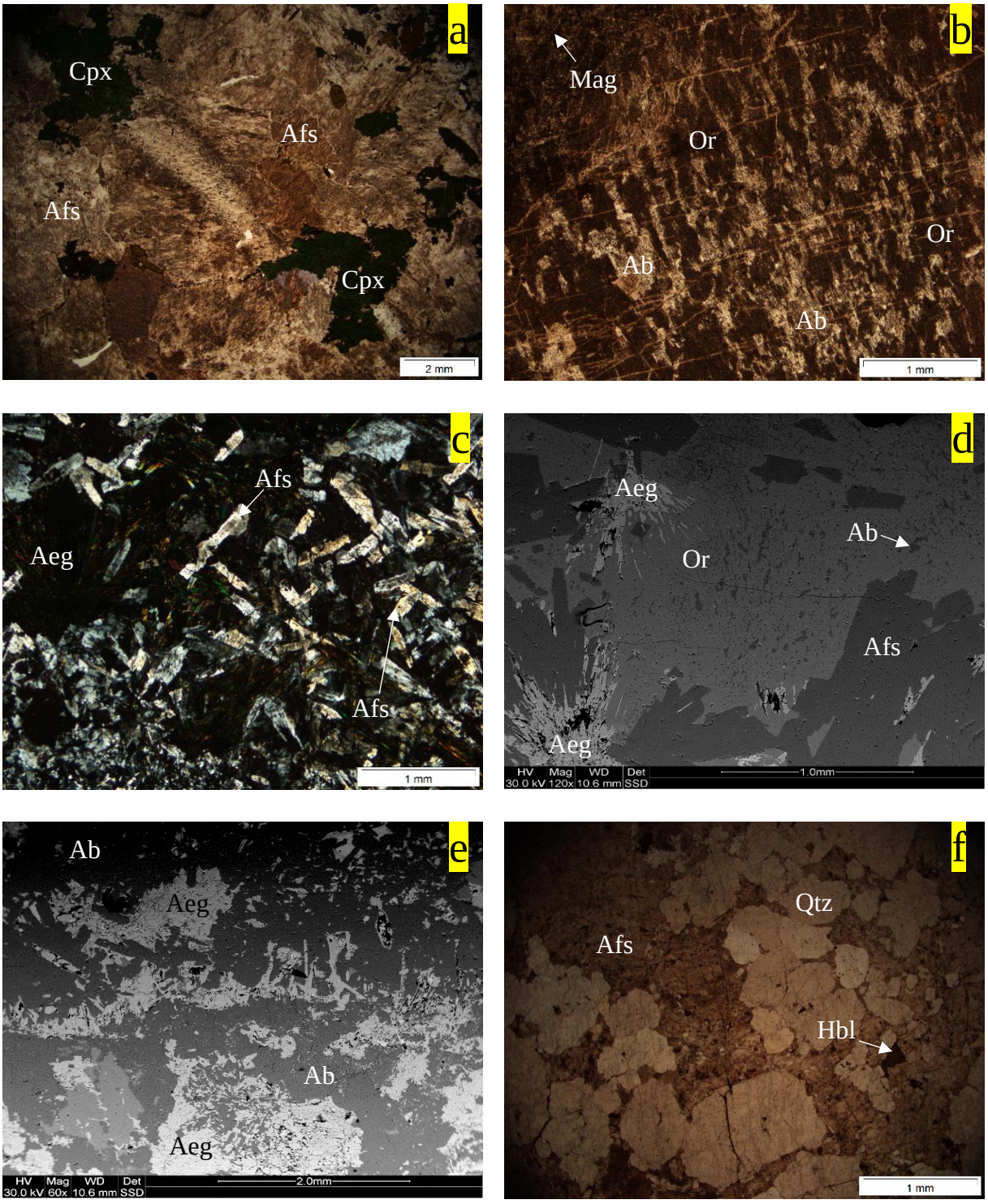
a
Cpx
Afs
Afs
Cpx
2 mm
b
Mag
Or
Or
Ab
Ab
1 mm
c
Afs
Aeg
Afs
1 mm
d
Aeg
Ab
Or
Afs
Aeg
HV Mag WD Det
30.0 kV 120x 10.6 mm SSD
1.0mm
e
Ab
Aeg
Ab
Aeg
HV Mag WD Det
30.0 kV 60x 10.6 mm SSD
2.0mm
f
Qtz
Afs
Hbl
1 mm

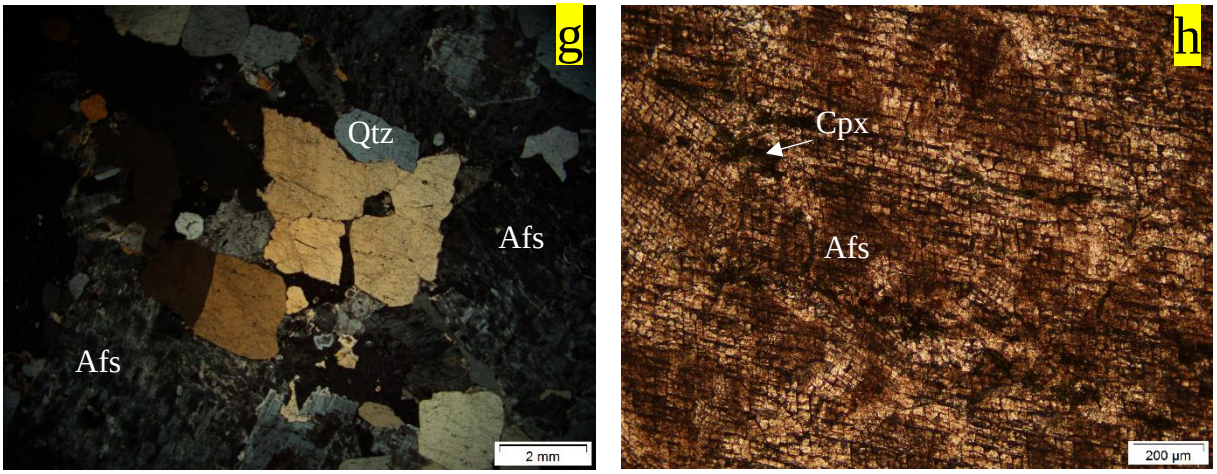

Figure 3. 11: Minerals and textures in feldspar fenite and quartz feldspar fenite (a) PPL image showing coarse-grained subhedral perthitic feldspar and coarse-grained anhedral clinopyroxene. Sample 4-48-4. (b) PPL image showing coarse-grained altered patch perthitic feldspar with domains of K and microcline and albite with some fine-grained anhedral magnetite grains. Sample 5-52-1. (c) XPL image showing radiating clusters of needle-like aegirines and tabular-shaped medium-grained alkali feldspars. Sample 4-48-10. (d) BSE image showing coarse-grained microcline with albite inclusions, and radiating clusters of needle-like coarse-grained aegirine. Sample 5-50-1. (e) BSE image showing coarse-grained anhedral-subhedral albite crystals and subhedral aegirines, note that there is no K-spar in this zone. Sample 5-50-1. (f) PPL image showing coarse-grained subhedral alkali feldspar, medium- to coarse-grained anhedral to subhedral quartz crystals with fine-grained anhedral clinopyroxene and medium-grained anhedral hornblende. Sample 5-56-2. (g) XPL image of coarse-grained anhedral to subhedral quartz with coarse-grained alkali feldspar. Sample 5-56-1. (h) PPL image showing a clinopyroxene vein within a coarse-grained perthitic feldspar. Sample 5-56-1. Perthitic feldspar (Afs), clinopyroxene (Cpx), microcline (Mc), albite (Ab), magnetite (Mag), aegirine (Aeg), quartz (Qtz), hornblende (Hbl).

Metasomatic alteration of plagioclase and quartz possibly to nepheline is only observed in some quartz-feldspar fenite samples (Fig. 3.12a and Fig 3.12b). The same alteration textures are not seen in the feldspar fenite.

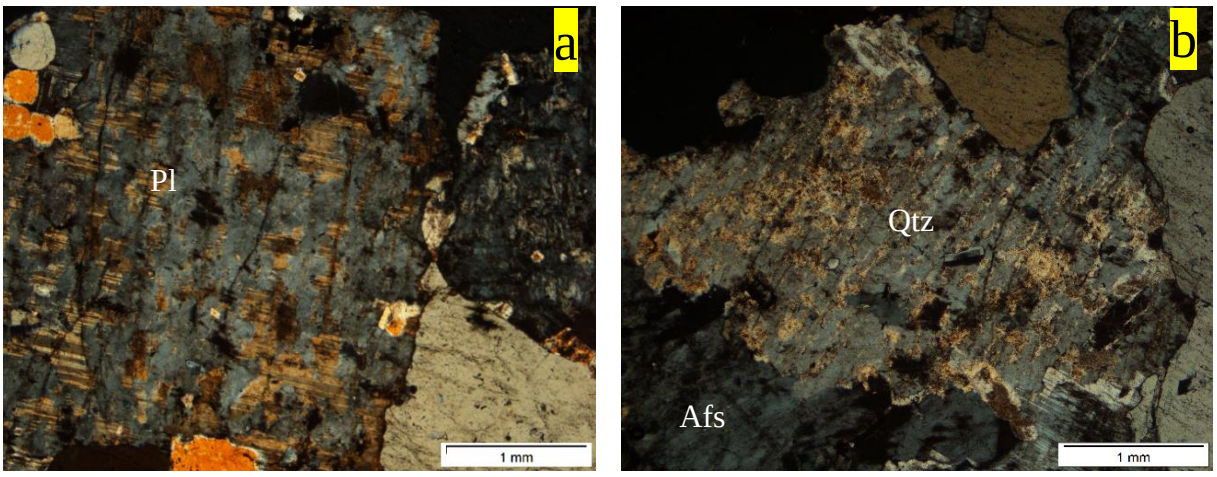

Figure 3. 12: Metasomatic alteration textures in quartz-feldspar fenite (a) XPL image showing an alteration of coarse-grained subhedral plagioclase feldspar of the Bushveld Nebo granite. Note that the altered anhedral mineral may be nepheline. Sample 5-56-1. (b) XPL image showing the alteration of coarse-grained subhedral quartz of the Bushveld Nebo granite possibly to nepheline. Sample 5-56-1. Plagioclase (Pl), quartz (Qtz).

3.6 Conclusion of Metasomatic Alteration

Nearly all dolomites of the carbonatite are interpreted as the result of the replacement of early calcite. This replacement occurred in two stages: In the first stage, a few of the calcite crystals are totally replaced by dolomite, and the others only show dolomite rims. In the second stage, the same replacement of calcite to dolomite occurred, however it is only observed in SEM-EDS, showing dark-coloured dolomite rims around light-coloured calcite and dolomite (Fig. 3.3b).

As can be seen in section of alteration assemblages of mafic fenites, the main metasomatized products are nepheline and aegirine, however these minerals are also the primary minerals of nepheline syenites. In some of the thin sections, nepheline and analcite are found together, which is an indication of partly metasomatic alteration of nepheline syenite, because nepheline tends to be altered to analcite during metasomatism (Fall et. al, 2007).

Ijolite in the Spitskop Complex is characterized by equal amounts of euhedral equant nepheline crystals and euhedral acicular clinopyroxenes, whereas mafic fenites consist of anhedral nepheline and anhedral-subhedral clinopyroxene. So although optically, ijolite can be distinguished from mafic fenite, it is impossible to separate them in the field.

In some thin sections of mafic fenites, the trace of Upper Zone gabbros are seen, and therefore the comparison of mafic fenites with the Upper Zone gabbros can be made.

In addition to fluids altering the Bushveld mafic rocks, the fluids emanating from the alkaline intrusions and/or carbonatites have also altered the Bushveld granite resulting in two types of granitic fenite. Quartz is common in quartz-feldspar fenite (Fig. 3.11f and Fig. 3.11g), and not in feldspar fenite (Fig. 3.11a-e), because the effect of metasomatism decreases from north to south. Additionally, aegirine is common in feldspar fenite, however there are no aegirine crystals in the quartz-feldspar fenite.

3.7 Discussion on Alteration Assemblages

Metasomatic alteration and mineral transformation are not always traceable, because most of the time only the final form of the minerals is seen in thin sections. However, sometimes the remnants of the original mineral are found together with the new metasomatic mineral, and this gives a unique opportunity to understand the sequence of processes that have taken place during metasomatism.

Thin section petrography demonstrates that a few analcite veins and zones and some sodalite crystals are found near nepheline within the ijolite. Secondly SEM-EDS results show an alteration of nepheline to analcite and sodalite. Therefore analcite and sodalite may be the metasomatic alteration products of nepheline, and the reaction between them is:

$NaAlSiO_4 + H_4SiO_4 \rightarrow NaAlSi_2O_6.H_2O + H_2O$

nepheline from fluid analcite

$6\ Na_4(Al_4Si_4O_{16}) + 8NaCl \rightarrow 4\ Na_8(Al_6Si_6O_{24})Cl_2$

nepheline from fluid sodalite

Additionally, Drüppel et. al (2005) demonstrated in their study that Na-rich fluids from carbonatites may transform nepheline to sodalite, whereas Fall et. al (2007) showed that saline fluids may transform nepheline to analcite.

Transparent nephelines are the earliest crystallizing phase in both the Mare- and Spitskop Hills igneous rocks and clinopyroxenes are the latest crystallizing phase within the nepheline syenites. Analcite is also common as an alteration product of nepheline.

It is very hard to understand the genesis of mafic fenites. Fortunately some of the thin sections give some mineralogical clue of the original unmetasomatized rock. The Upper Zone ferrogabbros of the Bushveld Complex variably contain plagioclase, ortho- and clinopyroxene and magnetite plus cumulus fayalite and cumulus apatite in certain zones. During alteration plagioclase is replaced by nepheline or analcite, orthopyroxene and fayalite are replaced by clinopyroxene, and clinopyroxene is replaced by sodic clinopyroxene, such as aegirine. The remnants of plagioclase from the ferrogabbro are also noted. The other parts of the thin section contain anhedral nephelines and aegirine-augite.

The alteration reactions of the mafic fenites are shown below:

$-(CaAl_2Si_2O_8 + NaAlSi_3O_8) + (MgSiO_3 + FeSiO_3) + 3Na? \rightarrow 3\ NaAlSiO_4 + (Na, Ca)(Fe, Mg, Al)Si_2O_6$

plagioclase orthopyroxene from fluid nepheline aegirine-augite

$-\ Ca(Mg, Fe^{2+})Si_2O_6 + Na^+ + Fe^{3+} \rightarrow NaFe^{3+}Si_2O_6 + 0{,}5\ Mg^{2+} + 0{,}5\ Fe^{2+} + Ca^{2+}$

augite from fluid aegirine

Even in the same outcrop two different metasomatic evolutions and progressive alteration of the feldspar are observable in the feldspar fenite. Therefore there is a gradual metasomatism in feldspar fenite and this event can occur even over a small distance.

Chapter 4.

Geochemistry

In this geochemistry chapter, the whole rock geochemistry of the rocks of the Spitskop Complex, associated fenites derived from Bushveld Upper Zone gabbros-ferrogabbros and Bushveld Nebo Granites will be presented and discussed. This is based on a suite of samples collected in the field, crushed, milled and analysed by XRF and ICP-MS for major, minor and trace elements. Full details of samples and the results of the analysis are presented in supplementary data. A summary of the different rock types analysed is shown in Table 5:

Table 5: Total number of samples of rocks of the Spitskop Complex and number of the samples that are used for XRF and ICP-MS analysis.

Rock Type	Number of Samples	XRF	ICP-MS
Calcite carbonatite	7	4	4
Calcite-dolomite carbonatite	3	3	3
Dolomite carbonatite	8	6	6
Nepheline syenite	13	6	6
Ijolite	3	1	1
Mafic fenites	57	7	7
Granitic fenites	27	7	7

The main reason for sampling and analysing these rocks is to gain a new and better geochemical perspective for metasomatic alteration processes. With the XRF and ICP-MS results it was expected to see some elemental correlations and differences between different types of rocks, especially the mafic- and granitic fenites.

Previous geochemical work on the Spitskop Complex includes the work of Harmer (1992) who worked on the geochemistry of the Spitskop Complex and some of his data is also used in this chapter. Briefly, he undertook whole-rock elemental- and isotopic analyses of ijolite, nepheline syenite and carbonatite of the Spitskop Complex and mineral chemistry of clinopyroxene, alkali feldspar and nepheline of the ijolite and the nepheline syenite. Additionally, Ionov and Harmer (2002) undertook an extensive trace element- and rare earth element analysis of the calcite-dolomite carbonatite. They analysed different carbonate minerals, mainly primary- and interstitial calcite and dolomite crystals, magnetite and apatite of the calcite-dolomite

carbonatite, and some of their results will be briefly discussed in the section on trace element geochemistry.

The first part of this chapter describes and discusses the geochemistry of the rocks of the Spitskop Complex, carbonatites and nepheline syenites. The second part is concerned with the geochemistry of the metasomatically altered rocks and their parental unmetasomatized rocks, the mafic fenites compared with the Upper Zone rocks of the Bushveld Complex and the granitic fenites compared with Bushveld Nebo Granites.

4.1 Carbonatites

4.1.1 Major element geochemistry

According to the chemical classification of carbonatites (Woolley and Kempe, 1989) the ratio (CaO/(CaO + MnO + FeO + Fe_2O_3 + MgO)) discriminates between the different types of carbonatite. For carbonatites from the Spitskop Complex calcite carbonatites have a ratio between 0.87 to 0.97; whereas dolomite carbonatites are between 0.53 to 0.66. One sample has a ratio of 0.33 and therefore should fall within the ferrocarbonatite field. However, this is because of the high magnetite content of this dolomite carbonatite sample (Fig. 4.1).

Calcite-dolomite carbonatites lie between 0.79 and 0.86, which is very close to the calcite-dolomite carbonatite boundary. Although the chemical classification shows that some can be classified as dolomite carbonatite, the mineralogy supports that they should be regarded as calcite-dolomite carbonatites.

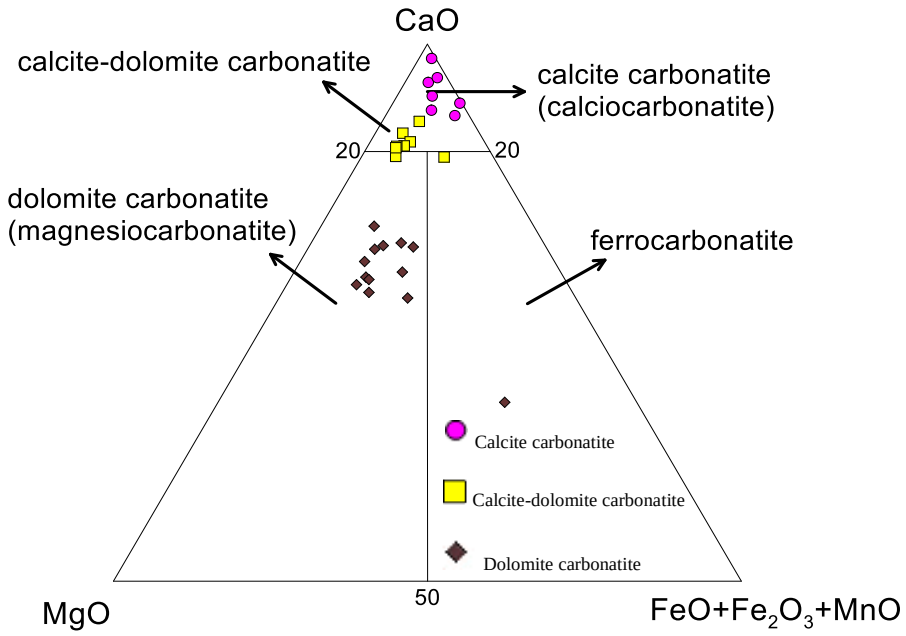

Figure 4. 1: Chemical classification of the Spitskop carbonatites. Note that there is no separate field in Woolley and Kempe's (1989) diagram for calcite-dolomite carbonatite. Harmer's (1992) data is also used.

The main difference between different kinds of carbonatite is the amount of CaO and MgO in the samples which reflects the variation in calcite and dolomite content in the carbonatite. Samples from the Spitskop carbonatite include calcite-, calcite-dolomite- and dolomite carbonatites and the major element variation of calcium and magnesium is also shown in Figure 4.2.

Different carbonatites show a linear trend on the MgO-CaO diagram. Calcite carbonatite has the highest CaO wt.% and the lowest MgO wt. %., whereas dolomite carbonatite has the lowest CaO wt.% and the highest MgO wt. %, and the calcite-dolomite carbonatites are located between these two carbonatites in the diagram (Fig. 4.2a). CaO content ranges from 48.79 to 55.41 wt. % for calcite carbonatite, from 44.42 to 48.23 wt. % for calcite-dolomite carbonatite and from 28.78 to 35.32 wt. % for dolomite carbonatite. MgO content ranges from 0.2 to 3.06 wt. % for calcite carbonatite, from 4.49 to 8.7 for calcite-dolomite carbonatite and from 11.99 to 17.66 wt. % for dolomite carbonatite. Dolomite carbonatite contains more MnO than the other carbonatites, however the distribution is dispersed (Fig. 4.2b).

The major element geochemistry of the Spitskop Complex is very limited because SiO_2, Al_2O_3, Na_2O, K_2O and TiO_2 contents are close to zero, and Fe_2O_3, FeO and P_2O_5 contents do not show any specific trends. The SiO_2 content of the carbonatites are less than 4.17 wt. %, whereas Al_2O_3, Na_2O, K_2O and TiO_2 are less than 1 wt. %.

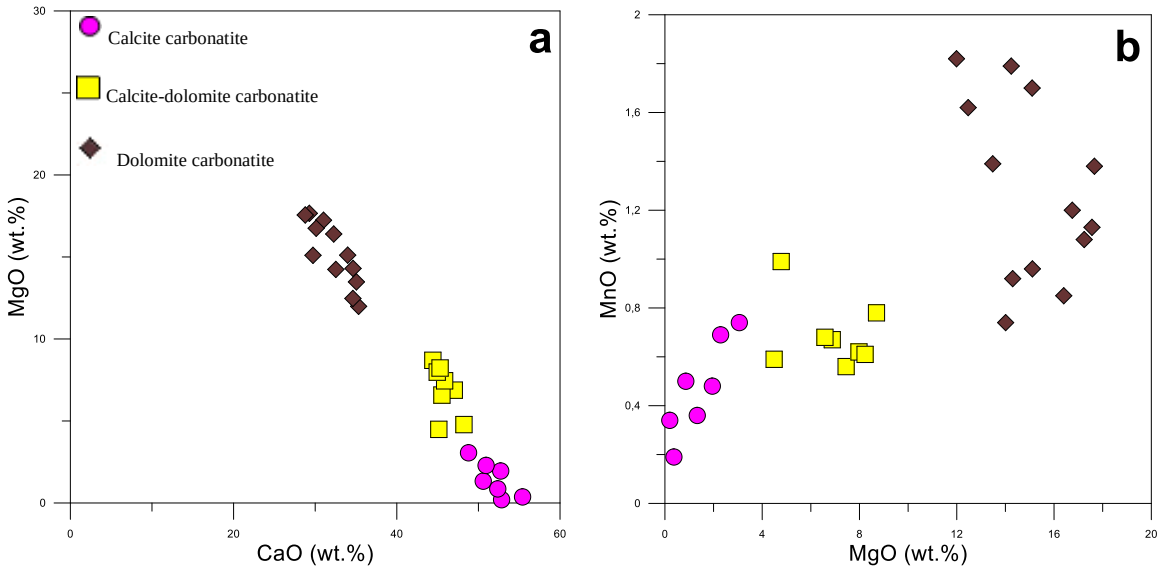

Figure 4. 2: Selected Harker diagrams of major element compositions of the Spitskop carbonatites. (a) MgO versus CaO contents, (b) MnO versus MgO contents.

4.1.2 Trace element geochemistry

Trace element averages of the carbonatites from the most abundant elements to the least abundant elements are shown in Table 6. The carbonatites exhibit a significant variation in Sr content from 261 to 2571 ppm with an average of 1273 ppm. Calcite carbonatite is the most Sr-enriched rock, with an average of 1827 ppm, whereas dolomite carbonatite has an average of 1149 ppm. Calcite-dolomite carbonatite is the least Sr-enriched rock with an average of 989 ppm.

Ba contents are also very variable from 11 to 989 ppm with an average of 205 ppm. The highest Ba contents are found in calcite carbonatite with an average of 495 ppm, whereas averages for calcite-dolomite carbonatite and dolomite carbonatite are 149 and 83 ppm respectively. Together with Sr and Ba, the next most abundant trace elements in the carbonatites are Y, Zn, Nb, Sc and Pb which occur with abundances between 30 to 80 ppm.

Cu, Th, Rb, Co, Ni, Ga and Mo are the least enriched elements in carbonatites with less than 10 ppm. Zr, V, Cr and U are also found in very minor amounts between 10 to 20 ppm.

Table 6: Trace element averages of all carbonatites, calcite carbonatite, calcite-dolomite carbonatite and dolomite carbonatite from the most enriched elements to the least enriched elements.

Elements	Average	Cal. Carb. Ave.	Cal-Dol. Carb. Ave.	Dol. Carb. Ave
Sr	1273 ppm	1827 ppm	989 ppm	1149 ppm
Ba	205 ppm	495 ppm	149 ppm	83 ppm
Y	77 ppm	75 ppm	62 ppm	87 ppm
Zn	61 ppm	21 ppm	33 ppm	99 ppm
Nb	48 ppm	8 ppm	5 ppm	90 ppm
Sc	34 ppm	48 ppm	44 ppm	26 ppm
Pb	29 ppm	18 ppm	28 ppm	35 ppm
Zr	20 ppm	15 ppm	19 ppm	23 ppm
V	15 ppm	20 ppm	17 ppm	12 ppm
Cr	12 ppm	16 ppm	11 ppm	12 ppm
U	12 ppm	3 ppm	6 ppm	20 ppm
Cu	10 ppm	13 ppm	8 ppm	8 ppm
Th	9 ppm	5 ppm	7 ppm	14 ppm
Co	5 ppm	7 ppm	5 ppm	4 ppm
Rb	2 ppm	2 ppm	2 ppm	2 ppm

Ni	2 ppm	2 ppm	2 ppm	3 ppm
Ga	1 ppm	2 ppm	< 1 ppm	< 1 ppm
Mo	< 1 ppm	< 1 ppm	1 ppm	< 1 ppm

Chondrite-normalized multi-element diagrams have been used to look at the variation in abundances in a range of trace elements within the carbonatites. All of the diagrams and patterns are very similar and they illustrate that there is very little difference between trace element abundance patterns for the three different types of carbonatite. Calcite carbonatite and calcite-dolomite carbonatite are depleted in V, Cr, Co, Ni, Cu, Zn, Ga, Rb and Mo relative to chondrite, whereas they are enriched in Sc, Sr, Y, Nb, Ba, Pb, Th and U (Fig. 4.3a and 4.3b). The Zr value is almost the same as the chondrite values. Dolomite carbonatites show a depletion in the same elements as the calcite- and calcite-dolomite carbonatite, and they are strongly enriched in Sr, Y, Nb and U (Fig. 4.3c). On average, all three carbonatites show similar patterns in terms of trace elements abundances, however calcite carbonatite shows an enrichment in Ga and Ba, and dolomite carbonatite is more enriched in Zn, Nb, Th and U, and is depleted in Cr relative to other carbonatites (Fig. 4.3d).

Figure 4.3 shows that the high field strength elements Th, U, Pb and REEs are compatible in carbonatites and these elements are most compatible in dolomite carbonatite. The large ion lithophile element Ba, is mostly compatible in calcite carbonatite and Sr is compatible in all carbonatites, whereas the high field strength element Nb, is only compatible in dolomite carbonatite. Incompatible elements in carbonatites are the large ion lithophile element Rb and high strength element Zr. Ba is also incompatible in dolomite carbonatite.

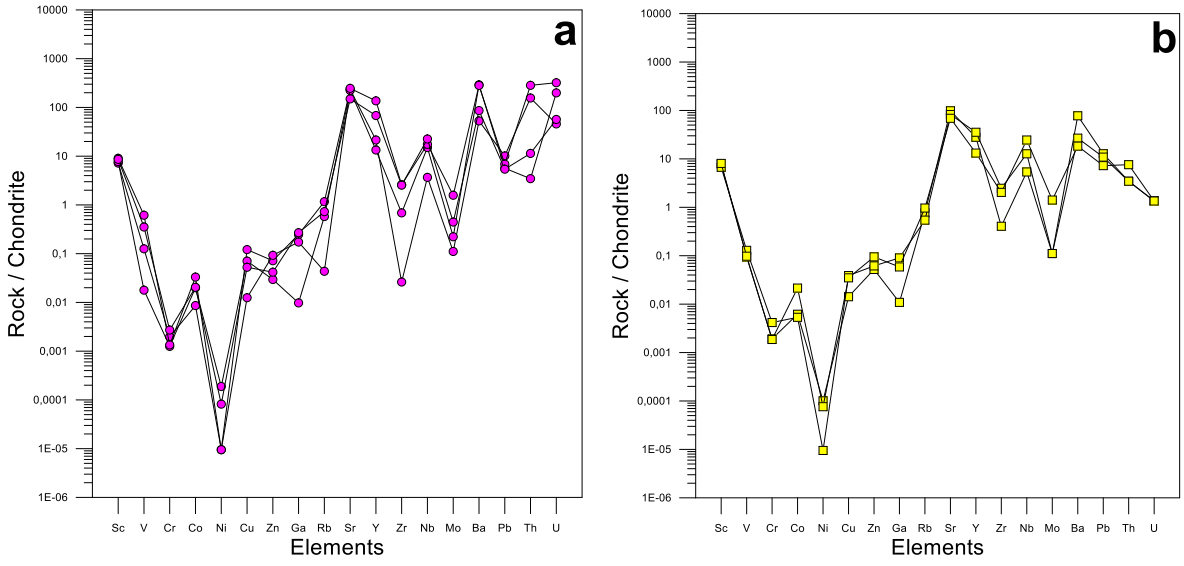

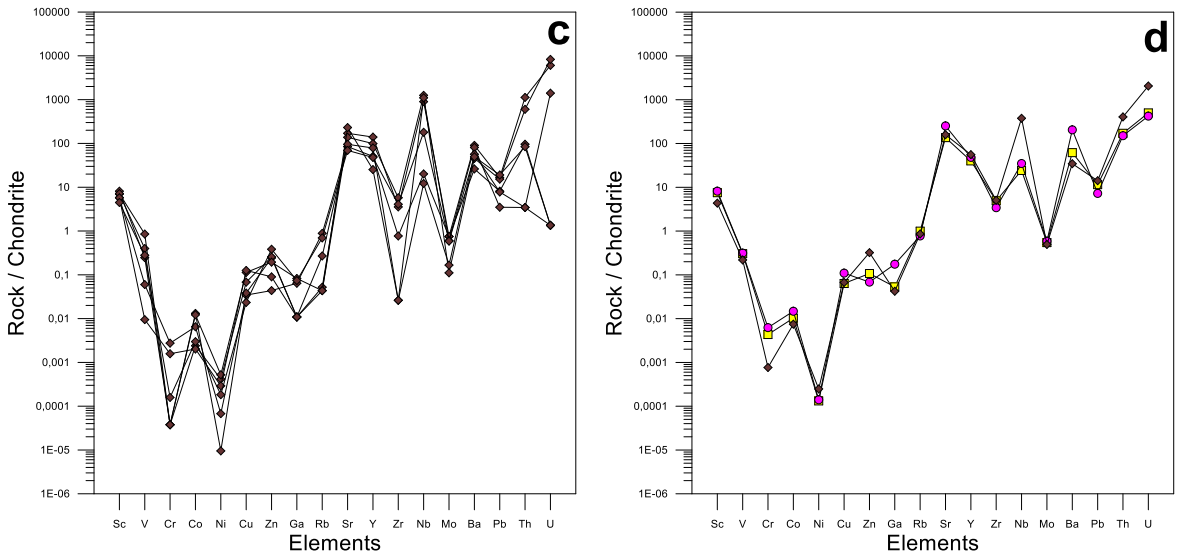

Figure 4. 3: Chondrite-normalized trace element abundance diagrams for whole rocks of (a) calcite carbonatite, (b) calcite-dolomite carbonatite, (c) dolomite carbonatite and (d) the average abundances. Chondrite values are taken from McDonough and Sun (1995).

Correlations between selected trace elements and also between trace elements and MgO have been investigated using binary Harker diagrams. These show that there are positive correlation trends between Co and Sc, between Zn and Pb (Fig. 4.4a and 4.4b), and between Pb and MgO (Fig. 4.4c). The relationship between Co and Sc is interesting, in the dolomite carbonatite the slope of the trend is low, however in the other two carbonatites the slope is steeper. Additionally, there is a negative correlation between Co and MgO, although there is quite a lot of scatter in the individual points (Fig. 4.4d). All of these diagrams show discrimination between the different types of carbonatite, other trace elements do not show any significant pattern.

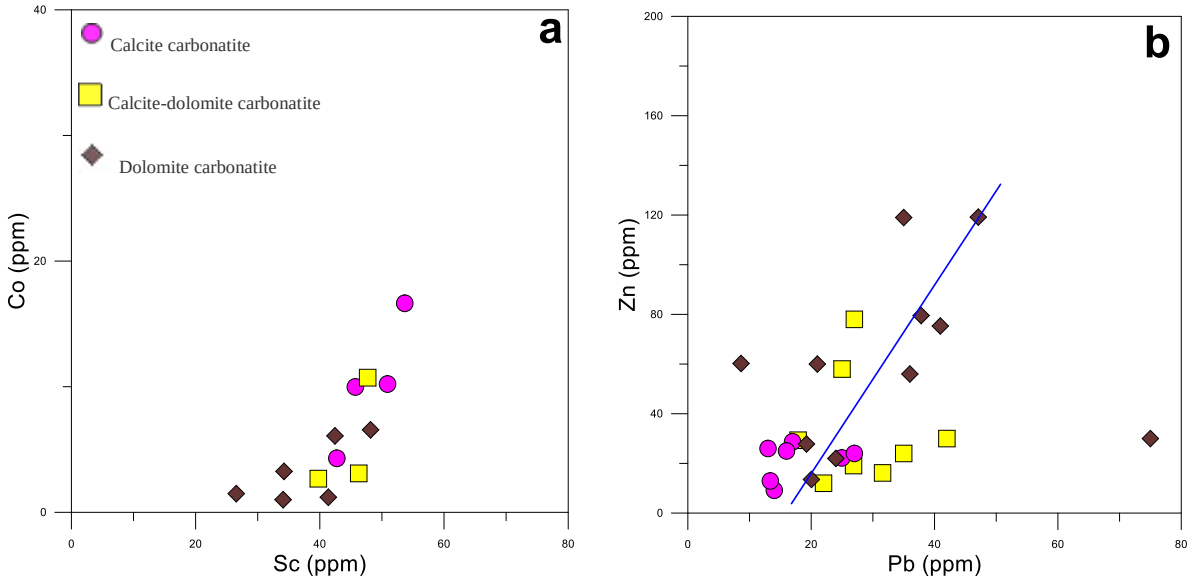

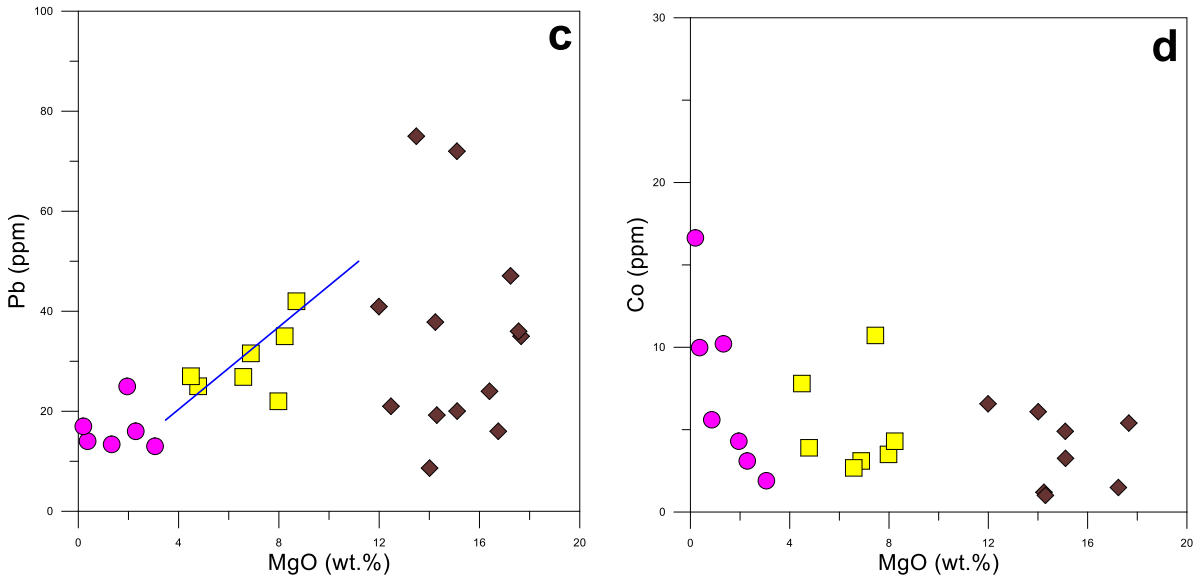

Figure 4. 4: Selected Harker diagrams of trace element compositions in the Spitskop calcite carbonatite, calcite-dolomite carbonatite and dolomite carbonatite. (a) Co versus Sc contents, (b) Zn versus Pb contents, (c) Pb versus MgO contents and (d) Co versus MgO contents.

4.1.3 REE geochemistry

The REE content of the carbonatites is greater than the other rocks of the Spitskop Complex. Nevertheless, they do not contain enough REE to be considered as economically important.

The average total REE contents for the different carbonatites are shown in Table 7, which shows that the dolomite carbonatite is the most REE-enriched carbonatite while calcite carbonatite is the least REE-enriched. The ratio between total REE average and total LREE average of the carbonatites are very similar for all the carbonatite types; 1.09 for calcite carbonatite, 1.07 for dolomite carbonatite and 1.05 for calcite-dolomite carbonatite.

Table 7: Carbonatite types and their total REE-, LREE- and HREE averages.

Rocks	TREE Average	LREE Average	HREE Average
Calcite carbonatite	428.3 ppm	390.5 ppm	37.8 ppm
Cal-Dol. carbonatite	714.4 ppm	682.2 ppm	32.2 ppm
Dolomite carbonatite	739.5 ppm	689.5 ppm	50 ppm

Chondrite-normalized REE patterns for all the carbonatites show a similar, relatively steep fractionated pattern. Some calcite carbonatite samples show an enrichment in HREE, especially Dy and Ho (Fig. 4.5a). The calcite-dolomite carbonatites have higher LREE contents than the calcite carbonatite, although the HREE contents can sometimes show similar patterns (Fig. 4.5a and 4.5b). Typically the HREE contents of calcite-dolomite carbonatites are lower than the calcite carbonatite (Table 7). The dolomite carbonatite

analyses show elevated levels of all REE compared to the other two carbonatite types, however some samples are similar to the calcite carbonatite in terms of their enrichment in HREE. The content of LREE is less varied than the HREE (Fig. 4.5a-c).

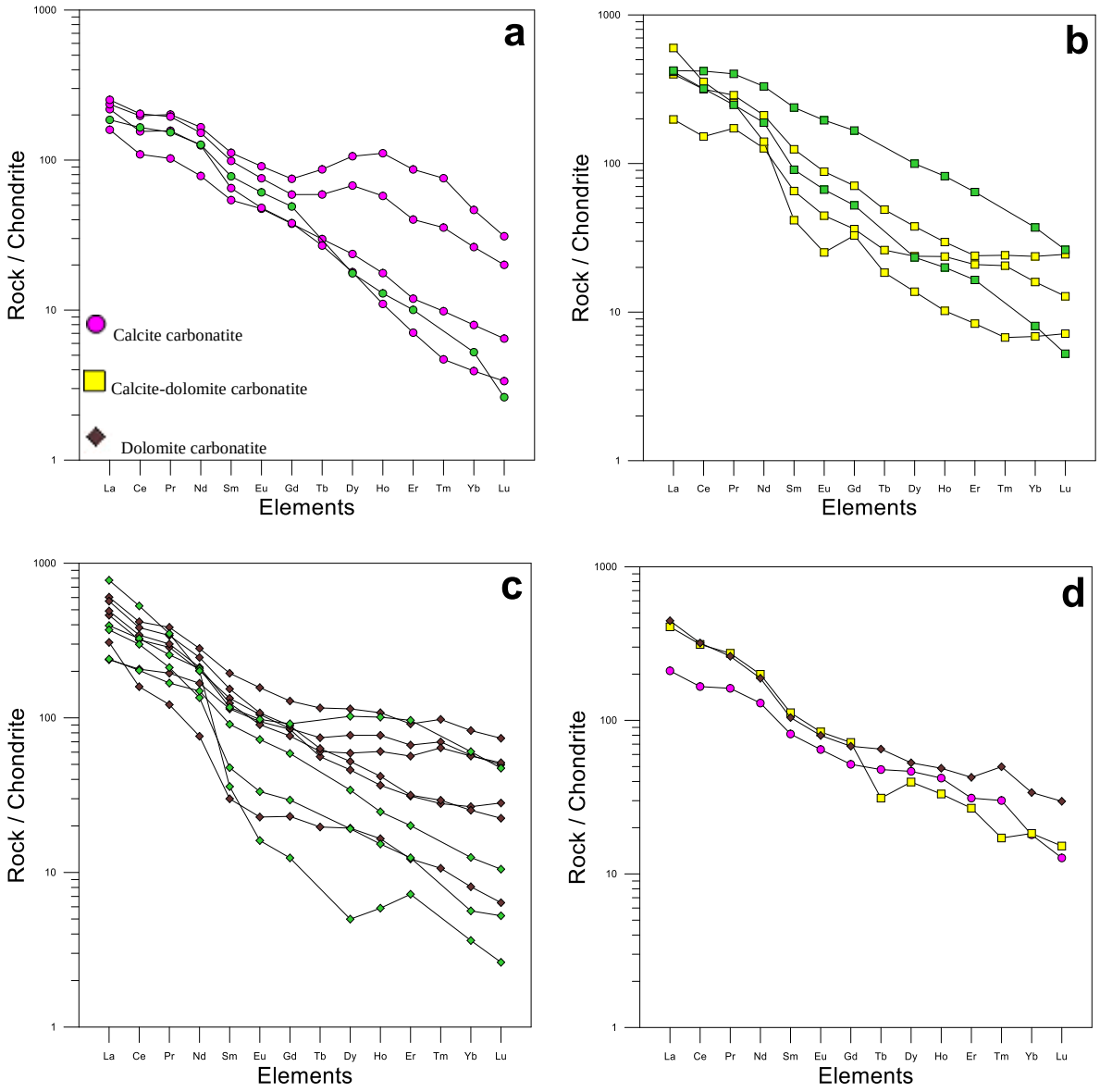

Figure 4. 5: Chondrite-normalized REE diagrams of (a) calcite carbonatite, (b) calcite-dolomite carbonatite, (c) dolomite carbonatite and (d) average of the carbonatites of the Spitskop Complex. Chondrite values are taken from Sun and McDonough (1989). Note that samples of Harmer (1992), which contain all REE data are shown as green in diagrams.

4.2 Nepheline Syenites and Ijolite

Nepheline syenites of the Spitskop Complex (Spitskop Hill nepheline syenites and Mare Hill nepheline syenites) are compared with the nepheline syenites of the Pilanesberg Complex, because both of the localities are part of the Pilanesberg Alkaline Province and their ages are similar (1341 Ma for Spitskop (Harmer, 1999) and 1395 Ma for the Pilanesberg Complex (Elburg and Cawthorn, 2017). The Pilanesberg Complex is located approximately 290 km west

of the Spitskop Complex. Geochemical data of Pilanesberg nepheline syenites (56 analyses) have been taken from Elburg and Cawthorn (2017). Nepheline syenite data from Harmer (1992) have also been used for the comparison (39 analyses).

4.2.1 Major element geochemistry

The chemistry of Spitskop-Mare nepheline syenite is very consistent and there is little variation, it is comparable with published data from the Pilanesberg. Most major elements, (Al_2O_3, MgO, CaO, TiO_2, P_2O_5 and Na_2O + K_2O) decrease with increasing SiO_2 content (Fig. 4.6a-g). Additionally, the Na_2O content increases with decreasing K_2O (Fig. 4.6 b). In contrast, CaO and MgO contents are associated with enrichment in Al_2O_3 (Fig. 4.6h and 4.6i) and P_2O_5 increases with increasing TiO_2 content, although this data is quite scattered (Fig. 4.6j). All diagrams show that there is very little difference in major elements between the Mare nepheline syenite and Spitskop nepheline syenite.

Conversely, the Pilanesberg nepheline syenites are more dispersed in terms of major element composition and in most cases they do not show a clear linear trend compared to the Spitskop-Mare nepheline syenites (Fig. 4.6 a-j). Additionally, Spitskop-Mare nepheline syenites are more enriched in Na_2O, whereas they are depleted in MgO, CaO and TiO_2 compared to the Pilanesberg analyses.

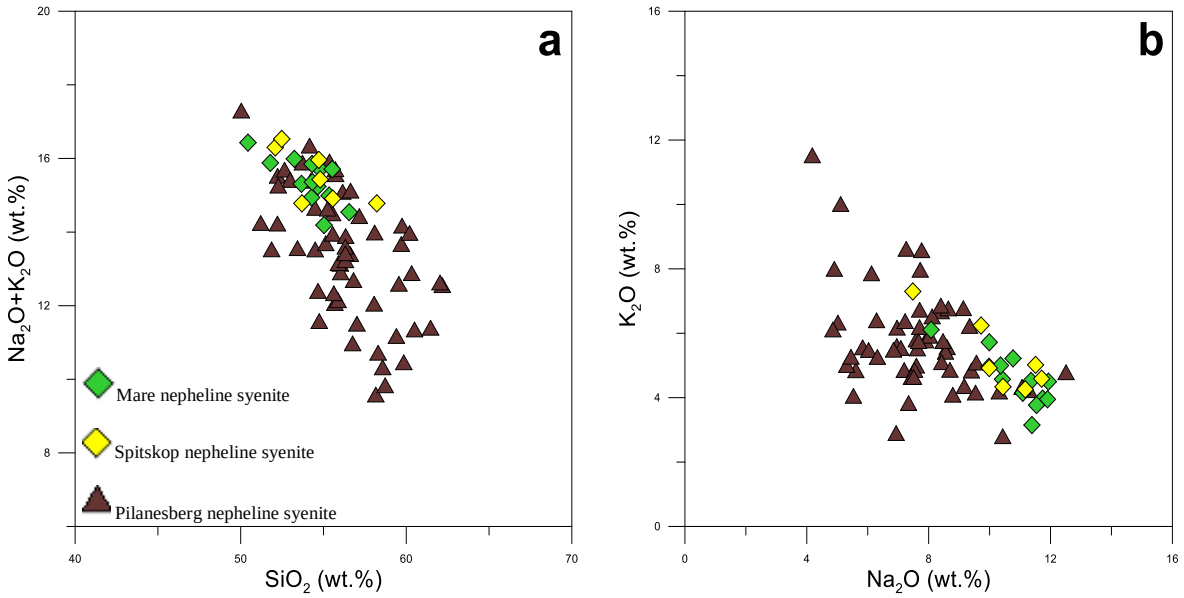

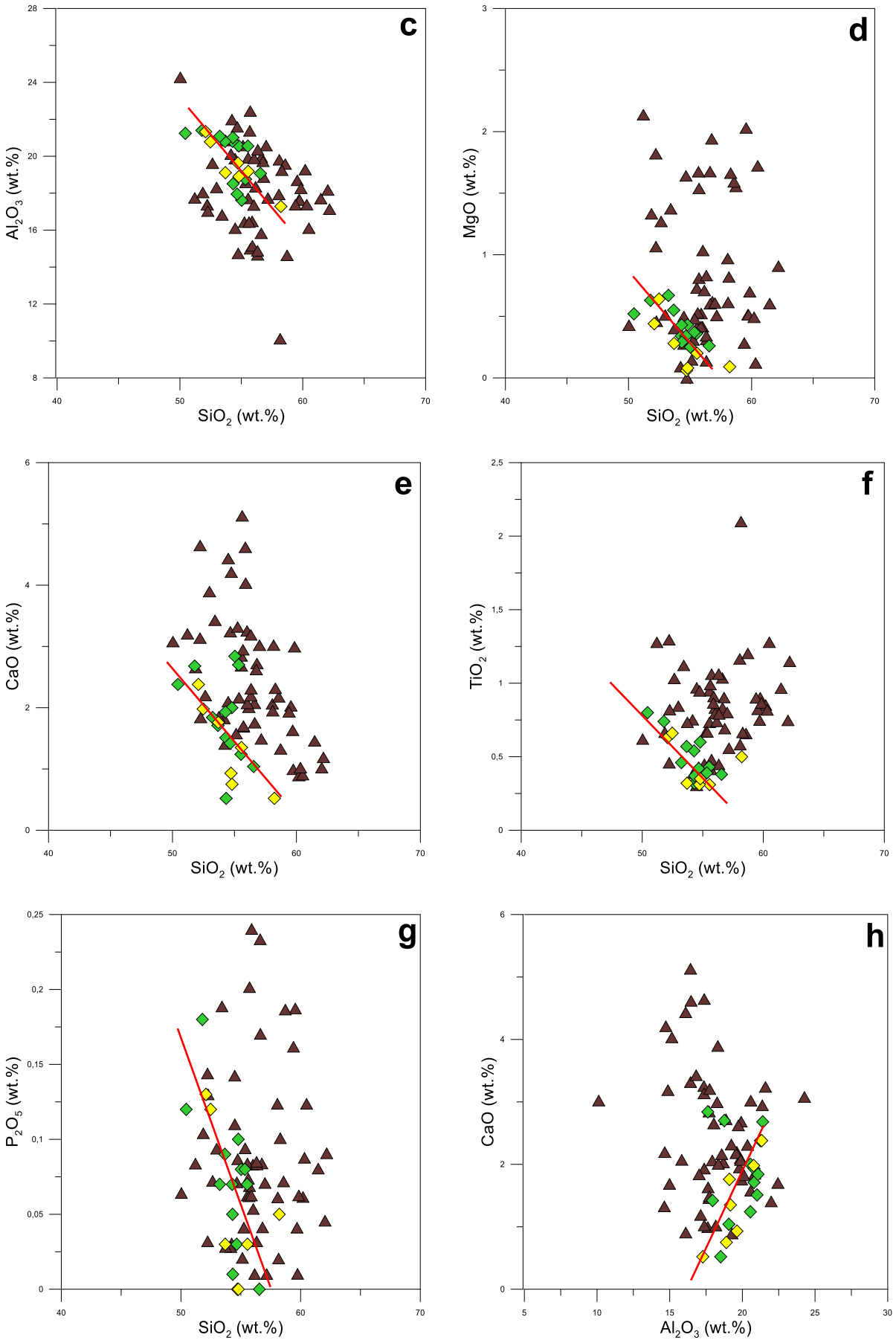
c
Al_2O_3 (wt.%)
SiO_2 (wt.%)
d
MgO (wt.%)
SiO_2 (wt.%)
e
CaO (wt.%)
SiO_2 (wt.%)
f
TiO_2 (wt.%)
SiO_2 (wt.%)
g
P_2O_5 (wt.%)
SiO_2 (wt.%)
h
CaO (wt.%)
Al_2O_3 (wt.%)

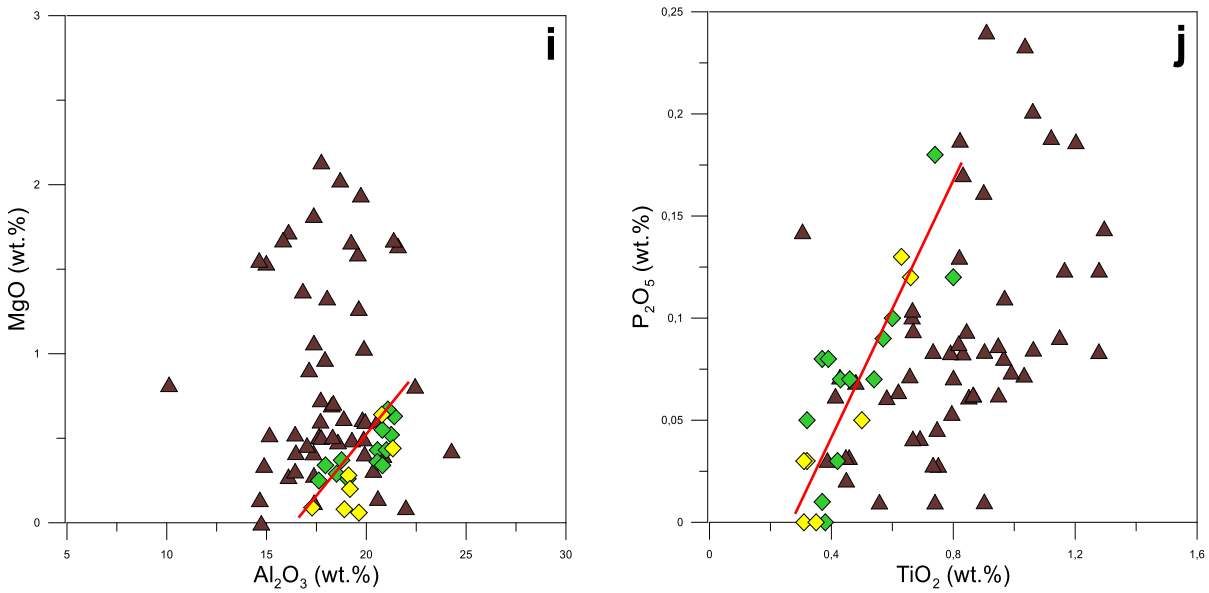

Figure 4. 6: Selected Harker diagrams of major element composition of the Mare nepheline syenite, Spitskop nepheline syenite and Pilanesberg nepheline syenite. (a) Na_2O+K_2O versus SiO_2 contents, (b) K_2O versus Na_2O contents, (c) Al_2O_3 versus SiO_2 contents, (d) MgO versus SiO_2 contents, (e) CaO versus SiO_2 contents, (f) TiO_2 versus SiO_2 contents, (g) P_2O_5 versus SiO_2 contents, (h) CaO versus Al_2O_3 contents, (i) MgO versus Al_2O_3 contents and (j) P_2O_5 versus TiO_2 contents. Pilanesberg nepheline syenite data are from Elburg and Cawthorn (2017).

4.2.2 Trace element geochemistry

Trace element geochemistry of Mare Hill, Spitskop Hill and Pilanesberg nepheline syenites is compared with published data from the Rietfontein nepheline syenites (Table 8), which are located 4-5 km west of the main research area. Rietfontein nepheline syenites are therefore unlikely to have been affected by the fenitizing fluids from Spitskop. Trace element concentrations of Rietfontein nepheline syenite are generally slightly higher than the Mare and Spitskop Hill nepheline syenites, however trace element concentrations of Pilanesberg nepheline syenites are much greater than the other nepheline syenites, except for Ba and Co.

Ba and Sr are the most abundant trace elements in the Mare and Spitskop nepheline syenites with an average of 1134 ppm and 568 ppm respectively; followed by Zr and Rb.

Zn, V, Pb, Ga, Nb, Y contents range from 15 to 86 ppm, whereas Cu, Cr, Co, Th, U, Sc, Ni and Mo exhibit low abundances with typically less than 10 ppm.

Table 8: Average trace element data for nepheline syenites of Mare, Spitskop, Rietfontein and Pilanesberg in descending order of abundance. Data for the Rietfontein nepheline syenite and Pilanesberg nepheline syenite are taken from Harmer (1992) and Elburg and Cawthorn (2017) respectively.

Elements	**Mare Neph. Syenite Average**	**Spitskop Neph. Syenite Average**	**Rietfontein Neph. Syenite Average**	**Pilanesberg Neph. Syenite Average**
Ba	1357 ppm	962 ppm	1275 ppm	942 ppm
Sr	590 ppm	587 ppm	686 ppm	2182 ppm
Zr	177 ppm	193 ppm	299 ppm	2393 ppm
Rb	102 ppm	128 ppm	104 ppm	191 ppm
Zn	55 ppm	76 ppm	86 ppm	No data
V	42 ppm	34 ppm	48 ppm	99 ppm
Ga	23 ppm	26 ppm	No data	No data
Pb	22 ppm	18 ppm	16 ppm	53 ppm
Nb	20 ppm	20 ppm	24 ppm	366 ppm
Y	13 ppm	10 ppm	24 ppm	81 ppm
Cu	6 ppm	9 ppm	6 ppm	No data
Cr	6 ppm	No data	18 ppm	No data
Co	6 ppm	4 ppm	20 ppm	3 ppm
Th	4 ppm	6 ppm	7 ppm	34 ppm
U	4 ppm	5 ppm	6 ppm	13 ppm
Sc	2 ppm	2 ppm	11 ppm	4 ppm
Ni	2 ppm	1 ppm	4 ppm	2 ppm
Mo	1 ppm	1 ppm	No data	No data

The chondrite-normalized trace element patterns of the nepheline syenites show similar patterns and similar levels of enrichment for individual elements for all samples. For Spitskop and Mare nepheline syenites, there is an enrichment in abundance of Rb, Sr, Zr, Nb, Ba, Th and U (Fig. 4.7a and 4.7b). Trace element patterns of Pilanesberg nepheline syenites show similar enrichments or depletions to the Mare-Spitskop nepheline syenites (Fig. 4.7c).

The chondrite-normalized patterns of data averages from Mare, Spitskop, Rietfontein and Pilanesberg samples clearly show that the trace element patterns are very similar, however, the Pilanesberg nepheline syenites are more enriched in most of the trace elements (Fig. 4.7d).

As can be seen in Figure 4.7 some of the large ion lithophile elements, (Rb and Ba), are mostly compatible in the Spitskop-Mare as well as Rietfontein nepheline syenites. Nepheline syenites show positive anomalies of these elements 200 times greater than the primitive mantle. In addition, some of the high field strength elements, (Th, U, Ce, Pb, Zr and Nb), are also compatible. From these elements, Th, U and Pb are the most compatible HFSEs, whereas Ce, Zr and Nb are enriched only 10 to 30 times more than the primitive mantle. Most of the REEs, especially HREEs are incompatible in nepheline syenites. They show 3 to 10 times enrichment relative to the primitive mantle. Only a few LREEs show slight enrichment between 10-20 times relative to the primitive mantle.

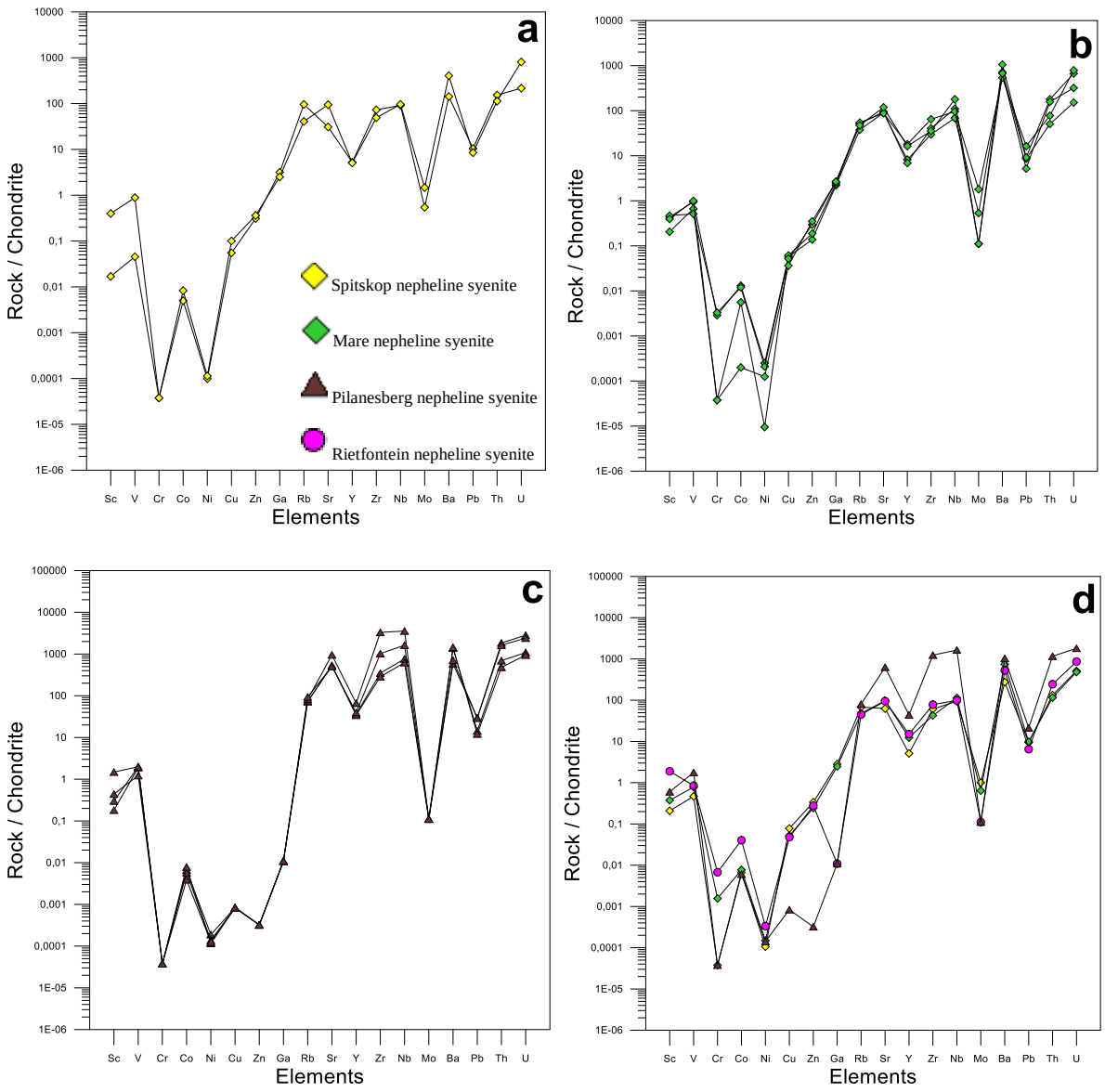

Figure 4. 7: Chondrite-normalized trace element abundance diagrams for whole rocks of (a) Spitskop nepheline syenite samples, (b) Mare nepheline syenite samples, (c) Pilanesberg nepheline syenite samples, and (d) average values of Spitskop-, Mare- and Pilanesberg nepheline syenite. Normalized values are taken from McDonough and Sun (1995).

Within the Mare nepheline syenite data there appears to be a linear relationship between LIL such as Sr and Ba and also between HFS elements such as Y and Nb. Trace element data for the Mare nepheline syenites and the Pilanesberg samples typically show little overlap between data sets with the Pilanesberg samples being enriched in Th, Sr Nb and Y relative to the Mare nepheline syenites (Fig. 4.8.a-e).

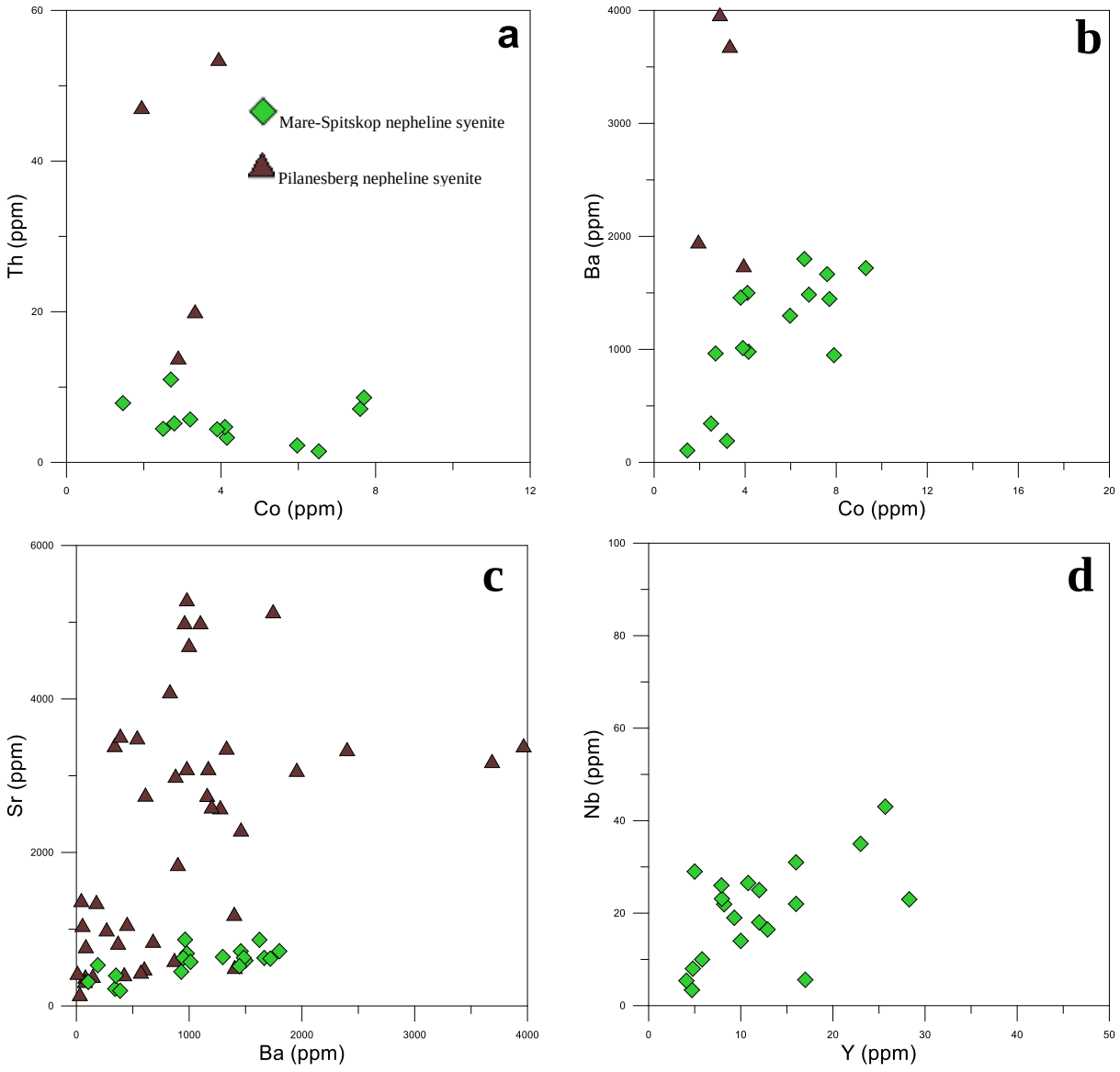

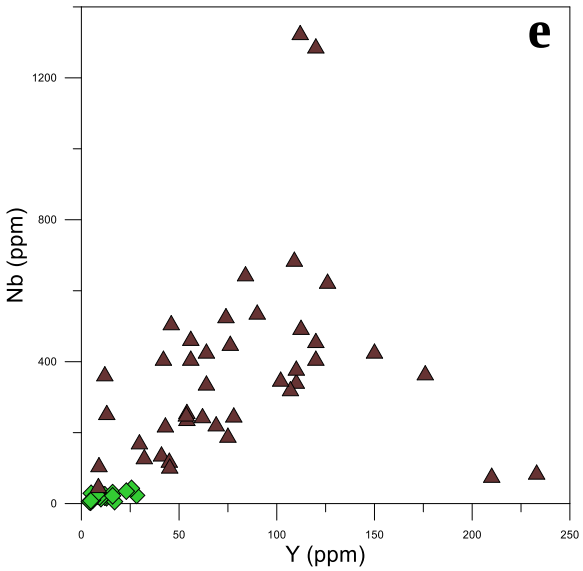

Figure 4. 8: Harker diagrams showing the trace element compositions of nepheline syenites of the Mare, Spitskop and Pilanesberg areas. (a) Th versus Co contents, (b) Ba versus Co contents, (c) Sr versus Ba contents, (d) Nb versus Y contents of Spitskop-Mare nepheline syenite, and (e) Nb versus Y contents of Spitskop-Mare and Pilanesberg nepheline syenite together. Pilanesberg nepheline syenite data are from Elburg and Cawthorn (2017).

4.2.3 REE geochemistry

Total REE abundances within the nepheline syenites lie between 58 and 129 ppm, with an average of 95.7 ppm. The average REE values of Mare and Spitskop nepheline syenites and the Rietfontein nepheline syenite clearly show that total REE of Mare and Spitskop is almost twice that of Rietfontein. The Pilanesberg data set show an even greater enrichment, ten times that of the other data. In the Mare and Spitskop nepheline syenites, the LREE have greater abundances than the Rietfontein nepheline syenites although this contains higher HREE than Mare and Spitskop (Table 9).

Table 9: Nepheline syenites and their total REE-, LREE- and HREE averages. Data for the Rietfontein nepheline syenite is taken from Harmer (1992).

Rocks	TREE Average	LREE Average	HREE Average
Mare neph. syenite	93.9 ppm	84.1 ppm	9.8 ppm
Spitskop neph. syenite	99.6 ppm	89.4 ppm	10.2 ppm
Rietfontein neph. syenite	49.3 ppm	35.8 ppm	13.5 ppm
Pilanesberg neph. syenite	1007.2 ppm	974.5 ppm	32.7 ppm

The chondrite-normalized REE diagrams of Mare- and Spitskop nepheline syenites have an uncommon shape with a concave upwards overall pattern. They show a relatively steep decrease

from La to Gd, followed by a slight increase from Gd to Lu (Fig. 4.9a and 4.9b). The Rietfontein nepheline syenites have similar REE patterns, but in addition to this, they can show a decrease from Yb to Lu, so that they display a wavy REE pattern (Fig. 4.9c). The Pilanesberg nepheline syenites show a steep fractionation pattern, with LREE contents more variable than the HREEs (Fig. 4.9d).

Average values of Spitskop and Mare nepheline syenites show a smooth trend from La to Gd and the HREEs are almost horizontal, whereas the average values of Rietfontein show a broadly horizontal pattern. The Pilanesberg nepheline syenites are much more enriched in REE compared to the nepheline syenites of the Spitskop Complex (Fig. 4.9e).

Although there is only one analysis of the Spitskop ijolite this shows a similar REE pattern to that of the Spitskop nepheline syenites (Fig. 4.9f).

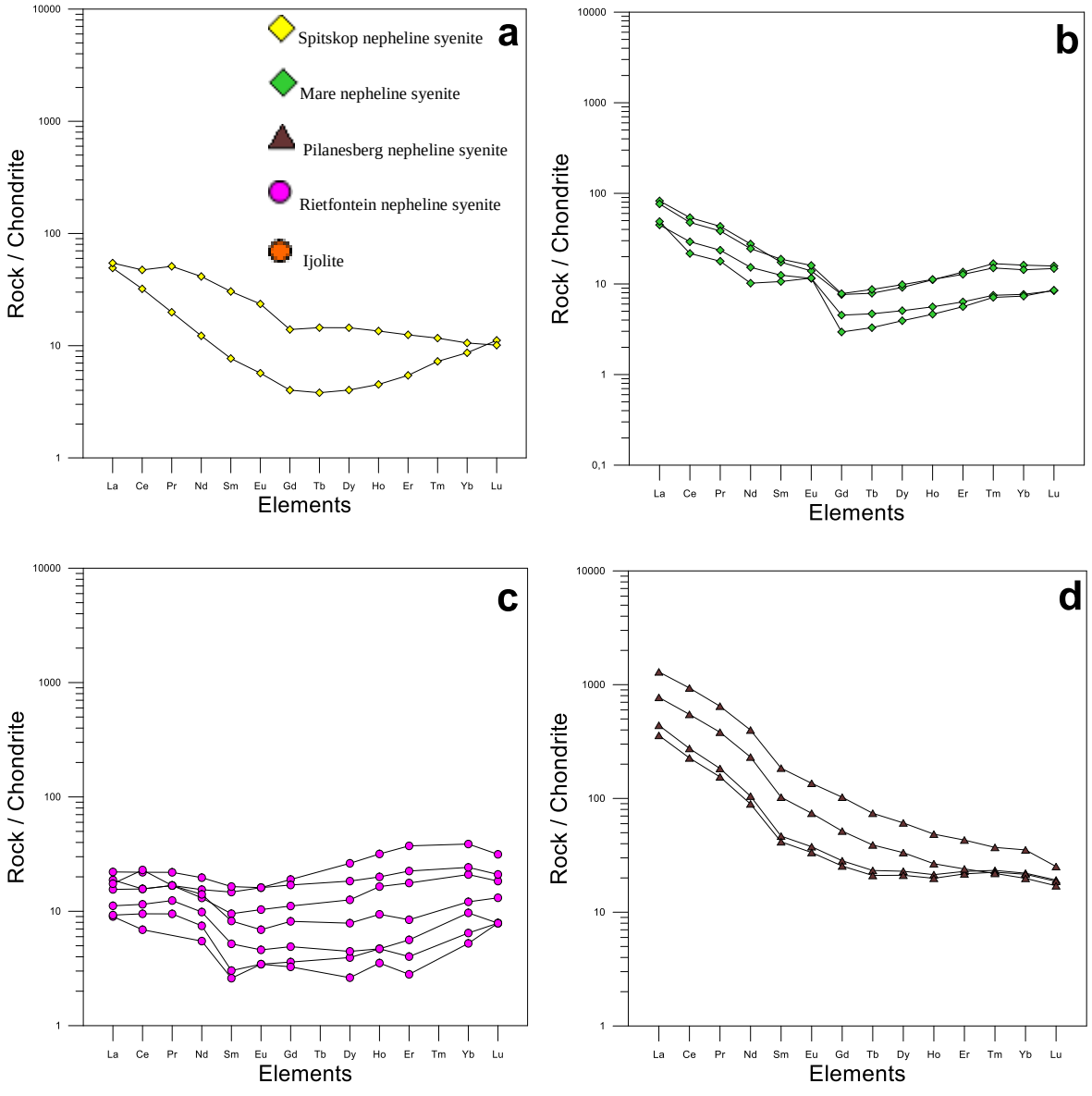

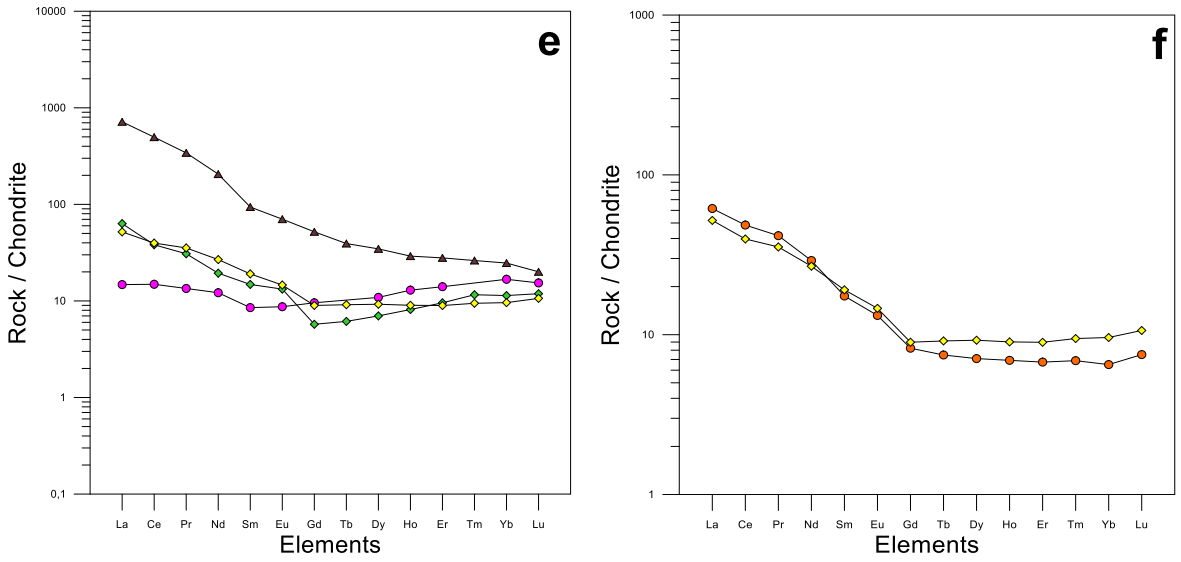

Figure 4. 9: Chondrite-normalized rare earth element diagram of (a) Spitskop nepheline syenites, (b) Mare nepheline syenites, (c) Rietfontein nepheline syenites, (d) Pilanesberg nepheline syenites, (e) average values of Spitskop, Mare, Rietfontein and Pilanesberg nepheline syenites, and (f) Spitskop nepheline syenite average and Spitskop ijolite. Pilanesberg nepheline syenite data are from Elburg and Cawthorn (2017) and Rietfontein REE data are from Harmer (1992). Chondrite values are taken from Sun and McDonough (1989).

4.3 Mafic Fenites

The geochemistry of the mafic fenites has been investigated in order to confirm the nature of the parental rock as deduced from field exposures and mineralogy and also to understand the metasomatic processes in terms of element mobility. From both field exposures and mineralogically, the mafic fenites strongly resemble Bushveld Upper Zone gabbros-ferrogabbros, therefore in this section the geochemistry of the mafic fenites of the Spitskop Complex are compared with Bushveld Upper Zone gabbros from two different localities using analyses from the literature.

For this comparison, geochemical data of Upper Zone gabbros have been taken from van Tongeren (2011) and Scoon and Mitchell (2012). Upper Zone samples of van Tongeren were obtained from Magnet Heights, eastern Bushveld, which is located approximately 30 km northeast of the Spitskop Complex, whereas other Upper Zone gabbro analyses, taken from Scoon and Mitchell (2012), are from the Roossenekal area, eastern Bushveld, approximately 20 km southeast of Spitskop. These localities are chosen because both of them are close to the Spitskop Complex and the geochemical results are well defined. There are 19 analyses from Scoon and Mitchell (2012) and 5 analyses from van Tongeren (2011).

4.3.1 Major element geochemistry

Generally, Upper Zone gabbros contain plagioclase, pyroxenes (ortho- and clinopyroxene) and magnetite, and major element data from these rocks contain CaO, MgO and FeO contents that are higher than those of the mafic fenites, although some samples of the mafic fenites contain similar amounts of MgO or CaO to the Upper Zone gabbros (Fig. 4.10a and 4.10b).

Conversely, the, Na_2O and K_2O content of the mafic fenites are greater than the Upper Zone gabbros (Fig. 4.10a-h). The Na_2O content of the mafic fenites is between 8.7 and 14.5 wt.%, whereas the Na_2O content of the Upper Zone gabbros are between 1 and 4 wt.% (Fig. 4.10c). Except for one sample, all the mafic fenites contain K_2O between 1.5 to 4 wt.%, whereas the Upper Zone gabbros-ferrogabbros contain less than 0.5 wt% K_2O (Fig. 4.10d). The main difference between these rock types is more clearly seen in Figure 4.10e, where the combined values of Na_2O+K_2O dramatically distinguishes between the mafic fenites and the Upper Zone gabbros. One mafic fenite sample has a K_2O content of 0.03 wt.%, which is less than the Upper Zone gabbros and is the lowest K_2O value for the mafic fenites, but this is balanced by the sample having the highest Na_2O content of the mafic fenites with 14.47 wt.%.

The low values ofMgO+CaO in the mafic fenites are easily seen in Figure 4.10f. The Upper Zone gabbros contain up to 20 wt.% of MgO+CaO, whereas the MgO+CaO content in mafic fenites lies between 4.7 and 14.5 wt.%. Additionally, the TiO_2 content of the Upper Zone rocks are greater than the mafic fenites (Fig. 4.10g).

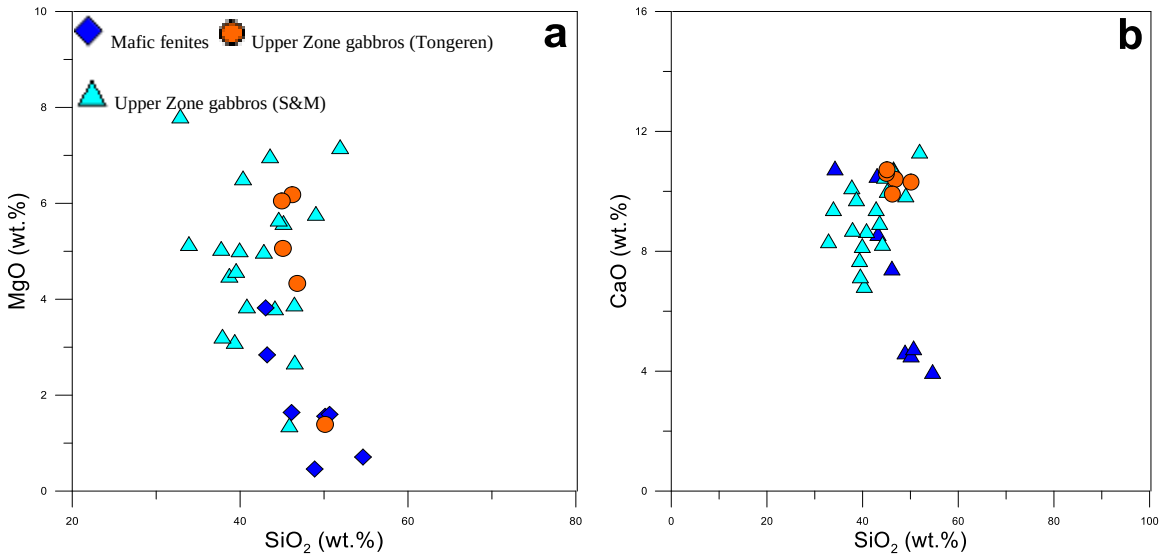

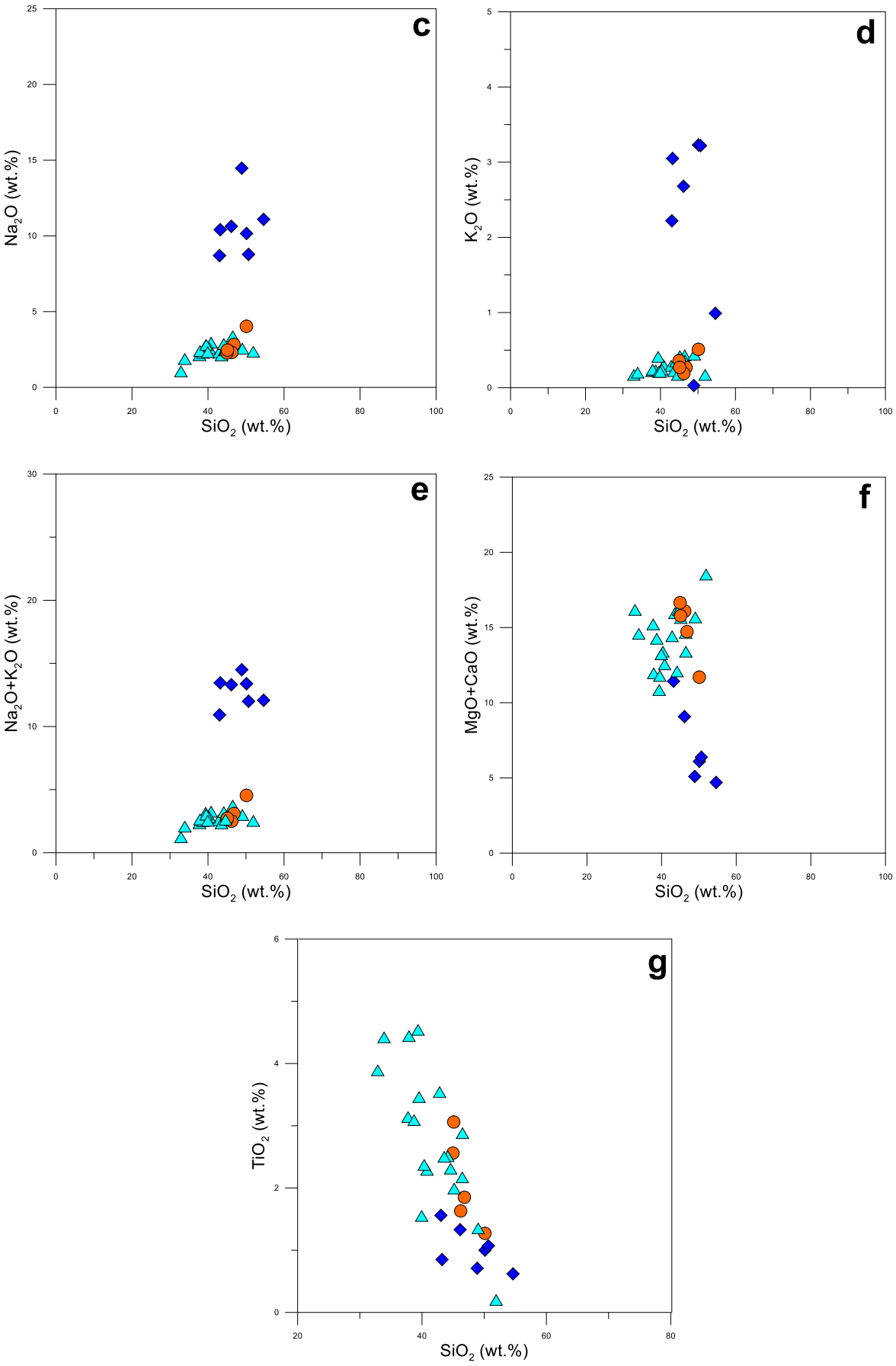
c
Na2O (wt.%)
SiO2 (wt.%)
d
K2O (wt.%)
SiO2 (wt.%)
e
Na2O+K2O (wt.%)
SiO2 (wt.%)
f
MgO+CaO (wt.%)
SiO2 (wt.%)
g
TiO2 (wt.%)
SiO2 (wt.%)

Figure 4. 10: Selected Harker diagrams of major element composition of the Spitskop mafic fenites, Bushveld Upper Zone gabbros of van Tongeren (2011) and Bushveld Upper Zone gabbros of Scoon and Mitchell (2012). (a) MgO versus SiO_2 contents, (b) CaO versus SiO_2 contents, (c) Na_2O versus SiO_2 contents, (d) K_2O versus SiO_2 contents, (e) Na_2O+K_2O versus SiO_2 contents, (f) MgO+CaO versus SiO_2 contents and (g) TiO_2 versus SiO_2 contents.

4.3.2 Trace element geochemistry

Trace element contents of the Spitskop mafic fenites are compared with the Upper Zone rocks from van Tongeren (2011) and from Scoon and Mitchell (2012) (Table 10). Absolute abundances of trace elements from the two Upper Zone suites of analyses are comparable and notably different from the mafic fenites. However, the patterns on multi-element diagrams shows peaks of Sr, Ba and U for all rocks and low values for Cr, Co, Ni and Mo.

The highest trace element contents found in the mafic fenites are for Ba and Sr with an average of 1198 ppm and 704 ppm respectively. The Upper Zone rocks contain an average Ba content of 130 ppm, while the average Sr content is only 287 ppm (van Tongeren) and 271 ppm (Scoon and Mitchell).

Zr, V, and Zn are other relatively abundant trace elements in the mafic fenites with averages of 199 ppm, 141 ppm and 89 ppm respectively. Upper Zone rocks are typically more enriched in V, with 537 ppm and 503 ppm, however the Zr content is low, it is only 15-19 ppm and the Zn content is 92-115 ppm for averages of the two Upper Zone suites.

Cu, Rb, Nb, Ga, Y and Co contents lie between 17 ppm and 55 ppm in the mafic fenites, whereas the abundance of these elements varies considerably in the Upper Zone rocks, from 1 ppm to 20 ppm, except for Cu, which has a concentration of 257 ppm. Nb and Rb averages in Upper Zone rocks are 1 ppm and 5 ppm, whereas the same elements are more abundant in the mafic fenites, with 30 ppm and 54 ppm respectively.

Sc, Cr, Pb, Ni, Th, U and Mo are the least abundant elements in the mafic fenites with less than 10 ppm on average. Pb, Th, U and Mo contents are also low in the Upper Zone rocks, however the Sc content of the Upper Zone rocks is 38 ppm and Ni content lie between 41 and 62 ppm on average.

Table 10: Trace element averages of the Spitskop mafic fenites and the Upper Zone data of van Tongeren (2011) and Scoon and Mitchell (2012) from the most enriched elements to the least enriched elements.

Elements	Mafic fenites	Upper Zone (van Tongeren)	Upper Zone (Scoon and Mitchell)
Ba	1198 ppm	130 ppm	No data
Sr	704 ppm	287 ppm	271 ppm
Zr	199 ppm	19 ppm	15 ppm
V	141 ppm	537 ppm	503 ppm
Zn	89 ppm	92 ppm	116 ppm
Cu	55 ppm	257 ppm	187 ppm
Rb	54 ppm	5 ppm	5 ppm
Nb	30 ppm	1 ppm	1 ppm
Ga	25 ppm	20 ppm	No data
Y	17 ppm	8 ppm	12 ppm
Co	17 ppm	No data	85 ppm
Cr	9 ppm	3 ppm	16 ppm
Sc	7 ppm	39 ppm	No data
Pb	7 ppm	3 ppm	No data
Ni	5 ppm	63 ppm	41 ppm
Th	2 ppm	1 ppm	No data
U	1 ppm	1 ppm	No data
Mo	1 ppm	No data	No data

Chondrite-normalized diagrams of trace elements of mafic fenites demonstrate that the different samples show a similar pattern but with varying enrichments and depletions for some elements (e.g. Sc, Cr, Ni, Mo, Ba, Th and U). Elements that show consistent values within a narrow range are V, Cu, Zn, Ga, Sr, Y and Pb (Fig. 4.11a and 4.11b). Chondrite-normalized diagrams of the Upper Zone gabbros show very similar patterns, and also some similarity with the mafic fenites. A comparison of the average values of mafic fenites and Upper Zone gabbros clearly show that the mafic fenites are more enriched in most of the trace elements, except Sc, V, Ni, Cu and U (Fig. 4.11c).

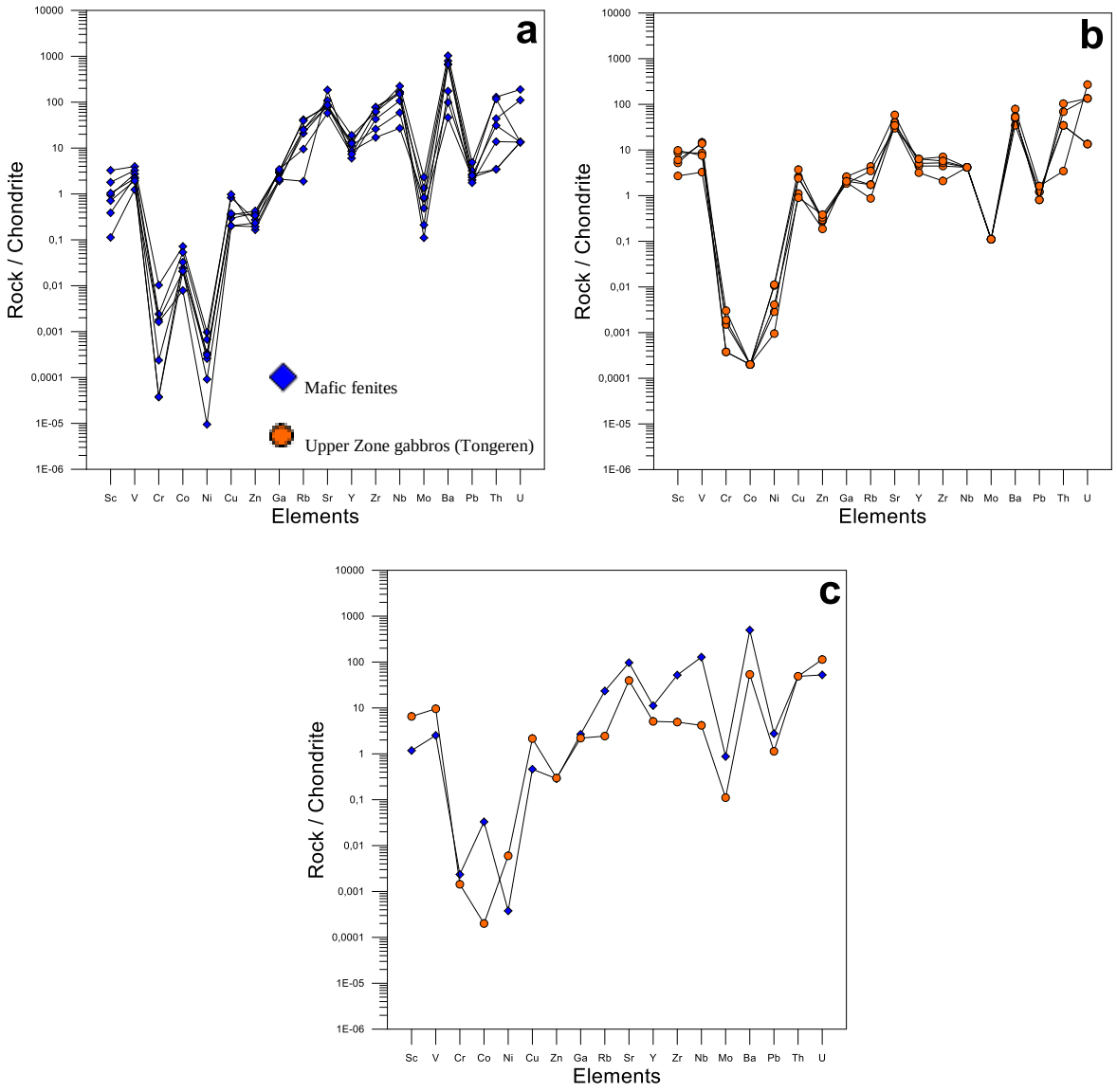

Figure 4. 11: Chondrite-normalized trace element abundance diagrams for whole rocks of (a) Spitskop mafic fenites, (b) Bushveld Upper Zone gabbros and (c) average values of the mafic fenites and the Upper Zone gabbros. Trace element values of the Upper Zone gabbros are from van Tongeren (2011). Normalized values are taken from McDonough and Sun (1995).

There is a positive correlation between increasing Sc and increasing V, Co and Ni in the mafic fenites, however there is no correlation in the gabbros between these elements (Fig. 4.12a-c). Additionally there are also positive well-constrained trends between V, Co and Ni for the mafic fenites and again the Upper Zone gabbros show much greater variation (Fig. 4.12d and 4.12e). Other approximately linear trends are observed between Nb and Ga, Y and Zn, as well as Nb and Zr, (Fig. 4.12f-h).

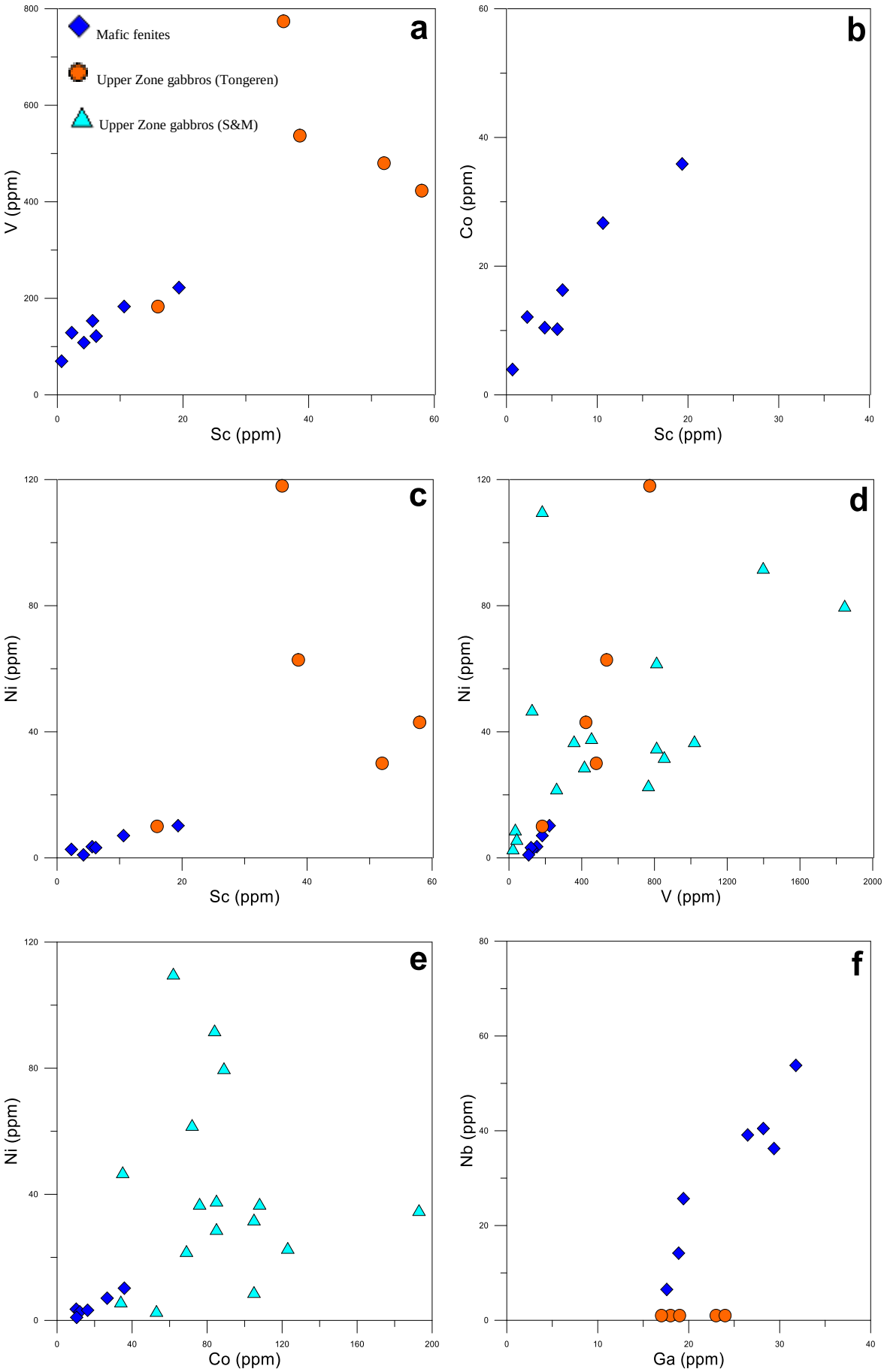
a
Mafic fenites
Upper Zone gabbros (Tongeren)
Upper Zone gabbros (S&M)
V (ppm)
Sc (ppm)
b
Co (ppm)
Sc (ppm)
c
Ni (ppm)
Sc (ppm)
d
Ni (ppm)
V (ppm)
e
Ni (ppm)
Co (ppm)
f
Nb (ppm)
Ga (ppm)

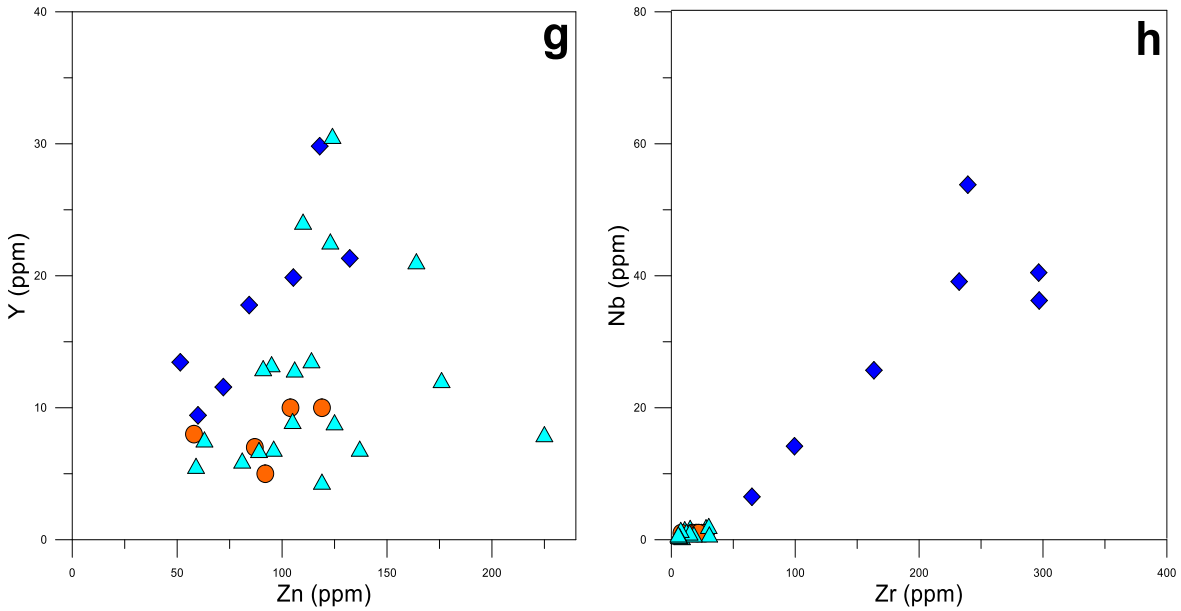

Figure 4. 12: Harker diagrams showing the trace element compositions of Spitskop mafic fenites. (a) V versus Sc contents, (b) Co versus Sc contents, (c) Ni versus Sc contents, (d) Ni versus V contents, (e) Ni versus Co contents, (f) Nb versus Ga contents, (g) Y versus Zn contents, (h) Nb versus Zr contents. Trace element values of the Upper Zone gabbros are from van Tongeren (2011) and Scoon and Mitchell (2012). Note that some diagrams do not contain Upper Zone trace element compositions because of unavailability of data.

4.3.3 REE geochemistry

The total REE concentration in the mafic fenites is greater than that of the Upper Zone gabbros with abundances between 41 ppm and 162 ppm and an average of 90 ppm, whereas the Upper Zone gabbros contain 10 ppm to 34 ppm TREE with an average of 24 ppm (Table 11).

Table 11: Total REE-, LREE- and HREE averages of mafic fenites and the Upper Zone gabbros.

Rocks	TREE Average	LREE Average	HREE Average
Mafic fenites	90 ppm	81 ppm	9 ppm
Upper Zone gabbros	24 ppm	20 ppm	4 ppm

The chondrite-normalized REE diagrams of mafic fenites generally show a fractionated pattern from La to Eu, followed by a steeper decrease from Eu to Gd, and a slight rise from Gd to Lu (Fig. 4.13a) with some variation between different samples.

The chondrite-normalized REE diagrams of the Upper Zone gabbros demonstrate very similar almost flat patterns with a slight decrease from La to Lu, and positive Eu and occasionally Tm anomalies. The content of LREE is more varied than the HREE (Fig. 4.13b) and three of the samples contained Tm below detection limits.

The comparison of chondrite-normalized REE average values of the mafic fenite and Upper Zone gabbros clearly show that mafic fenites are almost 5 times more enriched in REE than the Upper Zone gabbros, additionally their REE patterns are very different (Fig. 4.13c).

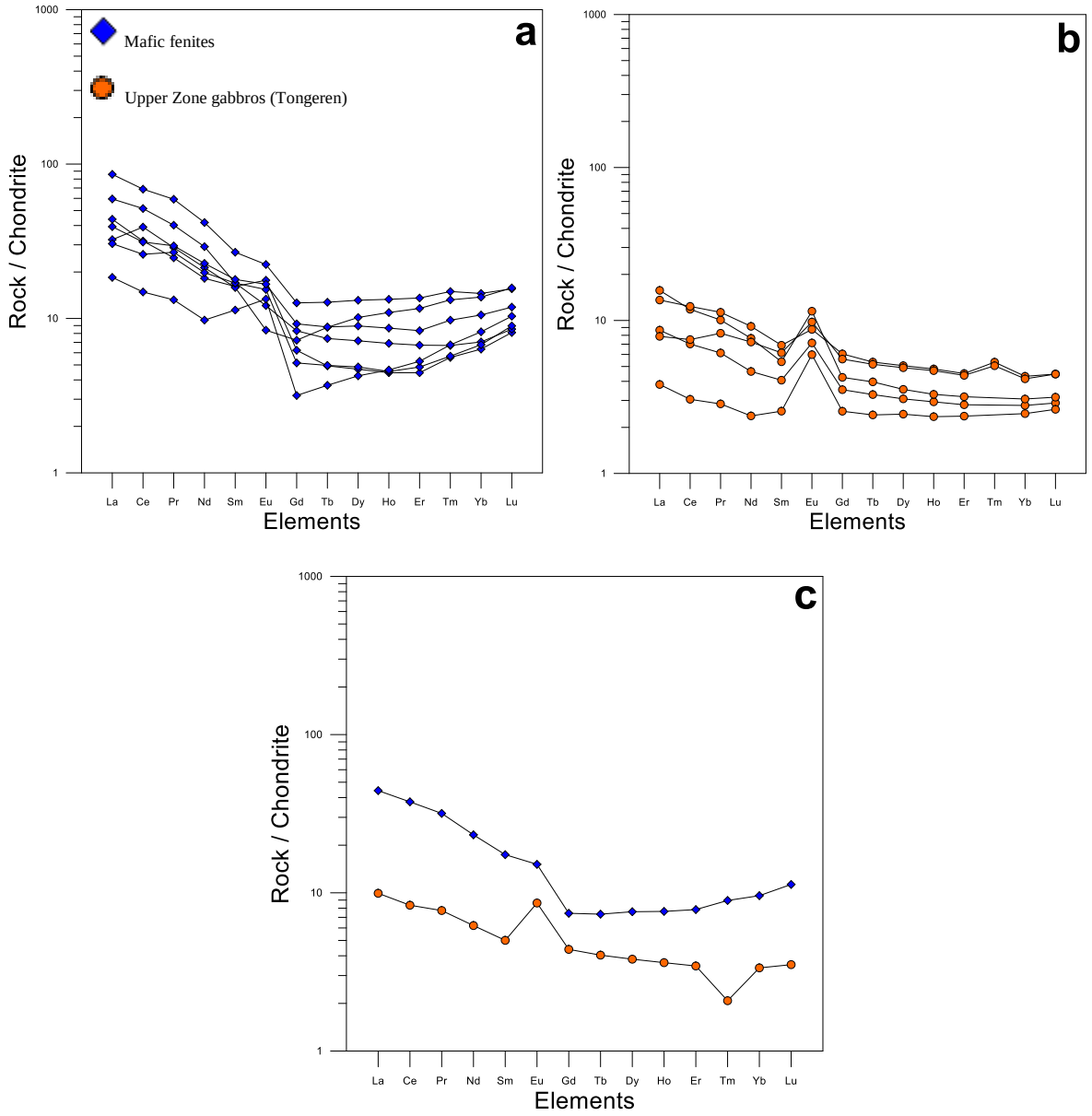

Figure 4. 13: Chondrite-normalized rare earth element diagrams of (a) mafic fenites, (b) the Bushveld Upper Zone gabbros, (c) their average values. The values of the Bushveld Upper Zone gabbros were taken from van Tongeren (2011). Normalized values are taken from Sun and McDonough (1989).

4.3.4 Isocon geochemistry

Isocon diagrams are an effective way to show metasomatic alteration and to estimate changes in element concentrations. Grant (1986) developed the isocon diagrams in which the altered composition of a rock is plotted against its original composition assuming that a correct identification of the unaltered rock has been made. Immobile elements define the isocon line,

whereas other elements represent mobility in terms of gains and losses. One major advantage of isocon diagrams is that they show the complete range of elements, both majors and traces which have been analysed. These isocon diagrams have been constructed using four different samples of mafic fenites and they are used with four different Upper Zone gabbro samples from van Tongeren (2011). Van Tongeren's data are used for these diagrams because her samples were taken closer to the Spitskop Complex than the Scoon and Mitchell samples.

It is apparent that Al_2O_3, SiO_2 and MnO are the least mobile elements. Na_2O, K_2O and P_2O_5 are the main major elements, whose concentrations are enriched more in mafic fenites (Fig. 4.14). Only in one sample is the K_2O concentration of mafic fenites less than the Upper Zone gabbros. In contrast, there are significant losses of CaO, MgO and TiO_2 from the mafic fenites during the alteration processes (Fig. 4.14 a-d).

For the trace elements, there is a significant loss in V, Sc and Cu contents in mafic fenites, whereas Zn and Ga remain immobile in all samples. In all except one sample (Fig. 4.14d), all mafic fenites are characterized by the gain of other trace elements and REEs (Fig. 4.14a-c), and in this one sample most of the trace elements fall into the immobile isocon zone, which represents the least mobile elements in the sample.

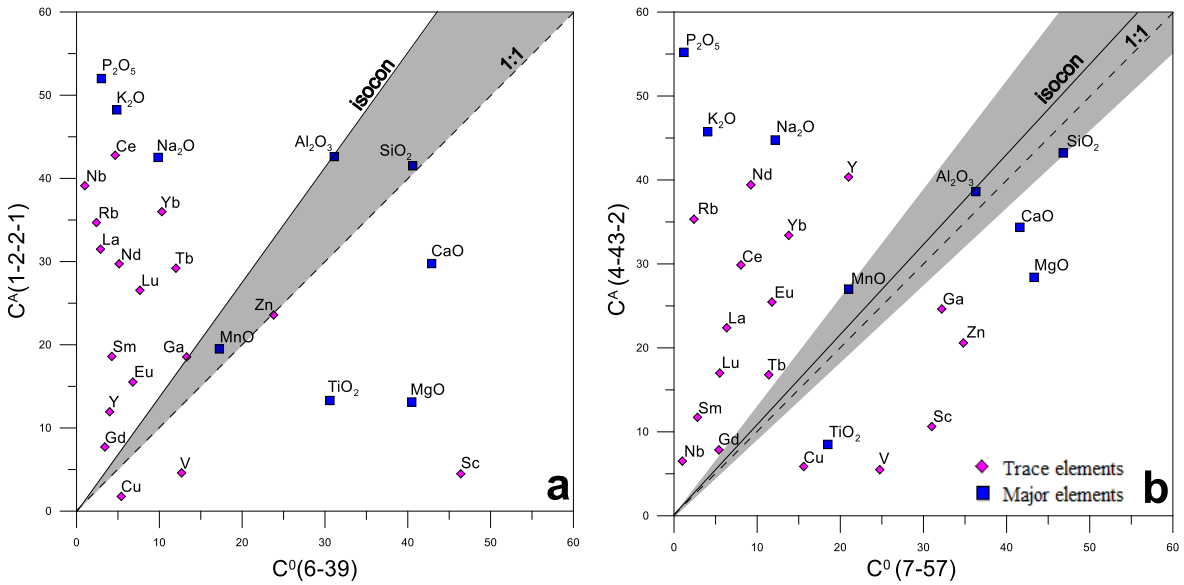

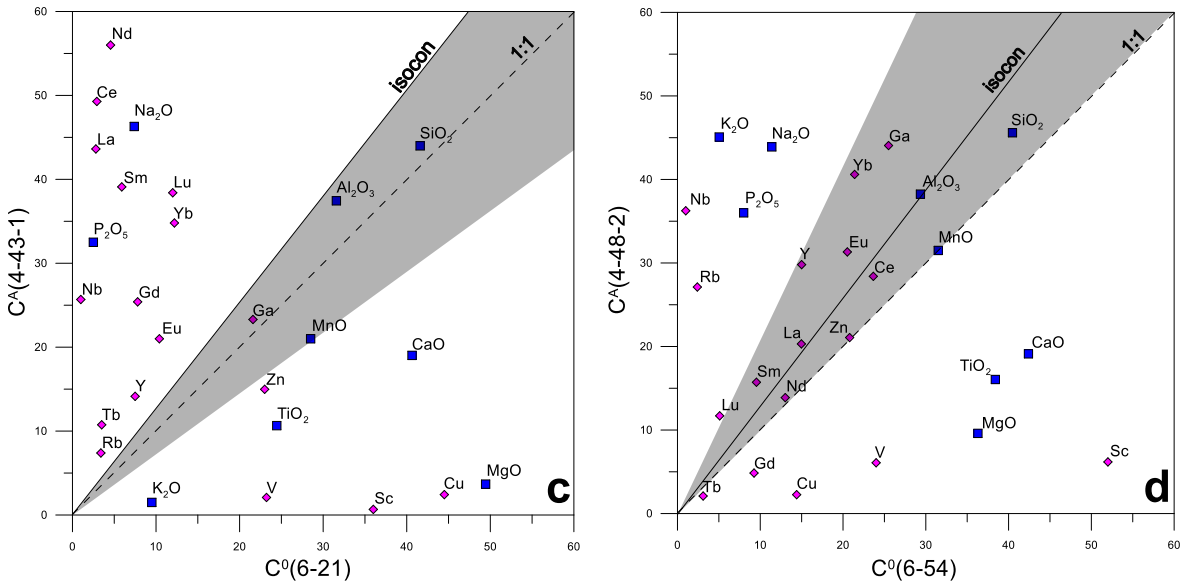

Figure 4. 14: Isocon diagram of mafic fenite samples versus Bushveld Upper Zone gabbros. The X-axis represent the concentration of the Upper Zone gabbros, and the Y-axis represent the concentration of the mafic fenites. The concentration of major- (blue square) and trace elements (purple diamonds) are multiplied by a constant for each element for easy representation. (a) mafic fenite sample 1-2-2-1 versus original Bushveld Upper Zone gabbro 6-39; (b) mafic fenite sample 4-43-2 versus original Bushveld Upper Zone gabbro 7-57; (c) mafic fenite sample 4-43-1 versus original Bushveld Upper Zone gabbro 6-21; (d) mafic fenite sample 4-48-2 versus original Bushveld Upper Zone gabbro 6-54. The grey zone represents the elements that can be immobile during metasomatism. Isocon line is within or in the boundary of this grey zone. The values of Bushveld Upper Zone gabbro samples are taken from van Tongeren (2011).

4.4 Granitic Fenites

There are two different granitic fenites based on mineralogical composition; a feldspar fenite, which is the most altered type of fenite, and a quartz-feldspar fenite, which is the least altered type of granitic fenite (see Chapter 3). It is likely that the original parental rock of the granitic fenites is Nebo Granite, and in this chapter the difference between the two fenites is investigated geochemically and compared with the original, unmetasomatized Nebo granite.

For the comparison, geochemical results of the Nebo granite are taken from Kleeman and Twist (1989) and Hill et. al. (1996). The data of Kleeman and Twist (1989) comes from the Groblersdal area, approximately 40 km southwest of the Spitskop Complex. This data is mainly used for the comparison of major- and trace elements of the Nebo granite with the granitic fenites. Geochemical results of Hill et. al. (1996) are from four different localities; Dennilton, Enkeldoorn, Sekhukhune and Zaaiplaats. Dennilton and Enkeldoorn are located to the southwest of Spitskop, whereas Sekhukhune and Zaaiplaats are located to the northeast and

northwest of the Spitskop Complex respectively. These results are mainly used for the comparison of trace elements as well as REE data of the Nebo Granite with the granitic fenites.

The main reason of selecting five different localities for data from the Nebo Granites is to show the geochemical similarities of these localities and also to show how the Spitskop granitic fenites differ from these. Twelve samples of Kleeman and Twist (1989) are used for major element- and trace element comparisons, whereas 10 samples of Hill et al. (1996) are used for trace element- and REE comparisons.

4.4.1 Major element geochemistry

All major element Harker diagrams show that the quartz-feldspar fenites plot in a similar position to the unaltered Nebo granite analyses from Kleeman and Twist (1989) and Hill et al. (1996). Conversely, the more altered feldspar fenites do not plot in the same position but typically occur as an extension of any linear array formed by the other samples. The feldspar fenites contain higher contents of K_2O, Na_2O, MgO, TiO_2 and MnO but slightly lower SiO_2 contents than the quartz-feldspar fenites and the normal Nebo Granite (Fig. 4.15a-f).

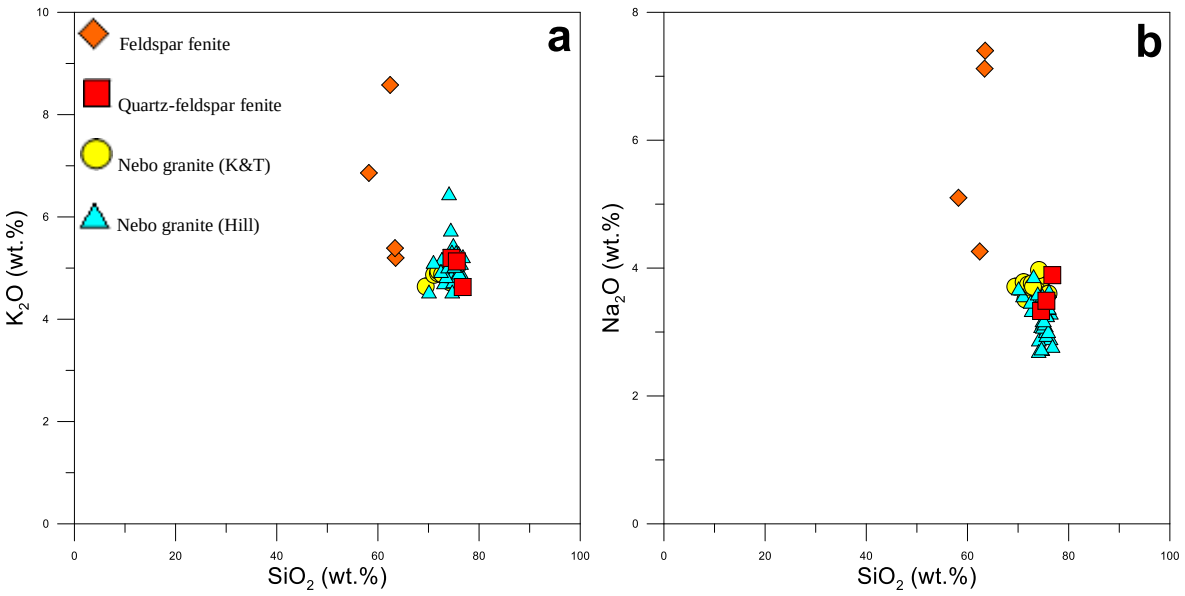

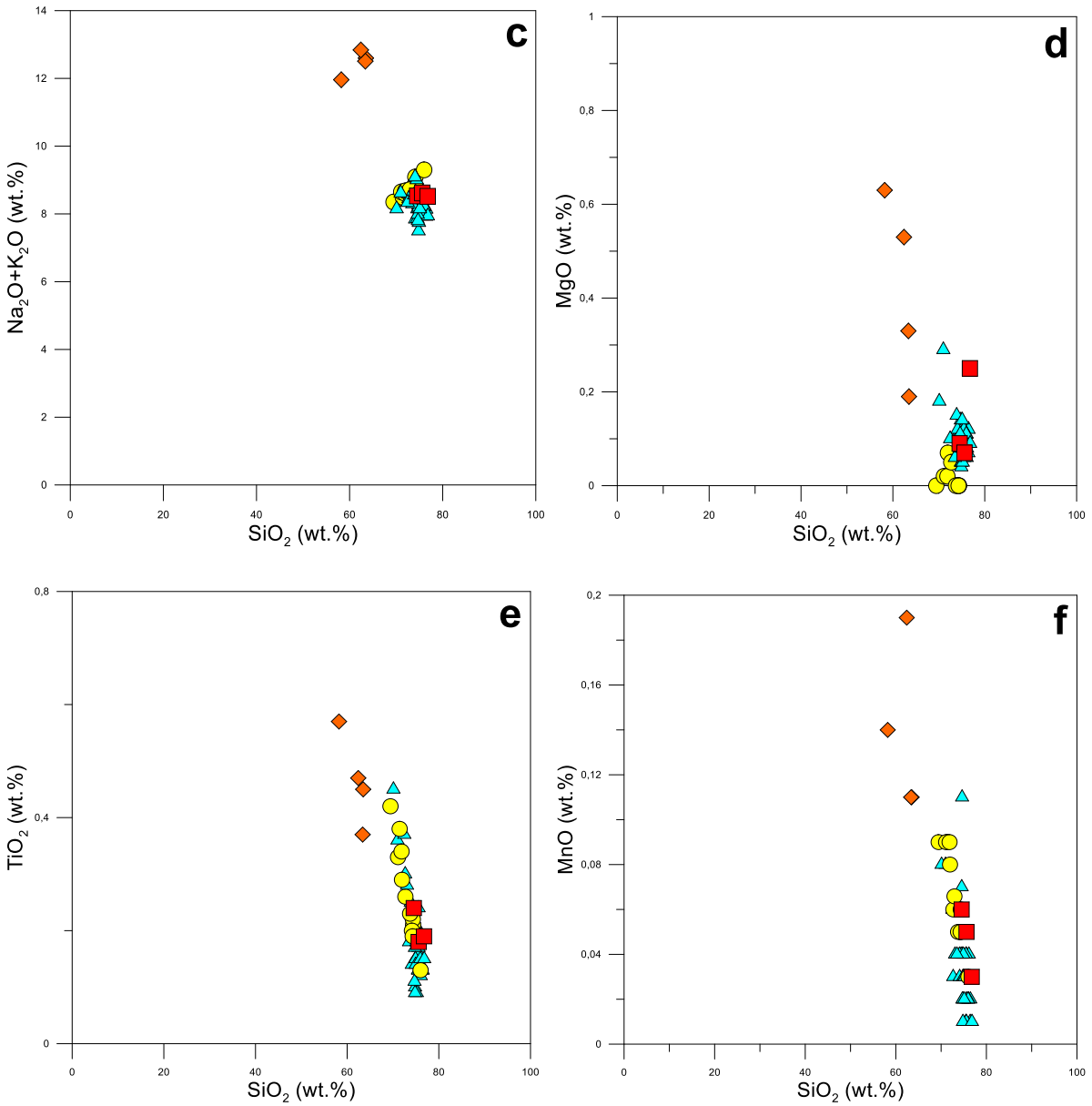

Figure 4. 15: Selected Harker diagrams showing major element compositions of Spitskop feldspar fenite, quartz-feldspar fenite and Nebo granite (Kleeman and Twist (1989) and Hill et al. (1996)). (a) K_2O versus SiO_2 contents, (b) Na_2O versus SiO_2 contents, (c) Na_2O+K_2O versus SiO_2 contents, (d) MgO versus SiO_2 contents, (e) TiO_2 versus SiO_2 contents and (f) MnO versus SiO_2 contents. The values of Nebo granites are taken from Kleeman and Twist (1989) and Hill et al. (1996). The samples of Kleeman and Twist are shown as yellow and the samples of Hill are shown as turquois.

4.4.2 Trace element geochemistry

Trace element abundances of the feldspar fenite and the quartz-feldspar fenite are compared with the Bushveld Nebo granite from Kleeman and Twist (1989) (Table 12). Generally, the levels of trace elements in the three different rock units are similar.

Table 12: Trace element averages of the feldspar fenite and the quartz feldspar fenite of the Spitskop Complex and the Bushveld Nebo Granite from Kleeman and Twist (1989) from the most enriched elements to the least enriched elements.

Elements	Feldspar Fenite	Quartz-Feldspar Fenite	Nebo Granite (Kleeman and Twist)
Ba	1424 ppm	949 ppm	1141 ppm
Zr	44 ppm	265 ppm	431 ppm
Sr	267 ppm	66 ppm	74 ppm
Rb	126 ppm	162 ppm	193 ppm
Zn	72 ppm	61 ppm	88 ppm
V	40 ppm	5 ppm	No data
Ga	32 ppm	20 ppm	20 ppm
Nb	26 ppm	16 ppm	27 ppm
Y	23 ppm	43 ppm	74 ppm
Cu	16 ppm	16 ppm	5 ppm
Pb	11 ppm	25 ppm	23 ppm
Th	9 ppm	13 ppm	26 ppm
Cr	9 ppm	3 ppm	No data
Sc	4 ppm	1 ppm	2 ppm
Ni	2 ppm	3 ppm	9 ppm
Mo	2 ppm	1 ppm	13 ppm
Co	1 ppm	2 ppm	No data
U	< 1 ppm	< 1 ppm	7 ppm

Chondrite-normalized diagrams of the trace element content of the feldspar fenites show that the samples exhibit broadly similar patterns, with quite a lot of variation (Fig. 4.16a). Rb, Sr, Zr, Nb, Ba and Th are enriched between 10 to 100 times compared to chondrite values. In contrast, Cr, Co and Ni show a depletion relative to the chondrite values, whereas Sc, V and Mo of feldspar fenite display similar concentrations to the chondritic values.

Chondrite-normalized samples of quartz-feldspar fenite demonstrate very similar patterns and concentrations and their results are also similar to the feldspar fenite. The most significant difference between feldspar fenite and quartz-feldspar fenite is that Sc and V concentrations are below the chondrite level (Fig. 4.16b). The Nebo granites show similar consistent patterns with

the quartz-feldspar fenite in terms of enrichment and depletion of the same trace elements (Fig. 4.16c).

The average values of these three rocks show that most of the elements of Nebo granite are more enriched than the fenitic rocks, however Sc, V, Cr, Co and Cu do not follow this pattern (Fig. 4.16d).

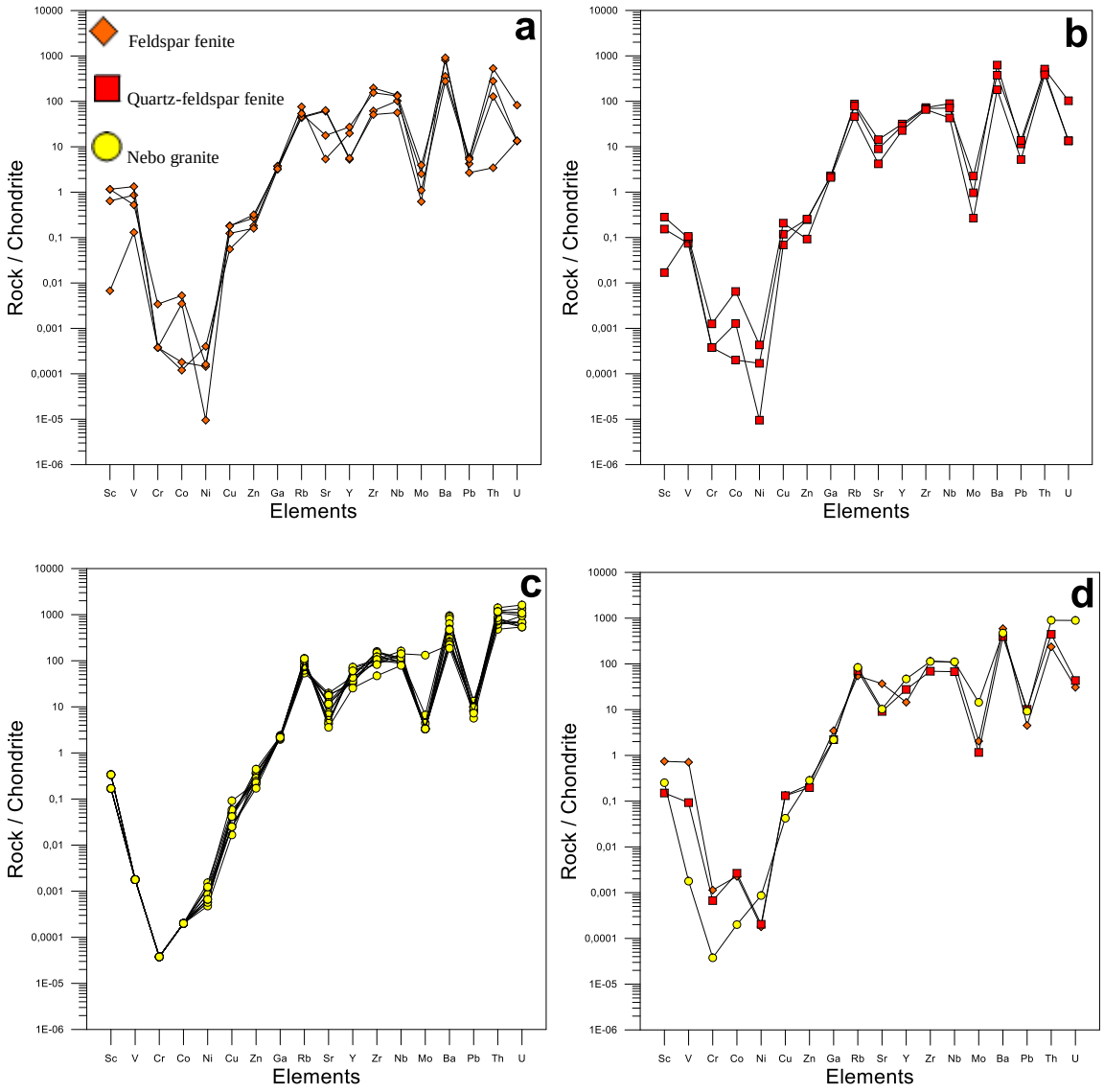

Figure 4. 16: Chondrite-normalized trace element abundance diagrams for whole rocks of (a) Spitskop feldspar fenite, (b) Spitskop quartz-feldspar fenite, (c) Nebo granite and (d) their average values. Trace element values of the Nebo granite are taken from Kleeman and Twist (1989) and Hill et. al. (1996). Chondrite values are taken from McDonough and Sun (1995).

There is a positive correlation trend between TiO_2 and Zr, and Sr and Zr for the quartz-feldspar fenite and the Nebo granite, while the feldspar fenite does not show the same correlation (Fig. 4.17a). For Zr and Sr the Nebo and the quartz-feldspar fenites show a positive correlation while the feldspar fenite shows a negative correlation (Fig. 4.17b). There is also a positive correlation

overall between Y and Th for all data from the three granite groups. Additionally, there is a gradual increase in absolute concentration of both Y and Th from feldspar fenite to quartz-feldspar fenite and to Nebo granite (Fig. 4.17c).

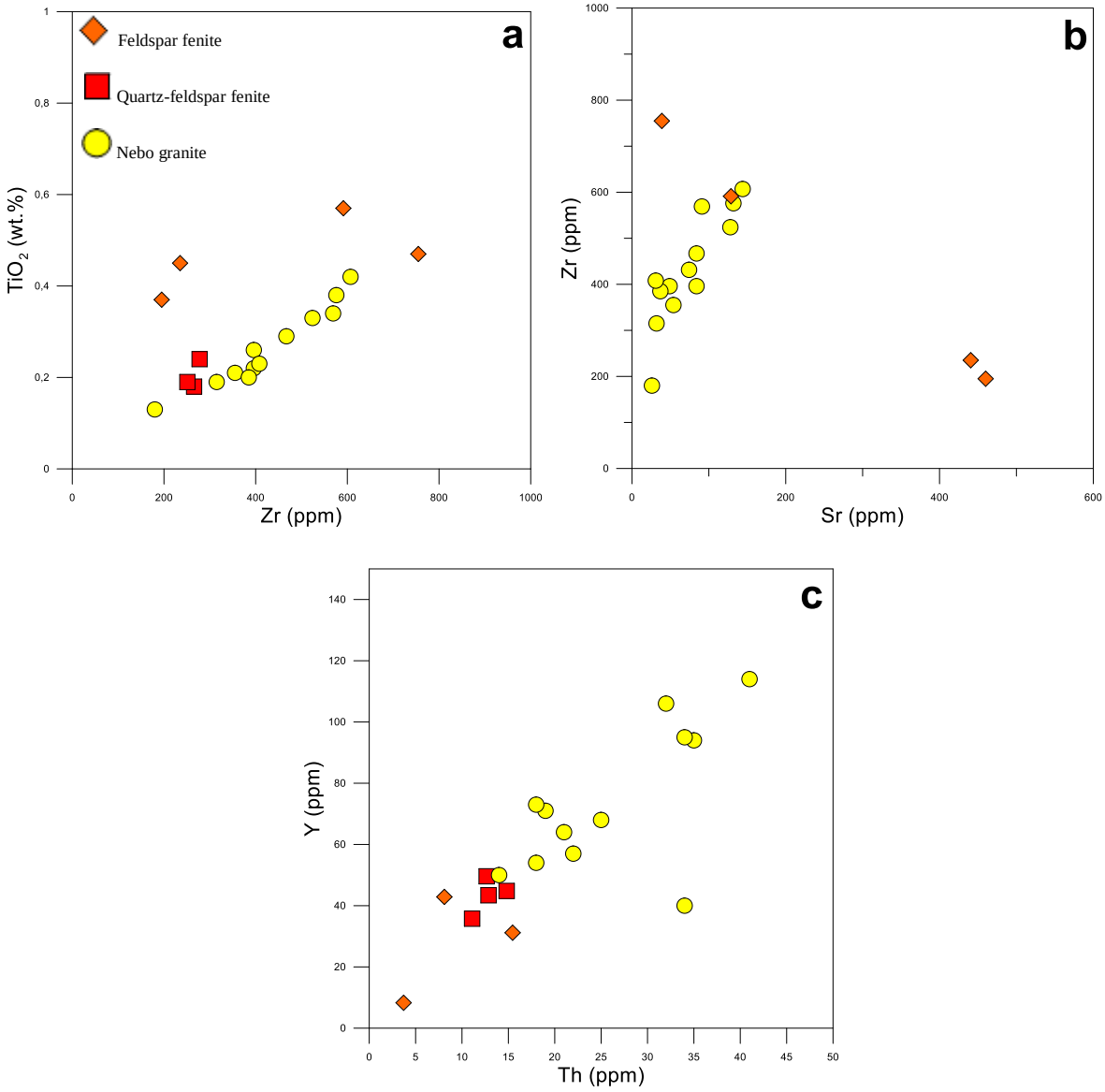

Figure 4. 17: Selected Harker diagrams showing important trace element compositions of Spitskop feldspar fenite, quartz-feldspar fenite and Nebo granite. (a) TiO_2 versus Zr contents, (b) Zr versus Sr contents, and (c) Y versus Th contents. Data for the Nebo granites are from Kleeman and Twist (1989).

4.4.3 REE geochemistry

Total REE contents for the feldspar fenite, quartz-feldspar fenite and the Nebo granite are displayed in Table 13, which shows that the Nebo granite is the most enriched rock with an average of 413 ppm TREE, whereas quartz-feldspar fenite and feldspar fenite contain on average 258 ppm and 209 ppm TREE respectively.

Table 13: REE-, LREE- and HREE averages of feldspar fenite, quartz-feldspar fenite and the Nebo granite. *Note that 1 LREE (Pr) and 4 HREEs (Dy, Ho, Er, Tm) are missing in Nebo granite.

Rocks	TREE Average	LREE Average	HREE Average
Feldspar fenite	209 ppm	195 ppm	14 ppm
Quartz-feldspar fenite	258 ppm	238 ppm	20 ppm
Nebo granite*	413 ppm	401 ppm	12 ppm

The chondrite-normalized REE diagrams of feldspar fenite have unusual irregular patterns with variation between samples. One sample contains more LREEs than the others, and shows a steep decrease in abundance from La to Ho and then a slight rise from Ho to Lu on the chondrite normalized plot (Fig. 4.18a). The other three samples show a drop from La to Gd, while the HREE either display a horizontal shape or a slight rise (Fig. 4.18a).

The REE results of the quartz-feldspar fenite are more consistent, the chondrite-normalized REE diagrams show a drop from La to Eu, and then a slight rise or fall from Eu to Lu. The LREE content of quartz-feldspar fenite is less varied than the HREE (Fi. 4.18b).

The chondrite-normalized REE diagrams of Nebo granite all have a very similar pattern, a steep drop from La to Nd, followed by a negative Eu anomaly and a slight drop from Gd to Lu (Fig. 4.18c). The LREE is less varied than the HREE content, which is the same as the quartz feldspar fenite.

The average chondrite-normalized REE values of the Nebo granite, quartz-feldspar fenite and feldspar fenite show that there is a gradual decrease in REE content from the original, unmetasomatized Nebo granite to the least metasomatized quartz-feldspar fenite and then the most metasomatized feldspar fenite (Fig. 4.18d). The negative Eu anomaly of the Nebo granite is an exception where the value for the Nebo granite is less than the average of the fenitized samples. Although the REE pattern for the quartz-feldspar fenite is similar to that of the Nebo granite the lack of Eu anomaly in the quartz-feldspar fenite is greater than that in the Nebo Granite.

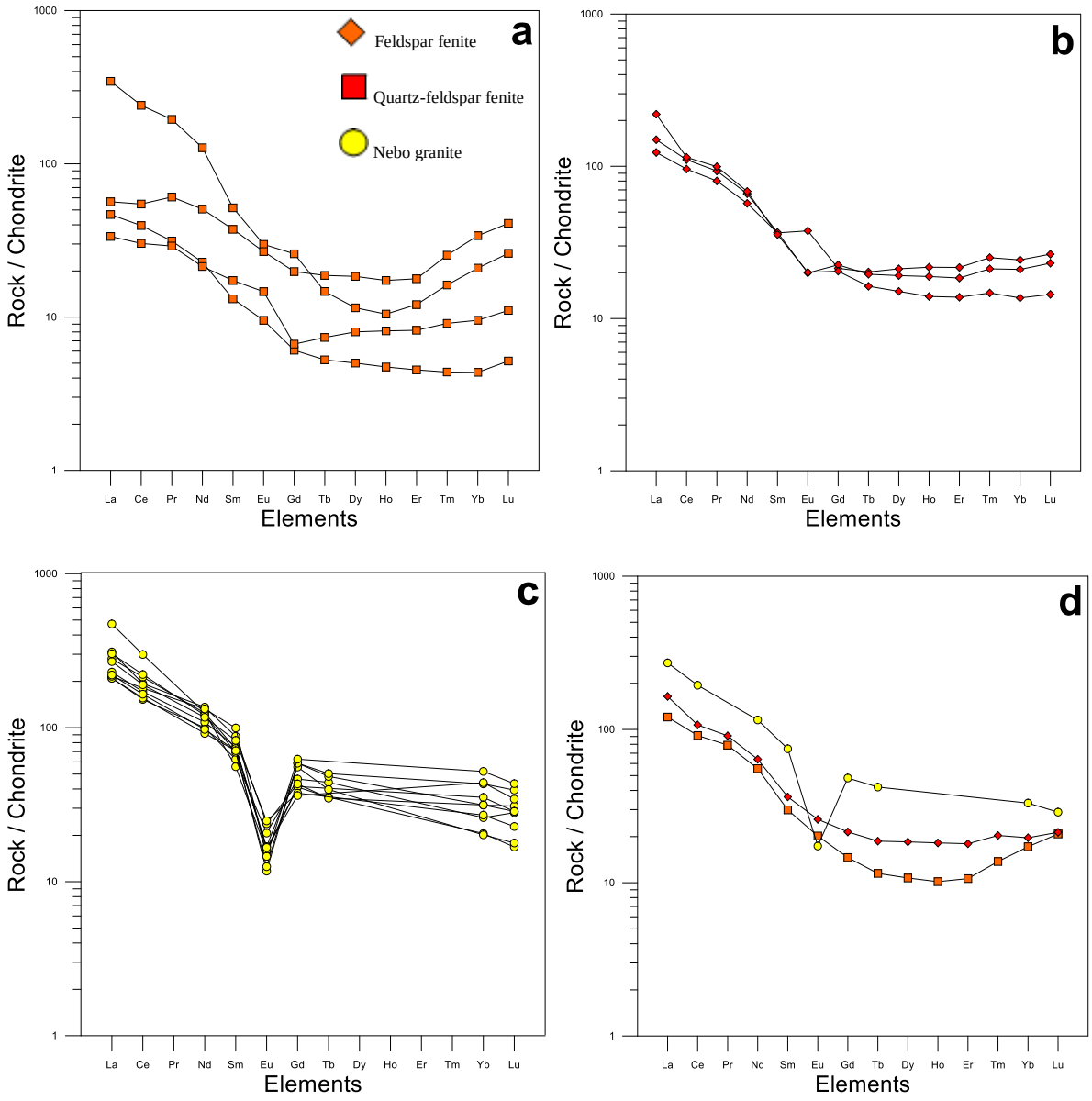

Figure 4. 18: Chondrite-normalized REE diagrams of (a) feldspar fenite, (b) quartz-feldspar fenite and (c) Bushveld Nebo granite and (d) average values of them. Pr, Dy, Ho, Er and Tm data are missing in the Nebo granite. REE values of the Nebo granite are taken from Hill et. al. (1996). Chondrite values are taken from Sun and McDonough (1989).

4.4.4 Isocon geochemistry

Isocon diagrams of granitic fenites have been used to show the mobility of major- and trace elements during metasomatism. Quartz-feldspar fenites and feldspar fenites of the Spitskop Complex are compared with the original, unmetasomatized Bushveld Nebo granite using isocon diagrams.

The first two diagrams illustrate a comparison between the least metasomatized quartz-feldspar fenite and the unmetasomatized Nebo granite (Fig. 4.19a and 4.19b). As can be seen, all of the major elements, except MgO and CaO, lie near or on the 1:1 line and were therefore relatively

immobile. The MgO content is higher in quartz-feldspar fenite, whereas CaO is slightly lower in the same rock. However, the main difference is found in trace elements, most of the trace elements have higher values in the Nebo granite than the quartz-feldspar fenite. Only the concentration of Pb, Eu and Cu are higher in quartz-feldspar fenites, although they are close to the 1:1 line. Ga, Sc and Zn also appear to have been immobile during metasomatism.

The mobility of major- and trace elements is greater in the isocon diagrams of the feldspar fenite (Fig. 4.19c-f). MgO, Na_2O and K_2O were in all cases mobile, however in some samples either Na_2O or K_2O can be found in the grey isocon zone, which means that it is less mobile or possibly immobile. SiO_2 content decreases during alteration and Al_2O_3 is thought to be immobile. The feldspar fenites contain more MnO, P_2O_5 and TiO_2 than the Nebo granite, however in Figure 4.19d P_2O_5 lies on the 1:1 line.

Trace elements of Ga, Sc, Eu and Cu are greater in the feldspar fenite, whereas the other trace elements are elevated in the Nebo granite. Except for Nb, there are no trace elements within the grey isocon zone.

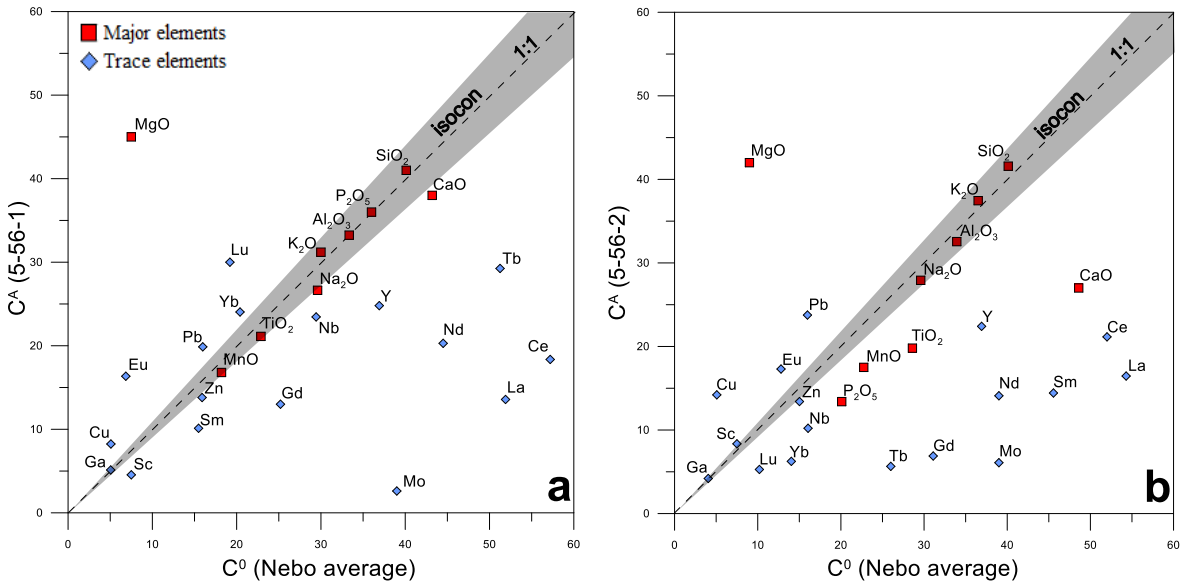

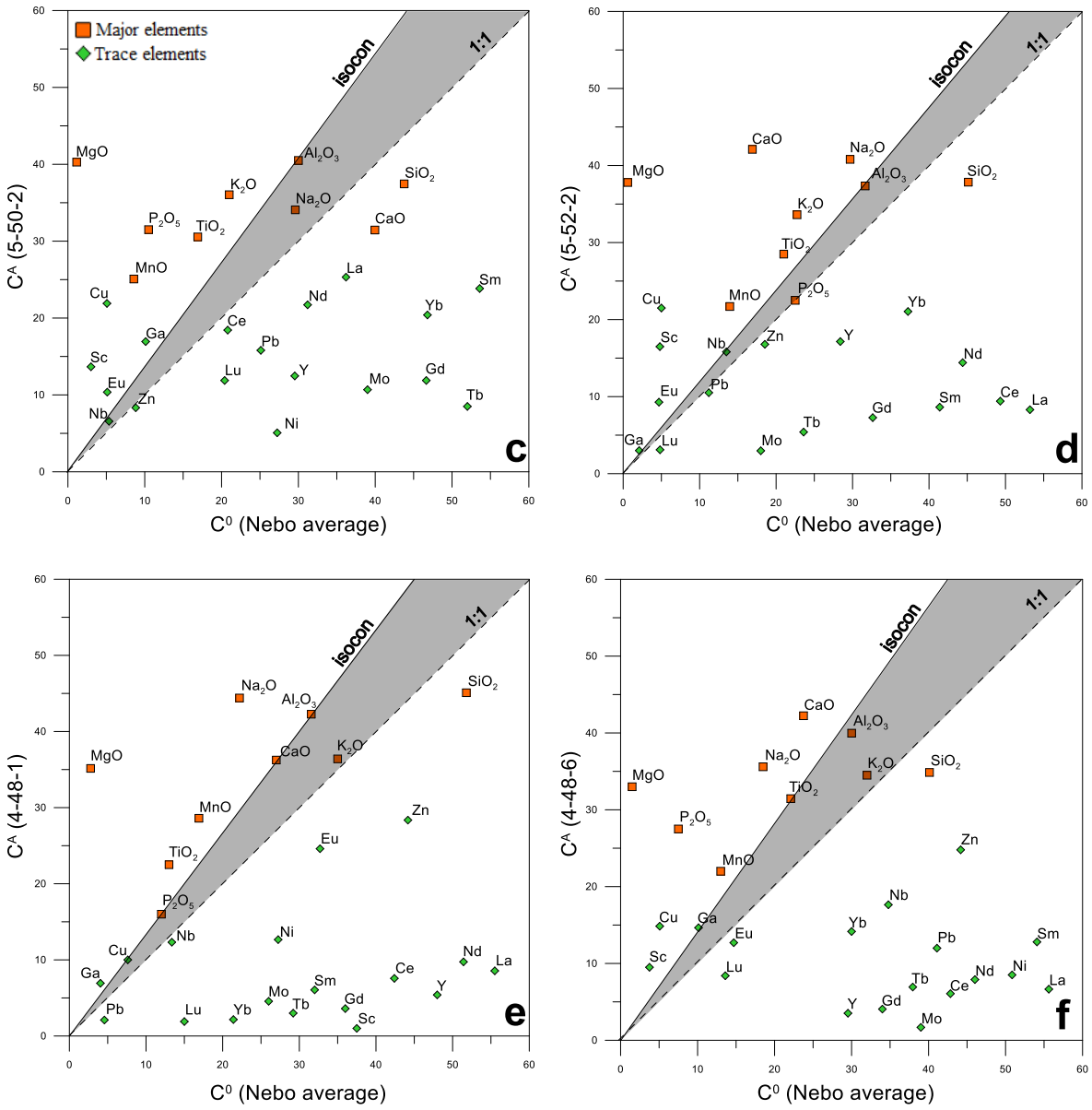

Figure 4. 19: Isocon diagram of quartz-feldspar fenite and feldspar fenite samples versus Nebo granite samples. The average value of Nebo granite is used for the isocon diagrams. The concentration of major- (red square for quartz-feldspar fenite, orange square for feldspar fenite) and trace elements (light blue diamonds for quartz-feldspar fenite, green diamonds for feldspar fenite) are multiplied by a constant for easy representation. (a) quartz-feldspar fenite sample 5-56-1 versus Bushveld Nebo granite average, (b) quartz-feldspar fenite sample 5-56-2 versus Bushveld Nebo granite average, (c) feldspar fenite sample 5-50-2 versus Bushveld Nebo granite average, (d) feldspar fenite sample 5-52-2 versus Bushveld Nebo granite average, (e) feldspar fenite sample 4-48-1 versus Bushveld Nebo granite average and (f) feldspar fenite sample 4-48-6 versus Bushveld Nebo granite average. The grey zone represents the elements that can be immobile during metasomatism. The values of Bushveld Nebo Granite samples are taken from Kleeman and Twist (1989) and Hill (1996).

4.5 Summary of Geochemistry Results

Major element results from the carbonatite analyses show that all types of carbonatites have very similar major element concentrations except for variations in CaO, MgO and MnO content.

The CaO and MgO concentrations determine the type of carbonatite. Trace element and REE patterns of the different carbonatites are typically similar to each other.

Nepheline syenites of the Spitskop Complex show some metasomatic alteration patterns and these patterns are well seen in REE diagrams. U-shaped and flat-like patterns of REE are a possible sign of metasomatism and these patterns are seen in all nepheline syenite samples. Additionally, the REE diagram of ijolite gives the same REE pattern as nepheline syenite.

Major element data of the mafic fenites show distinct Na_2O-K_2O and P_2O_5 enrichments relative to the parental Upper Zone gabbros. Most of the trace elements and all REE of the mafic fenites are more enriched than Upper Zone gabbros, however some trace elements such as Sc, V, Ni, Cu and U are more depleted than Upper Zone gabbros.

For the feldspar fenite Na_2O, K_2O and MgO enrichments occur, whereas SiO_2 content decreases with increasing metasomatic alteration. In some isocon diagrams, Na_2O or K_2O stays within the isocon zone in feldspar fenite, because sometimes Na-metasomatism dominates the rock, so the K_2O content looks as though it was immobile, or sometimes K-metasomatism is greater than Na-metasomatism, therefore Na_2O contents appears immobile. So there is a negative correlation between Na_2O or K_2O contents of the metasomatic rocks. However, MgO content is not associated with this Na-K correlation. Additionally, quartz-feldspar fenite has a very similar major element concentration to the Nebo granite, except for the MgO content. MgO is enriched in quartz-feldspar fenite, whereas there is only a slight change in Na_2O and K_2O.

It is obvious that the mobility of the trace elements changes with increased metasomatism, most of the trace elements have the highest concentrations in the Nebo granite, rather than in the quartz-feldspar fenite, with the feldspar fenite most depleted, however some trace elements, such as Cu, Sc and sometimes Eu, are more enriched in quartz-feldspar fenite and feldspar fenite than the Nebo granite.

Feldspar fenite samples do not show the same trace element patterns, because the metasomatism is heterogeneous for each sample, however when the effect of the metasomatism decreases, as in the quartz-feldspar fenite, the samples display more similar trace element patterns (e.g. same trace element ratios). In this case, different samples of the quartz-feldspar show similar trace element patterns.

The REE data for fenitized rocks and their associated parental rocks show that compositionally the fenites lie between the Nebo granite and the Upper Zone rocks (Fig. 4.20). This results in

altered Upper Zone rocks becoming more REE-enriched, whereas altered Nebo granite is depleted in REE. Additionally, it is seen that the unaltered Upper Zone country rocks defines the lower REE boundary and the Nebo Granite defines the upper REE abundances.

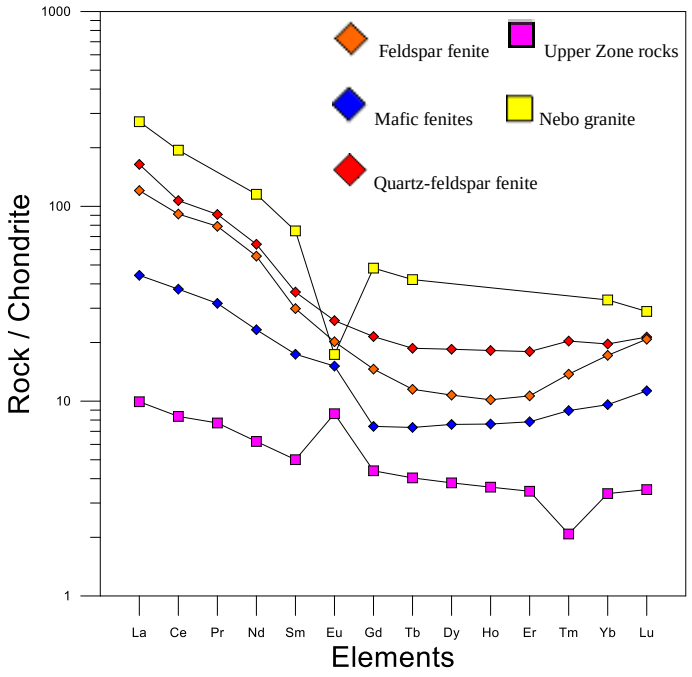

Figure 4. 20: Chondrite-normalized REE diagram of the fenites of the Spitskop Complex (quartz-feldspar fenite, feldspar fenite and mafic fenite) and their parental rocks (Nebo granite and Upper Zone rocks). Normalized values are taken from Sun and McDonough (1989).

In the Spitskop Complex, the mobility of REE is clearly seen between different groups of rocks. One of the interesting things is that the metasomatic fluids caused a depletion of REE in the felsic rocks, whereas the same fluids are the reason of the enrichment in REE in a mafic rock. However, this enrichment is dispersed through the whole rock across a broad zone and is therefore not an economic proposition.

Secondly, when there is a depletion of an element in one fenitized rock, there is a concomitant enrichment of the same element in another fenitized rock. For example during the metasomatism V, Cu, Rb, Y, Sc, Nb are lost from the Upper Zone rocks, whereas there is an enrichment of these elements in granitic fenites.

Ba, Sr and Ga do not follow this pattern, these elements are enriched in all fenitic rocks compared with their parental rocks. Interestingly, there is a decrease in Ba, Sr and Ga from the calcite carbonatite to the dolomite carbonatite.

4.6 Discussion

In carbonatites, apatite and interstitial calcite are major hosts for REE enrichment, therefore it is crucial to understand the relationship between these minerals and carbonatites. It is known that apatite can host high amounts of REE and it is a common mineral in carbonatites, however the REE-enriched interstitial calcite is interesting. It contains REE up to 100 times more than the euhedral calcite, and the shape of the REE patterns are irregular (Ionov and Harmer, 2002). These irregular patterns are also seen in whole rock samples of the mafic- and granitic fenites. The reason that the calcite-dolomite carbonatite and dolomite carbonatite have higher REE concentrations than the calcite carbonatite is that calcite-dolomite carbonatite contains interstitial calcites, whereas dolomite carbonatite has interstitial calcite and apatite. Late stage magmatic minerals are suggested to control the distribution of REE and trace elements.

The major element data of the mafic fenites suggests that Na-K-enriched fluids reacted with mafic fenites and during this process there was a loss of MgO and CaO. Similar Na-K enrichment is also seen in granitic fenites. Therefore Na and K are the main major elements of the metasomatic fluids. For the mafic fenites most of the major elements do not show any correlation or consistent patterns, and the main reason is that the metasomatic processes is not homogeneous in each sample. The samples, which are close to the thick metasomatic veins or the source of the metasomatic fluid, are affected more than the other samples. However, the mafic fenites are more enriched in trace elements and REE compared with unaltered Upper Zone rocks. So these elements must be transported via fluids from somewhere else. One interesting observation is that the average values of trace elements as well as REEs of the mafic fenites and nepheline syenites are very similar to each other (Fig. 4.21a and 4.21b).

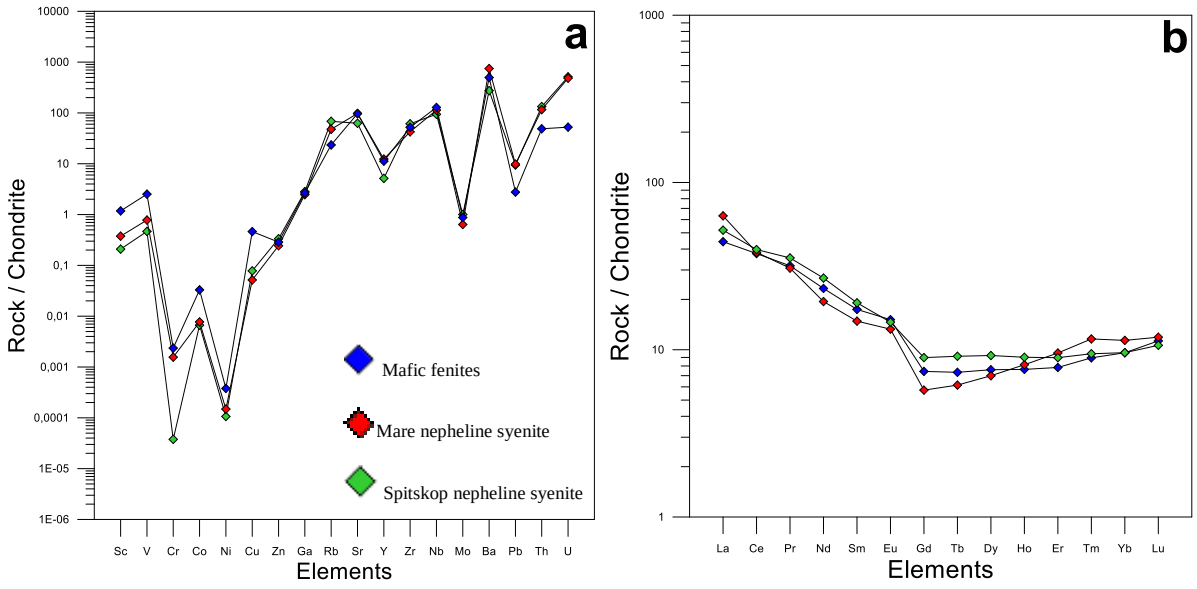

Figure 4. 21: Trace elements and REE diagrams of the mafic fenites, Mare nepheline syenite and Spitskop nepheline syenite (a) chondrite-normalized trace element abundance diagram for whole rock averages of the mafic fenites and nepheline syenites and (b) chondrite-normalized REE diagram of average values of mafic fenites and nepheline syenites. Chondrite values are taken from McDonough and Sun (1995).

The geochemistry data for the granitic fenites clearly show that there is a distinct relationship between the metasomatic fluids and the major element-, trace element- and REE concentrations. When metasomatic fluids affect the Nebo granite intensively, they form feldspar fenite, therefore feldspar fenite contains higher Na_2O and K_2O. Quartz-feldspar fenite is formed between feldspar fenite and the Nebo granite and represents the transition between the two rocks. It is known from the geochemistry of the mafic fenites that during the metasomatism mafic fenites are depleted in MgO, and this MgO then appears to be enriched in granitic fenite.

There is a gradual decrease in REE from the Nebo granite to quartz-feldspar fenite and to feldspar fenite. This indicates that when Na-K-Mg-enriched fluids reacted with the Nebo granite, they transported REE and also most of its trace elements to another area. However, the negative Eu anomaly of the Nebo granite is not reflected in the fenites as they have a similar or greater Eu content than the Nebo granite. This event can also suggest that the REE- and trace elements of the Nebo granite could be transported into another rock, in this case the mafic fenites could be the ideal candidate. Mafic fenites are more enriched in REE and trace elements than the original Upper Zone rocks. Additionally, the Upper Zone rocks have a positive Eu anomaly and this positive anomaly disappears in mafic fenites. However the Eu content of mafic fenites is still higher than the Upper Zone rocks, which shows that other rocks of the Spitskop Complex (carbonatites, nepheline syenite or ijolite) may be involved in this chaotic element transport.

Major elements-, trace elements- and REE results of Spitskop fenitized rocks and their parental rocks suggest that there may occured an element equalization process during the fenitization event of the Spitskop Complex. This means that hot Na-K-enriched fluids reacted with felsic and mafic rocks, depleted some of the major- and trace elements from one rock and added them to another rock. After a time the element concentrations of both of the rocks converged. In Spitskop felsic rocks had more REE than the mafic ones, and during the fenitization some of the elements of felsic rocks transferred to mafic rocks. However how intense is this transfer is still unknown, because there may be some element contributions also from carbonatite via hot fluids.

Chapter 5.

Conclusions, Discussion and Suggestions

5.1 Spitskop Alkaline Complex

The Spitskop Complex is an intrusive complex dated at 1.3 Ga (Harmer, 1992) which intruded into the Bushveld Complex on the Kaapvaal Craton. The major components of the complex are calcite carbonatite, calcite-dolomite carbonatite, iron-bearing dolomite carbonatite with an apatite rich zone, and alkaline rocks such as pyroxenite, ijolite and nepheline syenite (Fig. 5.1). These alkaline units are cut by a plug of carbonatite, which is the youngest component of the complex. Rocks of the complex intrude Bushveld granite and granophyre which have been variably fenitized (Strauss and Truter, 1950). The carbonatite is heart-shaped in plan, measures 1.6 km across and it is one of the best known carbonatites in the region, as well as in South Africa (Verwoerd, 1967).

Fluid-rock interactions are important to help to develop an understanding of the genesis of carbonatites, alkali intrusions and the associated REE mineralization. This study investigated the Spitskop alkaline complex to constrain the nature of the fluids, the reaction with the host rock and mobility of REE. Mineralogical changes induced by fluid-rock interaction were examined petrologically, mineralogically and geochemically.

5.2 Fenites

A variety of metasomatic fluids can have formed during the crystallization of magma and these may host incompatible elements. Most of the information on fluid chemistry comes from fluid inclusion and experimental studies of carbonatites and associated alkaline rocks (Kamenetsky and Kamenetsky, 2010; Williams-Jones and Palmer, 2002).

Fluids can play an important role in the mineralization of rare earth elements. The mobility or immobility of REE has attracted scientists because of their importance for potential ore deposits as well as for carbonatite genesis. Although typically considered immobile elements Yongliang and Yusheng (1991) suggested that during the hydrothermal activity REE can be mobile, and that detailed experimental studies should be done to understand the REE behaviour.

In general, fenitic rocks commonly have perthitic and granophyric textures, reaction rims and replacement coronas (see Chapter 3). In addition Na-K replacement in feldspars may also be

indicative of fenitization. Most of the fenitic alteration zones are irregular in shape, because of irregular fluid flow and fracture zones.

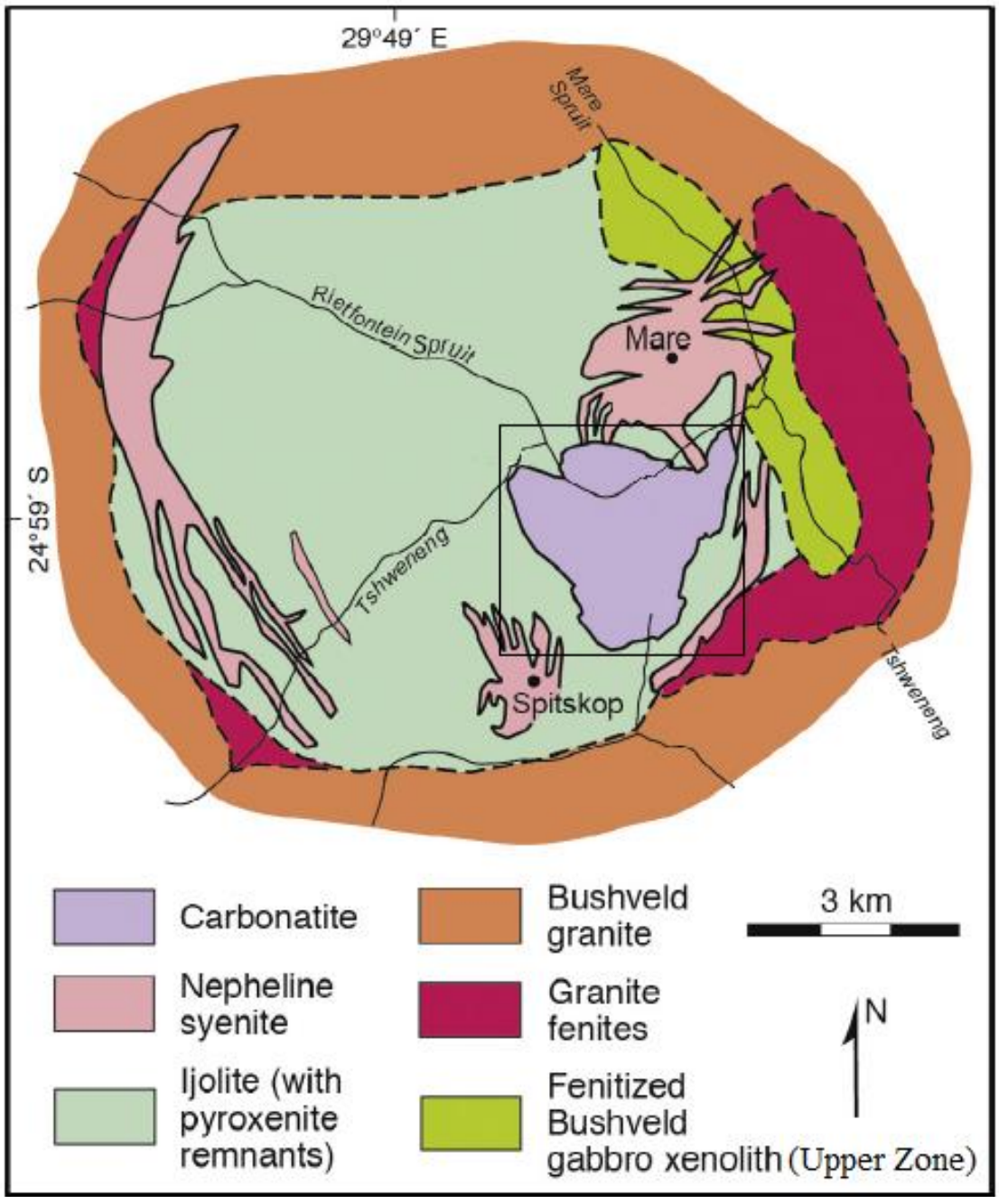

Figure 5. 1: Geological map of the Spitskop Complex displaying carbonatite, nepheline syenite, ijolite and fenitized rocks surrounded by Bushveld granite (Gose et al., 2013).

Fenites have often formed around carbonatites and alkaline rocks such as ijolite and nepheline syenite. There is a consensus that the source of the Na and K components of fluids may be either the carbonatites or alkaline silicate rocks (Elliott et. al., 2018).

In the Spitskop Complex the Nebo granites are close to the carbonatite, and the final product of fenitization, granite fenite, contains abundant K-feldspars and sometimes alkali pyroxenes and alkali hornblendes. Additionally, mafic rocks of the Bushveld Complex Upper Zone also occur near both carbonatite and ijolite. They are transformed into mafic fenites, which contain up to 50 % of aegirine or aegirine-augite. These and other minerals in mafic fenites are also affected by Na-K fenitization (see details in Chapter 3).

Most of the fenitized zones around the complex are in fresh outcrops, where mineral identification is relatively straight-forward, however some vein- and contact zones are very altered, where it is much more difficult to identify minerals, even under the microscope.

5.2.1 Mafic Fenites – implications from Spitskop

It is shown that mafic rocks of the Bushveld Complex tend to transform to an ijolitic rock, which consists mainly of nepheline and clinopyroxene (Chapter 3). They resemble to ijolitic rock because of the mineral content. The transformation of plagioclase to nepheline and to analcite/sodalite is clearly observed. In some thin sections analcite is seen as an incomplete rim around nepheline, therefore it is suggested that the transformation occurred in multiple steps. Some of the other studies (Drüppel et. al, 2005 and Fall, 2007) also support this alteration of plagioclase. Olivine, ortho- and clinopyroxenes tend to transform into Na-rich clinopyroxene.

Coarse-grained perthitic veins are only found in mafic fenites, which are thought to be one of the last processes of metasomatism (Chapter 2). Additionally, plagioclase crystals within magnetites of the mafic fenites are similar to the plagioclase-bearing magnetitite zone of the Upper Zone. Some of the plagioclase crystals within magnetite transformed to nepheline. Therefore it is thought to be that Upper Zone magnetitite layers also transformed to mafic fenites.

Although it is possible to compare the mafic fenites around the world with the Spitskop mafic fenites in terms of mineralogy, it is not possible to compare them geochemically, because there are not any significant geochemical datasets from these other complexes. The main reason for this is that the original composition of the mafic rocks is not certain in most cases whereas at Spitskop there is excellent control on the composition of the original rocks.

5.2.2 Granitic Fenites – implications from Spitskop

In the Spitskop complex granite fenites are mostly coarse-grained, which imply that the alteration process must be slow enough to form coarse-grained syenitic rocks (Fig. 5.3).

Because in most cases both quartz and plagioclase are absent during albitization, albite must be the replacement product of plagioclase and quartz of the Nebo granite. Albite is richer in Na and Si than plagioclase, therefore in this metasomatic reaction fluids must have been rich in Na and Si components. After the alteration Al and Ca are removed from the rock and it is thought that they either partitioned into the fluid or formed another mineral.

In some cases, the metasomatic fluids also affected the whole outcrops, such that some granite fenite outcrops are composed mainly of albite, resulting in a feldspar fenite. Detailed mineralogical and petrological information is given in Chapter 3.



Figure 5. 2: Fenitized outcrops in the Spitskop Complex. After alkali metasomatism, granitic rocks transformed to syenitic rocks.

5.2.3 Fenites – implications

Fenitization in the Spitskop Complex is a multi-stage process, as element mobilities caused the fluid to evolve through several different processes. Rock-fluid interaction resulted in the addition of Na and K as a major feature in the Spitskop Complex. Removal and addition of other major elements from one rock into another was different for each fenite type. Trace elements and REE were also mobile during fenitization, Na-K enriched fluids reacted with country rocks and during this stage all the rocks that are affected from these fluids had similar trace elements and REE composition.

After the fenitization process, all fenites tend to have similar REE patterns at Spitskop, which is a u-shaped concave upwards pattern, and similarities are also seen in the trace element distribution. Fenitizing fluid reacted with the host rock; if the fluid itself contained more REE than the host, REE would have been mobilized into the host Upper Zone gabbros, however where the fluid contained less REE than the parent rock, REE's were removed into the fluid phase as interpreted for the Nebo granite.

Generally, many of the carbonatite/alkaline complexes such as Mbozi Complex, Tanzania, Messum Complex, Namibia and Khariar Complex, India, which contain at least one mafic-ultramafic rock, have similar alteration reactions to the reactions at the Spitskop Complex with plagioclase having been transformed in mafic fenites to nepheline and nepheline occasionally to analcite. In almost all other complexes where mafic fenites have formed plagioclase was either altered to nepheline as at the Mbozi Complex in Canada, or to scapolite as in West Finnmark, or to zeolite as at Blue Mountains in Canada (Table 14).

This similarity is also applicable for clinopyroxenes, Spitskop augites transformed to aegirine-augite and later to aegirine and in some cases to amphibole, a feature that is very common in other complexes (Mbozi Complex, Breivikbotn Complex, Montviel Complex). Olivine and orthopyroxenes are also transformed to clinopyroxenes at the Spitskop Complex and other complexes as well (Gifford Creek Complex, Pollen Complex, Bekkarfjordness and Stjernoy). Therefore when mafic rocks alter to mafic fenites, the common primary minerals such as plagioclase, olivine, ortho- and clinopyroxenes tend to transform to nepheline and Na-rich clinopyroxenes.

5.3 Implications for REE Mineralization and Exploration

Carbonatites and alkaline rocks are main sources of rare earth elements (REE), therefore their alteration processes and element mobilities are one of the most important aspects of this study. Fenitizing fluids can contain REE and these elements were transported to the surrounding fenitized country rocks altering the composition of the fluids and changing the LREE/HREE ratio of the fenitized rock, resulting in unusual REE patterns. With intense fenitization, HREE can be greater than LREE, or individual elements may show a peak, or elements can create a wavy or u-shaped patterns, which are not common in country rocks. It is known that many rocks in the world (felsic-, mafic-, ultramafic- and alkaline rocks) contain small or relatively high amount of REEs and the ratio between the elements demonstrate similar inclined patterns with a slight decrease from LREE to HREE. However, Spitskop fenites behave differently from other

rocks in that they show anomalous REE patterns, with the various anomalous positive and negative peaks (Fig 5.4).

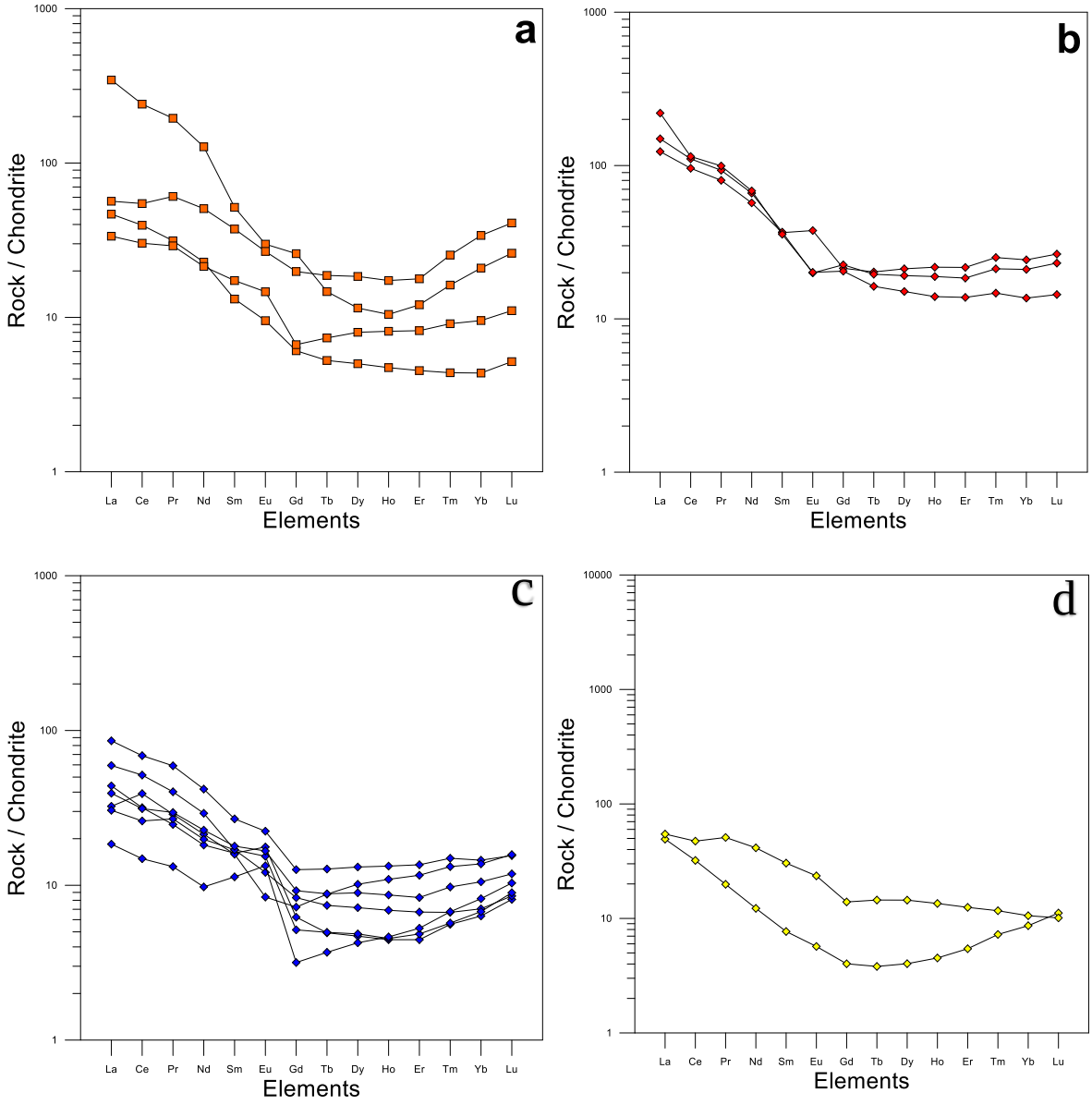

Figure 5. 3: Chondrite-normalized rare earth element diagram of (a) Spitskop feldspar fenites, (b) quartz-feldspar fenites, (c) mafic fenites, and (d) fenitized nepheline syenite. Chondrite values are taken from Sun and McDonough (1989).

After comparing fenites and their parental rocks, it is seen that additional REE transfered to the fenites during metasomatism process, however the source of the fluids, whether it is carbonatite or nepheline syenite, is not exactly clear.

It is difficult to find a fenitized rock when there is no carbonatite/alkaline rock outcrops in the field, however it is known that carbonatites and alkaline rocks occur mostly within stable intraplate environments and there are some specific environments where carbonatites/alkaline

rocks are more frequent, such as in the East African Rift Valley System. With systematic sampling in promising areas for carbonatites, this anomalous REE patterns can be found in some rocks, and it suggests that this rock is close to a carbonatite complex, and this may lead to the discovery of unexposed carbonatite complex. However, more geochemical research should be made in different fenites globally to see if they also show similar anomalous REE patterns.

5.4 Conclusions

There are many carbonatite or alkaline rock complexes that contain felsic fenites, however there are only few complexes (Table 14), which include mafic fenites and the Spitskop Complex is one of them. Although many fenite classifications have been made by different authors, there is a lack of detailed knowledge of mafic fenites and their fenitizing process because geochemical studies are missing, therefore it is not possible to compare them with other fenites and use them as a tool for exploration.

Fenites of the Spitskop Complex show both sodic and potassic metasomatism and the fenitization evolved in multiple steps. Spitskop is a unique complex, where both felsic and mafic fenites are seen together and Spitskop mafic fenite is one of the most studied mafic fenites. The original composition of the rocks that have been fenitized are well known because they are part of the well-studied Bushveld Complex, therefore the results in this study are more certain.

Alteration minerals of the Spitskop complex show that there is a systematic change of minerals, from plagioclase to albite or nepheline, from olivine and orthopyroxene to clinopyroxene, from nepheline to analcite and from clinopyroxene to amphibole. These alteration products mostly represent mafic fenites, whose alteration patterns were not clear in the literature.

The alteration products of the Spitskop mafic fenites are very similar with the other carbonatite complexes, which contain mafic-ultramafic rocks (Table 14). This concludes that the alteration reactions between mafic rock and mafic fenites are similar or the same.

The REE content of Spitskop carbonatites is up to 740 ppm on average and they are not economic, however they provide important information about the REE mobility of the fenites and the country rocks, mafic fenites have greater REE content than their parent rocks, however granitic fenites are depleted in REE compared with the Nebo granite. During the fenitization

process the REE content of the mafic protoliths increases, while the REE content of the felsic protoliths decreases and both of the protoliths tend to have similar REE content and ratios.

For the fenitized rocks Na_2O and K_2O enrichments occur, whereas SiO_2 content decreases in granitic fenites and CaO, MgO and FeO contents decrease in mafic fenites. Trace elements of the fenites also change positively or negatively during the fenitization, however they do not show unique REE patterns.

5.5 Discussion

5.5.1 Discussion of the Mafic Fenites at Spitskop

The Upper Zone gabbros of the Bushveld Complex contain pyroxenes, plagioclase, magnetite, cumulus apatite and fayalite. Where these have been fenitized, some thin sections show mineralogical relics of the original rock (Fig. 3.8d-f). After fenitization, plagioclase has been replaced by nepheline or analcite, orthopyroxene and fayalite are replaced by clinopyroxene, and clinopyroxene is replaced by sodic clinopyroxene.

Mafic fenites show Na_2O, K_2O and P_2O_5 enrichments relative to unmetasomatized Upper Zone gabbros. They also show a significant increase in REE compared to the Upper Zone gabbros, and this suggests that either the REE may come from other country rocks, which contain more REE than the Upper Zone gabbros, or that they were transported by fluids from the carbonatite or alkalic magma into the country rocks.

Although there are relatively few occurences of mafic fenites world-wide, the mineralogy of the mafic fenites of the Spitskop Complex can be compared with the other mafic fenites documented elsewhere (Table 14). Interestingly, most of them show similar alteration processes. This suggests that similar fluids were involved.

Table 14: Mafic fenites in the world.

Location	Associated Rocks	Fenitized Rocks	Alteration/New Minerals	References
1. Callander Bay, Ontario, Canada	Carbonatite, neph. sye., gneiss, garn. amphibolite	Garnet amphibolite	plagioclase→ albite	Currie and Ferguson, 1972
2. Blue Mountain, Ontario, Canada	Neph sye, amphibolite, granite, syenite	Amphibolite	plagioclase→zeolite	Payne, 1968

3. Mbozi Complex, Tanzania	Neph sye, gabbro, gneiss, pyroxenite	Gabbro	augite → aegirine-augite augite → amphibole Ca-amphibole → Na-amphibole plagioclase → nepheline nepheline → zeolite	Brock, 1968
4. Breivikbotn, Soroy, Norway	Carbonatite, Neph. sye., gabbro	Gabbro	nepheline and augite-aegirine albite → zeolite plagioclase → scapolite ilmenite → titanite pyroxene → hornblende hornblende → biotite and chlorite	Sturt and Ramsay, 1965
5. Spitskop Complex, South Africa	Carbonatite, neph. sye., ijolite, gabbro, granite	Gabbro	plagioclase → nepheline olivine → augite-aegirine orthopyroxene → augite-aegirine augite-aegirine → aegirine aegirine → amphibole	This Study
6. Montviel Complex, Canada	Carbonatite, granite, clinopyroxenite, ijolite, syenite	Clinopyroxenite	augite → augite-aegirine augite-aegirine → aegirine augite-aegirine → biotite	Nadeau et. al., 2015
7. Stjernoy, West Finnmark, Norway	Carbonatite, neph. sye., gabbro, hornblendite, syenite	Gabbro and hornblendite	clinopyroxene → hornblende orthopyroxene → hornblende plagioclase → scapolite plagioclase → albite	Heier, 1961
8. Mianning-Dechang Belt, SW China	Carbonatite, syenite, quartz diorite	Quartz diorite	aegirine-augite → biotite	Liu et. al, 2015
9. Messum Complex, Namibia	Neph. sye., syenite, granite, granophyre, gabbro, anorthosite	Gabbro	Ca-plagioclase → Na-plagioclase plagioclase → nepheline augite → amphibole	Mathias, 1956

10. Lyons River, Gifford Creek Complex, W. Australia	Ultrabasic sills	Ultrabasic sills	olivine → Na-pyroxene olivine → Na-amphibole	Pearson and Taylor, 1996
11. Pollen Complex, Finnmark, Norway	Carbonatite, gabbro, diorite, syenite	Gabbro	olivine → pyroxene-spinel symplectite olivine → Ca-poor pyroxene	Robins and Tysseland, 1983
12. Bekkarfjordness and Stjernoy, Norway	Carbonatite, Neph. sye., gabbro, gneiss	Gabbro	olivine → diopside plagioclase → nepheline	Robins, 1984
13. Khariar Alkaline Complex, SE India	Syenite, neph. sye., ijolite, meta gabbro, metadolerite, diorite	Metagabbro Metadolerite	plagioclase → nepheline plagioclase → nepheline and clinopyroxene	Upadhyay, 2012
14. Amba Dongar, Gujarat, W India	Carbonatite, nephelinite	Nephelinite	nepheline → analcite and natrolite nepheline → hydromuscovite pyroxene → phlogopite	Viladkar, 2015
15. Brava, Cape Verde Island	Carbonatite, ijolite	Ijolite	nepheline → cancrinite pyroxene → biotite and Fe-rich opaque material	Le Bas, 2008
16. Jasra Complex, India	Clinopyroxenite, gabbro, monzodiorite, neph. sye.	?	olivine → orthopyroxene olivine → phlogopite nepheline → analcite clinopyroxene → amphibole plagioclase → nepheline?	Melluso et. al, 2012
17. Richat Dome, Mauritania	Carbonatite, gabbro, rhyolite, kimberlite	Gabbro	pyroxene → amphibole pyroxene → biotite pyroxene → chlorite	Matton and Jebrak, 2014
18. Sung Valley Complex, NE India	Carbonatite, pyroxenite, ijolite, syenite	Pyroxenite	diopside → Na-pyroxene diopside → amphibole diopside → phlogopite	Viladkar et. al, 1994
19. Purulia Complex, West Bengal, India	Carbonatite, alkali-pyroxenite	Alkali-pyroxenite	diopside → biotite diopside → amphibole	Chakrabarty and Sen, 2010

5.5.2 Discussion of the Granitic Fenites at Spitskop

In Bushveld granite quartz, K-feldspar, plagioclase and biotite/hornblende are the common minerals however thin section observations of granitic fenites of the Spitskop Complex show that there is a progressive fenitization from unaltered granite to quartz-feldspar fenite and then to feldspar fenite. In quartz-feldspar fenites these minerals are transformed to aegirine, alkali amphibole, perthitic feldspar and there is less quartz. In feldspar fenite the original minerals have been transformed to aegirine and albite.

Feldspar fenites contain higher Na_2O and K_2O than quartz-feldspar fenites and the Nebo granites. MgO is enriched in the granite fenite and it is thought that MgO comes from reactions in the mafic fenite as the mafic fenites contain less MgO than the original Upper Zone gabbros. The metasomatic event also caused a decrease of REE in granites. There is a progressive depletion in REE from the Nebo granite to quartz-feldspar fenite and to feldspar fenite, this may also suggest that the REE of the Nebo granite may have been transported into the mafic fenites as the mafic fenites are enriched in REE and trace elements compared to the original Upper Zone rocks.

Evidence for metasomatism can be divided into two different scales in the granitic fenites of the Spitskop Complex:

- Macroscopic scale:

The effect of metasomatism is first seen in the field where unaltered rock and altered metasomatic rock are found together or found in close proximity, such as the Bushveld Nebo granites and the granite fenites. When these rock types are found together in a small outcrop, a sharp transition between rocks is commonly seen, including features such as reaction rims and coronas. Otherwise, when fluids affected large areas homogeneously, a smooth transition zone between altered- and unaltered rocks is observable. In the Spitskop complex, smooth transitional changes between unaltered granites and metasomatic granites are very common.

Albitization is a common type of process for most metasomatized rock types, as well as for the fenites of the Spitskop Complex. The reaction between the minerals and saline fluids are the main reason for the albitization, and the transformation of plagioclase to albite is one of the main results (Drüppel et al., 2005). It is found either at a small scale, such as in veins within fractures, or on a large scale, such as albitization of a whole outcrop. Figure 5.2 shows an

example of the small scale of albitization. This kind of albitization occurs when fluids move through a weak zone or a fracture of a rock, react with the rock and change its mineralogy.



Figure 5. 4: Small scale of albitization zones of metasomatic rocks. (a) is taken from quartz-feldspar fenite and (b) is taken from feldspar fenite. Pink zones are albititic zones.

- Microscopic scale:

Feldspar fenites contain mostly perthite, which is an alteration product and consists of microcline and albite. Radiating clusters of acicular clinopyroxenes are seen in a few thin sections. Progressive albitization is also observed.

Biotite of the Nebo granite is not observed in the thin sections of granitic fenites, however up to 5% of alkali amphiboles occur.

5.5 Suggestions for Further Work

Although fenites and fenitization process are important for REE mineralization, detailed descriptions of fenites are absent in literature. Additionally, the fenitization also continues vertically downwards and most of the alteration zones are buried and there is not enough drilling data to understand the 3D dimensions of the fenitization. To understand the fenite alteration zones and how the REE mineralization/mobility changes with depth, drilling should be undertaken in some of the promising complexes to understand the alteration zones clearly.

Detailed mineralogy and geochemistry of fenites from drill cores can be very useful for REE exploration.

It is known that fenites are the result of an alteration by carbonatites and alkaline rocks and many carbonatite complexes are documented by Woolley and Kjarsgaard (2008). Fenites in these complexes should be investigated in detail and mineralogical and geochemical similarities should be documented. Finding similarities or contrasts between different complexes will give a better understanding as to how fenitization works. Fenitization processes of the granitic rocks are already known, however the same is not the case for mafic rocks. Working on different complexes which contain mafic fenites will help to understand the fenitization and REE mobility better. The data of Spitskop Complex should be compared with other carbonatite and alkaline complexes, which contain mafic rocks. Similar alteration patterns in mafic fenites will help to find other promising mafic rocks and this can lead to discovery of new carbonatite complexes. The REE geochemistry of Spitskop Complex also shows interesting patterns, however these results should be compared with other fenites to see whether there are similar patterns or not.

One of the key gaps in understanding fenites is to separate magmatic syenites from syenites formed by fenitization. The feldspar fenite at Spitskop Complex contains up to 90 % alkali feldspar and it represents syenite formed by fenitization. The REE diagrams of feldspar fenite have unusual patterns, increases and decreases from LREE to HREE and u-shaped patterns, however magmatic syenites generally show a decrease from La to Lu. Therefore, the uncommon REE shape patterns can be used to separate unfenitized syenite and syenite formed by fenitization process when it is difficult to identify them in the field. Some fenitized syenites can be detected with this method.

The same pattern is also useful to separate magmatic nepheline syenite and nepheline syenite formed by fenitization. Geochemistry data suggests that the nepheline syenite at Spitskop may not be a magmatic nepheline syenite, rather it may be a product of fenitization, because REE pattern of the nepheline syenite are almost the same as the fenites of the Spitskop Complex and differ from other Pilanesberg nepheline syenites such as those in Pilanesberg, which are not fenitized (Fig. 5.5).

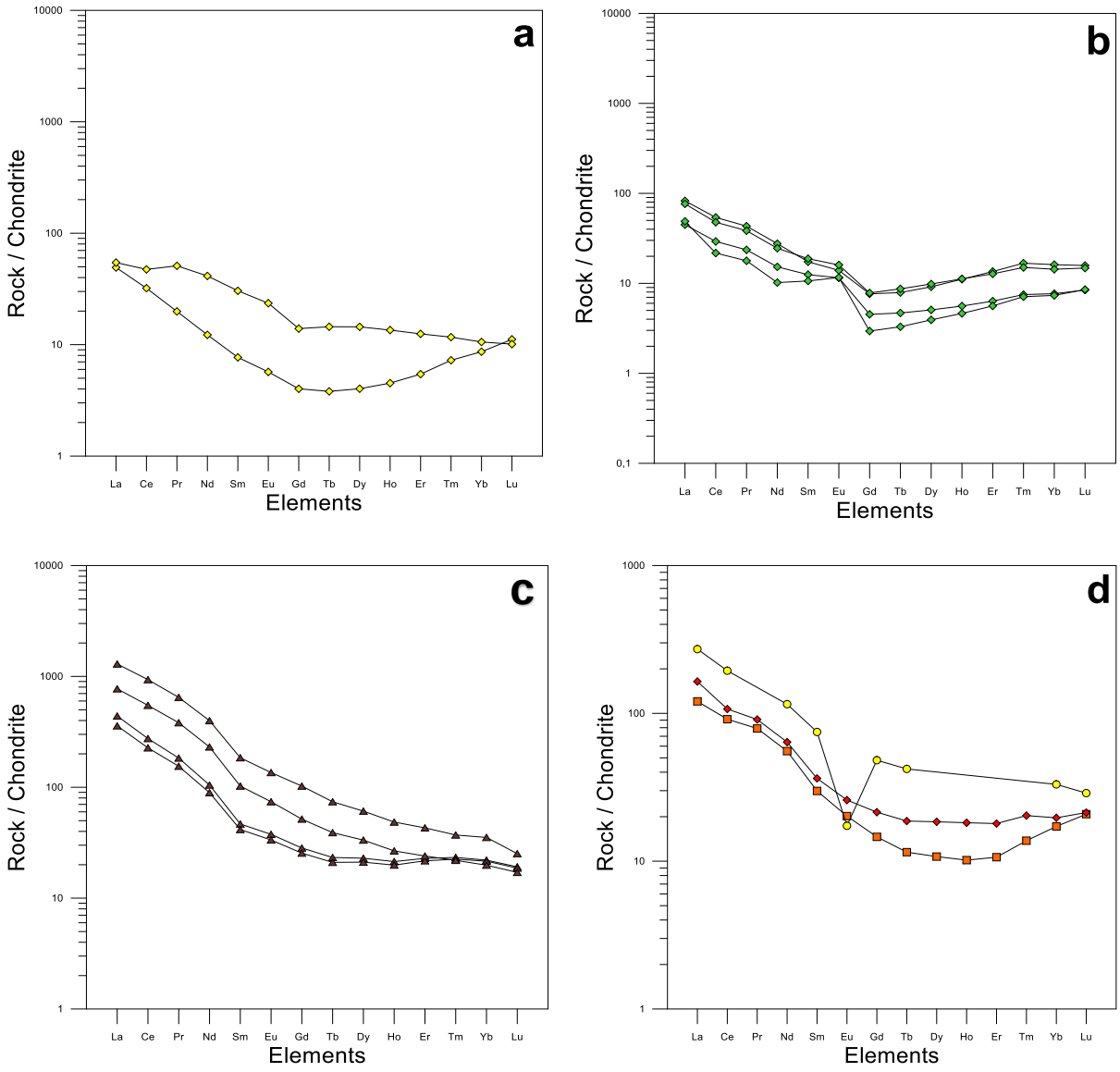

Figure 5. 5: Chondrite-normalized rare earth element diagram of (a) fenitized Spitskop nepheline syenites, (b) fenitized Mare nepheline syenites, (c) Pilanesberg nepheline syenites, and (d) average values of the Spitskop Nebo granite (yellow), quartz-feldspar fenite (red) and feldspar fenite (orange). Pilanesberg nepheline syenite data are from Elburg and Cawthorn (2017) and Nebo granite are taken from Hill et. al. (1996). Chondrite values are taken from Sun and McDonough (1989).

References

Bardina, N.Y., Popov, V.S., (1994). Fenites: systematics, formation conditions and significance for crustal magma genesis. *Zapiski Vseross. Mineral. Obshcheswa* 113, 485–497.

Bell, K., Tilton, G.R., (2001). Nd, Pb and Sr isotopic compositions of East African carbonatites: evidence for mantle mixing and plume inhomogeneity. *Journal of Petrology* 42, 1927–1945.

Beukes, N. J. & Cairncross, B., (1991). A lithostratigraphic-sedimentological reference profile for the late Mozaan Group, Pongola Sequence: application to sequence stratigraphy and correlation with the Witwatersrand Supergroup. *South Africa Journal of Geology*, 94, 44-69.

Brandl, G., de Wit, M. J., (1997). The Kaapvaal Craton. In: de Wit, M. J., Ashwal, L. D. (Ed.). *Greenstone Belts*. Clarendon Press, Oxford, pp. 581 – 607.

Brey, G.P., Bulatov, V.K., Girnis, A.V., (2009). Influence of water and fluorine on melting of carbonated peridotite at 6 and 10 GPa. *Lithos*, 112: 249-259.

Brock, P., (1968). Metasomatic and intrusive nepheline-bearing rocks from the Mbozi syenite-gabbro complex, southwestern Tanzania. *Canadian Journal of Earth Science*, 5, 387–419.

Brögger, W.G., (1921). Die eruptivegestein des kristianiagebietes, IV. Das fengebiet in telemark. *Norvegen. Naturv. Klasse* 9, 150–167.

Chakrabarty, A., Sen, A.K., (2010). Enigmatic association of the carbonatite and alkali-pyroxenite along the Northern Shear Zone, Purulia, West Bengal: a saga of primary magmatic carbonatite. *Journal of the Geological Society of India*, 76, pp. 403-413.

Cheney, E. S., (1996). Sequence stratigraphy and plate tectonic significance of the Transvaal succession of southern Africa and its equivalent in Western Australia. *Precambrian Research*, 79, 3-24.

Currie, K. L., Ferguson, J., (1972). A study of fenitization in mafic rocks, with special reference to the Callander Bay complex. *Canadian Journal of Earth Science* 9, 1254-1261.

De Wit, J. M., Roering, C., Hart, R. J., Armstrong, R. A., De Ronde, C. E. J., Green, R. W. E., Tredoux, M., Peberdy, E., Hart, R. A., (1992). Formation of an Archean continent. *Nature,* 357, 553-562.

Drüppel, K., Hoefs, J., Okrusch, M., (2005). Fenitizing processes induced by ferrocarbonatite magmatism at Swartbooisdrif, NW Namibia. *Journal of Petrology* 46: 377-406.

Eby, G. N., (1975). Abundance and distribution of the rare earth elements and yttrium in the rocks and minerals of the Oka carbonatite complex, Quebec. *Geochimica et Cosmochimica Acta* 39, 597- 620.

Elburg, M. A., Cawthorn, R. G., (2017). Source and evolution of the alkaline Pilanesberg Complex, South Africa. *Chemical Geology* 455, 148-165.

Elliott, H.A.L., Wall, F., Moore, K., Mariano, A.N., Lauri, L., (2016). Fenites: Initial results from investigations into REE micro-mineral assemblages. HiTech AlkCarb Expert Council 2: Fenite and geophysics as exploration tools Abstract Volume, 35–37.

Elliott, H.A.L., Wall, F., Chakhmouradian, A.R., Siegfried, P.R., Dahlgren, S., Weatherley, S., Finch, A.A., Marks, M.A.W., Dowman, E., Deady, E., (2018). Fenites associated with carbonatite complexes: A review. *Ore Geology Reviews*, 93, 38–59.

Fall, A., Bodnar, R. J., Szabo, C., Pal-Molnar, E., (2007). Fluid evolution in the nepheline syenites of the Ditrau Alkaline Massif, Transylvania, Romania. *Lithos* 95, 331-345.

Friese, A. E. W., Charlesworth, E. G., McCarthy, T. S., (1995). Tectonic processes within the Kaapvaal craton during the Kibaran (Grenville) orogeny: structural, geophysical and isotopic constraints from the Witwatersrand basin and environs. *Economic Geology Research Unit, University Witwatersrand, Johannesburg, Information Circular* 292, 67p.

Gose, W. A., Hanson, R. E., Harmer, R. E., Seidel, E. K., (2013). Reconnaissance paleomagnetic studies of Mesoproterozoic alkaline igneous complexes in the Kaapvaal Craton, South Africa. *Journal of African Earth Sciences*, 85, 22-30.

Grant, J.A., (1986). The Isocon Diagram - A simple solution to Gresens' equations for metasomatic alteration. *Economic Geology*, 81, 1976-1982.

Guzmics, T., Mitchell, R. H., Szabo, C., Berkesi, M., Milke, R. & Abart, R., (2011). Carbonatite melt inclusions in coexisting magnetite, apatite and monticellite in Kerimasi calciocarbonatite, Tanzania: melt evolution and petrogenesis. *Contributions to Mineralogy and Petrology*, 161, 177–196

Hall, A. L., (1910). Annual Report of the Geological Survey of the Transvaal for 1910, Pretoria, 58-60.

Hanson, R.E., Harmer, R.E., Key, R.M., Blenkinsop, T.G., Bullen, D.S., Dalziel, I.W.D., Gose, W.A., Hall, R.P., Kampunzu, A.B., Mukwakwami, J., Munyanyiwa, H., Pancake, J.A., Seidel, E.K., Ward, S.E., (2006). Mesoproterozoic intraplate magmatism in the Kalahari craton: a review. *Journal of African Earth Sciences* 46, 141–167.

Harlov, D. E., Austrheim, H., (2012). *Metasomatism and the chemical transformation of rock: the role of fluids in terrestrial and extraterrestrial processes.* Lecture notes in earth system sciences, Springer Science and Business Media, London.

Harmer, R. E., (1992). The Geochemistry of Spitskop and Related Alkaline Complexes. PhD Thesis, University of Cape Town, 287 pp.

Harmer, R. E., (1999). The petrogenetic association of carbonatite and alkaline magmatism: Constraints from the Spitskop Complex, South Africa. *Journal of Petrology* 40, 525–548.

Harmer, R. E., Gittins, J., (1998). The case for primary, mantle-derived carbonatite magma. *Journal of Petrology* 39, 1895–1903.

Heier, K.S., (1961). Layered gabbro, hornblendite, carbonatite and nepheline syenite on Stjernøy, North Norway. *Norsk Geologisk Tidsskrift*, 41, 109–155.

Hill, M., Barker, F., Hunter, D. R., Knight, R., (1996). Geochemical characteristics and origin of the Lebowa Granite Suite, Bushveld Complex. *International Geology Review* 38, 195-227.

Holmes, A., (1958). Spitskop Carbonatite, Eastern Transvaal. *Geological Society of America Bulletin* 69, 1525–1526.

Hornig-Kjarsgaard, I., (1998). Rare earth elements in sövitic carbonatites and their mineral phases. *Journal of Petrology*, 39, 2105-2122.

Ionov D., Harmer R.E., (2002). Trace element distribution in calcite-dolomite carbonatites from Spitskop: inferences for differentiation of carbonatite magmas and the origin of carbonates in mantle xenoliths. *Earth and Planetary Science Letters* 198:495–510.

Jones A.P., Genge M., Carmody L., (2013). Carbonatite melts and carbonatites. *Reviews in Mineralogy and Geochemistry*, 75: 289-322.

Kalt, A., Hegner, E., Satir, M. (1997). Nd, Sr and Pb isotopic evidence for diverse lithospheric mantle sources of East African Rift carbonatites. *Tectonophysics* 278, 31-45.

Kamenetsky, V.S., Kamenetsky, M.B., (2010). Magmatic fluids immiscible with silicate melts: examples from inclusions in phenocrysts and glasses, and implications for magma evolution and metal transport. *Geofluids* 10, 293–311.

Kinnaird, J. A., (2005). The Busveld large igneous province. Review Paper, University of the Witwatersrand, Johannesburg, 39 p.

Kleeman, G.J., Twist, D., (1989). The compositionally-zoned sheet-like granite pluton of the Bushveld Complex: Evidence bearing on the nature of A type magmatism. *Journal of Petrology*, 30, 1383-1414.

Kretz, R., (1983). Symbols of rock-forming minerals. *American Mineralogist*, 68, 277-279.

Le Bas, M. F., (1987). Nephelites and Carbonatites. Geological Society, London, Special Publications, 30(1):53-83.

Le Bas, M. J., (2008). Fenites associated with carbonatites. *Canadian Mineralogist* 46, 915-932.

Le Maitre, R. W., (2002). *Igneous Rocks: A Classification and Glossary of Terms* 2nd Edition.

Lee, W. J., Wyllie, P. J., (1994). Experimental data bearing on liquid immiscibility, crystal fractionation, and the origin of calciocarbonatites and natrocarbonatites. *International Geological Review*, 36, 797-819.

Lee, S. A., Webb, S. J., Jones, M. Q. W., Durrheim, R. J., Ganerod, M., (2013). A 3D potential field model of the Pilanesberg Complex shape and structure. 13th SAGA Biennial Conference and Exhibition.

Liu Y., Zhu Z. M., Chen C., Zhang S. P., Sun X., Yang Z. S. and Liang W., (2015). Geochemical and mineralogical characteristics of weathered ore in the Dalucao REE deposit, Mianning-Dechang REE Belt, western Sichuan Province, southwestern China. *Ore Geology Reviews* 71, 437–456.

Loubet, M., Bernat, M., Javoy, M. & Allegre, C. J., (1972). Rare earth contents in carbonatites. *Earth and Planetary Science Letters* 14, 226-32.

Mariano, A. N., (1989). Nature of economic mineralization in carbonatites and related rocks. In K. Bell ed., *Carbonatites: Genesis and Evolution*. Unwin Hyman, London, pp. 149-175.

Mathias, M., (1956). The petrology of the Messum igneous complex, south-west Africa. *Transactions of the Geological Society of South Africa*, 59, 35 pp.

Matton, G., Jebrak, M., (2014). The eye of Africa (Richat dome, Mauritania): an isolated cretaceous alkaline-hydrothermal complex. *Journal of African Earth Science* 97:109–124.

McDonough W.F., Sun S.S., (1995). The composition of the Earth. *Chemical Geology* 120, 223-253.

McDougall, I., (1963). Potassium–argon age measurements on dolerites from Antarctica and South Africa. *Journal of Geophysical Research* 68, 1535–1545.

Melluso, L., Srivastava, R. K., Petrone, C. M., Guarino, V., Sinha, A. K., (2012). Mineralogy, magmatic affinity and evolution of the Early Cretaceous alkaline complex of Jasra, Shillong Plateau, northeastern India. *Mineralogical Magazine*, 76, 1099–1117.

Mitchell, A. H. G., Garson, M. S. (Eds.), (1981). *Mineral Deposits and Global Tectonic Settings*. Academic Press, London. 405 pp.

Mitchell, R.H., (2009). Peralkaline nephelinite–natrocarbonatite immiscibility and carbonatite assimilation at Oldoinyo Lengai, Tanzania. *Contributions to Mineralogy and Petrology* 158, 589–598.

Moller, P., Morteani, G. & Schley, F., (1980). Discussion of REE distribution patterns of carbonatites and alkaline rocks. *Lithos* 13, 171-9.

Nadeau, O., Cayer, A., Pelletier, M., Stevenson, R., Jebrak, M., (2015). The Paleoproterozoic Montviel carbonatite-hosted REE–Nb deposit, Abitibi, Canada: geology, mineralogy, geochemistry and genesis. *Ore Geology Reviews* 67, 314–335.

Naumann, K. F., (1826). *Lehrbuch der Mineralogie*. Leipzig, Engelman, 209 pp.

Nelson, D. R., Chivas, A. R., Chappell, B. W., McCulloch, M. T., (1988). Geochemical and isotopic systematics in carbonatites and implications for the evolution of ocean-island sources. *Geochimica et Cosmochimica Acta* 52, 1-17.

Olsson, J.R., Söderlund, U., Klausen, M.B. & Ernst, R.E., (2010). U–Pb baddeleyite ages linking major Archean dyke swarms to volcanic-rift forming events in the Kaapvaal craton (South Africa), and a precise age for the Bushveld Complex. *Precambrian Research* 183, 490–500.

Payne, J.G., (1968). Geology and geochemistry of the Blue Mountain nepheline syenite. *Canadian Journal of Earth Science* 5, p. 269-273.

Pearson, J.M., Taylor, W.R., (1996). Mineralogy and geochemistry of fenitized alkaline ultrabasic sills of the Gifford Creek Complex, Gascoyne Province, Western Australia: *Canadian Mineralogist* 34, p. 201-219.

Rankin, A. H., (2003). Carbonatite-associated rare metal deposits: composition and evolution of ore-forming fluids - the fluid inclusion evidence. In: Linnen, R. L., Samson, I. M. (Eds.), *Rare-Element Geochemistry and Mineral Deposits*: Geological Association of Canada Short Course Notes, vol. 17, pp. 299–314.

Robins, B., Tysseland, M., (1983). The geology, geochemistry and origin of ultrabasic fenites associated with the Pollen carbonatite, Finnmark, Norway. *Chemical Geology* 40:65-95.

Robins, B., (1984). Petrography and petrogenesis of nephelinized metagabbros from Finmark, northern Norway. *Contributions to Mineralogy and Petrology* 86: 170-177.

SACS, (1980). *Stratigraphy of South Africa*. Part 1 In: L.E. Kent (Compiler), Lithostratigraphy of the Republic of South Africa, Handbook Geological Survey of South Africa, 8. 690 pp.

Scoon, R.N., Mitchell, A.A., (2012). The upper zone of the Bushveld complex at Roossenekal, South Africa: Geochemical stratigraphy and evidence of multiple episodes of magma replenishment. *South African Journal of Geology* 115: 515–534.

Shand, S. J., (1921). The nepheline rocks of Sekukuniland. *Transactions of the Geological Society of South Africa*, 24, 111-149.

Strauss, C. A. and Truter, F. C., (1950). The alkali complex at Spitskop, Sekukuniland, Eastern Transvaal. *Transactions of the Geological Society of South Africa*., 53, 81-125.

Sturt, B. A., Ramsay, D. M., (1965). The alkaline complex of the Breivikboton area, Soroy, N. Norway. *Norg. geol. Unders.* 231, 1-142.

Sun, S., McDonough, W.F., (1989). Chemical and isotopic systematics of oceanic basalts: implications for mantle composition and processes. In: Sanders, A.D., Norry M.J., (Edition), Magmatism in the ocean basins. *Geological Society of London Special Publication* 42, 313-345.

Tegner, C., Cawthorn, R.G., Kruger, F.J., (2006). Cyclicity in the main and upper zones of the Bushveld Complex, South Africa: Crystallization from a zoned magma sheet. *Journal of Petrology* 47, 2257-2279.

Upadhyay, D., (2012). Alteration of plagioclase to nepheline in the Khariar alkaline complex, SE India: Constraints on metasomatic replacement reaction mechanisms *Lithos* 155 19-29.

Van Breemen, O., Dodson, M. H., (1972). Metamorphic chronology of the Limpopo Belt, southern Africa. *Geological Society of America Bulletin* 83: 2005-2018.

Van Niekerk, C. B., (1962). The age of the Gemspost Dyke from the Venterspost gold mine. *Transactions of the Geological Society of South Africa* 65, 105–111.

Van Tongeren, J. A., (2011). The 'Ins' and 'Outs' of the Bushveld Complex Upper Zone. Phd Thesis, Columbia University, 198 pp.

Verwoerd, W.J., (1964). The significance of fenitised granite pegmatites in the Spitskop Complex. *Transactions of the Geological Society of South Africa* 67, 219-227.

Verwoerd, W. J., (1967). *The carbonatites of South Africa and South West Africa*: Handbook Geological Survey of South Africa 6, 452p.

Verwoerd, W.J., (2006). The Pilanesberg Alkaline Province. In: Johnson, M.R., Anhaeusser, C.R., Thomas, R.J. (Eds.), *The Geology of South Africa*. Geological Society of South Africa, Johannesburg, pp. 81–394.

Viladkar, S.G., Schleicher, H., Pawaskar, P., (1994). Mineralogy and geochemistry of the Sung Valley carbonatite complex, Shillong, Meghalaya, India. *Neues Jahrbuch Mineralogie Monatshefte* 11, 499-517.

Viladkar, S.G., (2015). Mineralogy and geochemistry of fenitized nephelinites of the Amba Dongar Complex, Gujarat. *Journal of the Geological Society of India* 85, 87–97.

Williams-Jones, A.E., Palmer, D.A.S., (2002). The evolution of aqueous-carbonic fluids in the Amba Dongar carbonatite, India: implications for fenitisation. *Chemical Geology* 185, 283–301.

Wilson, J., Ferre, E.C. and Lespinasse, P., (2000). Repeated tabular injection of high-level alkaline granites in the eastern Bushveld, South Africa. *Journal of the Geological Society of London*, 157, 1077-1088.

Woolley A.R., Kempe D.R.C., (1989). Carbonatites: Nomenclature, average chemical compositions and element distribution. In Carbonatites: *Genesis and Evolution*. Bell K (ed) Unwin Hyman, London, p 1-14.

Woolley, A. R., (2001). *Alkaline Rocks and Carbonatites of the World. Part 3: Africa*. Bath: The Geological Society of London.

Woolley, A.R., and Kjarsgaard, B.A., (2008). Paragenetic types of carbonatite as indicated by the diversity and relative abundances of associated silicate rocks—evidence from global database: *Canadian Mineralogist* 46, p. 741–752.

Ying J., Zhou X. and Zhang H., (2004). Geochemical and isotopic investigation of the Laiwu-Zibo carbonatites from western Shandong Province, China, and implications for their petrogenesis and enriched mantle source. *Lithos* 75, 413-426.

Yongliang, X., Yusheng, Z., (1991). The mobility of rare-earth elements during hydrothermal activity: a review. *Chinese Journal of Geochemistry* 10: 296–306.

Zegers, T. E., de Wit, M. J., Dann, J., White, S. H., (1998). Vaalbarra, Earth's oldest assembled continent? A combined structural, geochronical, and paleomagnetic test. *Terra Nova*, 10, 250-259.

Zeh, A., Ovtcharova, M., Wilson, A. H., Schaltegger., U., (2015). The Bushveld Complex was emplaced and cooled in less than one million years- result of zirconology, and geotectonic implications. *Earth and Planetary Science Letters* 418, 103-114.

Zharikov, V.A., Pertsev, N.N., Rusinov, V.L., Callegari, E., Fettes, D.J., (2007). Metasomatism and metasomatic rocks. In: Recommendations by the IUGS Subcommision of the Systematics of Metamorphic Rocks. British Geological Survey.

Supplementary Data

1. Spitskop Carbonatites

Table 1: Spitskop calcite carbonatite major element geochemistry.

Samples	*SiO_2*	*Al_2O_3*	*Fe_2O_3*	*FeO*	*MnO*	*MgO*	*CaO*	*Na_2O*	*K_2O*	*TiO_2*	*P_2O_5*	*Cr_2O_3*	*NiO*	*LOI*	*Total*
6-69-1	3,03	0,86	0,18	1,44	0,48	1,95	52,73	0,00	0,01	0,03	0,15	0,01	0,00	39,04	99,91
7-85	1,01	0,17	0,10	0,85	0,19	0,37	55,41	0,00	0,00	0,03	0,04	0,01	0,00	41,92	100,12
8-90	0,57	0,10	0,66	5,33	0,34	0,20	52,84	0,03	0,00	0,06	4,70	0,02	0,00	34,80	99,64
8-92	1,54	0,12	0,67	5,40	0,36	1,33	50,59	0,00	0,00	0,07	3,26	0,01	0,00	36,38	99,73
S57	1,46	0,30	2,13	-	0,50	0,86	52,37	0,00	0,01	0,01	0,08	-	-	41,03	100,00
S86	3,33	0,05	3,04	-	0,74	3,06	48,79	0,73	0,01	0,06	2,58	-	-	38,30	100,71
S87	2,51	0,07	2,47	-	0,69	2,29	50,94	0,63	0,00	0,04	1,76	-	-	39,32	100,73

Table 2: Spitskop calcite carbonatite trace element geochemistry.

Samples	*Sc*	*V*	*Cr*	*Co*	*Ni*	*Cu*	*Zn*	*Ga*	*Rb*	*Sr*	*Y*	*Zr*	*Nb*	*Mo*	*Ba*	*Pb*	*Th*	*U*
6-69-1	42,74	7,06	5,23	4,30	0,00	14,55	22,20	2,28	2,68	1702,45	33,73	0,00	0,88	0,00	127,50	24,96	4,52	0,34
7-85	45,72	0,00	3,32	9,98	1,98	8,45	9,16	0,09	1,33	1623,20	20,98	2,62	3,61	0,20	699,37	14,02	0,00	1,47
8-90	53,68	34,37	3,56	16,64	0,00	1,50	28,69	1,59	0,00	1783,43	214,19	9,92	4,20	1,42	680,96	16,98	8,25	2,38
8-92	50,90	19,69	7,18	10,21	0,86	6,31	12,93	2,48	1,67	1083,95	107,06	9,69	5,42	0,40	207,68	13,38	0,33	0,42
S57	0,00	9,00	0,00	5,60	0,00	0,00	24,00	-	3,70	2571,00	24,00	49,00	0,00	-	130,00	27,00	15,00	11,00
S86	0,00	25,00	32,00	1,90	2,70	20,00	26,00	-	0,00	1645,00	71,00	17,00	23,00	-	633,00	13,00	1,20	0,00
S87	0,00	27,00	48,00	3,10	3,10	28,00	25,00	-	1,20	2381,00	60,00	3,20	13,00	-	989,00	16,00	1,20	0,00

Table 3: Spitskop calcite carbonatite rare earth element geochemistry.

Samples	*La*	*Ce*	*Pr*	*Nd*	*Sm*	*Eu*	*Gd*	*Tb*	*Dy*	*Ho*	*Er*	*Tm*	*Yb*	*Lu*
6-69-1	58,43	104,40	14,04	55,72	12,50	4,12	11,51	1,73	9,02	1,50	2,97	0,35	1,97	0,25
7-85	80,10	148,60	21,49	89,12	15,01	4,18	11,62	1,56	6,82	0,94	1,76	0,17	0,97	0,13

8-90	86,41	188,68	27,56	117,70	25,83	7,91	22,96	5,03	40,39	9,45	21,55	2,69	11,54	1,18
8-92	92,48	194,64	26,68	108,03	22,80	6,58	18,01	3,42	25,77	4,91	10,00	1,26	6,52	0,76
S57	68,00	158,00	21,00	90,00	18,00	5,30	15,00	-	6,70	1,10	2,50	-	1,30	0,10

Table 4: Spitskop calcite-dolomite carbonatite major element geochemistry.

Samples	*SiO_2*	*Al_2O_3*	*Fe_2O_3*	*FeO*	*MnO*	*MgO*	*CaO*	*Na_2O*	*K_2O*	*TiO_2*	*P_2O_5*	*Cr_2O_3*	*NiO*	*LOI*	*Total*
8-91	1,34	0,04	0,20	1,60	0,67	6,88	47,04	0,11	0,01	0,03	1,08	0,01	0,00	41,13	100,13
8-96	1,28	0,04	0,31	2,55	0,68	6,58	45,53	0,11	0,00	0,03	1,33	0,02	0,00	40,70	99,16
8-100	1,28	0,10	0,30	2,41	0,56	7,45	45,86	0,07	0,00	0,03	0,05	0,01	0,00	42,32	100,46
S21	0,21	0,04	2,26	-	0,78	8,70	44,42	0,00	0,00	0,02	0,13	-	-	44,21	100,77
S53	1,51	0,03	2,33	-	0,99	4,78	48,23	0,00	0,00	0,03	1,29	-	-	41,30	100,51
S55	0,53	0,04	1,95	-	0,62	7,98	44,95	0,00	0,00	0,00	2,44	-	-	41,51	100,30
S56	0,51	0,09	1,98	-	0,61	8,23	45,30	1,09	0,00	0,01	2,49	-	-	39,64	99,97
S91	4,16	0,16	6,94	-	0,59	4,49	45,15	0,93	0,00	0,10	5,85	-	-	32,84	101,36

Table 5: Spitskop calcite-dolomite carbonatite trace element geochemistry.

Samples	*Sc*	*V*	*Cr*	*Co*	*Ni*	*Cu*	*Zn*	*Ga*	*Rb*	*Sr*	*Y*	*Zr*	*Nb*	*Mo*	*Ba*	*Pb*	*Th*	*U*
8-91	46,27	5,26	5,06	3,1	1,06	1,71	16,17	0,00	1,76	712,79	43,9	1,55	1,29	0,00	186,77	31,58	0,00	0,00
8-96	39,76	7,25	11,05	2,68	0,00	4,66	19,12	0,83	1,25	598,42	55,8	9,44	3,06	0,00	64,72	26,87	0,00	0,00
8-100	47,71	5,47	4,94	10,72	0,8	4,19	29,33	0,54	2,22	499,94	20,71	7,76	5,9	1,27	44,21	17,88	0,22	0,00
S21	0,00	7,20	0,00	0,00	0,00	0,00	30,00	-	2,40	380,00	29,00	9,80	5,00	-	11,00	42,00	6,10	5,60
S53	0,00	22,00	0,00	3,90	0,00	0,00	58,00	-	2,40	1851,00	37,00	44,00	7,60	-	96,00	25,00	9,90	5,70
S55	0,00	5,70	0,00	3,50	0,00	0,00	12,00	-	3,00	822,00	173,00	22,00	0,00	-	46,00	22,00	12,00	8,60
S56	0,00	4,50	0,00	4,30	0,00	0,00	24,00	-	3,00	1756,00	68,00	34,00	0,00	-	150,00	35,00	8,00	6,00
S91	0,00	79,00	25,00	7,80	3,60	20,00	78,00	-	0,00	1294,00	76,00	22,00	12,00	-	597,00	27,00	3,30	0,00

Table 6: Spitskop calcite-dolomite carbonatite rare earth element geochemistry.

Samples	*La*	*Ce*	*Pr*	*Nd*	*Sm*	*Eu*	*Gd*	*Tb*	*Dy*	*Ho*	*Er*	*Tm*	*Yb*	*Lu*

8-91	72,68	145,30	23,66	90,08	15,09	3,88	11,08	1,52	9,06	2,01	5,20	0,73	3,95	0,49
8-96	146,41	302,72	39,53	150,03	28,81	7,67	21,66	2,84	14,37	2,52	5,97	0,86	5,88	0,93
8-100	219,75	339,46	35,00	99,69	9,59	2,19	10,04	1,07	5,23	0,87	2,08	0,24	1,70	0,27
S53	152,00	305,00	34,00	134,00	21,00	5,80	16,00	-	8,90	1,70	4,10	-	2,00	0,20
S55	155,00	401,00	55,00	235,00	55,00	17,00	51,00	-	38,00	7,00	16,00	-	9,20	1,00

Table 7: Spitskop dolomite carbonatite major element geochemistry.

Samples	*SiO_2*	*Al_2O_3*	*Fe_2O_3*	*FeO*	*MnO*	*MgO*	*CaO*	*Na_2O*	*K_2O*	*TiO_2*	*P_2O_5*	*Cr_2O_3*	*NiO*	*LOI*	*Total*
6-74-2	0,40	0,05	0,54	4,38	0,96	15,11	33,98	0,02	0,01	0,02	2,42	0,01	0,00	41,42	99,31
7-76-1	0,66	0,06	0,84	6,78	1,82	11,99	35,32	0,04	0,02	0,02	10,16	0,02	0,00	31,38	99,12
7-76-2	0,53	0,08	0,87	7,08	1,79	14,24	32,53	0,02	0,02	0,03	5,45	0,03	0,01	36,53	99,19
7-77	0,80	0,03	3,26	26,41	0,74	14,01	22,19	0,00	0,01	0,05	0,01	0,02	0,00	32,31	99,84
8-93	0,21	0,03	0,61	4,97	0,92	14,30	34,64	0,00	0,00	0,02	2,98	0,01	0,00	41,04	99,73
8-99	1,06	0,09	0,60	4,84	1,08	17,24	31,02	0,09	0,00	0,03	1,53	0,01	0,00	42,07	99,65
S05	0,00	0,03	5,55	-	1,20	16,75	30,12	0,00	0,00	0,00	1,75	-	-	42,90	98,48
S06	0,38	0,00	9,85	-	1,70	15,10	29,73	0,00	0,02	0,02	1,95	-	-	40,83	99,59
S27	0,12	0,02	6,26	-	1,62	12,47	34,62	0,00	0,00	0,00	7,82	-	-	37,84	100,96
S54	2,41	0,02	3,10	-	1,39	13,48	35,05	0,00	0,01	0,00	0,06	-	-	43,29	98,82
S58	0,32	0,08	6,14	-	1,38	17,66	29,28	0,00	0,01	0,00	0,05	-	-	44,94	99,87
S59	0,00	0,03	4,66	-	1,13	17,56	28,78	0,00	0,00	0,00	0,01	-	-	45,51	97,68
S61	0,16	0,01	4,70	-	0,85	16,40	32,27	0,00	0,01	0,00	1,37	-	-	43,57	99,35

Table 8: Spitskop dolomite carbonatite trace element geochemistry.

Samples	*Sc*	*V*	*Cr*	*Co*	*Ni*	*Cu*	*Zn*	*Ga*	*Rb*	*Sr*	*Y*	*Zr*	*Nb*	*Mo*	*Ba*	*Pb*	*Th*	*U*
6-74-2	34,24	3,36	7,29	3,26	0,71	4,14	13,55	0,59	2,04	612,97	79,65	2,94	4,84	0,67	62,99	20,04	2,78	0,00
7-76-1	48,17	13,78	0,00	6,57	0,00	4,6	75,32	0,00	0,12	1235,55	219,6	13,56	215,76	0,68	217,75	40,93	32,6	44,78
7-76-2	41,37	22,33	0,00	1,20	4,36	8,15	79,53	0,00	0,00	999,6	156,1	21,96	301,17	0,00	109,84	37,83	17,5	61,67
7-77	42,44	47,67	0,00	6,09	5,48	13,62	60,23	0,76	0,00	1676,6	39,73	0,00	264,21	0,54	195,78	8,63	0,00	10,43
8-93	34,09	0,53	4,17	1,01	3,05	15,1	27,81	0,00	0,62	694,38	123,71	0,00	2,93	0,15	136,38	19,24	0,00	0,00

8-99	26,55	15,7	0,42	1,49	1,92	2,81	119,18	0,68	1,6	502,23	74,99	15,57	43,26	0,53	119,46	47,09	2,44	0,00
S05	15,00	0,00	0,00	0,00	0,00	0,00	248,00	-	2,30	1561,00	43,00	0,00	31,00	-	23,00	16,00	19,00	5,40
S06	13,00	18,00	0,00	4,90	0,00	0,00	384,00	-	3,50	1181,00	48,00	50,00	201,00	-	75,00	72,00	17,00	26,00
S27	4,40	3,10	0,00	0,00	0,00	0,00	60,00	-	0,00	965,00	235,00	0,00	12,00	-	22,00	21,00	24,00	12,00
S54	0,00	7,00	0,00	0,00	0,00	0,00	30,00	-	3,70	261,00	5,00	6,90	3,80	-	11,00	75,00	8,60	11,00
S58	10,00	6,00	0,00	5,40	0,00	0,00	119,00	-	4,30	2181,00	32,00	40,00	4,10	-	38,00	35,00	12,00	12,00
S59	14,00	3,70	0,00	0,00	0,00	0,00	56,00	-	2,70	2582,00	29,00	47,00	3,80	-	34,00	36,00	8,50	6,50
S61	0,00	6,10	0,00	0,00	0,00	0,00	22,00	-	2,70	495,00	52,00	15,00	0,00	-	36,00	24,00	8,20	7,90

Table 9: Spitskop dolomite carbonatite rare earth element geochemistry.

Samples	*La*	*Ce*	*Pr*	*Nd*	*Sm*	*Eu*	*Gd*	*Tb*	*Dy*	*Ho*	*Er*	*Tm*	*Yb*	*Lu*
6-74-2	87,22	197,57	26,65	118,93	26,41	8,24	25,80	3,26	17,57	3,12	7,77	0,99	6,61	1,07
7-76-1	221,47	400,41	52,72	199,92	44,88	13,65	39,34	6,72	43,57	9,18	22,76	3,48	20,53	2,81
7-76-2	169,36	305,63	39,17	144,04	30,92	9,14	26,07	4,31	29,42	6,56	16,60	2,49	14,21	1,90
7-77	112,85	152,18	16,68	54,06	6,92	1,99	7,05	1,14	7,37	1,41	3,05	0,38	2,00	0,24
8-93	180,23	328,33	41,13	150,92	28,71	7,86	23,38	3,51	22,53	5,16	14,08	2,28	14,04	1,95
8-99	208,83	366,76	46,73	174,67	35,53	9,36	27,21	3,67	19,89	3,56	7,87	1,04	6,27	0,85
S27	145,00	312,00	35,00	148,00	27,00	8,50	28,00	-	39,00	8,60	24,00	-	15,00	1,80
S54	285,00	507,00	48,00	143,00	8,30	1,40	3,80	-	1,90	0,50	1,80	-	0,90	0,10
S59	136,00	286,00	29,00	96,00	11,00	2,90	9,00	-	7,30	1,30	3,10	-	1,40	0,20
S61	88,00	194,00	23,00	106,00	21,00	6,30	18,00	-	13,00	2,10	5,00	-	3,10	0,40

Table 10: Spitskop and Mare nepheline syenite major element geochemistry.

Samples	*SiO_2*	*Al_2O_3*	*Fe_2O_3*	*FeO*	*MnO*	*MgO*	*CaO*	*Na_2O*	*K_2O*	*TiO_2*	*P_2O_5*	*Cr_2O_3*	*NiO*	*LOI*	*Total*
3-23-1	54,79	20,56	0,44	3,63	0,11	0,43	2,00	11,74	3,97	0,60	0,10	0,01	0,00	1,37	99,75
3-23-2	55,53	20,55	0,43	3,47	0,10	0,36	1,24	9,99	5,72	0,43	0,07	0,01	0,00	1,91	99,80
3-24	55,03	17,62	0,54	4,38	0,14	0,25	2,84	8,08	6,11	0,37	0,08	0,00	0,00	4,21	99,66
3-25	50,44	21,24	0,58	4,64	0,17	0,52	2,38	11,93	4,50	0,80	0,12	0,00	0,00	2,51	99,82
3-31-3	58,22	17,28	0,60	4,89	0,12	0,09	0,52	7,48	7,30	0,50	0,05	0,00	0,00	2,41	99,47

3-32	53,70	19,11	0,65	5,32	0,14	0,28	1,76	10,44	4,34	0,32	0,03	0,01	0,00	3,67	99,78
S07	54,28	20,81	5,25	-	0,14	0,34	1,93	9,98	4,96	0,54	0,07	-	-	2,07	100,51
S08	51,79	21,40	4,90	-	0,13	0,63	2,68	11,36	4,52	0,74	0,18	-	-	1,02	99,47
S96	56,55	19,07	6,69	-	0,08	0,26	1,04	11,39	3,15	0,38	0,00	-	-	0,46	99,15
S97	54,31	21,01	5,23	-	0,09	0,43	1,51	11,90	3,95	0,32	0,05	-	-	1,36	100,26
S102	55,34	18,76	4,76	-	0,10	0,37	2,70	10,42	4,57	0,39	0,08	-	-	1,63	99,23
S147	53,67	20,80	5,28	-	0,09	0,55	1,71	11,54	3,77	0,57	0,09	-	-	1,81	100,02
S148	53,24	21,08	4,44	-	0,11	0,67	1,84	10,77	5,22	0,46	0,07	-	-	0,70	98,70
S149	54,66	17,95	6,50	-	0,10	0,34	1,42	11,09	4,15	0,42	0,03	-	-	0,68	97,44
S150	54,33	18,51	6,73	-	0,11	0,29	0,52	10,36	5,00	0,37	0,01	-	-	2,30	98,69
S10	52,09	21,33	4,88	-	0,15	0,44	2,38	11,71	4,59	0,63	0,13	-	-	1,06	99,52
S11	55,56	19,18	5,22	-	0,20	0,20	1,35	9,99	4,92	0,31	0,03	-	-	3,17	100,39
S17	54,72	19,63	5,51	-	0,12	0,06	0,93	9,72	6,24	0,31	0,00	-	-	1,66	99,03
S19	54,80	18,90	6,04	-	0,13	0,08	0,75	11,17	4,26	0,35	0,00	-	-	3,07	99,69
S141	52,48	20,78	5,02	-	0,08	0,64	1,98	11,51	5,02	0,66	0,12	-	-	1,27	99,67

2. Spitskop-, Mare-, Rietfontein- and Pilanesberg Nepheline Syenites

Table 11: Spitskop and Mare nepheline syenite trace element geochemistry.

Samples	*Sc*	*V*	*Cr*	*Co*	*Ni*	*Cu*	*Zn*	*Ga*	*Rb*	*Sr*	*Y*	*Zr*	*Nb*	*Mo*	*Ba*	*Pb*	*Th*	*U*
3-23-1	2,58	52,79	7,61	6,53	2,63	6,87	42,82	20,20	86,39	648,17	12,91	113,52	16,48	0,48	1725,2	21,15	1,47	1,12
3-23-2	1,22	37,33	0,00	2,79	0,00	7,36	58,17	22,00	119,01	683,84	10,80	154,22	26,51	0,00	2542,08	22,67	5,17	4,95
3-24	2,77	28,71	8,72	5,97	2,20	6,23	91,78	24,17	124,97	637,51	28,28	247,00	22,99	1,62	1298,03	40,44	2,25	5,82
3-25	2,34	55,69	0,00	0,00	1,31	4,36	108,71	24,44	108,44	860,81	25,68	135,13	43,04	0,00	1623,59	12,79	4,56	2,36
3-31-3	0,00	2,55	0,00	2,50	1,04	6,63	95,62	29,13	220,39	223,78	8,20	279,30	21,94	0,49	343,51	25,76	4,46	1,60
3-32	2,37	49,62	0,00	4,15	1,19	12,06	112,24	22,99	93,92	684,20	7,95	187,84	23,12	1,32	979,59	20,93	3,28	6,00
S07	0,00	51,00	0,00	4,10	0,00	1,40	48,00	-	86,00	591,00	12,00	115,00	18,00	-	1500,00	24,00	4,70	0,00
S08	0,00	62,00	0,00	7,60	0,00	0,00	37,00	-	100,00	626,00	12,00	164,00	25,00	-	1666,00	12,00	7,10	8,20
S96	0,00	30,00	0,00	8,40	0,00	0,00	43,00	-	89,00	198,00	4,70	162,00	3,40	-	388,00	0,00	0,00	0,00
S97	0,00	17,00	0,00	6,20	0,00	0,00	43,00	-	114,00	394,00	17,00	335,00	5,60	-	351,00	0,00	0,00	0,00
S102	0,00	36,00	0,00	3,80	0,00	0,00	55,00	-	87,00	712,00	5,00	315,00	29,00	-	1458,00	0,00	0,00	0,00

S147	0,00	42,00	0,00	7,90	0,00	0,00	34,00	-	89,00	624,00	10,00	154,00	14,00	-	949,00	22,00	0,00	0,00
S148	0,00	49,00	0,00	9,30	0,00	0,00	30,00	-	113,00	617,00	9,30	132,00	19,00	-	1720,00	0,00	0,00	0,00
S149	0,00	0,00	0,00	0,00	0,00	0,00	0,00	-	94,00	446,00	5,80	134,00	10,00	-	930,00	0,00	0,00	0,00
S150	0,00	40,00	1,80	6,80	0,00	9,50	65,00	-	115,00	628,00	16,00	136,00	31,00	-	1485,00	18,00	0,00	0,00
S10	0,00	58,00	0,00	7,70	0,00	0,00	53,00	-	94,00	518,00	7,90	150,00	26,00	-	1446,00	18,00	8,60	7,80
S11	0,00	33,00	0,00	2,70	0,00	0,00	137,00	-	112,00	863,00	23,00	252,00	35,00	-	964,00	35,00	11,00	0,00
S17	0,00	36,00	0,00	3,90	0,00	0,00	36,00	-	148,00	573,00	4,10	150,00	5,40	-	1012,00	9,80	4,40	6,80
S19	0,00	18,00	0,00	3,20	0,00	0,00	46,00	-	129,00	531,00	4,80	207,00	8,00	-	190,00	8,40	5,70	5,10
S141	0,00	44,00	0,00	6,60	0,00	0,00	55,00	-	102,00	713,00	16,00	123,00	22,00	-	1800,00	6,20	0,00	0,00

Table 12: Spitskop and Mare nepheline syenite rare earth element geochemistry.

Samples	*La*	*Ce*	*Pr*	*Nd*	*Sm*	*Eu*	*Gd*	*Tb*	*Dy*	*Ho*	*Er*	*Tm*	*Yb*	*Lu*
3-23-1	16,45	28,00	3,23	10,84	2,89	1,00	1,39	0,27	1,93	0,48	1,58	0,27	1,90	0,32
3-23-2	17,93	20,78	2,44	7,25	2,46	1,01	0,90	0,19	1,50	0,39	1,40	0,25	1,82	0,33
3-24	30,32	51,73	5,92	19,64	4,01	1,21	2,34	0,46	3,49	0,95	3,37	0,60	4,00	0,60
3-25	28,04	45,68	5,27	17,46	4,34	1,39	2,39	0,50	3,75	0,95	3,18	0,54	3,56	0,56
3-31-3	18,09	30,72	2,72	8,71	1,78	0,50	1,23	0,22	1,53	0,38	1,35	0,26	2,14	0,43
3-32	20,01	45,31	6,98	29,42	7,03	2,05	4,26	0,84	5,50	1,15	3,11	0,42	2,62	0,39

Table 13: Rietfontein nepheline syenite major element geochemistry.

Samples	*SiO_2*	*Al_2O_3*	*Fe_2O_3*	*FeO*	*MnO*	*MgO*	*CaO*	*Na_2O*	*K_2O*	*TiO_2*	*P_2O_5*	*Cr_2O_3*	*NiO*	*LOI*	*Total*
S01	53,13	17,36	7,29	-	0,26	0,26	2,16	11,75	3,79	0,65	0,09	-	-	2,85	99,80
S02	55,52	16,99	6,18	-	0,15	0,11	1,12	10,64	4,02	0,54	0,05	-	-	4,03	99,57
S03	50,24	18,15	7,26	-	0,32	0,32	2,62	11,99	3,38	0,51	0,09	-	-	4,20	99,42
S12	55,75	17,42	6,28	-	0,12	0,12	1,84	10,39	4,69	0,27	0,02	-	-	3,07	100,11
S13	51,32	19,66	6,20	-	0,15	0,25	2,22	11,45	4,55	0,42	0,04	-	-	2,87	99,35
S14	51,25	19,41	6,77	-	0,12	0,48	2,42	10,78	4,50	0,44	0,02	-	-	3,14	99,56
S30	54,24	18,60	6,53	-	0,22	0,16	1,59	11,22	4,13	0,38	0,03	-	-	2,56	99,76
S31	50,31	19,29	7,44	-	0,27	1,75	3,65	12,07	2,95	0,88	0,53	-	-	0,80	100,01

S32	52,23	19,16	7,28	-	0,20	0,23	1,72	11,71	3,9	0,43	0,02	-	-	2,12	99,18
S38	53,80	20,79	4,62	-	0,12	0,34	1,88	11,79	4,03	0,42	0,00	-	-	1,80	99,72
S151	53,99	17,60	7,94	-	0,11	0,31	0,46	12,95	2,82	0,52	0,04	-	-	2,82	99,68
S152	50,63	15,94	6,62	-	0,20	0,51	3,47	12,57	3,90	0,55	0,05	-	-	4,63	99,23
S153	56,22	16,68	7,10	-	0,22	0,30	0,80	10,74	2,91	0,60	0,00	-	-	3,30	99,05
S154	52,66	19,35	5,99	-	0,13	0,42	1,87	11,64	4,81	0,33	0,02	-	-	2,41	99,76
S155	54,41	18,44	6,50	-	0,13	0,23	1,05	10,46	5,01	0,40	0,07	-	-	3,26	100,08
S156	52,99	16,89	8,82	-	0,19	0,32	0,94	11,18	3,59	0,75	0,02	-	-	2,46	98,30
S187	51,49	18,00	7,01	-	0,19	0,20	1,65	12,17	4,32	0,39	0,02	-	-	3,32	98,95
S187V	53,29	21,89	0,46	-	0,03	0,00	0,90	12,67	5,03	0,01	0,02	-	-	5,38	100,38
S188	54,16	19,04	4,71	-	0,17	0,14	1,40	11,37	4,99	0,30	0,04	-	-	3,68	100,08
S189	53,29	19,31	5,52	-	0,11	0,09	1,37	11,18	5,56	0,26	0,00	-	-	3,24	99,98
S186.a1	52,60	18,99	6,99	-	0,15	0,39	1,74	11,18	5,33	0,43	0,04	-	-	1,30	99,30
S186.a2	53,31	19,23	6,52	-	0,14	0,34	1,68	12,06	3,92	0,38	0,05	-	-	1,41	99,29
S186.b1	53,92	19,21	6,75	-	0,14	0,34	1,54	10,66	5,52	0,35	0,05	-	-	0,98	99,57
S186.b2	53,28	19,42	6,69	-	0,15	0,33	1,58	11,28	5,01	0,36	0,04	-	-	1,39	99,69
S186.c	55,14	19,35	5,29	-	0,13	0,27	1,25	10,51	5,84	0,27	0,00	-	-	1,41	99,64

Table 14: Rietfontein nepheline syenite trace element geochemistry.

Samples	*Sc*	*V*	*Cr*	*Co*	*Ni*	*Cu*	*Zn*	*Ga*	*Rb*	*Sr*	*Y*	*Zr*	*Nb*	*Mo*	*Ba*	*Pb*	*Th*	*U*
S01	0,00	41,00	0,00	5,80	0,00	0,00	95,00	-	120,00	494,00	72,00	447,00	21,00	-	1065,00	36,00	6,50	6,50
S02	0,00	8,50	0,00	2,50	0,00	0,00	114,00	-	124,00	581,00	33,00	450,00	15,00	-	823,00	17,00	5,40	6,90
S03	0,00	55,00	0,00	5,90	0,00	0,00	153,00	-	91,00	827,00	48,00	191,00	21,00	-	1255,00	21,00	8,30	6,40
S12	55,00	38,00	0,00	3,90	0,00	0,00	0,00	-	100,00	861,00	6,80	159,00	5,10	-	1876,00	10,00	6,40	7,70
S13	0,00	67,00	0,00	5,90	0,00	0,00	63,00	-	91,00	839,00	5,20	161,00	17,00	-	1823,00	6,80	5,50	3,20
S14	0,90	77,00	0,00	4,70	0,00	0,00	51,00	-	88,00	857,00	3,50	117,00	10,00	-	1719,00	0,00	0,00	0,00
S30	0,00	37,00	0,00	4,20	0,00	0,00	75,00	-	114,00	611,00	32,00	195,00	7,50	-	871,00	15,00	5,50	8,10
S31	2,10	91,00	0,00	16,00	0,00	3,20	146,00	-	70,00	775,00	34,00	282,00	50,00	-	703,00	15,00	12,00	7,10
S32	0,00	50,00	0,00	5,00	0,00	0,00	87,00	-	94,00	474,00	20,00	152,00	8,80	-	883,00	15,00	0,00	0,00
S38	0,00	34,00	0,00	3,10	0,00	0,00	29,00	-	70,00	865,00	4,00	90,00	10,00	-	1752,00	0,00	0,00	0,00
S151	0,00	71,00	0,00	7,80	0,00	0,00	78,00	-	82,00	873,00	19,00	158,00	19,00	-	988,00	0,00	0,00	0,00

S152	0,00	40,00	3,00	7,50	0,00	0,00	138,00	-	95,00	999,00	14,00	361,00	47,00	-	1330,00	0,00	0,00	0,00
S153	0,00	4,50	0,00	7,50	0,00	0,00	131,00	-	89,00	447,00	75,00	1268,00	59,00	-	395,00	12,00	6,50	5,90
S154	0,00	48,00	0,00	5,80	0,00	0,00	56,00	-	104,00	808,00	5,00	124,00	7,90	-	1472,00	0,00	0,00	0,00
S155	0,00	14,00	0,00	4,90	0,00	0,00	71,00	-	129,00	703,00	7,50	172,00	0,00	-	743,00	0,00	0,00	0,00
S156	0,00	17,00	1,90	7,60	0,00	0,00	74,00	-	112,00	316,00	30,00	467,00	20,00	-	403,00	6,40	0,00	0,00
S187	0,00	40,00	25,00	74,00	2,00	7,00	114,00	-	102,00	648,00	43,00	1124,00	58,00	-	1343,00	12,00	10,00	0,00
S187V	0,00	0,00	0,00	5,00	5,00	6,00	118,00	-	113,00	977,00	26,00	733,00	53,00	-	1268,00	0,00	0,00	0,00
S188	0,00	35,00	16,00	5,00	0,00	5,00	187,00	-	113,00	1002,00	25,00	164,00	36,00	-	2208,00	28,00	0,00	0,00
S189	9,00	37,00	45,00	6,00	0,00	8,00	66,00	-	123,00	865,00	7,00	97,00	9,00	-	1328,00	19,00	0,00	0,00
S186.a1	4,40	88,00	16,00	94,00	0,00	6,00	70,00	-	114,00	418,00	17,00	116,00	10,00	-	1410,00	0,00	0,00	0,00
S186.a2	9,00	69,00	0,00	74,00	0,00	5,00	62,00	-	102,00	573,00	19,00	104,00	6,00	-	1424,00	0,00	0,00	0,00
S186.b1	4,60	63,00	0,00	41,00	0,00	6,00	65,00	-	115,00	340,00	14,00	109,00	7,00	-	1325,00	0,00	0,00	0,00
S186.b2	0,00	65,00	0,00	51,00	0,00	5,00	65,00	-	108,00	487,00	15,00	103,00	70,00	-	1484,00	0,00	0,00	6,00
S186.c	4,60	51,00	0,00	56,00	0,00	6,00	58,00	-	129,00	514,00	15,00	83,00	5,00	-	1989,00	11,00	0,00	6,00

Table 15: Rietfontein nepheline syenite rare earth element geochemistry.

Samples	*La*	*Ce*	*Pr*	*Nd*	*Sm*	*Eu*	*Gd*	*Tb*	*Dy*	*Ho*	*Er*	*Tm*	*Yb*	*Lu*
S01	5,70	15,00	2,30	11,00	3,40	1,40	5,80	-	10,00	2,70	9,30	-	9,60	1,20
S02	6,90	15,00	2,30	9,30	2,20	0,90	3,40	-	4,80	1,40	4,40	-	5,20	0,70
S03	8,10	21,00	3,00	14,00	3,80	1,40	5,20	-	7,00	1,70	5,60	-	6,00	0,80
S12	3,30	6,60	0,00	3,90	0,60	0,30	1,10	-	1,50	0,40	1,40	-	2,40	0,30
S13	4,10	11,00	1,70	7,00	1,20	0,40	1,50	-	1,70	0,40	1,00	-	1,60	0,30
S151	6,40	22,00	2,30	10,00	1,90	0,60	2,50	-	3,00	0,80	2,10	-	3,00	0,50
S154	3,40	9,10	1,30	5,30	0,70	0,30	1,00	-	1,00	0,30	0,70	-	1,30	0,30

Table 16: Pilanesberg nepheline syenite major element geochemistry from Elburg and Cawthorn (2017).

Samples	*SiO_2*	*Al_2O_3*	*Fe_2O_3*	*FeO*	*MnO*	*MgO*	*CaO*	*Na_2O*	*K_2O*	*TiO_2*	*P_2O_5*	*Cr_2O_3*	*NiO*	*LOI*	*Total*
OWF	59,70	17,64	0,00	0,00	0,31	0,51	1,63	7,90	5,77	0,75	0,04	-	-	1,64	99,13
OWF	58,16	10,12	0,00	0,00	1,12	0,82	3,02	5,53	4,05	2,10	0,02	-	-	0,81	98,47

OWF	59,75	17,63	0,00	0,00	0,54	0,51	0,99	8,61	5,56	0,90	0,01	-	-	0,99	98,57
OWF	52,23	17,37	0,00	0,00	0,68	1,07	4,65	11,30	4,23	0,46	0,03	-	-	4,72	98,54
OWF	62,18	17,13	0,00	0,00	0,25	0,91	1,19	6,95	5,60	1,15	0,09	-	-	0,00	99,23
OWF	50,04	24,27	0,00	0,00	0,29	0,43	3,08	12,51	4,79	0,62	0,06	-	-	2,91	96,44
OWF	61,47	17,71	0,00	0,00	0,50	0,60	1,46	5,84	5,56	0,97	0,08	-	-	1,50	100,90
OWF	55,55	17,72	0,00	0,00	0,51	0,73	2,85	10,32	4,19	0,95	0,06	-	-	2,16	98,11
OWF	56,02	17,36	0,00	0,00	0,44	0,42	3,25	6,96	6,17	0,83	0,08	-	-	2,36	98,58
OWF	60,20	19,28	0,00	0,00	0,27	0,49	0,89	8,55	5,42	0,85	0,06	-	-	-	97,57
OWF	52,22	17,37	7,78	1,25	0,86	1,82	3,14	8,47	5,76	1,30	0,14	-	-	2,70	99,30
OWF	59,55	18,69	2,98	0,79	0,40	2,03	2,03	7,60	5,00	0,82	0,19	-	-	2,14	98,00
OWF	60,50	16,10	0,00	0,00	0,16	1,72	0,91	5,02	6,33	1,28	0,12	-	-	0,99	96,45
OWF	54,50	16,10	0,00	0,00	0,68	0,28	4,44	9,17	4,36	0,97	0,11	-	-	5,66	95,67
OWF	55,73	14,99	0,00	0,00	0,83	1,54	1,69	9,34	6,23	1,06	0,20	-	-	3,68	97,17
OWF	58,06	17,93	0,00	0,00	0,61	0,97	2,06	7,20	4,86	1,17	0,12	-	-	1,47	97,78
OWF	62,04	18,17	0,00	0,00	0,28	0,00	1,02	7,09	5,54	0,75	0,05	-	-	1,38	98,41
OWF	58,73	14,64	0,00	0,00	1,15	1,55	1,33	6,93	2,90	1,20	0,19	-	-	1,57	96,95
OWF	59,41	17,37	0,00	0,00	0,76	0,28	1,93	7,34	3,83	0,90	0,16	-	-	0,80	98,89
OWF	56,62	15,83	0,00	0,00	0,80	1,68	2,07	7,59	5,81	1,04	0,23	-	-	0,65	98,33
OWF	59,85	18,26	0,00	0,00	0,49	0,70	2,99	5,61	4,85	0,87	0,06	-	-	3,67	98,94
OWF	54,24	21,98	0,00	0,00	0,40	0,09	1,41	11,06	4,33	0,39	0,03	-	-	-	98,22
OWF	55,14	20,58	0,00	0,00	0,72	0,15	1,58	9,54	4,16	0,45	0,02	-	-	-	95,79
IWF	55,56	19,92	0,00	0,00	0,46	0,41	2,68	8,03	5,92	0,73	0,08	-	-	1,78	96,43
IWF	56,16	18,35	0,00	0,00	0,28	0,71	2,01	8,41	6,68	0,74	0,01	-	-	0,52	99,17
IWF	58,09	19,81	0,00	0,00	0,18	0,61	1,95	6,13	7,86	0,58	0,06	-	-	1,37	99,32
IWF	56,82	18,87	0,00	0,00	0,45	0,62	2,72	6,29	6,40	0,69	0,04	-	-	1,84	98,82
IWF	56,64	19,95	0,00	0,00	0,24	0,60	1,75	5,11	10,01	0,83	0,17	-	-	0,91	100,67
IWF	57,17	17,74	0,00	0,00	0,53	0,51	1,49	7,70	6,73	0,56	0,01	-	-	0,34	99,00
IWF	51,21	17,74	8,18	1,06	0,95	2,14	3,21	9,41	4,84	1,28	0,08	-	-	2,49	97,26
IWF	52,65	19,62	5,93	1,19	0,45	1,27	2,2	7,72	7,97	1,03	0,07	-	-	2,07	98,43
IWF	54,49	19,87	4,88	2,92	0,41	0,50	2,1	9,57	5,09	0,31	0,14	-	-	2,39	100,39
IWF	57,02	20,58	0,00	0,00	0,40	0,61	3,02	6,03	5,48	0,80	0,07	-	-	1,55	99,66
IWF	56,76	19,73	0,00	0,00	0,48	1,94	2,62	4,86	6,12	0,90	0,08	-	-	3,27	97,96

IWF	54,67	21,59	0,00	0,00	0,50	1,64	3,24	7,54	4,86	0,43	0,07	-	-	1,79	99,40
IWF	55,68	21,37	0,00	0,00	0,51	1,67	2,95	7,43	4,64	0,41	0,06	-	-	1,79	98,04
IWF	58,58	19,58	0,00	0,00	0,38	1,59	2,18	5,31	5,01	0,66	0,07	-	-	2,67	99,38
IWF	58,30	19,24	0,00	0,00	0,40	1,66	2,32	5,45	5,27	0,66	0,10	-	-	2,11	100,72
IWF	54,16	20,11	0,00	0,00	0,27	0,00	1,82	7,77	8,58	0,75	0,03	-	-	1,45	98,02
IWF	53,73	20,85	0,00	0,00	0,27	0,40	1,85	7,26	8,62	0,73	0,03	-	-	1,53	97,21
IWF	55,72	22,45	0,00	0,00	0,14	0,81	1,7	4,18	11,53	0,48	0,07	-	-	2,91	99,29
IWF/OWF	56,04	19,88	0,00	0,00	0,39	1,03	2,07	4,90	8,00	0,80	0,05	-	-	4,17	97,96
GF	55,90	15,15	0,00	0,00	0,68	0,52	4,03	7,63	5,53	0,91	0,24	-	-	2,57	98,27
GF	55,88	16,47	0,00	0,00	0,63	0,42	4,62	7,51	4,64	0,87	0,06	-	-	2,71	98,63
GF	55,25	16,43	0,00	0,00	0,44	0,31	3,32	8,11	6,52	0,67	0,04	-	-	0,84	98,21
GF	55,63	16,43	0,00	0,00	0,54	0,53	5,13	6,85	5,49	0,99	0,07	-	-	2,36	97,28
GF	56,32	14,66	0,00	0,00	0,77	0,14	2,19	10,43	2,80	0,45	0,03	-	-	-	93,91
GF	55,36	18,58	0,00	0,00	0,56	0,48	2,16	9,14	6,78	0,67	0,09	-	-	-	95,82
GF	56,34	20,35	0,00	0,00	0,35	0,31	2,31	7,70	6,19	0,79	0,08	-	-	-	96,13
GF	51,86	18,04	5,49	6,43	0,8	1,33	2,65	8,43	5,10	0,67	0,10	-	-	1,28	97,33
GF	53,43	16,82	7,87	1,35	0,97	1,37	3,43	8,70	4,86	1,12	0,19	-	-	3,54	98,31
GF	52,98	18,31	5,99	1,50	0,59	0,51	3,90	8,65	6,77	0,84	0,09	-	-	2,64	98,19
GF	56,32	14,88	0,00	0,00	0,96	0,34	3,19	7,23	6,38	1,06	0,09	-	-	3,06	97,17
GF	60,32	17,38	0,00	0,00	0,72	0,12	1,02	8,79	4,09	0,82	0,09	-	-	0,99	98,80
GF	54,75	14,74	0,00	0,00	1,05	0,00	4,21	6,32	5,26	0,95	0,09	-	-	4,09	99,08
GF	52,27	17,03	0,00	0,00	0,54	0,46	1,84	8,40	6,86	0,82	0,13	-	-	2,64	97,70

Table 17: Pilanesberg nepheline syenite trace element geochemistry from Elburg and Cawthorn (2017).

Samples	*Ba*	*Rb*	*Sr*	*Y*	*Zr*	*Nb*	*La*	*Nd*	*Th*	*U*	*Hf*	*Sc*	*Zn*	*Cu*	*Ni*	*Pb*
OWF	900,00	156,00	1850,00	78,00	1600,00	250,00	370,00	-	-	-	-	-	-	-	-	-
OWF	450,00	220,00	1070,00	150,00	2600,00	430,00	870,00	-	-	-	-	-	-	-	-	-
OWF	44,00	130,00	1380,00	120,00	7000,00	1290,00	410,00	-	-	-	-	-	-	-	-	-
OWF	980,00	150,00	5300,00	210,00	1600,00	80,00	1260,00	-	-	-	-	-	-	-	-	-
OWF	870,00	150,0	600,00	54,00	1200,00	260,00	400,00	-	-	-	-	-	-	-	-	-
OWF	540,00	130,00	3500,00	110,00	2300,00	345,00	560,00	-	-	-	-	-	-	-	-	-

OWF	680,00	190,00	850,00	120,00	2500,00	460,00	970,00	-	-	-	-	-	-	-	-	-
OWF	1170,00	140,00	3100,00	120,00	2900,00	410,00	720,00	-	-	-	-	-	-	-	-	-
OWF	980,00	270,00	3100,00	64,00	3310,00	430,00	670,00	-	-	-	-	-	-	-	-	-
OWF	603,00	130,00	490,00	-	840,00	197,00	-	-	-	-	-	-	-	-	-	-
OWF	-	-	-	-	-	-	-	-	-	-	-	-	-	-	-	-
OWF	-	-	-	-	-	-	-	-	-	-	-	-	-	-	-	-
OWF	1404,00	195,00	509,00	233,00	848,00	89,00	618,00	-	-	-	-	-	-	-	-	-
OWF	613,00	119,00	2754,00	84,00	2779,00	648,00	1253,00	-	-	-	-	-	-	-	-	-
OWF	370,00	187,00	825,00	75,00	922,00	193,00	875,00	-	-	-	-	-	-	-	-	-
OWF	269,00	243,00	998,00	56,00	2106,00	466,00	-	-	-	-	-	-	-	-	-	-
OWF	572,00	170,00	447,00	30,00	778,00	174,00	117,00	-	-	-	-	-	-	-	-	-
OWF	146,00	168,00	393,00	112,00	5648,00	1328,00	-	-	-	-	-	-	-	-	-	-
OWF	55,00	220,00	1056,00	109,00	3799,00	689,00	-	-	-	-	-	-	-	-	-	-
OWF	-	187,00	821,00	69,00	1169,00	225,00	-	-	-	-	-	-	-	-	-	-
OWF	178,00	161,00	1355,00	126,00	3059,00	627,00	-	-	-	-	-	-	-	-	-	-
OWF	31,00	238,00	155,00	-	743,00	341,00	-	-	-	-	-	-	-	-	-	-
OWF	-	234,00	168,00	-	1728,00	343,00	-	-	-	-	-	-	-	-	-	-
IWF	80,00	208,00	384,00	107,00	1282,00	324,00	844,00	-	-	-	-	-	-	-	-	-
IWF	1160,00	146,00	2750,00	54,00	1520,00	240,00	200,00	-	-	-	-	-	-	-	-	-
IWF	1460,00	200,00	2300,00	41,00	1000,00	140,00	220,00	53,00	-	-	-	-	-	-	-	-
IWF	880,00	200,00	3000,00	64,00	1900,00	340,00	400,00	-	-	-	-	-	-	-	-	-
IWF	340,00	290,00	3400,00	9,00	630,00	110,00	130,00	-	-	-	-	-	-	-	-	-
IWF	1400,00	390,00	1200,00	56,00	2700,00	410,00	290,00	-	-	-	-	-	-	-	-	-
IWF	-	-	-	-	-	-	-	-	-	-	-	-	-	-	-	-
IWF	-	-	-	-	-	-	-	-	-	-	-	-	-	-	-	-
IWF	-	-	-	-	-	-	-	-	-	-	-	-	-	-	-	-
IWF	76,00	205,00	327,00	102,00	1105,00	351,00	-	-	-	-	-	-	-	-	-	-
IWF	1887,00	147,00	3688,00	43,00	953,00	222,00		-	-	-	-	-	-	-	-	-
IWF	10,00	248,00	432,00	62,00	918,00	248,00	-	-	-	-	-	-	-	-	-	-
IWF	-	-	-	-	-	-	-	-	-	-	-	-	-	-	-	-
IWF	425,00	256,00	414,00	110,0,	1753,00	382,00		-	-	-	-	-	-	-	-	-
IWF	-	-	-	-	-	-	-	-	-	-	-	-	-	-	-	-

IWF	3686,00	162,00	3192,00	45,00	1345,00	122,00	136,00	-	20,06	8,07	24,65	1,77	-	-	2,00	35,28
IWF	3966,00	170,00	3396,00	45,00	1122,00	106,00	125,00	-	13,93	6,96	20,35	1,07	-	-	1,00	29,83
IWF	1277,00	423,00	2589,00	9,00	153,00	51,00	93,00	-	-	-	-	-	-	-	-	-
IWF/OWF	2401,00	142,00	3347,00	32,00	1196,00	132,00	313,00	-	-	-	-	-	-	-	-	-
GF	1100,00	150,00	5000,00	46,00	3200,00	510,00	760,00	-	-	-	-	-	-	-	-	-
GF	830,00	120,00	4100,00	74,00	2800,00	530,00	750,00	300,00	-	-	-	-	-	-	-	-
GF	1200,00	190,00	2600,00	42,00	2300,00	410,00	1000,00	-	-	-	-	-	-	-	-	-
GF	960,00	130,00	5000,00	90,00	3000,00	540,00	1030,00	-	-	-	-	-	-	-	-	-
GF	-	180,00	1956,00	176,00	8287,00	369,00	-	-	-	-	-	-	-	-	-	-
GF	1332,00	209,00	3366,00	12,00	3569,00	366,00	-	-	-	-	-	-	-	-	-	-
GF	390,00	123,00	3522,00	-	753,00	169,00	-	-	-	-	-	-	-	-	-	-
GF	-	-	-	-	-	-	-	-	-	-	-	-	-	-	-	-
GF	-	-	-	-	-	-	-	-	-	-	-	-	-	-	-	-
GF	-	-	-	-	-	-	-	-	-	-	-	-	-	-	-	-
GF	1745,00	171,00	5143,00	76,00	8908,00	452,00	499,00	-	53,56	20,89	227,18	8,79	-	-	1,00	72,86
GF	84,00	227,00	779,00	112,00	4559,00	497,00	520,00	-	-	-	-	-	-	-	-	-
GF	999,00	103,00	4704,00	13,00	2421,00	257,00	212,00	-	-	-	-	-	-	-	-	-
GF	1955,00	222,00	3077,00	54,00	3287,00	253,00	233,00	-	47,17	17,81	74,57	2,62	-	-	1,00	71,85

Table 18: Pilanesberg nepheline syenite rare earth element geochemistry.

Samples	*La*	*Ce*	*Pr*	*Nd*	*Sm*	*Eu*	*Gd*	*Tb*	*Dy*	*Ho*	*Er*	*Tm*	*Yb*	*Lu*
IWF	220	320	19,00	53,00	5,70	1,70	3,00	0,50	3,10	0,70	1,90	0,30	1,80	0,30
GF	750	1700	88,00	300,00	28,00	6,60	6,50	0,90	5,50	0,90	2,30	0,40	3,00	0,30
RF	345	500	40,00	110,00	9,50	2,80	4,80	0,70	4,10	0,90	2,10	0,90	1,90	0,20
RF	320	580	60,00	200,00	20,00	4,50	8,50	1,00	5,50	1,00	2,60	0,40	2,80	0,30

3. Spitskop Ijolite

Table 19: Spitskop ijolite major element geochemistry.

Samples	*SiO_2*	*Al_2O_3*	*Fe_2O_3*	*FeO*	*MnO*	*MgO*	*CaO*	*Na_2O*	*K_2O*	*TiO_2*	*P_2O_5*	*Cr_2O_3*	*NiO*	*LOI*	*Total*
2-11-1	44,72	21,90	0,67	5,40	0,15	2,49	7,83	11,74	3,31	0,70	0,93	0,01	0,00	0,52	100,35

Table 20: Spitskop ijolite trace element geochemistry.

Samples	*Sc*	*V*	*Cr*	*Co*	*Ni*	*Cu*	*Zn*	*Ga*	*Rb*	*Sr*	*Y*	*Zr*	*Nb*	*Mo*	*Ba*	*Pb*	*Th*	*U*
2-11-1	6,00	103,42	8,32	13,82	4,70	32,32	54,05	19,64	64,96	508,97	16,52	74,92	12,59	0,76	55,18	4,46	0,44	0,00

Table 21: Spitskop ijolite rare earth element geochemistry.

Samples	*La*	*Ce*	*Pr*	*Nd*	*Sm*	*Eu*	*Gd*	*Tb*	*Dy*	*Ho*	*Er*	*Tm*	*Yb*	*Lu*
2-11-1	22,61	46,43	5,71	20,69	4,03	1,15	2,52	0,43	2,70	0,59	1,68	0,25	1,61	0,29

4. Spitskop Mafic Fenites

Table 22: Spitskop mafic fenites major element geochemistry.

Samples	*SiO_2*	*Al_2O_3*	*Fe_2O_3*	*FeO*	*MnO*	*MgO*	*CaO*	*Na_2O*	*K_2O*	*TiO_2*	*P_2O_5*	*Cr_2O_3*	*NiO*	*LOI*	*Total*
1-2-2-1	46,13	18,53	1,10	8,94	0,26	1,64	7,44	10,63	2,68	1,33	0,52	0,01	0,00	0,95	100,16
4-42-6	43,04	15,20	1,41	11,41	0,26	3,82	10,53	8,70	2,22	1,56	0,86	0,01	0,00	0,74	99,78
4-43-1	48,88	18,72	0,64	5,17	0,14	0,46	4,64	14,47	0,03	0,71	0,13	0,00	0,00	5,18	99,17
4-43-2	43,22	19,31	0,99	7,98	0,18	2,84	8,59	10,41	3,05	0,85	0,92	0,01	0,00	1,33	99,67
4-48-2	50,66	17,38	1,04	8,45	0,21	1,60	4,78	8,78	3,22	1,07	0,36	0,01	0,00	2,36	99,92
4-48-11	50,13	18,62	0,92	7,49	0,23	1,56	4,54	10,16	3,23	1,00	0,37	0,00	0,00	1,67	99,93
6-65-2	54,64	17,42	0,72	5,77	0,2	0,71	3,99	11,09	0,99	0,62	0,18	0,01	0,00	3,32	99,65

Table 23: Spitskop mafic fenites trace element geochemistry.

Samples	*Sc*	*V*	*Cr*	*Co*	*Ni*	*Cu*	*Zn*	*Ga*	*Rb*	*Sr*	*Y*	*Zr*	*Nb*	*Mo*	*Ba*	*Pb*	*Th*	*U*

1-2-2-1	5,61	153,31	4,75	10,21	3,57	35,31	117,90	26,48	57,82	789,63	29,82	232,32	39,12	0,00	420,17	4,95	1,27	0,82
4-42-6	19,36	222,25	27,32	35,88	10,22	99,55	84,34	18,89	48,14	592,83	17,78	99,43	14,17	0,44	111,91	5,68	0,00	0,00
4-43-1	0,67	69,76	4,29	3,94	0,00	24,31	59,94	19,42	4,35	1341,54	9,43	163,52	25,68	1,22	1915,83	7,93	3,75	1,40
4-43-2	10,63	183,02	6,4	26,70	7,06	117,41	51,48	17,59	58,88	583,90	13,45	65,09	6,51	0,72	238,40	6,65	0,00	0,00
4-48-2	6,18	121,68	0,00	16,28	3,24	45,18	105,35	29,37	90,40	630,04	19,87	296,95	36,25	0,19	1620,57	6,25	0,90	0,00
4-48-11	2,29	128,84	0,63	12,10	2,71	42,05	132,24	28,20	95,75	572,80	21,32	296,51	40,48	0,75	1596,96	4,35	0,40	0,00
6-65-2	4,22	108,33	0,00	10,44	0,96	24,36	72,01	31,78	21,89	418,19	11,57	239,31	53,80	2,09	2484,76	12,05	3,40	0,00

Table 24: Spitskop mafic fenites rare earth element geochemistry.

Samples	*La*	*Ce*	*Pr*	*Nd*	*Sm*	*Eu*	*Gd*	*Tb*	*Dy*	*Ho*	*Er*	*Tm*	*Yb*	*Lu*
1-2-2-1	31,49	65,82	8,11	29,74	6,20	1,95	3,86	0,74	5,00	1,13	3,38	0,53	3,60	0,59
4-42-6	11,89	37,41	3,94	15,18	3,67	0,73	2,21	0,51	3,87	0,93	2,89	0,47	3,41	0,60
4-43-1	21,81	49,28	5,51	20,75	3,92	1,05	2,55	0,43	2,73	0,59	1,67	0,24	1,75	0,33
4-43-2	11,21	24,90	3,68	14,09	3,92	1,34	1,58	0,29	1,85	0,39	1,21	0,20	1,68	0,34
4-48-2	6,77	14,21	1,81	6,94	2,62	1,16	0,97	0,21	1,62	0,40	1,32	0,24	2,03	0,39
4-48-11	14,42	29,93	4,05	16,17	4,13	1,45	2,82	0,51	3,41	0,74	2,08	0,35	2,61	0,45
6-65-2	16,11	30,36	3,39	12,94	3,73	1,54	1,91	0,29	1,79	0,38	1,11	0,20	1,57	0,31

5. Bushveld Upper Zone

Table 25: Upper Zone major element geochemistry from Scoon and Mitchell (2012) and Tongeren (2011).

Samples	*SiO_2*	*Al_2O_3*	*Fe_2O_3*	*FeO*	*MnO*	*MgO*	*CaO*	*Na_2O*	*K_2O*	*TiO_2*	*P_2O_5*	*Cr_2O_3*	*NiO*	*LOI*	*Total*
S1	46,47	14,28	19,02	-	0,23	3,90	10,75	2,81	0,43	2,17	0,05	-	-	-0,93	99,18
S2	40,81	13,43	27,49	-	0,35	3,86	8,69	2,95	0,30	2,29	1,53	-	-	-2,06	99,62
S3	37,75	10,50	29,91	-	0,36	5,06	10,15	2,12	0,22	3,14	2,39	-	-	-2,18	99,41
S4	32,88	5,04	40,47	-	0,47	7,82	8,35	1,06	0,17	3,89	2,07	-	-	-3,14	99,09
S5	46,51	17,03	16,88	-	0,18	2,69	10,70	3,37	0,36	2,88	0,04	-	-	-0,57	100,06
S6	38,72	11,71	28,50	-	0,34	4,50	9,75	2,28	0,23	3,09	2,11	-	-	-1,97	99,27
S7	33,90	10,92	31,97	-	0,32	5,16	9,42	1,87	0,20	4,42	3,01	-	-	-1,93	99,25
S8	39,36	15,46	26,70	-	0,22	3,12	7,72	2,75	0,41	4,54	0,08	-	-	-0,75	99,62

S9	42,83	12,68	24,23	-	0,26	5,00	9,42	2,29	0,29	3,54	0,05	-	-	-1,50	99,10
S10	49,03	14,89	16,06	-	0,22	5,79	9,88	2,55	0,44	1,35	0,02	-	-	-0,43	99,81
S11	45,17	14,76	19,46	-	0,20	5,60	10,03	2,43	0,42	1,99	0,05	-	-	-0,48	99,63
S12	44,15	18,20	20,02	-	0,16	3,82	8,26	2,86	0,35	2,51	0,04	-	-	-0,52	99,87
S13	40,35	16,66	24,61	-	0,20	6,53	6,86	2,58	0,24	2,37	0,02	-	-	-0,92	99,50
S14	43,57	13,56	22,65	-	0,23	6,99	8,96	2,11	0,22	2,50	0,01	-	-	-0,99	99,81
S15	37,90	16,31	27,00	-	0,15	3,23	8,73	2,40	0,24	4,44	0,01	-	-	-1,17	99,26
S16	39,53	18,60	23,07	-	0,14	4,60	7,18	2,80	0,21	3,46	0,01	-	-	-0,32	99,29
S17	39,94	18,19	20,27	-	0,14	5,03	8,19	2,32	0,21	1,55	0,02	-	-	3,84	99,69
S18	44,60	14,70	19,69	-	0,19	5,67	10,50	2,45	0,17	2,31	0,01	-	-	-0,60	99,70
S19	51,92	17,09	9,05	-	0,16	7,18	11,34	2,35	0,17	0,20	0,01	-	-	-0,26	99,21
B07-057	46,81	18,15	-	13,50	0,14	4,33	10,40	2,83	0,27	1,85	0,02	-	-	-	98,33
B06-021	46,22	15,79	-	15,34	0,19	6,18	9,91	2,31	0,19	1,63	0,01	-	-	-	97,77
B06-054	50,12	22,98	-	8,07	0,08	1,39	10,31	4,03	0,51	1,27	0,02	-	-	-	98,77
B06-042	44,97	13,34	-	17,28	0,21	6,05	10,60	2,28	0,36	2,56	0,08	-	-	-	97,72
B06-039	45,10	13,53	-	18,03	0,23	5,06	10,72	2,46	0,27	3,06	0,03	-	-	-	98,49

Table 26: Upper Zone trace element geochemistry from Scoon and Mitchell (2012) and Tongeren (2011).

Samples	*Sc*	*V*	*Cr*	*Co*	*Ni*	*Cu*	*Zn*	*Ga*	*Rb*	*Sr*	*Y*	*Zr*	*Nb*	*Mo*	*Ba*	*Pb*	*Th*	*U*
S1	-	127,00	-	35,00	47,00	47,00	95,00	-	10,40	318,00	10,40	13,30	29,00	1,20	-	-	-	-
S2	-	22,00	-	53,00	3,00	54,00	91,00	-	4,00	296,00	4,00	13,00	3,40	-	-	-	-	-
S3	-	18,00	-	65,00	-	57,00	110,00	-	3,10	229,00	3,10	24,10	8,70	0,40	-	-	-	-
S4	-	35,00	12,00	105,00	9,00	101,00	164,00	-	6,80	113,00	6,80	21,10	15,20	1,30	-	-	-	-
S5	-	43,00	4,00	34,00	6,00	5,00	105,00	-	6,30	363,00	6,30	9,00	15,20	1,80	-	-	-	-
S6	-	32,00	-	76,00	-	97,00	123,00	-	3,90	257,00	3,90	22,60	8,20	-	-	-	-	-
S7	-	105,00	-	88,00	-	65,00	124,00	-	4,10	239,00	4,10	30,60	10,80	1,60	-	-	-	-
S8	-	415,00	-	85,00	29,00	129,00	125,00	-	10,30	311,00	10,30	8,90	28,00	1,90	-	-	-	-
S9	-	358,00	-	76,00	37,00	101,00	114,00	-	6,80	243,00	6,80	13,60	24,20	1,20	-	-	-	-
S10	-	262,00	-	69,00	22,00	201,00	106,00	-	13,50	258,00	13,50	12,90	30,20	2,10	-	-	-	-
S11	-	454,00	-	85,00	38,00	238,00	176,00	-	11,90	260,00	11,90	12,10	30,70	0,80	-	-	-	-
S12	-	812,00	5,00	72,00	62,00	247,00	137,00	-	8,70	300,00	8,70	6,90	18,30	0,80	-	-	-	-

S13	-	767,00	8,00	123,00	23,00	-	119,00	-	3,90	307,00	3,90	4,40	7,60	1,20	-	-	-	-
S14	-	854,00	-	105,00	32,00	238,00	225,00	-	4,80	238,00	4,80	8,00	12,20	1,20	-	-	-	-
S15	-	1846,00	25,00	89,00	80,00	505,00	96,00	-	0,60	280,00	0,60	6,90	14,80	1,10	-	-	-	-
S16	-	1020,00	10,00	108,00	37,00	542,00	63,00	-	2,80	292,00	2,80	2,80	7,60	1,50	-	-	-	-
S17	-	812,00	6,00	193,00	35,00	30,00	89,00	-	0,20	314,00	0,20	2,70	6,80	0,50	-	-	-	-
S18	-	1398,00	18,00	84,00	92,00	540,00	81,00	-	0,30	257,00	0,30	7,10	6,00	0,60	-	-	-	-
S19	-	183,00	53,00	62,00	110,00	171,00	59,00	-	1,60	286,00	1,60	5,50	5,60	0,80	-	-	-	-
B07-057	31,00	825,00	0,00	-	113,00	312,00	87,00	23,00	4,00	295,00	7,00	17,00	1,00	-	117,00	3,00	1,00	0,00
B06-021	36,00	774,00	4,00	-	118,00	445,00	92,00	18,00	2,00	248,00	5,00	8,00	1,00	-	84,00	3,00	1,00	0,00
B06-054	16,00	183,00	5,00	-	10,00	133,00	58,00	24,00	10,00	425,00	8,00	20,00	1,00	-	190,00	4,00	0,00	2,00
B06-042	52,00	480,00	0,00	-	30,00	288,00	104,00	17,00	8,00	217,00	10,00	27,00	1,00	-	131,00	2,00	2,00	1,00
B06-039	58,00	423,00	8,00	-	43,00	108,00	119,00	19,00	4,00	250,00	10,00	22,00	1,00	-	126,00	2,00	3,00	1,00

Table 27: Upper Zone rare earth element geochemistry from Tongeren (2011).

Samples	*La*	*Ce*	*Pr*	*Nd*	*Sm*	*Eu*	*Gd*	*Tb*	*Dy*	*Ho*	*Er*	*Tm*	*Yb*	*Lu*
B07-057	3,17	6,71	0,84	3,30	0,94	0,62	1,08	0,19	1,17	0,25	0,70	0,00	0,69	0,11
B06-021	1,40	2,92	0,39	1,69	0,59	0,52	0,78	0,14	0,93	0,20	0,59	0,00	0,61	0,10
B06-054	5,77	11,32	1,38	5,44	1,24	1,00	1,30	0,23	1,35	0,28	0,79	0,00	0,76	0,12
B06-042	4,99	11,83	1,55	6,51	1,59	0,76	1,85	0,31	1,93	0,41	1,12	0,19	1,07	0,17
B06-039	2,89	7,18	1,13	5,14	1,42	0,85	1,71	0,30	1,87	0,40	1,09	0,18	1,03	0,17

6. Spitskop Granite Fenite

Table 28: Spitskop granite fenites major element geochemistry.

Samples	*SiO_2*	*Al_2O_3*	*Fe_2O_3*	*FeO*	*MnO*	*MgO*	*CaO*	*Na_2O*	*K_2O*	*TiO_2*	*P_2O_5*	*Cr_2O_3*	*NiO*	*LOI*	*Total*
4-48-1	63,50	15,95	0,54	4,32	0,11	0,19	1,45	7,40	5,20	0,45	0,04	0,00	0,00	0,78	99,93
4-48-6	63,38	15,86	0,53	4,28	0,11	0,33	1,92	7,12	5,39	0,37	0,11	0,00	0,00	0,7	100,09
5-50-2	62,41	16,07	0,50	4,09	0,19	0,53	0,85	4,26	8,58	0,47	0,09	0,00	0,00	1,80	99,84
5-52-1	58,21	14,82	0,58	4,67	0,14	0,63	4,21	5,10	6,86	0,57	0,03	0,00	0,00	3,89	99,72
5-56-1	74,54	11,87	0,32	2,55	0,06	0,09	0,95	3,33	5,20	0,24	0,03	0,00	0,00	0,21	99,41

5-56-2	75,60	11,42	0,27	2,16	0,05	0,07	0,60	3,49	5,13	0,18	0,02	0,00	0,00	0,49	99,48
5-56-4	76,76	11,76	0,23	1,88	0,03	0,25	0,37	3,89	4,63	0,19	0,03	0,01	0,00	0,47	100,49

Table 29: Spitskop granite fenite trace element geochemistry.

Samples	*Sc*	*V*	*Cr*	*Co*	*Ni*	*Cu*	*Zn*	*Ga*	*Rb*	*Sr*	*Y*	*Zr*	*Nb*	*Mo*	*Ba*	*Pb*	*Th*	*U*
4-48-1	0,04	7,29	0,00	0,06	4,22	6,67	56,73	34,66	100,36	440,63	8,31	235,20	24,65	2,28	1959,16	10,50	3,71	0,00
4-48-6	3,80	48,29	0,00	0,09	1,52	14,85	49,58	29,31	104,71	460,02	8,81	195,07	13,57	0,56	2208,52	6,66	0,00	0,00
5-50-2	6,83	29,34	9,09	2,64	1,69	21,90	83,33	33,88	175,46	38,94	31,18	754,75	32,86	3,56	860,51	14,36	15,46	0,61
5-52-1	6,87	74,38	0,00	1,75	0,00	21,50	98,79	29,96	123,90	128,83	42,87	591,29	31,63	0,99	666,80	13,14	8,10	0,00
5-56-1	0,91	4,17	0,00	0,64	0,00	8,24	76,64	20,54	200,58	103,63	49,60	277,68	21,32	0,87	1506,57	28,39	12,66	0,00
5-56-2	1,67	5,49	0,00	0,00	1,78	14,21	78,87	20,98	180,34	65,01	44,82	265,59	17,01	2,03	905,46	33,94	14,82	0,76
5-56-4	0,00	5,93	3,33	3,24	4,53	24,92	28,66	19,34	105,66	30,45	35,75	251,05	10,32	0,24	434,13	12,90	11,09	0,00

Table 30: Spitskop granite fenite rare earth element geochemistry.

Samples	*La*	*Ce*	*Pr*	*Nd*	*Sm*	*Eu*	*Gd*	*Tb*	*Dy*	*Ho*	*Er*	*Tm*	*Yb*	*Lu*
4-48-1	17,13	37,85	4,30	16,24	3,04	0,83	1,86	0,31	1,91	0,40	1,13	0,16	1,08	0,20
4-48-6	12,32	28,93	3,98	15,20	4,00	1,28	2,04	0,43	3,05	0,69	2,04	0,32	2,37	0,42
5-50-2	126,63	230,43	26,70	90,50	11,92	2,60	7,92	0,85	4,38	0,89	3,00	0,58	5,18	0,99
5-52-1	20,75	52,27	8,32	36,03	8,64	2,33	6,06	1,09	7,02	1,48	4,43	0,90	8,43	1,56
5-56-1	45,23	91,81	10,97	40,59	8,44	3,28	6,54	1,17	8,08	1,85	5,39	0,89	6,02	1,01
5-56-2	54,88	105,78	12,76	47,00	8,50	1,73	6,89	1,13	7,29	1,61	4,60	0,76	5,21	0,88
5-56-4	80,64	109,61	13,62	48,65	8,23	1,75	6,26	0,95	5,75	1,19	3,44	0,52	3,39	0,55

7. Nebo Granite

Table 31: Nebo granite major element geochemistry from Kleeman and Twist (1989).

Samples	*SiO_2*	*Al_2O_3*	*Fe_2O_3*	*FeO*	*MnO*	*MgO*	*CaO*	*Na_2O*	*K_2O*	*TiO_2*	*P_2O_5*	*Cr_2O_3*	*NiO*	*LOI*	*Total*
S1	69,45	12,56	-	6,00	0,09	0,00	1,69	3,71	4,64	0,42	0,04	-	-	0,45	99,31
S2	71,45	12,10	-	4,56	0,09	0,02	1,48	3,51	4,98	0,38	0,05	-	-	0,42	99,25
S3	71,10	12,46	-	4,18	0,09	0,02	1,43	3,78	4,87	0,33	0,05	-	-	0,47	98,97
S4	71,87	12,16	-	4,39	0,09	0,02	1,27	3,71	4,90	0,34	0,04	-	-	0,42	99,40
S5	71,96	11,87	-	3,74	0,08	0,07	1,12	3,74	4,94	0,29	0,03	-	-	0,29	98,52
S6	72,70	12,16	-	3,74	0,06	0,05	1,13	3,76	4,88	0,26	0,02	-	-	0,52	99,30
S7	74,38	11,77	-	2,99	0,05	0,00	0,96	3,76	5,00	0,21	0,02	-	-	0,36	99,76
S8	74,33	11,56	-	3,19	0,06	0,00	0,83	3,73	4,72	0,22	0,07	-	-	0,42	99,31
S9	74,13	11,72	-	3,04	0,05	0,00	0,81	3,97	5,12	0,20	0,01	-	-	0,33	99,68
S10	73,74	11,69	-	3,32	0,05	0,00	0,92	3,65	5,15	0,23	0,02	-	-	0,47	99,46
S11	74,30	11,43	-	3,17	0,05	0,00	0,94	3,58	5,17	0,19	0,02	-	-	0,63	99,70
S12	76,01	11,48	-	1,92	0,03	0,00	0,41	3,60	5,70	0,13	0,01	-	-	0,41	99,85

Table 32: Nebo granite trace element geochemistry from Kleeman and Twist (1989).

Samples	*Ba*	*Rb*	*Sr*	*Y*	*Zr*	*Nb*	*La*	*Ce*	*Nd*	*Th*	*U*	*Hf*	*Ga*	*Sc*	*Zn*	*Cu*	*Ni*	*Pb*	*Mo*	*W*	*Sn*
S1	2294	147	144	71	607	27	59	118	73	19	5	11	21	2	109	5	6	14	6	6	5
S2	2139	124	132	50	576	25	48	94	60	14	4	8	18	2	113	2	5	21	3	6	5
S3	1935	143	128	54	524	21	57	108	70	18	7	11	19	1	118	5	6	30	4	6	5
S4	1534	180	91	73	569	28	59	123	81	18	5	9	21	2	138	5	7	33	3	6	5
S5	1174	169	84	64	467	23	68	140	85	21	4	10	20	2	86	6	12	20	3	8	5
S6	1137	170	84	57	396	21	76	170	84	22	5	5	19	2	73	3	9	20	3	8	5
S7	737	180	54	68	355	24	85	170	100	25	4	13	20	2	65	3	12	20	3	7	5
S8	633	228	49	106	396	32	83	170	114	32	7	9	21	1	88	6	7	25	3	10	6
S9	590	225	37	94	385	28	122	239	139	35	10	10	21	1	71	7	16	24	3	7	5
S10	540	232	31	114	408	39	106	210	127	41	12	11	22	1	76	5	9	25	3	13	6
S11	533	259	32	95	315	34	95	177	102	34	8	7	21	1	70	11	13	24	119	11	7
S12	449	255	26	40	180	19	74	149	80	34	8	7	20	1	53	3	7	18	3	6	5

Table 33: Nebo granite trace element geochemistry from Hill et al. (1996).

Samples	*Rb*	*Sr*	*Cs*	*Ba*	*Sc*	*Cr*	*Co*	*Y*	*Zr*	*Hf*	*Ta*	*Th*	*U*
SAT-1	599,00	34,00	5,80	263,00	1,90	46,00	1,38	46,00	169,00	6,76	6,70	64,00	12,70
SAT-2	276,00	91,00	10,40	609,00	2,70	27,00	3,18	55,00	215,00	7,71	3,00	41,20	12,10
SAT-9	178,00	61,00	2,36	792,00	2,03	-	1,15	68,00	265,00	9,34	1,38	27,70	6,51
SAT-16	202,00	32,00	1,04	232,00	1,10	-	0,75	123,00	233,00	9,07	1,52	45,10	11,64
SAT-20	277,00	32,00	6,30	377,00	1,10	33,00	1,04	94,00	209,00	8,66	3,70	34,80	12,90
ED-2	238,00	39,00	1,58	548,00	2,02	-	1,98	82,00	343,00	10,60	2,30	30,40	9,42
SAT-25	123,00	117,00	2,20	1840,00	3,20	35,00	1,52	57,00	444,00	14,10	1,40	11,40	4,20
GT1	315,00	34,00	9,73	454,00	1,96	-	1,51	109,00	350,00	13,20	3,29	31,00	9,36
UK4	177,00	58,00	4,11	754,00	2,11	-	2,09	67,00	320,00	10,60	1,64	28,7	6,94
N2	-	-	1,05	309,00	0,32	-	0,21	-	-	13,60	3,29	39,20	10,30

Table 34: Nebo granite rare earth element geochemistry from Hill et al. (1996).

Samples	*La*	*Ce*	*Pr*	*Nd*	*Sm*	*Eu*	*Gd*	*Tb*	*Dy*	*Ho*	*Er*	*Tm*	*Yb*	*Lu*
SAT-1	86,60	201,00	-	53,00	8,27	0,35	-	1,40	-	-	-	-	7,00	0,68
SAT-2	91,20	167,00	-	58,00	8,00	1,28	-	1,42	-	-	-	-	4,60	0,59
SAT-9	77,00	146,00	-	71,30	14,40	1,88	14,20	2,56	-	-	-	-	6,46	1,07
SAT-16	140,00	285,00	-	136,00	26,90	1,08	28,30	5,02	-	-	-	-	11,60	1,71
SAT-20	76,80	149,00	-	65,30	16,40	1,02	18,00	2,80	-	-	-	-	7,80	1,18
ED-2	84,30	164,00	-	77,20	17,40	1,40	12,70	-	-	-	-	-	8,75	1,09
SAT-25	65,50	125,00	-	61,00	12,70	4,04	14,00	2,00	-	-	-	-	4,40	0,59
GT1	79,20	173,00	-	94,20	23,00	1,27	19,10	-	-	-	-	-	12,90	1,65
UK4	98,70	182,00	-	83,10	19,10	2,16	11,50	-	-	-	-	-	6,71	0,87
N2	80,80	158,00	-	69,30	16,40	1,45	11,10	-	-	-	-	-	10,90	1,31

8. Spitskop Carbonatite Mineralogy

Table 35: Spitskop calcite carbonatite mineralogy.

Samples	*Calcite*	*Dolomite*	*Magnetite*	*Apatite*	*REE-Minerals*
6-69-1	85 %	-	-	-	15 %
6-69-2A	100 %	-	-	-	Acc.
6-69-2B	95 %	-	-	-	5 %
7-85	100 %	-	-	Acc.	-
8-88-1	85 %	-	Acc.	15 %	-
8-88-2A	60 %	-	5 %	25 %	-
8-88-2B	50 %	-	5 %	35 %	-
8-90	70 %	-	5 %	25 %	-
8-92A	65 %	-	5 %	30 %	-
8-92B	65 %	-	5 %	30 %	-

Table 36: Spitskop calcite-dolomite carbonatite mineralogy.

Samples	*Calcite*	*Dolomite*	*Magnetite*	*Apatite*	*REE-Minerals*	*Quartz*
8-91	85 %	10%	5%	-	-	-
8-96	80 %	20%	-	-	-	-
8-97A	90 %	5 %	5 %	-	-	-
8-97B	70 %	20%.	10 %	-	-	-
8-100A	60 %	10 %	5 %	25 %	-	-
8-100B	65 %	10 %	5 %	20 %	-	-
8-103-1A	60 %	10 %	15 %	10 %	-	5 %
8-103-1B	60 %	10 %	15 %	10 %	-	5 %

8-103-2A	40 %	15 %	15 %	15 %	-	15 %
8-103-2B	50 %	5 %	15 %	15 %	-	15 %

Table 37: Spitskop dolomite carbonatite mineralogy.

Samples	*Calcite*	*Dolomite*	*Magnetite*	*Apatite*	*REE-Minerals*
6-74-2	Acc.	90 %	10 %	Acc.	-
7-76-1	Acc.	95 %	5 %	Acc.	-
7-76-2	Acc.	95 %	5 %	Acc.	-
7-77	Acc.	90 %	5 %	5 %	-
8-93	Acc.	85 %	5 %	10 %	-
8-95A	Acc.	70 %	20 %	10 %	-
8-95B	Acc.	80 %	20 %	-	-
8-99	Acc.	70 %	5 %	25 %	-

Table 38: Spitskop- and Mare nepheline syenite mineralogy.

Samples	*Aeg-Aug*	*K-Feldspar*	*Sanidine*	*Nepheline*	*Sodalite*	*Calcite*	*Titanite*	*Biotite*	*Cancrinite*
3-23-1	30 %	-	35 %	30 %	5 %	-	Acc.	-	-
3-23-2A	20 %	15 %	45 %	15 %	5 %	-	-	-	Acc.
3-23-2B	20 %	40 %	30 %	10 %	Acc.	-	-	-	Acc.
3-24	20 %	65 %	-	5 %	Acc.	5 %	-	-	-
3-25	30 %	-	30 %	35 %	5 %	-	-	Acc.	-
3-30-1	35 %	30 %	-	15 %	Acc.	-	-	-	Acc.
3-31-1-1A	45 %	15 %	40 %	Acc.	-	-	-	-	-
3-31-1-1B	45 %	15 %	40 %	Acc.	-	-	-	-	-
3-31-1-2	40 %	20 %	40 %	Acc.	-	-	-	-	-
3-31-3	60 %	30 %	10 %	Acc.	-	-	-	-	-
3-31-3-1	30 %	50 %	5 %	20 %	-	-	-	-	-
3-31-3-2	40 %	20 %	30 %	10 %	-	-	-	-	-

3-32A	40 %	10 %	25 %	25 %	-	-	-	Acc.	Acc.
3-32-B	40 %	10 %	25 %	25 %	-	-	-	Acc.	Acc.

Table 39: Spitskop ijolite mineralogy.

Samples	*Aeg-Aug*	*Nepheline*	*Perthite*	*Magnetite*	*Titanite*	*Biotite*	*Sanidine*	*Hornblende*	*Sodalite*
2-11-1-1	30 %	40 %	30 %	-	Acc.	-	-	-	Acc.
2-11-1-2	30 %	55 %	10 %	Acc.	5 %	-	-	-	-
2-11-1-3	30 %	45 %	10 %	Acc.	15 %	-	-	-	-

Table 40: Spitskop mafic fenites mineralogy.

Samples	*Aeg-Aug*	*Nepheline*	*Perthite*	*Magnetite*	*Titanite*	*Biotite*	*Sanidine*	*Hornblende*	*Sodalite*
1-1-1	25 %	40 %	10 %	10 %	-	15 %	-	-	-
1-2-1-1	30 %	50 %	15 %	5 %	-	-	Acc.	-	-
1-2-2-1-1	30 %	30 %	5 %	10 %	10 %	15 %	-	-	-
1-2-2-1-2	30 %	30 %	15 %	10 %	5 %	10 %	-	-	-
1-2-2-2	20 %	20 %	50 %	10 %	-	-	-	-	-
1-3-1	20 %	20 %	40 %	10 %	-	-	-	-	-
1-4	-	25 %	20 %	15 %	-	5 %	10 %	25 %	-
1-4-1	30 %	35 %	20 %	5 %	10 %	Acc.	-	-	Acc.
1-4-2	20 %	35 %	40 %	5 %	-	Acc.	Acc.	-	Acc.
1-6-1	-	5 %	-	85 %	-	10 %	-	-	-
1-6-2	15 %	25 %	-	50 %	-	10 %	-	-	Acc.
1-8-2-1	5 %	10 %	10 %	60 %	10 %	Acc.	-	5 %	-
1-8-2-2	-	5 %	-	90 %	5 %	Acc.	-	-	-
2-9-1	50 %	35 %	15 %	-	-	-	-	-	-
2-12-1-1A	15 %	20 %	-	60 %	5 %	-	-	-	-
2-12-1-1B	15 %	20 %	-	60 %	5 %	-	-	-	-
2-12-1-2A	60 %	35 %	-	5 %	-	-	-	-	-

2-12-1-2B	60 %	35 %	-	5 %	-	-	-	-	-
2-14-3A	5 %	20 %	-	70 %	5 %	Acc.	-	Acc.	-
2-14-3B	5 %	20 %	-	70 %	5 %	Acc.	-	Acc.	-
2-14-4-1	5 %	15 %	-	40 %	20 %	10 %	-	10 %	-
2-14-4-2	10 %	20 %	-	50 %	10 %	5 %	-	5 %	-
2-14-5-1	15 %	10 %	-	60 %	10 %	5 %	-	-	Acc.
2-14-5-2	30 %	30 %	40 %	Acc.	Acc.	-	-	-	-
2-14-6-1	5 %	15 %	-	70 %	5 %	5 %	-	-	-
2-14-6-2A	30 %	45 %	-	15 %	10 %	Acc.	-	-	-
2-14-6-2B	30 %	45 %	-	15 %	10 %	Acc.	-	-	-
2-15-1	35 %	50 %	-	5 %	10 %	Acc.	-	-	Acc.
2-16-1A	25 %	35 %	40 %	Acc.	-	Acc.	-	-	Acc.
2-16-1B	25 %	35 %	40 %	Acc.	-	Acc.	-	-	-
2-16-2A	40 %	55 %	-	-	5 %	-	-	-	-
2-16-2B	40 %	55 %	-	-	5 %	-	-	-	-
4-40	20 %	30 %	-	50 %	-	Acc.	-	-	-
4-42-1	20 %	75 %	-	-	5 %	-	-	-	-
4-42-6A	15 %	70 %	15 %	Acc.	Acc.	-	-	-	Acc.
4-42-6B	-	60 %	-	10 %	-	Acc.	-	30 %	Acc.
4-43-1	30 %	50 %	10 %	5 %	5 %	-	-	-	Acc.
4-43-2A	30 %	40 %	30 %	Acc.	-	-	-	-	Acc.
4-43-2B	30 %	40 %	30 %	Acc.	-	-	-	-	Acc.
4-48-2A	30 %	15 %	50 %	5 %	-	Acc.	-	-	-
4-48-2B	30 %	15 %	50 %	5 %	-	Acc.	-	-	-
4-48-11-1	50 %	15 %	30 %	5 %	-	Acc.	-	-	-
4-48-11-2A	35 %	-	60 %	5 %	-	Acc.	-	-	-
4-48-11-2B	35 %	-	60 %	5 %	-	Acc.	-	-	-
6-64-1A	20 %	-	75 %	5 %	-	Acc.	-	-	-
6-64-1B	20 %	5 %	65 %	10 %	-	Acc.	-	-	-
6-64-1	15 %	10 %	75 %	-	-	-	-	-	-
6-64-2A	40 %	-	45 %	15 %	-	-	-	-	-
6-64-2B	40 %	-	45 %	15 %	-	Acc.	-	-	-

6-65-2	35 %	25 %	30 %	Acc.	10 %	Acc.	-	-	-
6-66-3	15 %	65 %	-	-	-	-	-	-	-

Table 41: Spitskop granite fenites mineralogy.

Samples	*Aeg-Aug*	*Nepheline*	*Titanite*	*Perthite*	*Magnetite*	*Hornblende*	*Sodalite*	*Biotite*	*Plagioclase*	*Quartz*
4-42-4	25 %	65 %	10 %	-	-	-	Acc.	-	-	-
4-46-1	35 %	30 %	5 %	30 %	Acc.	-	-	-	-	-
4-46-2	25 %	15 %	5 %	50 %	5 %	-	-	Acc.	-	-
4-48-1	25 %	15 %	5 %	40 %	5 %	-	-	Acc.	-	10 %
4-48-4	15 %	10 %	-	70 %	-	-	-	-	-	-
4-48-6	25 %	15 %	-	50 %	-	-	-	-	-	-
4-48-7	45 %	10 %	-	45 %	-	-	-	-	-	-
4-48-10	30 %	-	-	35 %	-	-	-	-	-	35 %
5-49A	15 %	-	-	60 %	-	-	-	-	-	25 %
5-49B	15 %	-	-	60 %	-	-	-	-	-	25 %
5-50-1	10 %	-	-	60 %	-	-	-	-	-	30 %
5-50-2	10 %	-	-	60 %	-	-	-	-	-	30 %
5-52-1	-	-	-	70 %	-	10 %	-	-	-	20 %
5-52-2	-	-	-	30 %	-	50 %	-	-	-	20 %
5-56-1	-	-	-	50 %	-	10 %	-	-	5 %	35 %
5-56-2	-	-	-	50 %	-	10 %	-	-	5 %	35 %
5-56-4	-	-	-	50 %	-	10 %	-	-	5 %	35 %